Contribution à la modélisation déterministe spatialisée de l'érosion hydrique des sols à l'échelle des petits bassins versants cultivés

Silvio José Gumiere

Thèse présentée au Centre International d'Études Supérieures en Sciences Agronomiques

Montpellier SupAgro

Discipline : Eaux Continentales et Société

présenté par

Silvio José GUMIERE

pour obtenir le grade de

Docteur du Centre International d'Études Supérieures en Sciences Agronomiques Montpellier SupAgro

---

« Contribution à la modélisation déterministe spatialisée de l'érosion hydrique des sols à l'échelle des petits bassins versants cultivés ».

Soutenue le 10 décembre 2009 devant le jury composé de :

Vincent GUINOT	Président	Université de Montpellier 2
Victor JETTEN	Rapporteur	ITC (Pays Bas)
John WAINWRIGHT	Rapporteur	Université de Sheffield
Olivier CERDAN	Examinateur	BRGM (Orléans)
Damien RACLOT	Examinateur	IRD (Tunisie)
Yves LE BISSONNAIS	Directeur de thèse	INRA (Montpellier)

Remerciements

Je remercie le département Environnement et Agronomie de l'INRA d'avoir financé mes travaux. L'achèvement de ce travail a impliqué de nombreuses collaborations qu'il est important de rappeler. Je voudrais remercier en premier Yves Le Bissonnais. Il a suivi l'évolution de ce travail pendant ces trois années avec beaucoup de patience, de sérénité et de disponibilité. Son aide a été d'une grande importance pour moi sur le plan scientifique, linguistique et humain. D'un coté par sa grande compétence scientifique et de l'autre par ses qualités humaines remarquables, il a été toujours prêt à aider à trouver des solutions. Je lui exprime toute ma gratitude. Damien Raclot était à l'origine du modèle, il a suivi l'avancement du travail à distance en apportant des idées précieuses pour le développement du modèle et l'écriture des articles. Je le remercie aussi pour les nombreuses discussions scientifiques au cours desquelles il a su me conseiller et me faire profiter de ses compétences scientifiques variées pour la modélisation de l'érosion. J'ai également eu le grand plaisir de travailler avec Bruno Cheviron, qui m'a accompagné pendant deux années dans les longues nuits et les week-ends devant l'écran à chercher des "bugs" dans les codes C++ et Latex, en écoutant Beethoven ou la scène finale du Commandeur, dans le Don Giovanni de Mozart. Et aussi pour contribuer à mon apprentissage de la langue française. Merci mon ami. Je voudrais remercier Roger Moussa pour sa bienveillance et pour les longues conversations sur la science, la vie et la modélisation, toujours accompagnées d'une bonne tasse au "café érosion". Je remercie aussi Jean-Stéphane, Jean-Christophe, Xavier, pour leur aide dans l'informatique et la modélisation. Je tiens a remercier nos professeurs François Colin et Stéphane Follain, pour leur amitié, pour les échanges scientifiques et pour les soirées à Vienne. Un grand merci à l'équipe technique pour son travail quotidien qui est d'assurer le fonctionnement opérationnel du laboratoire. Ces trois années ont été effectuées au sein de l'UMR LISAH à Montpellier où Marc Voltz, Jean Albergel et Patrick Andrieux m'ont accueilli. Je tiens à remercier l'ensemble du laboratoire LISAH où j'ai été super bien accueilli, ce qui a d'une certaine façons comblé le vide familial, l'éloignement d'avec le Brésil. Je remercie sincèrement les deux rapporteurs, Victor Jetten et John Wainwright, pour avoir consacré du temps à la lecture méticuleuse de mon manuscrit, ainsi que les autres membres du jury, Olivier Cerdan et Vincent Guinot pour avoir accepté d'évaluer mes travaux. Je remercie également les membres

du comité de pilotage, Joël Léonard, Cédric Legout, Frédéric Darboux et Christian Salles; leurs remarques m'ont toujours été très bénéfiques et furent indispensables à l'achèvement de ce travail. Je voudrais remercier tous les doctorants, post-doctorants et stagiaires du LISAH, Mauricio, Armand, Dennis, Nakié, Lai Ting, Lionel, Séverine, Simon, Rossano, Laurence, Abir, James, Jerome, Muriel, Aline, Sebastien et Rim, pour leur amitié, bonne humeur et pour les petites "fiesta" thématiques toujours bien arrosées. Je tiens à remercier mon ami Jorge qui est a l'origine de mon aventure en France. Je ne saurais suffisamment remercier Adriana: sans elle ma venue en France n'aurait jamais pu devenir réalité. Elle est ma famille ici en France et m'a soutenu dans toutes les circonstances de la vie. Pour tout ça mais surtout pour le reste, encore merci. Enfin je tiens à dédicacer ce travail à ma famille et ma belle famille au Brésil, qui ont toujours été là pour moi quand il le fallait.

Résumé

La pression anthropique liée à l'agriculture intensive est souvent à l'origine d'une accélération des processus érosifs, avec des taux d'ablation souvent supérieurs aux vitesses de formation des sols. En Europe et dans le monde, l'érosion hydrique affecte quasiment toutes les zones géographiques, à des degrés divers. La modélisation de l'érosion hydrique peut fournir des informations utiles pour la mise en œuvre de mesures antiérosives sur les bassins versants agricoles afin de conserver les ressources en sol et diminuer le transport de sédiments vers les cours d'eau. L'objectif général de cette thèse a été de mener une réflexion et une analyse critique sur la problématique de la modélisation de l'érosion hydrique, avec différents angles d'attaque : conceptuel, exploration de modèle et paramétrisation. Nous avons effectué dans un premier temps une analyse bibliographique sur deux des questions qui semblent les plus problématiques dans les modèles d'érosion actuels : la première sur la paramétrisation de l'érosion diffuse et la seconde sur le fonctionnement des éléments d'interfaces du paysage comme les bandes enherbées. Nous avons ensuite développé un modèle d'érosion hydrique distribué et à base physique applicable aux échelles du bassin versant et de l'événement pluvieux. Cette modélisation permet de prendre en considération les éléments d'interface du paysage tout en s'appuyant sur une paramétrisation distribuée facilitée par le recours aux systèmes d'information géographique (SIG). Le modèle développé a été calé et validé sur un bassin versant Méditerranéen, en utilisant une procédure de calage multi échelles. Un autre résultat de ce travail a été le développement d'un cadre général pour l'analyse de sensibilité des modèles d'érosion aux paramètres d'entrée et à leur distribution spatiale, et ceci pour des modèles distribués conçus pour différentes échelles d'espace et de temps. Cette procédure d'analyse a été appliquée à quatre modèles d'érosion (MHYDAS-Erosion, STREAM, MESALES et PESERA). Les résultats montrent des similitudes de comportement pour les différents modèles testés par rapport aux paramètres d'entrée.

Abstract

Anthropogenic activity associated with intensive agricultural production is often the origin of an acceleration in soil erosion processes, such that the rate of erosion will exceed the rate of soil formation. In Europe and the world, water erosion affects all types of landscapes to different degrees. Water erosion models may provide helpful information for the development and application of land management practices in catchments with soil and water conservation concerns. The objective of this work was to reflect on and then critically analyse the problem of water erosion modelling from different points of view: conceptually, model exploration and model parameterisation. From this reflection, and after a literature review, which focused on two of the main problems identified with present-day erosion models, namely model parameterisation and sedimentological connectivity, we have developed a physically based and distributed water erosion model, able to provide dynamic information about soil loss and sediment transport within small agricultural catchments during rainfall events. The model takes into account the effects of land management practices on sediment transport using a distributed GIS parameterisation. The model was calibrated and validated for a Mediterranean catchment, using an automatic and multi-scale calibration procedure. Another result from this work was the development of a sensitivity analysis framework to provide an exploratory analysis of distributed erosion models at different space and time scales. This framework has been applied to four water erosion models (MHYDAS-Erosion, STREAM, MESALES and PESERA). Results have shown a similarity in behaviour of the four erosion models with regards to input parameter variations.

Contents

List of Figures

List of Tables

Introduction Générale

1.1 Contexte et problématique

L'érosion hydrique des sols correspond à l'ensemble des phénomènes de déplacement de matériaux à la surface du sol sous l'action de l'eau. L'érosion hydrique peut recouvrir différents types d'érosion telle que l'érosion marine littorale, l'érosion fluviatile et l'érosion pluviale. Néanmoins, nous nous intéressons dans ce travail uniquement à l'érosion pluviale en zones agricoles, où les impacts de l'activité humaine sur les processus érosifs des sols peuvent être particulièrement importants.

Les problèmes économiques et environnementaux graves provoqués par l'érosion des sols sont de plus en plus fréquents. Les dommages les plus notables sont surtout ressentis par les collectivités locales. Ces dernières doivent faire face aux coûts engendrés par les coulées de boue dans les zones urbanisées, la détérioration des chaussées, la pollution des points de captage d'eau potable et la perte de capacité de production agricole (Boardman et al., 1994; Papy and Douyer, 1991).

Les modèles empiriques globaux peuvent donner des informations bien utiles concernant les charges en sédiment dans les rivières ou les pertes en terre à la sortie de grands bassins versants. Ces modèles utilisent fréquemment des équations dans lesquelles la perte en terre est déterminée en fonction du débit, mais les modèles deviennent alors spécifiques au site. Une autre limite de ces modèles est l'impossibilité de fournir des résultats de perte en terre d'une manière spatialisée au sein du bassin versant. Ils ne peuvent donc pas traiter des questions du type : "quel est l'impact des activités agricoles sur les processus d'érosion ?" ou "comment réduire le taux d'érosion ?". Pour lever ces limites, de nombreux efforts de recherche ont été investis depuis une dizaine d'années dans le développement de modèles distribués à base physique : WEPP (Laflen et al., 1997), LISEM (De Roo et al., 1996b), EUROSEM (Morgan et al.,

1998a), KINEROS (Woolhiser et al., 1990), SHETRAN (Ewen et al., 2000), PERFECT (Littleboy et al., 1992), ANSWERS (Beasley et al., 1980), GUEST (Yu et al., 1997), CREAMS (Knisel, 1980b), TOPOG (Haskins and Davey, 1991). Pourtant, les résultats des tests d'évaluation menés jusqu'à présent sur ce type de modèle ne sont pas très encourageants, comme le montrent les conclusions publiées à la suite des ateliers organisés par le réseau érosion du programme GCTE (Global Change and Terrestrial Ecosystem) (Boardman and Favis-Mortlock, 1998; Favis-Mortlock, 1998; Folly et al., 1999; Jetten et al., 2003, 1999; Nearing and Nicks, 1998; Takken et al., 1999).

Selon Boardman (2006), nous ne devrions pas être déçus par les résultats peu satisfaisants des modèles d'érosion car les modèles sont toujours en développement. En particulier, les manques peuvent indiquer les points à réviser pour de futures améliorations. Tous les efforts investis dans le perfectionnement des modèles à base physique ont permis de générer des pistes de recherches et d'améliorer nos connaissances des mécanismes des processus d'érosion. Cependant, comme le soulignent Parsons et al. (1997), Boardman (1998) et Bryan (2000), il est possible que tous les processus et interactions impliqués dans l'érosion des sols ne soient jamais complètement modélisés physiquement.

La modélisation distribuée à base physique de l'érosion permet cependant de fournir une estimation spatiale des "sources" et des "puits" de sédiment sur un bassin versant. Les modèles d'érosion hydrique sont généralement couplés à des modèles de ruissellement : les processus d'érosion sont alors calculés après les variables hydrologiques, qui peuvent donc être considérées comme des entrées du modèle d'érosion. Ceci explique la forte dépendance des modèles d'érosion par rapport aux paramètres hydrologiques, démontrée par de nombreux tests de sensibilité (De Roo et al., 1996a; Nearing et al., 1990; Veihe and Quinton, 2000).

Les modèles d'érosion distribués à base physique peuvent être classés dans deux groupes selon leur type de discrétisation spatiale. D'un coté les modèles qui s'appuient sur un découpage du bassin versant composé d'unités hydrologiques surfaciques sur les versants et de tronçons linéaires pour le réseau de drainage (Morgan et al., 1998b; Nearing et al., 1989; Smith et al., 1995), modèles que nous pouvons appeler "modèles basés sur des vecteurs" (point, ligne et polygone). D'un autre coté il existe les modèles "raster" qui sont basés sur un maillage régulier de l'espace, maillage pouvant provenir par exemple du modèle numérique du terrain. Ces modèles ont la particularité d'être

bi-dimensionnels (De Roo et al., 1996b; Ewen et al., 2000). Chacune des deux approches possède des avantages et des inconvénients en ce qui concerne la description des processus érosifs, leur paramétrisation et le résultat obtenu en sortie (Merritt et al., 2003). Le choix entre les deux types de modèles doit se faire en fonction des objectifs généraux de la modélisation, en particulier des données disponibles et du type de processus érosif à modéliser (Morgan, 2005). En effet, il existe un lien étroit entre le mode de discrétisation spatiale et la description des différents processus érosifs (par exemple la distinction entre les processus d'érosion diffuse et concentrée).

D'une manière générale, les efforts de modélisation réalisés ces dernières années ont permis d'améliorer la connaissance des processus érosifs. Selon Boardman (2006), seuls le développement et l'utilisation des modèles donnent la possibilité de quantifier les taux d'érosion et d'estimer le risque d'érosion dans des secteurs où nous n'avons pas de mesure d'érosion.

1.2 Objectifs

L'objectif général de ce travail a été de faire progresser la modélisation distribuée de l'érosion hydrique à travers d'une réflexion et d'une analyse critique des modèles existants. Différents angles d'attaque ont été retenus : conceptuel, exploration de modèle et paramétrisation. Un des fruits de cette réflexion a été l'élaboration d'une modélisation de l'érosion hydrique distribuée et à base physique applicable aux échelles du bassin versant et de l'événement pluvieux. Cette modélisation, basée sur une paramétrisation distribuée facilitée par le recours aux systèmes d'information géographique (SIG), tente de lever certaines limites des modèles existants. Un autre résultat de ce travail a été le développement d'un cadre général ("framework") pour l'analyse exploratoire de modèles distribués à différentes échelles d'espace et de temps.

L'objectif opérationnel de la modélisation proposée est de prendre en compte les aménagements de l'homme afin de pouvoir analyser l'impact des ces aménagements sur le déplacement des particules de terre, la localisation des "sources" et des "puits" des sédiments, et *in fine* de prévoir les taux d'érosion en tout point du bassin versant. Ce modèle devrait en particulier être capable de simuler l'influence d'aménagements anthropiques, comme les dispositifs anti-érosifs, sur la connectivité sédimentologique, dans le contexte de petits bassins versants agricoles. Nous avons choisi de développer ce

modèle sur la base de la segmentation spatiale et des processus du modèle hydrologique MHYDAS qui a été développé et validé sur des petits bassins versants agricoles.

1.3 Plan de la thèse

La partie **I** de la thèse est consacrée à une analyse bibliographique portant sur les concepts et les points de blocage généralement rencontrés dans les modèles d'érosion existants. Les chapitres 1 et 2 présentent deux aspects de cette analyse bibliographique sous forme de deux articles.

Le premier, publié dans *CATENA*, présente une synthèse sur la manière dont les modèles décrivent l'érodibilité diffuse ("interrill erodibility"), principal paramètre utilisé pour décrire le processus d'érosion diffuse. La question est examinée en particulier sous l'angle de la sensibilité des modèles d'érosion à ce paramètre. Le deuxième article, en cours de révision pour *Earth Surface Processes and Landforms*, fait le point sur la façon dont les modèles existants gèrent la connectivité sédimentologique. La réflexion vise également à définir des pistes d'amélioration pour cette gestion de la connectivité sédimentologique dans le cadre de modèles d'érosion destinés à des bassins versants agricoles.

La partie **II** de la thèse est focalisée sur le développement d'un nouveau modèle d'érosion hydrique distribué et à base physique: MHYDAS-Erosion. Le chapitre 3 présente un bref rappel sur le modèle hydrologique MHYDAS ayant servi de base pour le développement du modèle d'érosion. Le chapitre 4 décrit ensuite le modèle d'érosion sous la forme d'un article soumis à *Journal of Soil and Sediments*.

La partie **III** de ce travail est dédiée à l'analyse de sensibilité, la calibration et la validation du modèle développé. Le chapitre 5 présente la méthodologie utilisée pour l'analyse de sensibilité et l'exploration des modèles d'érosion. Ce chapitre est composé d'un article en révision pour *Water Resources Research*. Le chapitre 6 présente l'application de la procédure d'analyse de sensibilité proposé dans le chapitre 5 à quatre modèles d'érosion différents, incluant MHYDAS-Erosion. Ce chapitre est également proposé sous la forme d'un article en préparation pour *Water Resources Research* . Le chapitre 7, correspond à un article en préparation sur l'analyse de la sensibilité de MHYDAS-Erosion à la distribution spatiale des bandes enherbées affectant la connectivité sédimentologique. Le chapitre 8 présente une procédure de calibration et de

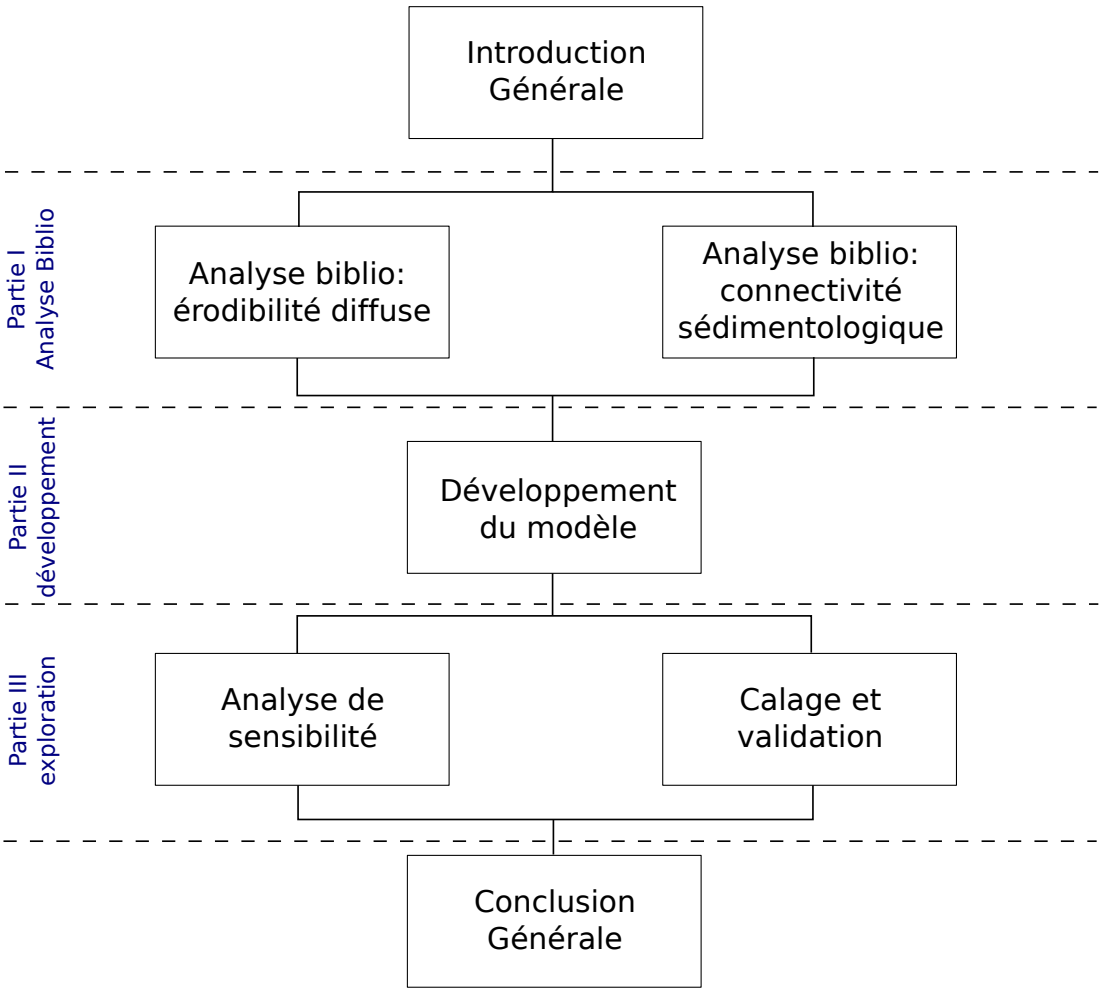

Figure 1.1: Schema synoptique du mémoire de thèse

validation multi-échelles de MHYDAS-Erosion sur le bassin versant expérimental de Roujan (France). Ce chapitre, rédigé sous la forme d'un article en préparation, est une synthèse d'un stage de Master 2 recherche que j'ai co-encadré. La figure 1.1 présente une vue synoptique de ce mémoire de thèse.

Part I

Analyse bibliographique sur certains concepts pour la modélisation de l'érosion

Introduction

Les tests d'évaluation des modèles ont souvent montré des résultats peu satisfaisants par rapport aux mesures de perte en sol (Boardman and Favis-Mortlock, 1998; Evans and Brazier, 2005; Favis-Mortlock, 1998; Folly et al., 1999; Jetten et al., 2003, 1999; Nearing and Nicks, 1998; Takken et al., 1999). Nombreuses sont les raisons de cette performance limitée, nous en énumérons ici certaines :

- La plupart des modèles d'érosion supposent que le ruissellement est généré seulement par le processus hortonien (Evans and Brazier, 2005), tandis que dans la réalité une grande part de l'écoulement superficiel peut provenir des pluies de faible intensité sur sol saturé ;
- Les modèles événementiels sont notamment sensibles aux conditions initiales, en général très difficiles à déterminer (Boardman, 2006);
- Les paramètres d'entrée des modèles ont une variabilité spatiale et temporelle qui vient s'ajouter à l'incertitude intrinsèque de leur mesure (Jetten et al., 2003);
- Le fonctionnement du bassin versant peut être différent selon l'intensité des événements hydrologiques (Jetten et al., 2003). Des barrières topologiques, existant dans le bassin versant pour les événements faibles ou moyens, peuvent complètement s'effacer au cours des forts événements, rendant ainsi obsolète la topologie initiale fixée dans le modèle;
- Certains facteurs du modèle sont considérés comme constants pendant la durée de l'événement, alors qu'ils ont un comportement dynamique.

Il y a eu beaucoup d'études sur la diminution des paramètres d'infiltrabilité du sol et de la rugosité superficielle sous l'influence des précipitations (Boiffin and Monnier,

1986; Torri et al., 1987). Ces études n'ont pas toujours été incorporées dans les modèles, de plus il s'agit souvent des expériences faites en conditions de laboratoire. Or *in situ*, les changements de la structure du sol peuvent être beaucoup plus rapides et plus prononcés. Par conséquent, l'anomalie entre le comportement des modèles et le comportement réel pourrait augmenter d'autant plus qu'il s'agit de forts événements pluviométriques.

Nearing (1998), soutient un autre point de vue sur la faible performance des modèles d'érosion, qui serait liée à une variabilité inévitable de la mesure de perte en terre. Wendt et al. (1986), cité par Nearing (1998) ont fait une étude sur la variabilité des valeurs d'érosion mesurées avec 40 répétitions sur des parcelles en sol nu dans des condition de ruissellement naturel: les coefficients de variation obtenus vont de 18 à 83 %. Dans cette étude, Wendt et al. (1986) n'ont pas trouvé de relation statistique entre les valeurs d'érosion et les caractéristiques des parcelles. Comme Nearing (1998, 2000); Nearing et al. (1999), qui défendent l'idée qu'une partie de la différence entre les valeurs mesurées et les valeurs simulées provient de la variabilité des mesures, propose une évaluation des modèles qui prenne en compte cette variabilité. La difficulté devient alors de caractériser cette variabilité des mesures, ce qui nécessite de multiplier ces mesures.

Selon Jetten et al. (2003), parmi toutes les raisons mentionnées ci-dessus, les principales explications des faibles performances des modèles d'érosion sont la variabilité spatiale et temporelle ainsi que l'incertitude sur les paramètres d'entrée du modèle. Ces imperfections affectent plus les modèles complexes à base physique que les modèles empiriques plus simples. Les modèles complexes comportant une meilleure description des processus érosifs devraient en principe, être capables de faire de meilleures prévisions en ce qui concerne la perte de sol d'un bassin versant donné. Mais ces modèles complexes ont généralement besoin d'un grand nombre de paramètres d'entrée, affectés d'une incertitude mal connue. Cette incertitude peut se propager et être parfois amplifiée par les processus itératifs utilisés pour les résolutions numériques des équations différentielles, ce qui détériore le résultat final.

La deuxième raison citée par Jetten et al. (2003) est le changement de comportement des bassins versants par rapport à l'intensité de l'événement pluviométrique. Cette problématique concerne la connectivité hydrologique et sédimentologique entre les objets qui composent le paysage. Par exemple, le degré de connexion entre les parcelles

agricoles et les canaux de drainage dépend du type d'interface entre les deux objets et de son action sur le flux de matière. Une bande enherbée qui se trouve entre une parcelle agricole et un canal de drainage agit comme un filtre qui retient tout ou partie des sédiments jusqu'à un débit donné, mais au-delà de ce débit la bande enherbée n'a plus d'effet significatif sur la charge en sédiments.

Dans le cadre de cette thèse il n'était pas envisageable de traiter simultanément toutes les limites indiquées. Nous avons choisi d'approfondir deux de ces questions : la première concerne le paramètre d'entrée relatif à l'érodibilité interrill et la seconde traite de la variabilité, au cours de la crue, du comportement des éléments d'interface du paysage en fonction des conditions hydrologiques. Les deux chapitres suivants présentent des analyses bibliographiques concernant ces deux questions.

Chapter 1

Soil Resistance to Interrill Erosion: Model Parameterization and Sensitivity

Même si l'érosion diffuse est généralement moins visible que l'érosion linéaire ou l'érosion ravinaire, elle peut causer d'important dégâts, notamment en ce qui concerne le dépôt de sédiments à l'aval des parcelles cultivées. L'érosion diffuse est souvent associée au ruissellement produit à la suite de la formation de croûte de surface et à des propriétés du sol comme la détachabilité ou la stabilité structural du sol. L'érodibilité d'un sol traduit la résistance inhérente au détachement des particules et à leur transport. À partir d'une synthèse bibliographique sur l'érodibilité diffuse du sol et ses différentes méthodes de détermination, nous avons identifié trois principaux types de méthodes : les méthodes basées sur la mesure de la stabilité structurale des agrégats ("aggregate stability"), les méthodes basées sur la mesure du splash ("splash cups") et les méthodes basées sur des placettes d'érosion ("mini-plots"). Les résultats de l'analyse bibliographique nous ont permis d'identifier les avantages et inconvénients liés à chaque méthode en vue de paramétrer les modèles d'érosion. Ce chapitre montre également la sensibilité des modèles d'érosion au paramètre d'érodibilité diffuse.

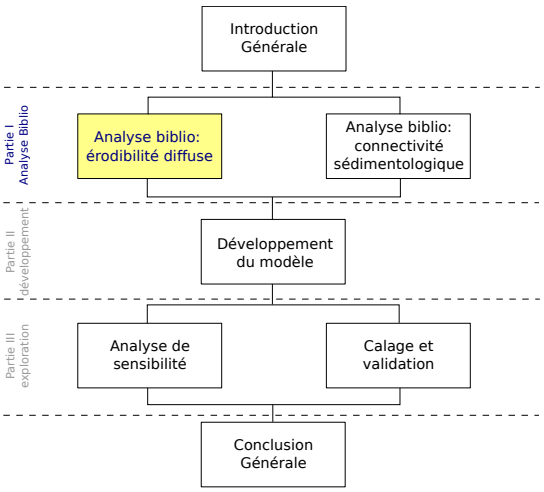

Soil Resistance to Interrill Erosion: Model Parameterization and Sensitivity[1]

Gumiere, S. J.; Le Bissonnais, Y. & Raclot, D. (published article in CATENA)

Abstract

Interrill erosion, which is less visible in the landscape than rill and gully erosion, may cause major sediment deposits in the lower part of cultivated fields. It is often associated with runoff resulting from sealing and crusting, and soil properties such as soil detachability or soil aggregate stability have been used to express soil resistance to interrill erosion processes, i.e., interrill erodibility. From a literature review including more than fifteen erosion models, we have identified three main methods used to measure these properties: aggregate stability and splash cup detachability, methods performed in the laboratory using only a few grams of soil, and standard plot methods that are based on field plot measurements. This difference makes the parameters involved in assessing interrill erodibility dependent upon the scale and the hydrological processes involved and difficult to compare. According to the literature, the sensitivity of actual erosion models to interrill erodibility is lower than the sensitivity to hydrological properties and rill erodibility parameters. This numerical study shows that erodibility measurements from the three major assessment methods give different results regarding the contribution of interrill erosion and show that the sensitivity of erosion modeling to interrill erodibility may in fact be greater than shown in the literature on global sensitivity analysis.

1.1 Introduction

The development of erosion models such as physically based, stochastic or empirical models involves simplifying reality in order to establish a balance between process representation and computational complexity. The universal soil loss equation (USLE) developed by Wischmeier and Smith (1978) has been the most widely used model of soil erosion at the field scale. However, this model was developed for long-term simulations, and its input parameters are annual averages. The USLE model concept lacks the ability to describe the spatial variability of soil erosion within a watershed for a single rain

[1]Gumiere, S. J.; Le Bissonnais, Y. & Raclot, D. Soil resistance to interrill erosion: Model parameterization and sensitivity, Catena, 2009, 77, 274-284

event. This is part of the reason why there has been a shift from empirical modeling to process-based dynamic modeling. As a result, a number of process-oriented dynamic models of soil erosion have been developed. Examples of such models are listed in Table 1.1. Estimates of spatial and temporal soil loss variabilities in these models are determined as a function of factors including soil resistance to rill and interrill erosion (Bryan, 2000; Knapen et al., 2007), slope characteristics (Kinnell, 1993; Watson and Laflen, 1986), vegetation and land use, rainfall erosivity (Rosewell, 1986; Salles and Poesen, 2000), and hydraulic factors (Kinnell, 2005). A conceptual framework showing the different processes involved with regard to rainfall and runoff characteristics has been proposed by Kinnell (2005).

The process of soil resistance to erosion is called erodibility. This complex concept is supposed to represent the combined effects of the various sub-processes that determine soil behavior in response to erosive agents (Bryan, 2000; Sheridan et al., 2000). All of the models cited in Table 1.1 use one or more parameter(s) to describe soil erodibility in order to account for the fact that some soils are intrinsically less resistant to erosive agents than others (Bryan, 1976).

The first approach was made for USLE development (Wischmeier and Smith, 1978), where the erodibility factor is called K. This empirical variable in the USLE is used for the characterization of both rill and interrill erosion processes, and it is determined by measurements of soil loss over a standard plot with 22 m in length and with a 9% slope (Foster et al., 1980; Knisel, 1980a). This simplification of erosion processes was later criticized by Laflen et al. (1991) and Zhu et al. (1995), who argued that it is not possible to describe two distinct processes with only one parameter.

More recent process-based models make an explicit distinction between rill and interrill erosion processes (De Roo et al., 1996b; Morgan et al., 1998a; Woolhiser et al., 1990). Parameters describing soil cohesion or critical shear strength are often used to express soil resistance to the rill erosion process (Knapen et al., 2007). For interrill areas, parameters like aggregate stability (De Roo et al., 1996b) or index of detachability (Morgan, 2001) are generally used.

Knapen et al. (2007) conducted an extensive literature review dedicated to soil resistance to concentrated flow. Knapen et al. (2007) analyzed the literature's data on the resistance of topsoils to concentrated flow erosion in terms of channel erodibility (k_c) and critical shear stress (τ_c) and then compared that data with other soil properties. However, there are few if any works in the literature that specifically review interrill erodibility and methods for its assessment. Thus, the resistance of soil to interrill erosion is still a grey area, and important research issues remain (Bryan, 2000). To understand

and to model interrill erosion appropriately, clear insight into the soil's resistance to this process and interrill erosion controlling parameters are of vital importance.

The literature indicates that the soil interrill erodibility is influenced by many soil properties, such as soil texture and organic matter content and quality (Wischmeier and Smith, 1978), water content (Bryan, 2000), and surface soil conditions like surface crusting (Darboux and Le Bissonnais, 2007; Le Bissonnais et al., 2005). Soil erodibility is also affected by cropping systems. Rachman et al. (2003) show that together with other soil properties, such as aggregate stability or shear stress, soil detachability is the most sensitive parameter for cropping systems. These authors suggest that measurements of soil properties related to erodibility, like splash detachment, aggregate stability and shear stress, might provide information to help orient and manage the application of different cropping systems.

Soil interrill erodibility for a large variety of soil types and surface conditions has been determined experimentally in the field and in the laboratory. Nevertheless different experimental procedures were used, and so far no attempt has been made to compare all of these results.

This paper presents a dataset of soil interrill erodibility values from the three major assessment methods, all of which are identified in the literature. The first method is the standard erosion plot using natural or simulated rain, the second is the splash cup method, and the third is the aggregate stability test. The main objectives of the study are (1) to present a state of the art parameterization of soil resistance to interrill erosion and a discussion of the soil interrill erodibility values for 12 typical soil textures based on different assessment methods; (2) to assess models' sensitivities to the erodibility parameter and discuss the application of the interrill erodibility factor in physically-based erosion models; and (3) to test the influence of the interrill erodibility parameter on the contribution of interrill erosion as calculated by models of the three assessment methods.

1.2 Interrill erodibility parameter in soil erosion models

Three different determination methods of interrill soil erodibility have been identified based on a literature review of erosion models: (i) standard erosion plots and derivation, (ii) splash cups, and (iii) aggregate stability tests. Table 1.1 shows the analyzed models and the erodibility assessment method.

Table 1.1: Erodibility assessment methods for erosion models

Model	Interrill and Rill	Erodibility Assessment	Reference
EUROSEM	yes	Splash Cups	Morgan et al. (1998a)
KINEROS	yes	Splash Cups	Woolhiser et al. (1990)
PSEM-2D	yes	Splash Cups	Nord (2005)
USLE	no	Stand. Plots	Wischmeier and Smith (1978)
CREAMS	no	Stand. Plots	Foster et al. (1980)
AGNPS	no	Stand.Plots	Young et al. (1987)
SWAT	no	Stand. Plots	Arnold and Williams (1995)
RUSLE	no	Stand. Plots	Renard et al. (1991)
WEPP	yes	Mini-Plots	Ascough et al. (1997)
USLE-M	no	Stand. Plots	Kinnell and Risse (1998)
USPED	no	Stand. Plots	Mitas and Mitasova (1998)
USLE-2D	no	Stand.Plots	Van Oost et al. (2000)
RUSLE 2	no	Stand. Plots	Desmet and Govers (1996)
LISEM	yes	Aggregate Stab.	De Roo et al. (1996b)

Below, we analyze the characteristics and consequences of these methods for interrill erodibility parameter assessment.

1.2.1 Standard erosion plots and derivations

In models based on or derived from the USLE (Universal Soil Loss Equation), a single erodibility value combining interrill and rill processes is inferred from the soil loss measured at the end of a standard erosion plot that is 22 m long and has a 9% gradient. In these standard conditions, other factors of the USLE (L, S, C and P) are considered unitary, and the factor K is defined as the slope coefficient between soil loss and R (the rainfall erosivity index). In practical terms for the USLE and the RUSLE (Revised Universal Soil Loss Equation), soil erodibility is the average long-term soil and

soil-profile response to the erosive power of rainfall. This means that the soil erodibility factor for the USLE is a lumped parameter that represents an integrated average annual value of the total soil profile reaction to a large number of hydraulic and erosive processes. These processes include rainwater infiltration into the soil profile, raindrop detachment with transport by raindrop splash (RD-ST), raindrop detachment with transport by raindrop-induced flow transport (RD-RIFT), raindrop detachment with transport by flow (RD-FT), flow detachment with transport by flow (FD-FT) (Kinnell, 2005), and localized deposition due to topography and tillage-induced roughness (Wischmeier, 1976). Normally, the measurements of soil loss and R are annual means as mentioned above, and their application to single event models is not necessarily relevant. Actual references for K come from a series of experiments over periods of 20 years in the eastern United States. Such experiments are expensive, and therefore few of them were conducted in other areas of the world. Rainfall simulations make it possible to perform many more experiments concerning soil erodibility determination. These experiments facilitate the establishment and measurement of empirical relationships between soil erodibility and other primary soil properties. From a statistical analysis of all these standard plot results, Wischmeier et al. (1971) proposed a nomograph where the erodibility factor is first a function of soil characteristics, such as texture and organic matter content, and second one of soil properties, like structure and permeability. The algebraic function of the nomograph is shown in eq.(1.1).

$$K = \frac{k_t \cdot K_o + k_s + k_p}{100} \tag{1.1}$$

where K is the soil erodibility factor; kt [1] is the texture sub factor; ko is the organic matter sub factor; ks is the soil structure sub factor and kp is the soil profile permeability sub factor. The nomographs relationship is derived from rainfall simulation data from 55 Midwestern soils of medium texture (Wischmeier et al., 1971). Because these soils only represent the medium-textured soils, the nomograph is well suited for a limited range of soil types. Correctional factors have been developed to facilitate estimates of erodibility from nomographs to other soil types. Figure 1.1 presents the range of erodibility values calculated with the nomograph for typical soils textures and for three values of the soils' organic matter content (0.5%, 2% and 4%) (Stewart et al., 1975).

The erodibility values range from [0.07- 1.0 $ton \cdot ha^{-1}$], with higher values for loam and sandy-loam and lower values for sand. In unit plot measurements, clay soils have medium soil erodibility, because they have good resistance to detachment by flow. However, sandy soils have the lowest soil erodibility values as shown in Figure 1.1.

[1] ici kt est utilisé en dehors du significat proposé dans la nomenclature

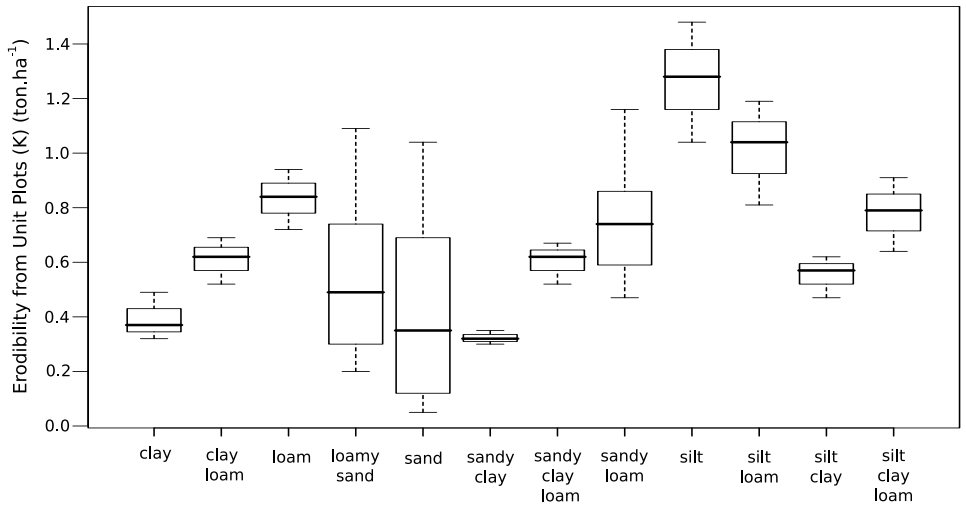

Figure 1.1: Soil Erodibility for USLE/RUSLE from (Stewart et al., 1975)

In fact, soils produce less sediment because of reduced runoff that results from high infiltrability; soil particles could be detached and splashed easily. However, sandy soils also have low transportability, and little runoff is available to detach and transport soil particles. The transport limitation of coarse-size particles has been observed by (Parsons et al., 1991) on a 35x18 m^2 plot. However, when runoff comes from upslope, sand may be very prone to erosion (Toy et al., 2002). Erodibility from standard plots as USLE was designed to allow prediction of soil erosion and recommendations for applying conservations practices.

Among the models based on standard erosion plots and their derivations, the WEPP (Water Erosion Prediction Project) is based on a particular concept of soil erodibility. It uses two erodibility parameters: one related to rill processes and another one related to interrill processes. The interrill erodibility parameter is determined using a mini-plot (0.6x1.2 m) without vegetation that is submitted to rainfall simulation. Like the erodibility from standard erosion plots, the measurement is made over the erosion rate and converted to erodibility. The WEPP interrill soil erodibility parameter is calculated

with:

$$Ki = \frac{D_i}{I^2 \cdot S_f} \tag{1.2}$$

where, D_i is the delivery of sediment from plot ($kg.m^{-2}.s^{-1}$), Ki is interrill erodibility ($kg.m^{-4}.s$), I is the effective rainfall intensity ($m.s^{-1}$), and Sf is a slope adjustment factor given by $S_f = 1.05 - 0.85e^{-4sin(\alpha)}$ where α is the slope of the surface toward a nearby rill.

As with erodibility from standard erosion plots, the WEPP model has developed an indirect way to determine soil interrill erodibility as a function of primary soil properties. For croplands, the erodibility values are based on experiments conducted in 1987 and 1989 by Elliott et al. (1989). Two different empirical equations of interrill soil erodibility were developed for croplands: one composed of soil with 30% or more sand (eq.(1.3)) and another for the soils with 30% or less sand (eq.(1.4)). The equation for the baseline (standard) erodibility is shown below.

$$K_{ib} = 2728000 + 19210000 \cdot vfs \tag{1.3}$$

$$K_{ib} = 6054000 - 5513000 \cdot clay \tag{1.4}$$

where vfs is the very fine sand (0.05 to 0.15mm) in the surface soil, and clay is the fraction of clay in surface soil.

The interrill erodibility equation for croplands uses the baseline erodibility with correction factors to account for various effects, including canopy cover, ground cover, roots, and sealing and crusting. These factors are calculated empirically and multiplied by the interrill baseline erodibility to find the adjusted interrill erodibility for croplands.

The suggested limit for the predicted values of erodibility to croplands is [0.5-12] in ($10^6.kg.m^{-4}.s$). In Figure (1.2) and Table (1.2) the range of values is [0.77-4.5 $10^6.kg.m^{-4}.s$], with the highest values for silty-loam and the lowest values for sandy-loam. Observing erodibility values from the standard erosion plot and mini-plot methods we note that the dependence of hydrological phenomena is maintained and that the capacity of soil runoff production is a very important factor.

Table 1.2: Erodibility from mini-plot assessment method values in $10^6.kg.m^{-4}.s$ for WEPP, source Elliott et al. (1989) and Laflen et al. (1991) , N is the number of samples

Soil Texture	N	Minimum	Average	Maximum
clay	3	1.70	2.13	2.50
clay loam	3	2.04	2.57	2.20
loam	9	1.45	2.24	3.17
loamy sand	2	0.77	2.45	4.12
sand	1	-	0.87	-
sandy clay	-	-	-	-
sandy clay loam	1	-	1.86	-
sandy loam	5	1.21	2.37	3.93
silt	-	-	-	-
silty loam	12	1.26	2.85	4.32
silty clay	1	-	1.85	-
silty clay loam	-	-	-	-

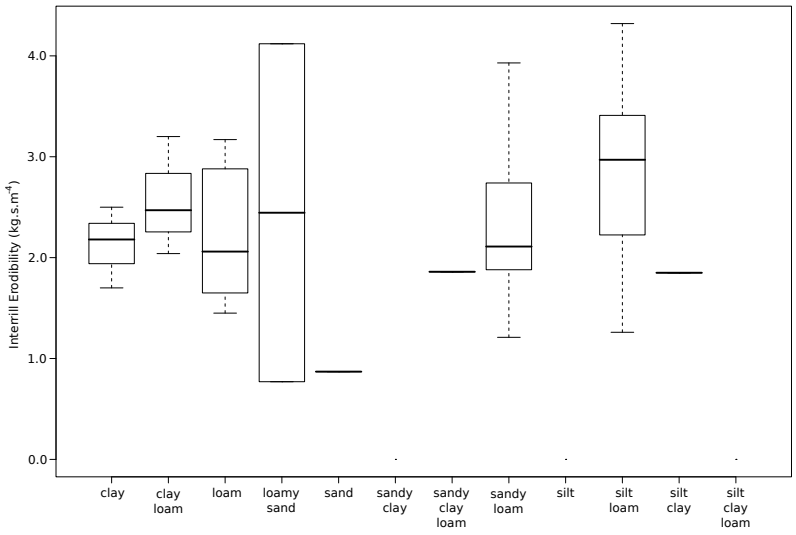

Figure 1.2: Soil Interrill Erodibility for WEPP croplands from (Elliott et al., 1989) values in $10^6.kg.m^{-4}.s$

1.2.2 Splash cups

A second method currently used for determining interrill soil erodibility is based on the measurement of soil detachability. This approach derives from the pioneer work of Ellison (1947). Several techniques have been developed to measure soil detachability using raindrops. One consists in embedding a circular cup into the topsoil in order to collect the soil particles that detach from the surrounding surface by the kinetic energy of rainfall (Bollinne, 1975; Savat and Poesen, 1981). Another procedure used to measure soil detachment with splash cups is the reverse of that previously shown: it consists in filling a cylinder with soil and measuring the mass of the sediment that detaches from this cylinder by rainfall kinetic energy (Morgan, 1978). In these two cases, raindrop detachment with transport by raindrop splash (RD-ST) is the only process involved. In addition the two type of tests generally use a little amount of soil.

Sreenivas et al. (1947) used round cups or funnels embedded in the soil to catch splashed particles. They considered the mass of the collected material divided by the surface area of the cup (with radius r in m), denoted here by m_r, as an indicator of the detachment rate on the surrounding soil. This method has been applied in subsequent studies, a number of which were reviewed by Poesen and Torri (1988). The index of detachability is determined by:

$$k = \frac{m_r}{KE} \tag{1.5}$$

where k is the detachability index ($g.J^{-1}$) , m_r is the mass of soil particles detached (g) and, KE is the total rainfall kinetic energy (J).

However, the splash rate (m_r) is dependent on the cup size, and the relationship between the cup size and splash rate is also influenced by the distribution of the distances over which the splashed particles travel. Given a particular amount of soil detached per unit of area outside the cup, more sediment will end up in the cup as the distance over which splashed particles travel increases. Poesen and Torri (1988) developed a correction factor for the splash cup diameter effect based on Savat and Poesen (1981) that had shown the mass of deposited splashed sediment decreases exponentially with the distance to the impact point. The equation developed by Poesen and Torri (1988) is shown in eq.(1.6).

$$m_{sr} = m_r \cdot e^{-0.054D} \tag{1.6}$$

where m_{sr} is the real mass of splashed soil material per unit area ($g.cm^{-2}$) and D is the splash cup diameter (cm).

Table 1.3: Erodibility from splash cups assessment method values in $g.J^{-1}$ source: Morgan (2001) and Morgan et al. (1998a), N is the number of samples

Soil Texture	N	Minimum	Average	Maximum
clay	1	-	0.05	-
clay loam	1	-	0.70	-
loam	1	-	0.80	-
loamy sand	1	-	0.30	-
sand	1	-	1.20	-
sandy clay	1	-	0.30	-
sandy clay loam	1	-	0.10	-
sandy loam	1	-	0.70	-
silt	1	-	1.00	-
silty loam	1	-	0.90	-
silty clay	1	-	0.50	-
silty clay loam	1	-	0.80	-

However, there are many geometric possibilities for the splash cups and comparing results from different geometry is very difficult. Therefore each one of the device's geometry has its own correction function. Poesen and Torri (1988) proposed to measure splash detachment in a field using a circular cup with a diameter larger than 10 cm in order to reduce the edge effect.

The analysis of splash processes and modeling was further refined by Legout et al. (2005); Van Dijk et al. (2002) and Leguédois et al. (2005) . These studies established theoretical splash distribution functions to interpret results from different experiments.

However, the literature does not provide enough references to the erodibility values of the splash cup method to establish a statistical analysis. Morgan (2001) proposed reference values for erodibility from splash cups; these values are shown in Figure 1.3 and Table 1.3 . Unfortunately these are only average values, and we have no information about their variability for either the texture classes or the number of soils tested.

The theoretical range of values for erodibility from splash cups is [0.01-10 $g.J^{-1}$] (Morgan, 2001; Morgan et al., 1998a). The real observed range of values is [0.05-1.2 $g.J^{-1}$] with a maximum value for sand and a minimum value for clay.

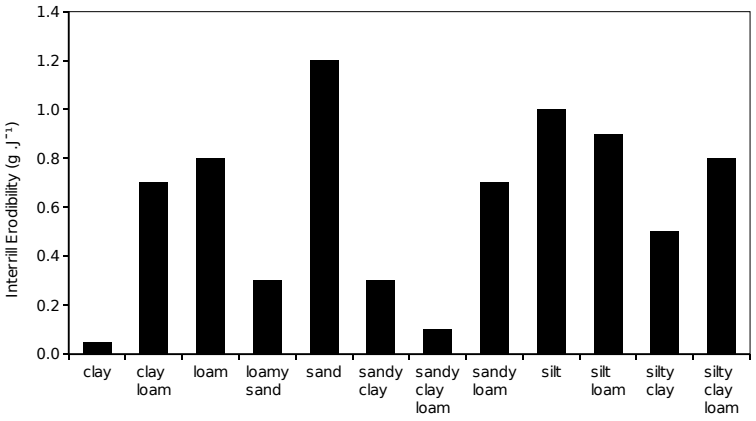

Figure 1.3: Soil Interrill Erodibility from splash cups from Morgan, 2001

1.2.3 Aggregate stability tests

A third method used for the determination of interrill soil erodibility is based on the measurement of soil aggregate stability. In the LISEM (Limburg Soil Erosion Model) (De Roo et al., 1996b), this parameter is determined with a drop test that consists in counting the number of drops necessary to reduce the mass of an aggregate by 50%. The range of value for aggregate stability is [1 to 200 or more] drops according these authors. It is important to note that the number of drops is inversely proportional to soil resistance. A complete experimental set of values for soil textures is not available in the literature; however, some papers such as (Dijk et al., 1996; Hessel et al., 2006; Liu et al., 2003) present aggregate stability values for different soil treatments and land-uses.

Hessel et al. (2006) present a set of values for clay loam soils submitted to different agricultural cultures in east Africa (coffee, banana, vegetables, wood plots, and maize). The erodibility values found by Hessel et al. (2006) for clay loam soils range from 22 to 376 drops; the lowest value is for coffee and the highest value is for wood plots.

Liu et al. (2003) present a set of values for silt soils submitted to different soil uses in the Chinese Plateau (steep slope, terrace, cropland, woodland, fallow and wasteland). The values of soil erodibility vary from 8 to 18 drops with cropland having the lowest

value and woodlands the highest. Dijk et al. (1996) present a set of values for silt soils submitted to different uses in South Limburg. The values of erodibility from this work range from 10 to 30 drops.

In addition to the drop test method, there are many other methods that can describe soil aggregate stability. Amezketa (1999) reviewed these methods. Le Bissonnais (1996) proposed a standardized method based on the most common and reproducible aspects of the classical methods of erodibility assessment. Le Bissonnais's method uses relatively large aggregates (3-5 mm), and performs various tests corresponding to different conditions of water impact on soil. These tests represent the mechanisms of aggregate breakdown in natural conditions, from intense rainstorms on dry soils to long low intensity rains on wet soils. Although the measurement of the aggregate stability of some isolated samples does not completely characterize a soil material submitted to erosive stress, it generally correlates well with the erosion measured on plots in controlled conditions or in the field (r = -0.85 from Amezketa et al. (1996) and r = -0.70; $p > 0.01$ from Barthés et al. (2000)). This has to be related to the fact that desaggregation, which is measured in the aggregate stability test, is most often the main process involved in soil erosion and particularly in interrill erosion (Bryan, 2000). However, some authors found no correlation between stability and measured erosion (Young, 1974). In some cases these results correspond to specific situations where runoff rate is high that it can transport stable micro- or macro-aggregates(Janeau et al., 2003). The intensity of the correlation between the erosion and aggregate stability also depends on the methods used for both measurements. For example, the smaller the aggregates used for stability tests, the greater the chance of erosion to affect stable aggregates and thus the chance for a contradiction between stability and erosion. It has been shown that stronger correlations between measured interrill erosion and aggregate stability were observed when using Le Bissonnais's test compared to other classical methods (Amezketa et al., 1996; Le Bissonnais et al., 2007). However, no erosion model using an aggregate stability tests like the erodibility parameter was found in the literature, although Yan et al. (2008) successfully used it as a substitute for the interrill erodibility parameter Ki that was considered irrelevant for an application of WEPP model.

Because of the absence of a sufficient data set for the drop test, only aggregate stability values from the Le Bissonnais method were plotted in figure 1.4 using data from table 1.4 . The results of the tests are plotted in 1/MWD (Mean Weight Diameter) to give the same aspect of for all of the presented erodibility graphics (high values indicate high erodibility).

The theoretical range value for 1/MWD is [0.2-40 mm^{-1}] (Le Bissonnais, 1996;

Table 1.4: Erodibility from aggregate stability assessment method, values in mm^{-1} source: Darboux et al. (2008) , N is the number of samples, MWD (Mean Weight Diameter)

Soil Texture	N	Minimum	Average	Maximum
clay	4	0.53	0.73	1.90
clay loam	11	0.50	0.67	1.41
loam	4	0.33	0.84	2.44
loamy sand	-	-	-	-
sand	-	-	-	-
sandy clay	-	-	-	-
sandy clay loam	-	-	-	-
sandy loam	9	0.74	1.19	1.82
silt	-	-	-	-
silty loam	61	0.32	1.12	2.72
silty clay	2	0.79	0.85	0.92
silty clay loam	11	0.40	0.77	1.79

Le Bissonnais and Singer, 1992). In Figure 1.4 the range value is [0.3-2.8 mm^{-1}] (Darboux et al., 2008) with a maximum value for silt-loam texture and a minimum value for loam.

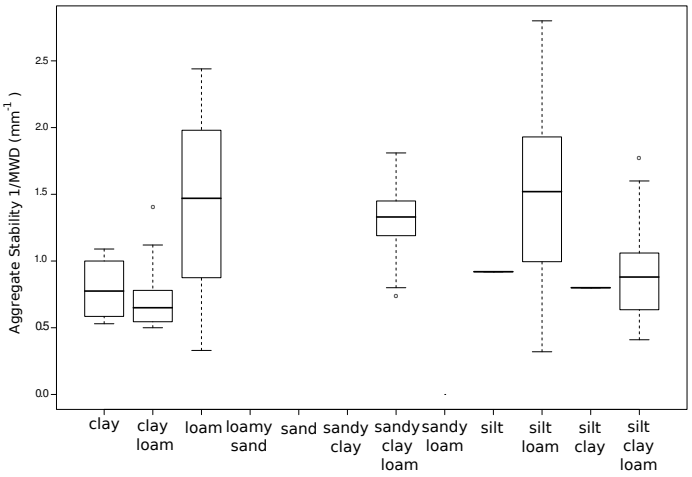

Figure 1.4: Aggregate stability for typical soil textures from Le Bissonnais method, from Darboux et al. (2008), MDW (Mean Weight Diameter)

1.2.4 Discussion on erodibility assessment methods

The three assessment methods presented are used to determine soil erodibility parameters and are different in terms of the erosion processes involved and the scale size samples. In the standard plot method, erodibility combines interrill and rill processes and depends on hydrological processes like infiltrability and runoff production capacity. For these reasons, soil with high clay and soil with high sand content has both low measured erodibility, the first because it has good aggregate stability and the second because of the intrinsic high infiltration capacity of sandy soils (Toy et al., 2002). Medium-textured soils with high silt content present high erodibility values in this method, because these soils generally produce high overland runoff due to surface crusting. This runoff provides greater energy for the detachment and transport of soil particles. Thus, runoff substantially influences the standard erosion plot method (Toy et al., 2002). Kinnell (1993) proposed a modification in the index of rainfall erosivity determination to allow the USLE/RUSLE models to calculate erosion for a single rainfall event. This modification consisted in multiplying the rainfall erosivity index by the runoff rate; consequently, this change in the erosivity index changed the soil erodibility. This modification improved erodibility assessment, because it made the erodibility

factor independent of runoff. However, it still remains the only global erodibility factor for both rill and interrill erosion, and it is impossible to separate soil loss from each process.

New erodibility parameters have been developed to predict erosion in the field more precisely. For example, WEPP uses two different erodibility parameters to account for the different processes of erosion; rill erodibility is determined from standard plots and interrill from 1.0 m^2 mini-plots where there is supposedly no rill erosion process (Elliott et al., 1989). This method accounts for the major erosional and hydrological processes that occur simultaneously during time tests at interrill areas (RD-ST, RD-RIFT and RD-FT) (Kinnell, 2005). Soils with high clay content have low erodibility values, whereas soil textures like loamy sand and silty loam have the highest erodibility values due to low cohesion between soil particles.

However, other "process-based" models such as AGNPS, SWAT or CREAMS calculate runoff and erosion separately using the K index derived from standard plots as an erodibility parameter. Therefore, there is a risk that these models give low erosion rates for high runoff conditions on sandy soils because of a low K value; whereas in reality high erosion may occur because of the detachability of sandy materials. Additionally, soil erodibility may vary in time. Soil in high moisture conditions induces an increased amount of runoff and a peak rate that produces increased erosion. Soil erodibility tends to be higher during the late winter and early spring than in late summer. The temperature during the summer months increases biological activity in the soil, which produces organic compounds that may decrease soil erodibility in these months.

Another soil property used as an interrill erodibility parameter is the index of rainfall detachability in erosion models, such as EUROSEM and PSEM-2D. This property is determined by splash cup measurements (Nord, 2005; Poesen and Torri, 1988). This method is a local method, and it depends on device geometry, as shown by Poesen and Torri (1988). The raindrop detachment with transport by raindrop splash (RD-ST), which depends primarily on aggregate stability, is the only erosion process taken into account. For this reason clay soils have the lowest erodibility value, and sand soils have the highest value. Soil aggregate stability is also used as an interrill erodibility factor. This soil property can be obtained by many methods Amezketa (1999). The aggregate stability test uses a small amount of soil aggregates: only one single aggregate in drop test (Low, 1954) and up to 10g in the wet sieving aggregates tests (Kemper and Rosenau, 1986). The only process analyzed is the aggregate breakdown. The organic matter content in soil often affects its aggregate stability Le Bissonnais (1996). This sensitivity to the organic matter content can be used to help recommend the appropriate

conservation practices.

Splash cups and aggregate stability methods do not integrate detached particle transportation. However, aggregate stability provides information about particles' size distribution and, therefore, about the transportability of the sediment (Legout et al., 2005).

Two inconveniences of local methods, like splash cups or aggregate stability tests, are that they cannot account for temporal evolution in soil structure or for changing from non-coherent to coherent soil (Bryan, 2000). With regard to non-coherent soils, soil's erosion resistance by flow (Knapen et al., 2007) or detachability (Savat and Poesen, 1981) is determined by the particles' size and mass. However, when the coherence of soil increases, individual particle's properties lose importance in the erosion process. In practice a few properties, particularly soil aggregation, consistency and shear strength, usually dominate erosion processes, and other properties are only indirectly effective (Bryan, 2000). These other properties may act simultaneously, influencing water movement into and over the soil, influencing soil resistance to entrainment and changing erosion processes. Thus, the most important aspect for an ideal erodibility parameter is to express soil loss response to a rainfall event, whatever the context and erosion factors. It should also reflect a parameter that is stable and directly related to soil loss.

A direct comparison of interrill values based on the three major assessment methods is not possible because these methods differ in terms of scale, physical concept and units of measure. However, the interrill erodibility assessment has an impact on erosion modeling sensitivity. We have observed this impact, first by looking at the erosion model sensitivity analysis in literature (part 3) and second, by numerically simulating interrill detachment calculated using various interrill erodibility assessment parameters in order to compare how they affect the results of detachment for different typical textural classes.

1.3 Models of sensitivity to interrill erodibility

Sensitivity analysis can be used for different purposes, such as for understanding model behavior in response to changes in parameter values, for helping identify model parameter optimization in the calibration process, for guiding model parameterization or for model validation (Ferreira et al., 1995; Walsh et al., 1994). There are many techniques for sensitivity analysis, including linear regression or correlation analysis, measures of sensitivity indices, Monte-Carlo method, etc (Helton, 1993; Saltelli et al.,

2000). The choice of method depends on the model type and the objective of the analyses. Several of them were used to measure erosion model sensitivity. Veihe and Quinton (2000) analyzed the sensitivity of EUROSEM, which uses splash cup measurements as soil interrill erodibility parameter. They applied there sensitivity analysis with a fixed rainfall intensity of 50 $mm.h^{-1}$. They applied the Monte Carlo method to test soil properties, such as the saturated hydraulic conductivity, the maximum volume moisture content, the initial volume moisture content, the effective net capillarity drive, the soil porosity, soil cohesion, median particle size and the detachability index of soil. Veihe and Quinton (2000) found that the EUROSEM output model is more sensitive to hydrological parameters like saturated hydraulic conductivity and net capillarity than to erosion parameter. The total soil loss output is 5 times less sensitive to the interrill erodibility parameter called the detachability index of soil in EUROSEM ($p < 0.1$) level of statistical significance) than to saturated hydraulic conductivity, and 1.3 times less sensitive than to the net capillarity ($p < 0.1$ level of statistical significance). Peak sediment discharge is 2 times less sensitive to the soil interrill erodibility ($p < 0.1$ level of statistical significance) than to saturated hydraulic conductivity. Veihe and Quinton (2000) concluded that the soil interrill erodibility represented in EUROSEM by index of detachability is a low to moderately sensitive parameter.

Nearing et al. (1990) analyzed the sensitivity of the WEPP model. The variables they tested were soil textures (clay content and sand content), topology parameters (slope length, slope gradient and rill spacing), hydrological variables (runoff, rainfall intensity and initial soil moisture), vegetation parameters (canopy cover, canopy height and incorporated residue), and soil properties (rill erodibility, interrill erodibility and critical shear stress). Nearing et al. (1990) found that soil detachment and sediment delivery output were more sensitive to saturated hydraulic conductivity and to rill erodibility parameter than to interrill soil erodibility and initial soil moisture. Soil detachment and sediment delivery was 6 times less sensitive to interrill erodibility than to rill erodibility for 50 $mm.h^{-1}$ and 3 times less sensitive to interrill erodibility than to rill erodibility for 100 $mm.h^{-1}$ rainfall intensity. This can be explained because the rill detachment rate is a function not only of rill erodibility, but also of the amount of sediment in the flow. Thus, when interrill contribution is high, the rill contribution is reduced; it is a compensating process, and this may explain the low sensitivity to interrill erodibility parameter. Soil interrill erosion is also a function of rainfall intensity, because the interrill contribution to the sediment load increases in proportion to the square of rainfall intensity. This is the reason for the double sensitive value for 100 $mm.h^{-1}$ rainfall intensity. Nearing et al. (1990) found that saturated hydraulic conduc-

tivity and soil interrill erodibility fall into the moderately sensitive range parameters. However, Nearing et al. (1990) also suggested that the influence of these factors on prediction depends on specific conditions, because the soil interrill erodibility might be considerable on short and low slope gradients.

De Roo et al. (1996b) analyzed the sensitivity of the LISEM (LImburg Soil Erosion Model). They have analyzed the hydraulic conductivity, slope gradient, initial soil moisture, Manning coefficient, leaf area index, soil cohesion and random roughness. Their analysis showed that the sediment discharge output was more sensitive to hydraulic conductivity than to the other tested parameters. However, the sensitivity to interrill erodibility represented in LISEM by the aggregate stability was not shown in this analysis.

Nord (2005) completed the PSEM-2D (Plot Soil Erosion Model 2D) sensitivity analysis using the linear method. The variables tested were median particle diameter, initial loose soil depth, rill soil erodibility, interrill soil erodibility, soil critical shear stress and the Darcy-Weisbach friction factor. The slope used in the analysis was 9% and rainfall intensity was 50 $mm.h^{-1}$. Nord (2005) found that the dominant erosion process in these conditions was rill erosion and that erosion was more sensitive to soil critical shear stress, rill erodibility, and the Darcy-Weisbach friction factor than to the others tested parameters. A decrease of 33% in soil critical shear stress led to an increase of 100% in soil loss. An increase of 100% in rill erodibility led to an increase in soil loss of 75% and an increase of 500% in interrill erodibility led to an increase of 40% in soil loss. Nord (2005) concluded that in their model, soil loss was poorly sensitive to soil interrill erodibility parameter.

The sensitivity analyses realized by the authors cited above show a low sensitivity of actual erosion models to interrill soil erodibility parameters and that models are globally more sensitive to hydrological parameters. However, the sensitivity analysis of erosion models as presented above may be overlapped by the test configuration that often uses conditions potentially more favorable to rill erosion than to interrill erosion in terms of rain intensity (100 $mm.h^{-1}$ for the Nearing et al. (1990) and 50 $mm.h^{-1}$ for the Nord (2005) and Veihe and Quinton (2000)), or slope (9%).

1.4 Numerical comparison of three major interrill erodibility assessment methods

We compared the three erodibility assessment methods using a numerical test that calculates the theoretical interrill contribution to total erosion using values of interrill

erodibility. The theoretical soil interrill detachment by rainfall was calculated over a virtual plot with 1.0 m^2 using three rainfall intensities (30, 60 and 90 $mm.h^{-1}$) during one hour. There was a particular equation for interrill detachment by rainfall related to each assessment method (Table 1.5).

Table 1.5: Interrill erosion equations for three assessment methods

Model and Method	Original Interrill Equation	Simplified Equation
WEPP (mini-plots)	$D_i = k_i \cdot I^2 \cdot Sf$	$D_i = k_i \cdot I^2$
EUROSEM (splash cups)	$D_i = k \cdot KE \cdot e^{-2h}$	$D_i = k \cdot KE$
LISEM (aggregate stab.)	$D_i = \left(\frac{2.82}{AG} \cdot KE \cdot e^{-1.48h} + 1.61\right) \cdot I$	$D_i = \left(\frac{0.29}{MWD} \cdot KE + 1.61\right) \cdot I$

where is the interrill detachment by rainfall $g \cdot s^{-1}$, I is the rainfall intensity in ($mm \cdot h^{-1}$), KE is the kinetic energy of rain ($J.m^{-2}$) calculated by $KE = 11.9 + 8.7log(I)$, ki is the erodibility from the mini-plots, k is the erodibility from splash cups and MWD is the erodibility from the aggregate stability test.

Three interrill detachment equations have been extracted from the existing erosion models as examples of interrill erodibility assessment methods. Thus, we selected erosion equations from WEPP, EUROSEM and LISEM to represent the mini-plot, splash cup and aggregate stability assessment methods, respectively. For this numerical test we have used the simplified/transformed equations, and we consider the slope adjustment factor (Sf) of the WEPP equation equal to 1 to express only the interrill detachment (Table 1.5). Likewise we did not consider the influence of water height (h) on the interrill in EUROSEM and LISEM equations, and the terms in these equations were instead considered equal to 1 (Table 1.5). Finally the LISEM equation was transformed to use MWD values instead of drop test values.

The results quantify the importance of the variability of interrill detachment by rainfall for a given texture class, when the available data-set reveals this variability, as it is the case for the mini-plots and aggregate stability test (Figure 1.5). This variability may be larger than the inter-textural variability, which may be explained by the influence of other soil properties, such as the organic matter content or the cation content that affects soil erodibility.

The relative ranking of the various textural classes' average erosion may be completely different from one assessment method to another. For example, the detachment rate for sandy soil is maximal for splash cup and aggregate stability tests, whereas it is minimal for the mini-plots. Conversely, the detachment rate is minimal for the

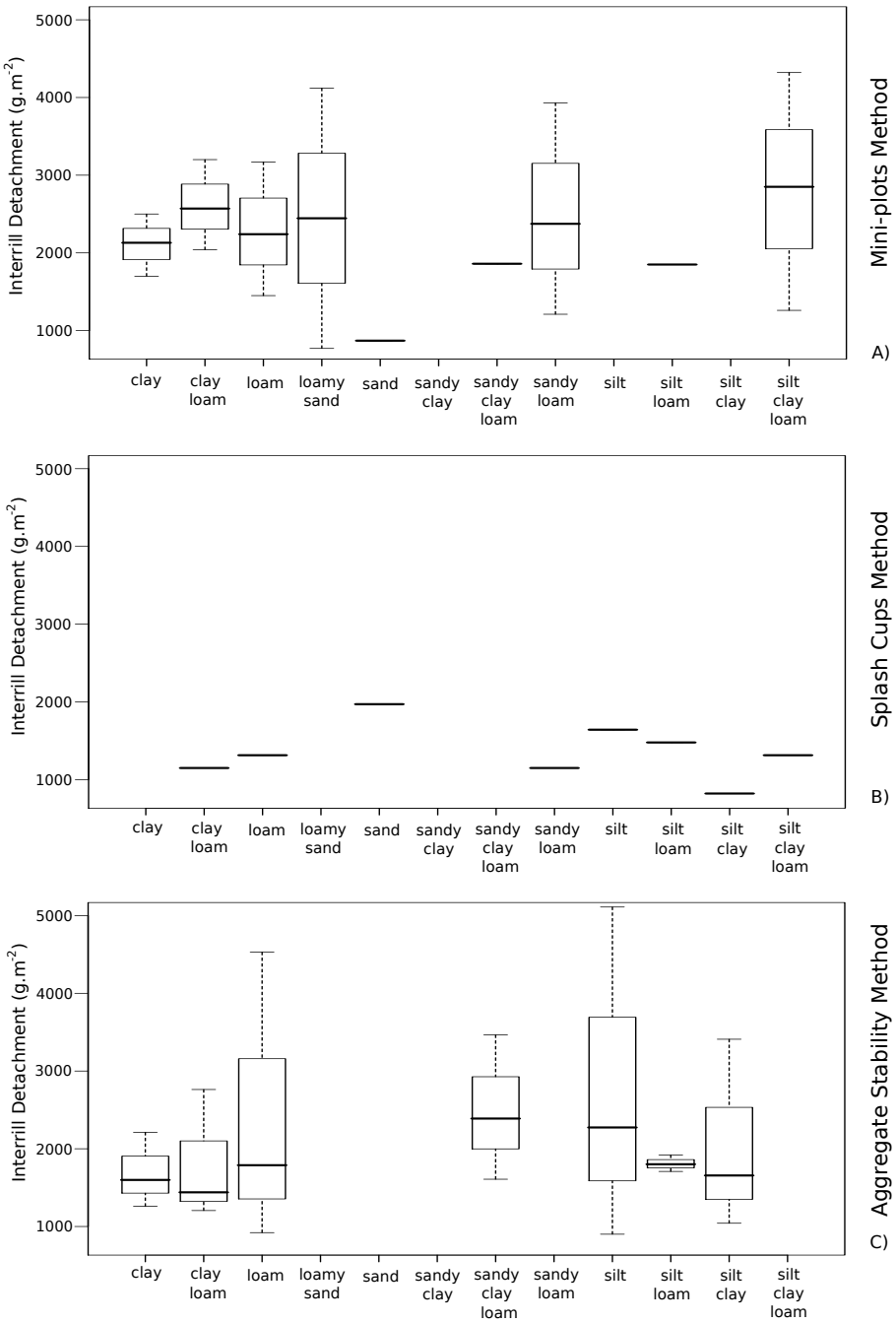

Figure 1.5: Box plot of theoretical interrill contribution to total erosion values for typical soil textures for three assessment methods rain intensity 60 $mm \cdot h^{-1}$

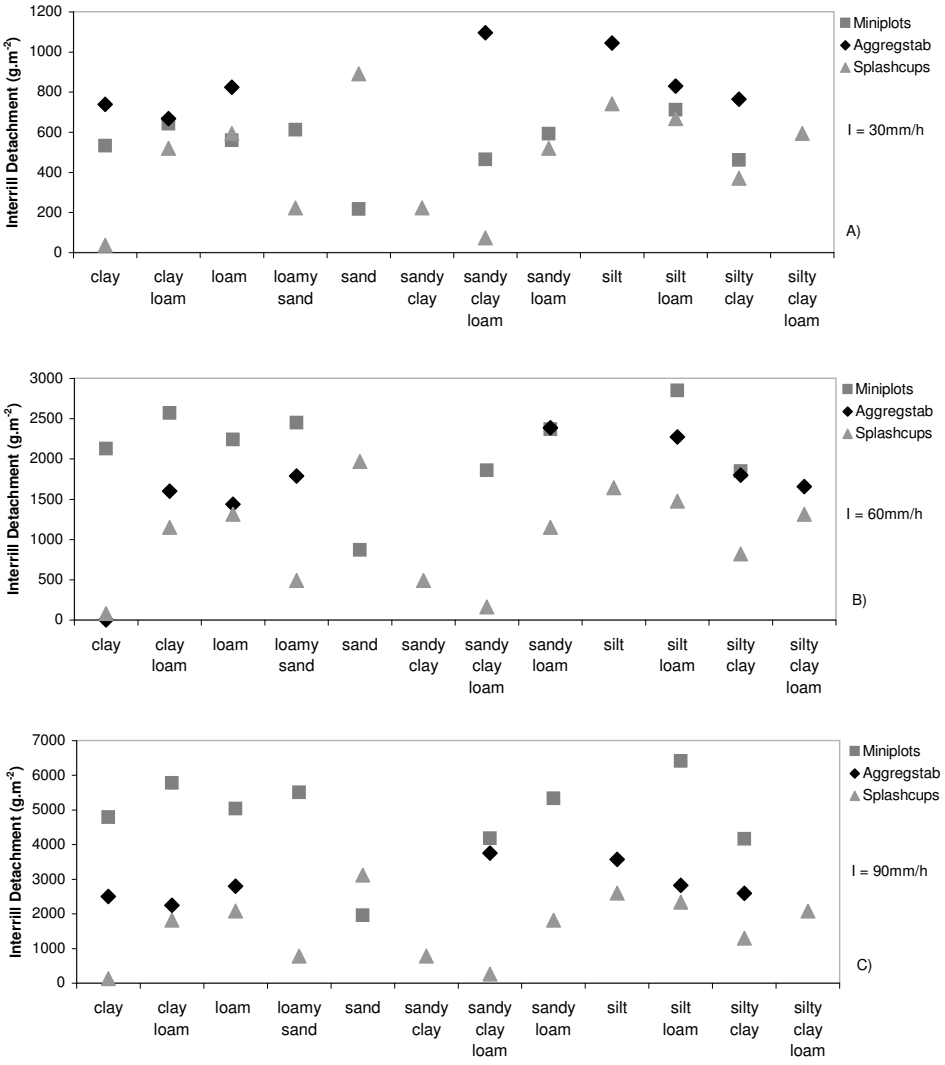

Figure 1.6: Theoretical interrill contribution to total erosion values for typical soil textures for three assessment methods with three intensities 30,60 and 90 $mm \cdot h^{-}1$

clay with splash cup method, whereas it is medium for the aggregate stability test and mini-plots. Such contradictions between models may be one of the reasons for the divergence between erosion models' results and the validation data gathered in evaluation tests (Jetten et al., 2003, 1999) .

This numerical test shows that the three different assessment methods may produce different values for interrill detachment by rainfall for the same textural class (e.g., CV for clay = 67%; CV for loam = 72%; CV for sand = 111%; CV for silt = 126%). Statistical tests with level of 95% of significance proved that detachment values evaluated through the three different methods are not equal regardless of the considered textural class. More importantly the relationships between the interrill detachments given by the three methods show the following results: (i) a positive and significant correlation between splash cups and aggregate stability methods ($R^2 = 0.99$) with a statistically significant level of 95% and (ii) a negative (but not statistically significant at 95%) correlation between the interrill detachment values for mini-plots and both splash cups and aggregate stability test. Although these results may be affected by the limited availability of erodibility data sets, they are in accordance with those obtained by Rachman et al. (2003).

In addition, if we look at the effect of rain intensity and its interaction with interrill detachment (Figure 1.6), we may observe a different ranking of the various texture classes for different rain intensities: interrill detachment by rainfall increases with rain intensity more in the case of mini-plots than that of aggregate stability tests or splash cups. This is due to the fact that the exponent of intensity within the WEPP equation is 2, whereas it is a logarithm for LISEM and EUROSEM.

1.5 Discussion and Conclusion

There is a large data set of references for soil erodibility values in the literature for standard plot methods. Thus, the scientific community frequently uses models based on this assessment method. However, the standard plot assessment method is used to assess lumped interrill and rill erodibility together with runoff. Therefore, the use of erodibility (as a parameter of specific interrill or rill erosion) in process-based models that calculate runoff and interrill and rill erosion separately seems inappropriate. For these models, we think that the aggregate stability test is a preferable approach for the parameterization of interrill erosion, because it specifically characterizes this process. Another advantage of the aggregate stability test is that it provides information about the size of potentially transported particles that indirectly indicates information about

the deposition process. Unfortunately, the data-set available in the literature for local erodibility assessment methods, such as splash cups and the drop test, is not sufficient for a comparative model application analysis. However, a large data set exists in the literature for standardized aggregate stability methods (Kemper or Le Bissonnais methods), which could be used as an interrill erodibility parameter in process-based models.

The erodibility values from the standard plot assessment methods are frequently high for loam soil textures and low for sand and clay soils textures, whereas sandy soils are more erodible than loam soil textures for splash cups and aggregate stability test. An erodibility assessment method like standard plots is strongly influenced by hydrological processes. Sandy soil generally has high infiltration capacity and low transportability, which results in reduced runoff production, particle transport and, consequently, erosion (intensity). Medium textured soils are more erodible based on unit plot and mini-plot assessment. As these soils tend to produce increased runoff, soil particles are easily detached and transported (Toy et al., 2002). In fact, erodibility assessment is influenced by the experimental scale of the method, with increasing effects of hydrological processes for increasing scales. That is one of the reasons for the difference between interrill erodibility values in the three different assessment methods. Making comparisons between interrill soil erodibility parameters from different methods is difficult, because some methods have few reference values for typical soil textures. However, the values of interrill detachment by rainfall from local assessment methods, i.e. splash cups and aggregate stability test, are positively correlated ($R^2 = 0.99$), with statistically significant level of 95%. Negative correlations, though not statistically significant at 95%, between interrill detachment values derived from mini-plots and both splash cups and aggregate stability test have been found. The sensitivity of erosion models' outputs to interrill erodibility is generally considered in the literature as low to moderate, compared with hydrological properties and other soil parameters. This result may be related to the reference conditions for the sensitivity analysis.

Whatever the method used, direct measurements are preferable to pedotransfer function derived values. We think that a universal pedotransfer function that predicts interrill erodibility for a large range of soils does not exist. Estimated values from pedotransfer functions (as nomograph for K) would be acceptable only if the strictly observe the validity application domain of the function. For this reason standardized and straightforward methods, such as the aggregate stability test, would be useful to make these direct measurements more easily accessible. A new interrill erosion equation based on this parameter is yet to be developed.

Chapter 2

Interface Effects on Sedimentological Connectivity of Agricultural Catchments in Erosion modelling: A Review

La connectivité sédimentologique des bassins versants agricoles peut-être influencée par des aménagements existants au sein du bassin versant. A priori les modèles distribués d'érosion hydrique peuvent donner des informations sur "où" et "quand" appliquer ces aménagements dans le bassin versant, afin de réduire l'exportation des sédiments. Ce chapitre a pour objectif d'analyser comment l'interaction entre les aménagements et la connectivité sédimentologique du bassin versant est gérée dans la modélisation de l'érosion, d'un point de vue à la fois théorique et expérimental, en prenant comme exemple les bandes enherbées. Ce chapitre montre également comment les modèles d'érosion actuels prennent en compte l'effet des aménagements sur la connectivité sédimentologique.

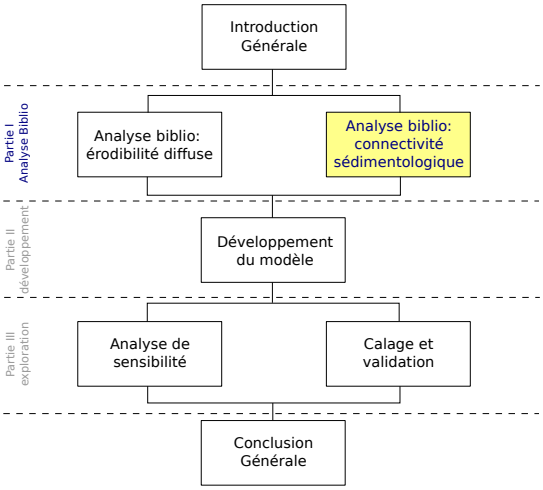

Interface Effects on Sedimentological Connectivity of Agricultural Catchments in Erosion modelling: A Review[1]

Gumiere, S. J.; Le Bissonnais, Y.; Raclot, D. & Cheviron, B. (article accepted with major revision in ESPL)

Abstract

Sedimentological connectivity of agricultural catchments may be affected by man-made structures (land management practices) established to reduce sediment exportation from agricultural plots to water streams. Distributed erosion models may in theory provide information about where and how these structures should be installed in catchments to reduce sediment exportation. The interaction between sediment exportation and land management practices is very complex in both theoretical and experimental points of view. Vegetated filters are a widely used land management practice which interacts with water flows, changing turbulence conditions, affecting in turn sediment transport and deposition processes. Experimental results have shown that the efficiency of sediment trapping in vegetated filters is influenced by flow characteristics, sediment size, vegetation type as well as by the slope and width of the filter in the streamwise direction. At the catchment scale the spatial organisation of management practices is crucial for the global sedimentological connectivity. Present-day erosion models propose different approaches to simulate the influence of management practices on soil loss and sediment export for agricultural catchments. Some of them use the Sediment Delivery Ratio (SDR) to describe sediment transport from source to sink areas. An alternative is to rely on process-based descriptions involving changes in roughness and infiltrability along flow paths to study the effect of management practices. From the literature review conducted here we identified the lack of an "intermediate" approach between very detailed descriptions of management practices not taking into account their distribution, and "black boxes" not offering sufficient understanding of the processes governing sediment filtration.

2.1 Introduction

In agricultural catchments, sediment transport between landscape objects such as cultivated fields and ditches, may be modified by human activities depending on the nature and characteristics of the interfaces between these objects. Some catchments are

[1] Gumiere, S. J.; Le Bissonnais, Y.; Raclot, D. & Cheviron, B., Interface Effects on Sedimentological Connectivity of Agricultural Catchments in Erosion modelling: A Review, Earth Surface Processes and Lanforms, 2009, accepted with major revision required

equipped with soil conservation practices like grass strips or terraces that trap sediment particles, others include drainage channels which accelerate natural flows and increase their erosive power. A useful concept to address the behaviour of the interfaces under variable runoff conditions is that of connectivity between landscape objects of agricultural catchments.

The linkages between runoff and sediment sources in upper regions and the corresponding sinks in lower regions of catchments are called hydrological and sedimentological connectivities (Croke et al., 2005). Bracken and Croke (2007) cited (i) the *landscape connectivity*, which refers to the physical coupling of landforms within a drainage basin *via* its topography, *e.g.* from agricultural plots to drainage channels, (ii) the *hydrological connectivity*, which refers to the transfer of water from one part of the landscape to another; (iii) the *sedimentological connectivity*, which relates to the physical transfer of sediments and attached pollutants through the drainage basin. The connectivity is therefore a function of topography and topology, as well as climate and anthropic impact.

The concept of connectivity is *a priori* relevant at any scale, in particular at the zonal, reach and hillslope-channel scales. Harvey (2001) established that zonal scale connectivity influences the transfer of sediments between major sources of sediments like rivers systems, while reach scale connectivity influences sediment transport between reach segments of a catchment. At hillslope-channel scale, connectivity affects the channel response to sediment supply from hillslopes.

Many studies have shown the importance of sedimentological connectivity in modelling sediment transport and erosion processes in natural catchments. Fryirs and Brierley (1999) in the Wolumla catchment (Australia) showed that hillslope was effectively not coupled with the channel network due to the presence of farm dams. Harvey (2001) argued that hillslope-channel connectivity plays a central role in channel geomorphological processes and that connectivity follows a pattern determined by the intensity and frequency of rain events. Michaelides and Wainwright (2002) in a hillslope-channel coupling model suggested that connectivity was determined by more than just topographic linkages: surface properties of the catchment, spatial variability of these properties as well as rainfall intensity and duration should also be taken into account. Wang et al. (2005) showed that the interface effects of buffer structures between landscape objects reduce the total suspended load of 73% for continuous runoff condition in a Chinese catchment.

Distributed erosion models may provide important information about the effects of soil loss and sediment exportation or redistribution for agricultural and water quality

concerns. Sedimentological connectivity has been used implicitly in erosion and sediment transport modelling as exemplified by the application of SDR (Sediment Delivery Ratio) (Young et al., 1987), which quantifies the physical transfer of material from hillslopes to channels through the catchment. This approach has traditionally been called a "black box" (Bracken and Croke, 2007) not aiming at a real understanding of the spatial and temporal patterns of sediment sources and sinks in the catchment. Others erosion models have used more physically based concepts to express sedimentological connectivity. These models generally rely on the concept of transport capacity of the flow to describe detachment and deposition processes (Ewen et al., 2000; Laflen et al., 1997; Morgan et al., 1998b). In addition, other models have applied empirical weight factors and efficiency functions determined by field observations to describe sediment transport from source to sink areas (de Vente and Poesen, 2005; Verstraeten et al., 2003; Vertessey et al., 2001; Viney et al., 2000). However, the common factor between these approaches is that none of them is directly linked to the amount of water passing through the landscape object. Among many works reviewing erosion models, Rustomji and Prosser (2001) discussed the use of sediment transport capacity in sediment transport modelling and Wheater et al. (1993) classified and reviewed the representation of the processes in conceptual, empirical and physics-based erosion models. Parsons et al. (2001) reviewed 14 agricultural erosion models in a very detailed description of functionality of the models. Merritt et al. (2003) reviewed 17 erosion and water quality models, concluding they provided knowledge about model structure, model limits, input/output procedure and complexity. However, these works do not give information about the approach used to treat interfaces inside erosion models. There are only few works in literature about sedimentological connectivity routines adopted in present-day erosion and water quality models. There are many data sources about the impact of management practices on sedimentological connectivity at the local scale but very few at the catchment scale. Thus, the two main objectives of this paper are: first, to present a review and a synthesis of the impacts of interfaces found in agricultural catchments and their effects on sedimentological connectivity focusing on vegetated filters, and second, to critically review how present-day water erosion models take interfaces into account.

2.2 Interfaces effect on sedimentological connectivity in agricultural landscape

2.2.1 Interfaces in agricultural landscape

Agricultural landscapes have more linkages (artificial drains, gullies, rills and channels) and discontinuities (terraces, hedges, vegetated waterways and grass strips) than natural landscapes. In agricultural catchments, human activities interfere with sediment fluxes in each component of the "connectivity cascade" (Warner, 2006). Agricultural catchments are characterised by a strong landscape transformation in terms of water flow directions, surface roughness, slope steepness, vegetation type and soil erodibility. These transformations affect both sediment production and sediment transport processes from one part of a catchment to another. The connectivity may be influenced by "new objects" placed in the catchment to control sediment transport and erosion processes. These management practices include grass strips, riparian vegetation, hedges, vegetated waterways, mulches, terraces and dams. Each practice affects sedimentological connectivity in a specific way, impacting the hillslope-channel and channel-channel sediment transport at the time scale of the rainfall events. Figure 2.1A) and B) shows the natural and anthropic drainage networks in a typical Mediterranean agricultural catchment.

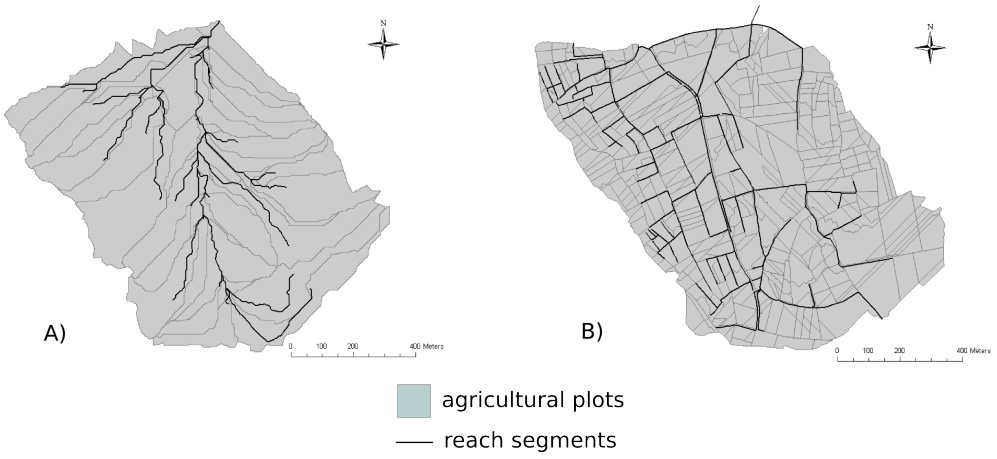

Figure 2.1: Example of a Mediterranean agricultural catchment. A) Represents the natural drainage network and B) the same catchment with an artificial network of ditches, adapted from Lagacherie et al. (2009)(submitted).

Figure 2.1A) was adapted from Lagacherie et al. (2009)(submitted) where the channel network was automatically extracted from the Digital Elevation Mapping (DEM), established from aerial photographs with a 2 m resolution. The technique used is based on the Band (1986) method, assuming that the channel network follows the steepest slope and that all extremities of the channel network drain the same source area. In Figure 2.1B) the channel network was measured *in situ*. From a qualitative point of view the man-made network channel (Figure 2.1B) has been changed compared to natural flow path (Figure 2.1A) of the catchment. The man-made ditches are often placed perpendicularly to the natural flow direction line, which might cause overbank phenomena during heavy rain events. Hillslope-channel and channel-channel interfaces have been investigated by Brunsden (1993), who describes the three types of coupling at this scale: not coupled, coupled and dis-coupled. Not coupled means no linkage exists between two components. Coupled objects have free transmission of materials and energy between them. Objects that were previously coupled but for some reason were disconnected during the event are called dis-coupled. The disconnection is often the result of sediment deposition obstructing the flow path. Conversely, some objects initially not coupled may become coupled during the rain event if overflowing occurs. In catchments with high connectivity, increases of erosion rates on hillslopes lead to increasing sediment inputs to the channels. On the contrary, increasing erosion rates on hillslopes of low connectivity catchments may cause local degradation of soils without any transmission effect. The coupling state of interfaces within a catchment is both spatially distributed and time-dependent. Parts of the catchment may be inactive or active sediment sources and may be connected or not connected to the drainage channel network. The time dependence of linkages is related to magnitudes of the considered events. Over short rain events, hillslopes are "a priori" not coupled to the drainage network, but when rain volumes and/or intensity reaches a threshold hillslopes become connected to the drainage network and sediments are transmitted down into the system. Some interface systems have filtering properties: they capture sediment particles by decelerating the running water. These objects are classified in literature as vegetative filters (Dillaha et al., 1989; Magette et al., 1989; Young et al., 1980) and may have a strong impact on sedimentological connectivity. In the following subsection we will focuses on these filters, describing experimental, theoretical and modelling aspects.

2.2.2 The case of vegetative filters (VF)

2.2.2.1 Experimental aspects

Vegetative filters are placed in catchments to reduce exportation of sediments, soil and pollutants from agricultural activities (Dillaha et al., 1989). As showed by Borin et al. (2005); Deletic and Fletcher (2006); Le Bissonnais et al. (2004) among others, grass strips act as filters, trapping sediment particles suspended in overland flow, thus reducing sedimentological connectivity. Sedimentological connectivity in agricultural catchments is the underlying concept of management practices aiming at controlling erosion, among which vegetative filters are widely used. The spatial disposition and characteristics of these vegetative filters may completely transform the connectivity pattern within a catchment. Increases of infiltrability and surface roughness provided by these vegetated filters may decrease flow transport capacity and thus reduce sedimentological connectivity. Ludwig et al. (1995) showed that interactions between land managements and topographic features possibly result in a complex hydro-sedimentological structure: the efficiency of VF depends on filter width and slope, particle size, vegetation type and incoming runoff, not necessarily in this order of importance. A literature review was undertaken to synthesise values of sediment removal in vegetated filters reported in experimental studies for different localisations, vegetation type, sediment size etc. These studies include (i) field experiments in agricultural plots, (ii) field experiments in agricultural catchments, (iii) flume experiments in laboratory using real vegetation and (iv) flume experiments in laboratory using synthetic vegetation. Table 2.1 and 2.2 summaries the results.

Table 2.1: Vegetated filters efficiency for homogeneous and heterogeneous vegetation [a] refers to homogeneous vegetation and [aa] refers to heterogeneous vegetation

Source Article	Country	Width (m)	Slope (%)	Vegetation type	Efficiency (%)	Sed. diam. (mm)	Discharge ($L.s^{-1}$)	Runoff (mm)
Roose and Bertrand (1971)[a]	Ivory Coast	4	7	cassava	80	-	-	138
	Ivory Coast	4	7	-	-	-	-	-
Neibling and Alberts (1979)[a]	USA	5	-	-	90	-	-	-
Hall et al. (1983)[a]	USA	6	14	-	76	-	-	-
Hayes and Hairston (1983)[a]	USA	2.6	2.35	-	60	-	-	-
Dillaha et al. (1989)[a]	USA	4.6	16	-	53.5	-	-	-
	USA	9.1	5	-	93	-	-	-
	USA	4.6	5	-	83.5	-	-	-
	USA	9.1	11	-	97.5	-	-	-
	USA	4.6	11	-	86	-	-	-
	USA	9.1	16	-	70.5	-	-	-
Magette et al. (1989)[a]	USA	4.6	2.7	-	64.3	-	-	-
	USA	9.2	4.1	-	80.3	-	-	-
	USA	4.6	4.1	-	65.8	-	-	-
	USA	9.2	2.7	-	92.4	-	-	-
	USA	9.2	2.7	-	88.3	-	-	-
	USA	4.6	2.7	-	82.8	-	-	-
	USA	8.5	3.25	-	85	-	-	-
	USA	4.3	3.25	-	75	-	-	-
Line (1991)[a]	USA	1.5	-	-	60	-	-	-
Schauder and Auerswald (1992)[a]	Germany	-	-	-	55	-	-	-
Parsons et al. (1994)[a]	USA	8.5	1.9	-	81	-	-	-
	USA	4.3	1.9	-	78	-	-	-
Coyne et al. (1995)[a]	USA	4.6	9	-	99	-	-	-
Ligdi and Morgan (1995)[a]	Lab.	-	15	synthetic	38	-	0.07	-
	Lab.	-	10	synthetic	75.8	-	0.04	-
	Lab.	-	5	synthetic	86.2	-	0.04	-
	Lab.	-	15	synthetic	38	-	0.04	-
	Lab.	-	5	synthetic	30	-	0.07	-
	Lab.	-	10	synthetic	81.5	-	0.07	-
Meyer et al. (1995)[a]	Lab.	0.2	5	vetiver	63	-	-	-
Arora et al. (1996)[a]	USA	20.12	3	-	87.6	-	-	-
	USA	20.12	3	-	83.6	-	-	-
Chaubey et al. (1993)[a]	USA	21.4	-	fescue	79	-	-	-
	USA	3.1	-	fescue	40	-	-	-
Daniels and Gilliam (1996)[a]	USA	3	4.9	-	59	-	-	-
	USA	6	4.9	-	61	-	-	-
	USA	3	2.1	-	45	-	-	-
	USA	6	2.1	-	57	-	-	-
Robinson et al. (1996)[a]	USA	3	7	fescue	70	-	-	-
	USA	9.1	12	fescue	85	-	-	-
	USA	9.1	7	fescue	85	-	-	-
	USA	3	12	fescue	80	-	-	-
Dijk et al. (1996) [a]	Netherlands	5	2.3	-	73	-	0.5	-
	Netherlands	4	5.2	-	78.5	-	0.5	-
	Netherlands	10	8.5	-	97.5	-	0.5	-
	Netherlands	5	8.5	-	92	-	0.5	-
	Netherlands	10	2.5	-	99	-	0.5	-
	Netherlands	1	5.2	-	49.5	-	0.5	-
	Netherlands	10	2.3	-	94	-	0.5	-
	Netherlands	5	2.5	-	64.5	-	0.5	-
Ghate et al. (1997)[a]	USA	24	3	Bermuda	89.6	-	0.43	-
	USA	24	1.5	Bermuda	72.8	-	0.43	-
Patty et al. (1997)[a]	France	12	15	-	97	-	-	-
	France	18	10	-	98	-	-	-
	France	6	10	-	87	-	-	-
	France	12	10	-	100	-	-	-
	France	18	10	-	100	-	-	-
	France	6	7	-	98.9	-	-	-
	France	12	7	-	99	-	-	-
	France	6	15	-	91	-	-	-
	France	18	7	-	99.9	-	-	-
Barfield et al. (1998)[a]	USA	13.7	9	-	99.7	-	-	-
	USA	4.5	9	-	97	-	-	-
	USA	9.1	9	-	99.9	-	-	-
Coyne et al. (1998)[a]	USA	9	9	-	99	-	-	-
	USA	9	9	-	98	-	-	-
	USA	4.5	9	-	95	-	-	-
Tingle et al. (1998)[a]	USA	2	3	-	94	-	-	-
	USA	3	3	-	96	-	-	-
	USA	0.5	3	-	88	-	-	-
	USA	4	3	-	98	-	-	-
	USA	1	3	-	93	-	-	-

Continued on the next page...

Table 2.2: Continuation of Table 1

Source Article	Country	Width (m)	Slope (%)	Vegetation type	Efficiency (%)	Sed. diam. (mm)	Discharge ($L.s^{-1}$)	Runoff (mm)
Lee et al. (2000)[a]	USA	13.7	3	$S+B^a$	90	-	0.66	-
	USA	6	3	$S+B^a$	76.5	-	0.66	-
	USA	3	3	$S+B^a$	65.5	-	0.66	-
	USA	7.1	5	$S+B^a$	70	-	-	-
Munoz-Carpena et al. (1999)[a]	USA	4.3	6	-	86	-	-	-
	USA	8.5	6	-	93	-	-	-
Schmitt et al. (1999)[a]	USA	7.5	6.5	-	85	-	-	-
Sheridan et al. (1999)[a]	USA	8	2.5	-	81	-	-	-
Fasching and Bauder (2001)[a]	USA	12.2	-	wheat grass	68	-	-	-
Appelboom et al. (2002)[a]	USA	0.9	-	-	56	-	-	-
Abu-Zreig et al. (2003)[a]	Canada	2	2.3	-	68	-	-	-
	Canada	15	2.3	-	98	-	-	-
Blanco-Canqui et al. (2004)[a]	USA	8	5	-	90	-	-	-
Le Bissonnais et al. (2004)[a]	France	3	4	ray grass	73	-	-	-
	France	6	4	ray grass	86	-	-	-
	France	6	4	ray grass	60	-	-	-
Borin et al. (2005)[a]	Italy	6	1.8	-	94	-	-	-
Helmers et al. (2005)[a]	USA	13	1	-	80	-	-	-
Gharabaghi et al. (2006)[a]	Canada	20	-	-	98	0	-	-
	Canada	2.5	-	-	50	0	-	-
Deletic and Fletcher (2006)[a]	Australia	24	1.6	-	74.6	0	5	-
	Australia	24	1.6	-	57.4	0	15	-
	UK	6.2	7.8	-	67	0.01	-	72
	Australia	24	1.6	-	87.7	0	2	-
	Australia	24	1.6	-	67.2	0	8	-
	Australia	24	1.6	-	59.1	0	12	-
Ghadiri et al. (2001)[a]	Lab.	0.3	5	vetiver	90.5	0.002-2	-	-
ShuHui et al. (2006)[a]	China	0.5	14	Setaria Sphacelota	85	-	-	-
Hussein et al. (2007)	Lab.	0.3	5	vetiver	88.4	0.26	-	30.6
	Lab.	0.3	3	vetiver	89.8	0.26	-	20.4
	Lab.	0.3	1	vetiver	94	0.26	-	10.2
Babalola et al. (2007)[a]	Nigeria	10	7	vetiver	66	1.1	-	19.4
Shiono et al. (2007)[a]	Japan	0.5	-	centipede	24	0.002-0.02	-	-
	Japan	1.5	-	centipede	54	0.002-0.02	-	-
	Japan	3	-	centipede	73	0.002-0.02	-	-
Young et al. (1980)[aa]	USA	27.4	4	-	79	-		
	USA	21.3	4	-	78	-		
Peterjohn and Correl (1984) [aa]	USA	60	5	-	94	-		
	USA	19	5	-	90	-		
Cooper et al. (1987)[aa]	USA	-	-	-	90	-		
	USA	-	-	-	84	-		
Dillaha et al. (1988)[aa]	USA	4.6	11	-	87	-		
	USA	4.6	16	-	76	-		
	USA	9.1	11	-	95	-		
	USA	9.1	16	-	88	-		
	USA	4.6	11	-	86	-		
	USA	4.6	16	-	53	-		
	USA	9.1	11	-	98	-		
	USA	9.1	16	-	70	-		
Lee et al. (2000)[aa]	USA	16.3	-	Panicum virtagatum L.	70	-		
	USA	16.3	-	Panicum virtagatum L.	70	-		
McKergow et al. (2003)[aa]	Australia	-	-	-	93	-		
	Australia	15	-	-	80	-		
Ward and Jackson (2004)[aa]	USA	-	-	-	99	-		
	USA	-	-	-	71	-		
Syversen and Borch (2005)[aa]	Norway	5	14-17	-	32	0.02-0.06		
	Norway	5	14-17	-	37	0.006-0.02		
	Norway	10	14-17	-	54	0.006-0.02		
	Norway	10	14-17	-	33	0.002-0.006		
	Norway	15	14-17	-	71	0.002-0.006		
	Norway	10	14-17	-	83	0.02-0.06		
	Norway	15	14-17	-	89	0.02-0.06		
	Norway	15	14-17	-	82	0.006-0.02		
	Norway	5	14-17	-	54	20-60		
	Norway	5	14-17	-	49	0.02-0.06		
	Norway	5	14-17	-	39	0.00006-0.002		
	Norway	10	14-17	-	25	0.00002-0.00006		
	Norway	10	14-17	-	23	0.000006-0.00002		
	Norway	15	14-17	-	57	0.000006-0.00002		
	Norway	10	14-17	-	24	0.00006-0.002		
	Norway	15	14-17	-	55	0.00006-0.002		
	Norway	15	14-17	-	51	0.00006-0.002		
	Norway	5	14-17	-	31	0.00006-0.002		

Table 2.1 and 2.2, shows 147 values of sediment removal efficiency for vegetated filters. These values have been obtained from 49 studies conducted in the whole world. Soil texture in the experimentations in Table 2.1 and 2.2 is mostly silt loam. The range of sediment removal efficiency in these studies is 24% to 100%.

Initially it was thought that sediment and pollutants removal efficiency of vegetated filters was dependent on their physical characteristics (i.e, width, slope and soil properties) (Norris, 1993). Figure 2.2 shows the scatter diagrams obtained from Table 2.1 and 2.2 between sediment removal efficiency, selected VF physical characteristics of width and slope, and flow discharge.

No statistically significant relationship was found between vegetated filter width and sediment removal efficiency (Figure 2.2A) for data in Table 2.1 and 2.2. According to Lacas et al. (2005) and relying on works by Vaucluse (2000), Dillaha et al. (1989), Lim et al. (1998), Schmitt et al. (1999), Spatz et al. (1997), Srivastava et al. (1996) and Tingle et al. (1998) vegetated filter width is not a determining parameter in sediment removal efficiency. As showed by Tingle et al. (1998), sediment deposition occurs in the first few meters of the vegetated filter: an increase in streamwise width of the filter has limited impact on the efficiency. this result can be explained by the fact that large particles, that represent the majority of sediment weight are trapped in the first few meters of VF, and only finer particles travel farther (Gharabaghi et al., 2006).

Based on the data from Table 2.1 and 2.2, no statistically significant relationship was found between VF slope and sediment removal efficiency (Figure 2.2B), showing that slope is not a determining parameter of sediment removal efficiency. However, Ghadiri et al. (2001) showed for grass strips that water behaves as if striking porous barriers, partly stopped and creating backwater regions with raised flow level. The length on which a variation in flow depth is reported varies with slope, vegetation density and flow rate. As pointed out by Ghadiri et al. (2001), the backwater length is exponentially related to the slope when flow rate and vegetation density are constant. The existence of backwater regions upslope from vegetated filter acts in favour of sedimentation processes and may increase sediment removal efficiency. Liu et al. (2008) proposed that sediment removal efficiency is maximum when vegetation filters are placed at an optimal slope of 9%. This was criticised by Fox and Sabbagh (2009) arguing that sediment and pollutant removal efficiency is at the first order dependent of flow conditions and runoff characteristics.

On the other hand, even though Figure 2.2C has only few points, it is possible to find a significant statistical (exponential) relationship between discharge and sediment removal efficiency: it is probably the hydrological response of vegetated filters that

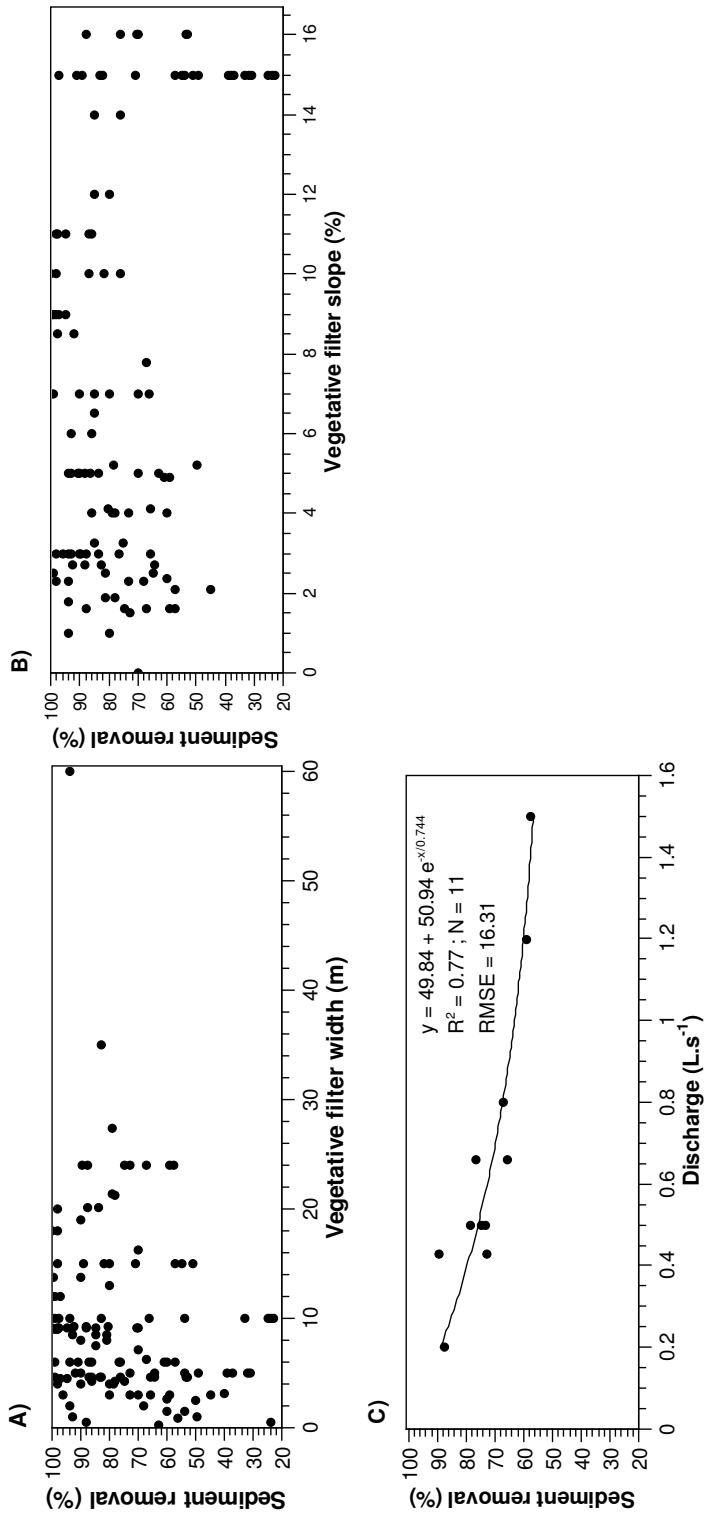

Figure 2.2: Scatter diagrams between vegetative filter and A) width of VF and sediment removal efficiency, B) slope of VF and sediment removal efficiency and C) discharge and sediment removal efficiency.

drives sediment removal efficiency. Sabbagh et al. (2009) also suggest that sediments and pollutants removal efficiency of vegetated filters is a result of VF physical characteristics and of the nature of runoff events. In addition, concentrated flows in vegetated filters act against sediment removal efficiency (USDA, 2000) as fast flow lines are able to carry more sediment loads.

Several works in Table 2.1 and 2.2 have shown that grass strips increase infiltrability of soil:Le Bissonnais et al. (2004) showed that runoff was significantly reduced on experiment made with 6-meter long grass strips; the authors observed a runoff reduction of 63 to 84%, consistent with a study by Abujamin et al. (1984) who reported a decrease of 50-60% in grass strips applications. Shrestha et al. (2005) showed that the vertical saturated hydraulic conductivity was increased with grass application, diverting flows into the topsoil. Schmitt et al. (1999) observed that infiltration rates double up when doubling grass strip width. Beside runoff reduction and consequently sediment transport capacity reduction, fine particles ($< 0.45\mu m$) may penetrate into the top soil layers via their porosity. In fact it has been noted that porosity of soils in vegetated filters is increased, possibly explained by the increase of organic matter content.

Based on experimentations related in literature, the sediment removal efficiency of vegetated filters results from the interaction of flow discharge characteristics, soil properties and vegetated filter specificities. Moreover, a global point of view on a catchment indicates that the impact of vegetated filters on sedimentological connectivity not only depends on single VF efficiency, but is also dependent on the spatial distribution of vegetated filters compared to the flow paths network.

2.2.2.2 Theoretical aspects

The efficiency of VF is a function of the energy reduction gradient generally associated with increasing surface roughness and infiltration rate, resulting in decreasing velocity and volume of overland flow. Several studies (Baptist et al., 2007; Nepf, 1999; Wilson et al., 2005; Wu et al., 1999) associate roughness elements due to vegetation with decreases in flow velocity and increases in near-bed shear stresses. Local resistance on the stems and boundary resistance on the bed enhance turbulence in comparison with the case of a flow without obstacles, which causes a decrease in transport capacity and results in more deposition. These results intuitively hold (1) for small but not negligible flow velocities for which the energy spent to maintain or create turbulence lacks for particle detachment and (2) for sufficiently sparse vegetation to allow turbulence apparition (a dense vegetation would prevent turbulence and allow only laminar flows). The key element is the influence of the vegetative drag force, *i.e.* the drag force

attributed to vegetation, and its propensity to affect flow characteristics.

For fluid flow over vegetative areas, the drag force may be described by:

$$F_D = \frac{1}{2} C_D \, \rho \, A \, U^2 \tag{2.1}$$

where C_D is the drag coefficient of vegetation, U is the flow velocity on the obstacles, A is the cross-sectional momentum-absorbing area of vegetation and ρ is the water density.

For submerged vegetation the drag coefficient (C_D) is equivalent to the widely-used Darcy-Weisbach friction coefficient f:

$$f = 4 \, C_D \, \frac{A}{b \, l} \tag{2.2}$$

where b is the width of the grass strip, l its length, A is the total momentum-absorbing area of the stems $A = \rho_{grass} d_{grass} h_{grass}$ with ρ_{grass} the density in number of stems per surface unit, d_{grass} the width of stems seen as cylinders and h_{grass} their height.

Many works have showed that the total effective roughness depends on the relative submergence of vegetation. Figure 2.3 A) and B) shows Darcy-Weisbach and Manning coefficients plotted against relative submergence from laboratory experiments involving varied water depths.

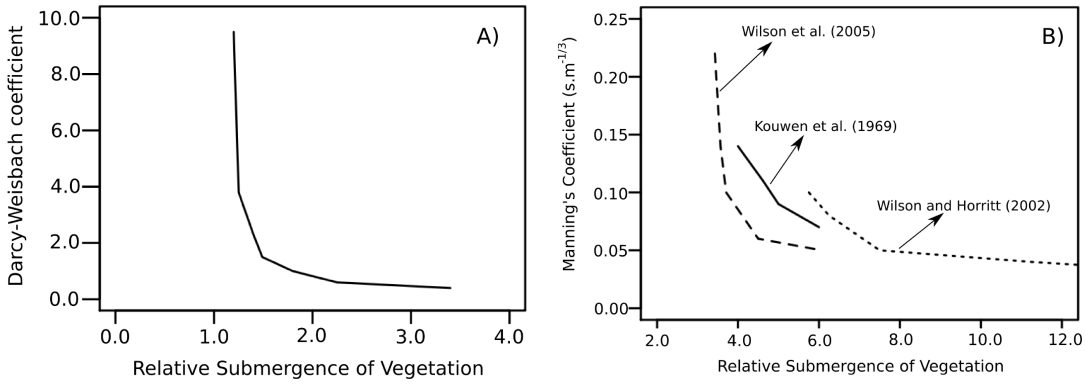

Figure 2.3: Roughness coefficients from grass filtering experiments in varied water depths and relative submergence, adapted from Wilson et al. (2005). A) Darcy-Weisbach coefficient and B) Manning coefficient.

Figure 2.3 indicates that hydraulic resistance of grass increases when relative submergence (flow depth divided by vegetation height) diminishes from complete submergence to marginal inundation. In other words, the efficiency of grass strips grows higher when flow depth is of the same order than grass height. The hydraulic resistance decreases with increasing relative submergence, tending to an asymptotic constant, thus

having progressively less effects on the flow, including on sediment deposition. The differences between the curves may be explained by the vegetation properties like vegetation type or vegetation density used in the mentioned studies. As proposed by Lawrence (1997) for relative submergence less than one, the hydraulic resistance decreases when relative submergence decreases, reaching a non-zero limit for extremely small water depths. This case of low relative submergence is often encountered in natural conditions though only theoretical or small-scale studies are available (Dunkerley, 2003) , either out of the scope of this paper or giving no directly exploitable information.

Drag forces in homogeneous VF may be due to (i) non-submerged vegetation or (ii) submerged vegetation.

(i) For non-submerged VF the most important parameter is vegetation density, either described as the number of vegetation blades per surface unit or equivalently as the proportion of cross-sectional surface area obstructed by vegetation (Baptist et al., 2007; Deletic, 2001). In these two works the flow regime inside vegetation is considered as laminar and the expected linear velocity profile is approximated by a constant velocity on the entire height of the stems. The drag force C_D is calculated from vegetation density which increases the particle "fall number" proportional to the ratio of settling velocity to flow velocity.

(ii) For submerged vegetation Baptist et al. (2007); Campana (1999); Hong (1995); Wu et al. (1999) proposed that velocity profile be divided into four categories. In the bed zone (i) velocity is highly influenced by the wall effect with a vertical logarithmic velocity profile. Inside the non-flexible vegetation zone (ii), velocity is uniform. In the flexible vegetation zone (iii), a logarithmic velocity profile is connected to that of zone (iv) above vegetation.

Many studies have proposed variations in roughness coefficient in function of flow depth (Baptist et al., 2007; Nepf, 1999; Wilson et al., 2005; Wu et al., 1999). They often divide VF into categories of homogeneous and heterogeneous vegetation (Figure 2.4).

A vegetation strip is said to be homogeneous when there is little variation in dimension and density of vegetation and no debris or tree branches forming obstacles on the surface. The land management practice used as an example here for this condition is a grass strip. Grass strips are densely vegetated, uniformly graded areas that receive overland flow from adjacent impervious surfaces. They are frequently planted with turf grass but filter strips may also employ native vegetation, such as meadow or prairie. Figure 2.4A illustrates the condition of homogeneous vegetation with sediment inflow

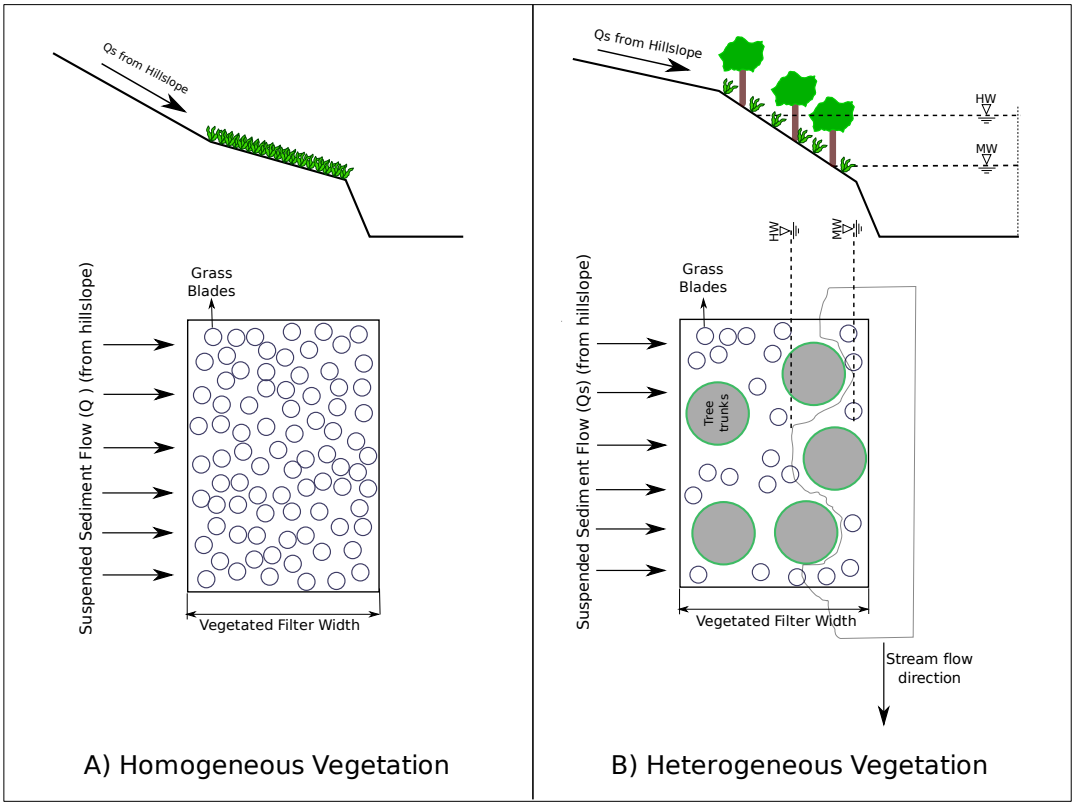

Figure 2.4: (A) Representation of an homogeneous vegetated strip. (B) Two flow conditions over an heterogeneous vegetated strip.

from an hillslope. Heterogeneous vegetation is considered when noticeable variations exist in dimension and density of vegetation, also allowing the presence of woody debris and tree branches on the surface. Riparian vegetation is an example of land management practice classed in this category. Riparian vegetative buffers consist of bands of either planted or indigenous vegetation on river banks and channels of catchments. They improve sediment and pollutant trapping by a combination of physical, chemical and biological processes (McKergow et al., 2003).

For heterogeneous vegetation, some works have proposed that water flow inside vegetation be divided into sub-regions characterised by different roughnesses. In this case the total roughness coefficient is taken as the sum of coefficients pertaining to different sub-regions (Masterman and Thorne, 1992). Some approaches take into account the interactions between high velocity regions in the mainstream and slow velocity regions

in the vegetated regions. In this context, Zhang and Su (2008) proposed three equations to determine appropriate drag coefficients in laminar, laminar-turbulent and fully turbulent flow regimes.

Whatever the conversion of C_D into Darcy-Weisbach, Manning, Chezy or composite and additive formulations of roughness coefficients, the existence of vegetation always reduces flow velocity and increases sediment deposition. However, under certain circumstances, rigid and emergent vegetation creates secondary circulation flow patterns and coherent lateral flow structures (Bennett et al., 2002), these deflections resulting in local bank scour. Bennett et al. (2002) showed that flow velocity was drastically reduced within regions where rigid vegetation has a high density, diverting accelerated flow filaments out of the dense region and toward the bank. This flow divergence creates mini-vortices with axis normal to the bed and rotation directions varied with vegetation position, confirming the possibility of scour bank.

The heterogeneous vegetation case includes the existence of LWD (large woody debris), FWD (fine woody debris) and FOD (fine organic debris). The influence of these objects in the flow is very complex, depending on discharge characteristics as well as of size and orientation of the debris. Wallerstein et al. (1997) classified their influence in function of their position in the flow (Underflow, Dam, Deflector, Flow Parallel) in a river. Considering an uniform and steady flow through a straight channel Petryk and Bosmajian (1975) presented an equation to predict the Manning coefficient specific to LWD, expressed by energy lost per unit channel length. It is the result of drag calculations on a series of solid obstructions. Using the same approach Shields and Smith (1992) estimated the Darcy-Weisbach friction factor (f_d) due to LWD:

$$f_d = 4R_H C_D D_A \tag{2.3}$$

$$D_A = \frac{\sum_{i=1}^{n} A_i}{BR_H l} \tag{2.4}$$

where R_H is the mean hydraulic radius (assumed equal to flow depth in wide-section assumptions), C_D is the drag coefficient for LWD, assumed equal to 1.0 by Petryk and Bosmajian (1975) and D_A is the roughness concentration due to LWD, A_i is the cross-sectional area of the i^{th} debris in the plane normal to the flow, B is the mean flow depth.

In shallow overland flow conditions the effect of LWD, FWD and FOD is to divide the flow into regions of near-zero velocity upstream from large obstacles and regions of fast flow filaments in constricted zones, as observed by (Dunkerley, 2003) in flume

experiments involving different topologies and non-submerged obstacles. Friction coefficients were found very dependent of the LWD disposition in space and not dependent of the LWD density.

2.2.2.3 Modelling aspects

The most cited model of water and sediment flow through vegetated filters is GRASSF, that has been developed at Kentucky University (Lexington, USA), from laboratory experiments using metal rods as vegetation stems (Barfield et al., 1979; Hayes et al., 1979, 1984; Tollner et al., 1976, 1977). This physically based model implies many parameters affecting sediment transport and deposition (sediment characteristics and concentration, vegetation type, slope and length of the filter). The varied flow is described by means of the continuity equation whereas steady state infiltration is considered, i.e. flow depth and discharge decrease when advancing into the filter.

Based on the same algorithms used in GRASSF, Munoz-Carpena et al. (1999) derived a complex model called VSFMOD, composed of two main sub-models attached to hydrology and sediment transport sub-model. This model is said "evolutive" as it includes computations of modifications in surface elevations due to deposition and in turn affecting flow characteristics through feedback effects. The core of the hydrology sub-model is a quadratic finite element routine describing overland flow in the kinematic wave approach. This sub-model also uses a modification of the Green-Ampt equation under unsteady rainfall (Chu, 1978) for water infiltration processes.

The sediment transport submodel allows a spatial variation of the Manning coefficient and slope steepness inside the vegetated filter, both controlled by sediment deposition. In fact vegetated filters in the model are divided into five zones (Figure 2.5) $O(t)$ the upper face of the wedge formed by coarse deposition, $A(t)$ the downslope face of the wedge (only particles transported as bedload), $B(t)$ the equilibrium deposition zone (deposition and transport occurring at the same time), $C(t)$ sediment load and coarse material deposition zone and $D(t)$ only sediment load deposition zone. All zones are recalculated for each time step. The calculation procedure for zones $O(t)$, $A(t)$ and $B(t)$ uses modified Manning equations for the flow and Einstein's total bedload transport equation. For zones $C(t)$ and $D(t)$ it uses the transport equation for suspended sediment derived by Tollner et al. (1976), based on the probabilistic approach of turbulent diffusion for non-submerged vegetation.

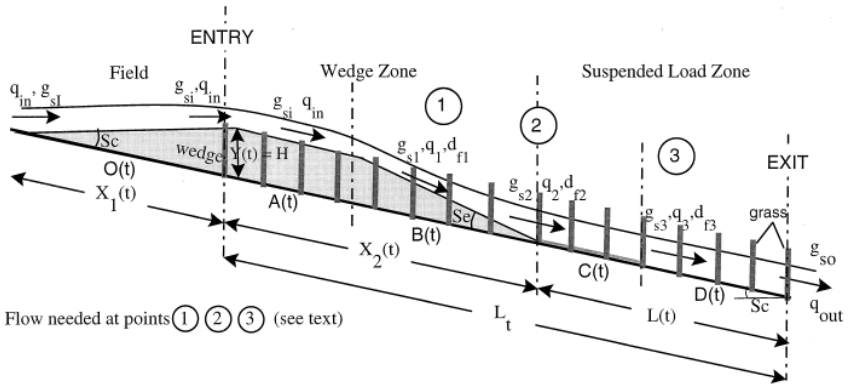

Figure 2.5: Vegetated filters description for the sediment transport submodel, from: Munoz-Carpena et al. (1999), in the Figure: q_{ini} flow rate, g_{si} sediment load, Sc soil slope, $Y(t)$ thickness of the deposited sediment layer at the entry of the filter, g_{s0} out filter sediment load, q_{out} out filter flow rate

Deletic (2001, 2005) later developed TRAVA, a deterministic model of sediment transport through vegetated filters. The model was based on the "Aberdeen equation" for trapping particles by medium grass. TRAVA is a complex hydrodynamic model designed for simulating transport during a single rain event. It is fully explained with a comprehensive sensitivity analysis in Deletic (2001). It is a 1-D model that contains two submodels. A runoff submodel simulates overland flow based on the Green-Ampt model for infiltration and the kinematic wave for overland flow. A sediment submodel simulates deposition using the "Aberdeen equation" (Deletic, 1999) and sediment outflows at the end of the grass filter. Sediment removal at the vegetated filter is calculated as an empirical function of the particle "fall number":

$$T_{r,s} = \frac{N_{f,s}^{0.69}}{N_{f,s}^{0.69} + 4.85} \tag{2.5}$$

$$N_{f,s} = \frac{lVs}{hV} \tag{2.6}$$

$$V = \frac{q}{hB_0} \tag{2.7}$$

where$T_{r,s}$ is the sediment removal efficiency of the vegetated filter, l is the length of the vegetated filter, Vs is the sedimentation velocity calculated by Stokes equation (laminar flow and sufficiently small sediment load), V is the velocity between the vegetation

blades, q is the overland flow rate per width unit, h is the depth of flow, B_0 is the open flow width (spacing between two nearby stems).

The specialised vegetated filters models as presented above are often very detailed and relying on a fine physical description of small-scale phenomena. Models like VSFMOD or GRASSF are able to compute changes of flow conditions caused by vegetation effects and variations in surface elevation due to deposition processes. They are therefore very demanding in terms of parameterisation and calculation times. Other models are a little bit simpler, like TRAVA in which sediment trapping efficiency is function of the particle "fall number". Both approaches were tested in laboratory and during field experiments. They give acceptable results Barfield et al. (1979); Deletic (2005); Munoz-Carpena et al. (1999) for a single vegetated filter. The limitation of these approaches is in fact that they pertain to isolated elements at the local scale only. No attempt was made yet to study the effects of any organisation or spatial distribution involving multiple elements.

2.2.3 Upscaling sedimentological connectivity from plot scale to catchment scale

Sedimentological connectivity is a complex concept combining landscape properties (topography, topology, soil type and moisture, native vegetation) with driving variables (rainfall intensity and cumulative amount) and human activities. Land management practices, exemplified in this work by vegetative filters, are often placed at the bottom end of hillslopes, interacting with the drainage network (grass strips) or directly alongside the channels (vegetated waterways). To optimise the localisation of the land management practices in the catchment, the CORPEN (1997) suggests distinguishing two functions of land management practices: (i) interception of the diffuse runoff or shallow flow by devices located according to the agricultural plots limits and (ii) interception of concentrated flow by devices located according to the channel network and its ramifications upstream.

Lecomte (1999) simulated nine different spatial distributions of grass strips in an agricultural catchment. She showed that for each distribution the global runoff reduction and sediment removal efficiency was changed, a change in localisation of the grass strips having more effect than a variation in size of the grass strips staying in the same position.

Fryirs et al. (2007) in a work on large-scale systems proposed that the effects of buffers in catchments depends on their scale and on the localisation of sediment conveyance channels: "the location of any given floodplain pocket determines whether its

primary role is to disconnect lateral or longitudinal linkages. In headwater zones, floodplains or alluvial fans disconnect lateral linkages by buffering slopes and valley floors at the zonal scale. However in lowland zones, floodplain accretion removes sediment from the [connectivity] cascade, thus also disrupting longitudinal sediment conveyance at the system scale". Catchment configurations (spatial distribution of objects) are key elements determining responses to rainfall and erosion events. The spatial distribution of land management practices in an agricultural catchment determines the capacity of any given part of the catchment to reduce or increase the global sedimentological connectivity (Cammeraat and Imeson, 1999; Fitzjohn et al., 1998).

The complexity of interactions between sediment flow and land management practices (e.g. vegetative filters) presented above makes difficult to take these elements into account in catchment scale erosion models. Thus, few models either conceptual or physically based represent the hydrodynamic impact of interface objects and their distribution in the catchment. In the following section we will expose how present-day erosion models take into account the influences of land management practices on sediment transport in agricultural catchments.

2.3 Sedimentological connectivity of agricultural landscape in catchments scale erosion modelling

Many erosion models such as EUROSEM, EMSS, WEPP, LISEM, SEMMED, LASCAM (Table 2.3) include soil conservation practices to predict the influence of these practices on sediment transport processes and therefore on sedimentological connectivity of the catchments. In this work we classify catchment scale erosion models in (i) those that apply the P-factor USLE approach, (ii) those that apply SDR and derivations and (iii) those that include new objects with specific physical parameters like roughness coefficient or infiltrability to represent land management practices (Table 2.3).

2.3.1 Catchment scale models that apply USLE P-factor approach

The USLE (Universal Soil Loss Equation) was originally developed in the 1970's for farmers as a tool to manage soil erosion processes at the field scale. The USLE relates erosion rate to six multiplicative factors:

$$E = R \times K \times L \times S \times C \times P \tag{2.8}$$

Table 2.3: Present-day erosion models and their description of sedimentological connectivity

Model	**Type**	**Sediment Connectivity Approach**	**Reference**
AGNPS	Conceptual	USLE + SDR	Young et al. (1987)
HSPF	Conceptual	SPP	Johanson et al. (1980)
LASCAM	Conceptual	SDR	Viney et al. (2000)
SWRRB-WQ	Conceptual	RUSLE	USEPA (1994)
STREAM	Empirical/Conceptual	SPP	Cerdan et al. (2002)
SEMMED	Empirical/Conceptual	RUSLE	de Jong et al. (1999)
SEDEM	Empirical/Conceptual	RUSLE	Van Rompaey et al. (2001)
SWIM	Empirical/Conceptual	RUSLE	
SedNet	Empirical/Conceptual	USLE + SDR	
SWAT	Empirical/Conceptual	USLE + SDR	Arnold et al. (1996)
EUROSEM	Physical	SPP	Morgan et al. (1998b)
SHETRAN	Physical	SPP	Ewen et al. (2000)
PERFECT	Physical	USLE + RUSLE	Littleboy et al. (1992)
ANSWERS	Physical	USLE + SPP	Beasley et al. (1980)
GUEST	Physical	SPP	Yu et al. (1997)
CREAMS	Physical	USLE	Knisel (1980a)
LISEM	Physical	SPP	De Roo et al. (1996b)
WEPP	Physical	SPP	Laflen et al. (1997)
TOPOG	Physical	SPP	Haskins and Davey (1991)
KINEROS	Physical	SPP	Woolhiser et al. (1990)

where E is the mean annual soil loss, R is the rainfall erosivity factor, K is the erodibility factor, L is the slope length factor, S is the slope steepness factor, C is the crop management factor and P is the land management practices factor.

By definition the P-factor is the ratio of soil loss with a specific land management practice to the soil loss from a plot without any practice application. The USLE proposes tables of P-factor values for different land management practices including contouring and vegetated strips. The P-factor is dimensionless with values ranging from 0 to 1. Zero indicates a perfect land management practice (no sediment passes) and one represents an inefficient land management practices (all sediment passes). P-factor is calculated in function of slope length, slope steepness and strip width (Table 2.4).

The P-factor values presented in Table 2.4 were empirically estimated using annual averages of soil loss on standardised plots. When "terraces" is chosen in the USLE, the P-factor value used is that of the contouring practice with corrections on the LS-factor

Table 2.4: P-factor from USLE for different erosion-control practices

Erosion-control Practice	slope (%)	P-factor value
Contouring	1-2	0.60
	3-5	0.50
	6-8	0.50
	9-12	0.60
	13-16	0.70
	17-20	0.80
	21-25	0.90
Stripcopping	1-2	0.45
	3-5	0.38
	6-8	0.38
	9-12	0.45
	13-16	0.52
	17-20	0.60
	21-25	0.68
Grass Strip 10% cover	1-2	0.55
	3-5	0.45
	6-8	0.45
	9-12	0.55
	13-16	0.65
Grass Strip 20% cover	1-2	0.50
	3-5	0.40
	6-8	0.40
	9-12	0.50
	13-16	0.55
Grass Strip 30% cover	1-2	0.40
	3-5	0.35
	6-8	0.35
	9-12	0.40
	13-16	0.50
Grass Strip 40% cover	1-2	0.35
	3-5	0.30
	6-8	0.30
	9-12	0.35
	13-16	0.40
Grass Strip 50% cover	1-2	0.30
	3-5	0.25
	6-8	0.25
	9-12	0.30
	13-16	0.35
Level bench terrace	-	0.14
Reverse-slope bench terrace	-	0.05
Outward-sloping bench terrace	-	0.35
Level retention bench terrace	-	0.01

Source: Wischmeier and Smith (1978); Roose (1977) and Chan (1981)

associated with the slope length represented by the horizontal spacing between terraces. But as shown by Chan (1981) this approach is not appropriate for bench terraces so he established new values of P-factor for bench terraces from researches in Taiwan (showed at the end of Table 2.4).

Models like AGNPS, PERFECT, SWIM use the P-factor from USLE to describe the influence of VF on sediment production and transport for agricultural catchment. Other models like CREAMS, SEMMED and SEDEM are based on the RUSLE that estimate annual sheet (diffuse) and rill (concentrated) erosion rates with revised parameters. They represent sedimentological connectivity with a modified transport capacity for each land management practice. The P-factor values in RUSLE are often experimentally determined and transport capacity equations for each land management practice (grass strips, riparian vegetation, hedge, terraces) is calculated in accordance.

In the RUSLE the P-factor for contouring, grass strips and strip-cropping is determined by Equation (2.9) (Wischmeier and Smith, 1978):

$$P = \frac{(g_p - B)}{g_p} \tag{2.9}$$

where P is the P-factor, g_p is the potential sediment load in the incoming flow and B is the amount of deposition provided by the vegetated filter, given as a percentage.

To compute erosion and sediment transport or deposition, the RUSLE proposes four cases, (i) net erosion occurs everywhere in the practice, (ii) net deposition occurs everywhere in the practice, (iii) both deposition and erosion occur in the practice and (iv) runoff ends up within the practice. For each case the RUSLE relies on specific equations to determine B and g_p using empirical parameters and basic erosion concepts referring to vegetation type and crop characteristics to determine the P-factor (Renard and Foster, 1983).

2.3.2 Catchment scale erosion model using SDR and Derivations

Some models based on the P-factor may also use the SDR concept to estimate the transport of sediments from source to sink areas. The SDR has been proposed to correct the gross soil loss rate simulated by the USLE (Wischmeier and Smith, 1978) and so to be able to assess erosion rate at catchment scale. The SDR is defined as the proportion of gross erosion that is transported from a given area in a given time. The SDR is a sediment transport efficiency (Lu et al., 2006), expressed as:

$$SDR = \frac{Y}{E} \tag{2.10}$$

where Y is the annual average sediment yield at the outlet per unit area and E is the average annual gross erosion from field over the same area (Richards, 1993; Walling, 1983). It represents the average sedimentological connectivity between sources and sink areas within the catchment in an unique value.

There are many factors that may influence the SDR including rainfall, vegetation, topography, soil properties, land management practices, agricultural managements and their complex interactions. There is no precise procedure to estimate the SDR in the handbook published by USDA (1972). The SDR is often estimated with the empirical SDR-area power function $SDR = \alpha A^{\beta}$, where A is the area of the catchment and α and β are empirical parameters linked to available field information about sediment transport and rainfall-runoff processes in the catchment (Lu et al., 2006). Field measurements have suggested that β values range from 0.01 to -0.025, meaning that the SDR decreases with increasing catchment areas. On the other hand, the relation between the SDR and the drainage area may widely change from one to another catchment: catchments with similar areas may have different values of α and β because of the topography and deposition zones existing in the catchment.

Other relationships were developed between the SDR and various physiographic attributes. For example in the model SWAT (Arnold et al., 1996), the SDR is calculated from the runoff by:

$$SDR = \left(\frac{q_p}{r_{ep}}\right)^{0.56} \tag{2.11}$$

where q_p is the peak runoff rate and r_{ep} is the peak rainfall excess rate. Intuitively, a humid catchment usually has a higher SDR due to more rainfall. The SDR is also associated with the rainfall pattern: a longer rainfall event with less intensity has a lower SDR than a short rainfall event with a higher rainfall intensity.

Williams and Berndt (1977) proposed another equation to predict the SDR in function of the slope steepness of the mainstream channel:

$$SDR = 0.627 SLP^{0.403} \tag{2.12}$$

where SLP is the slope steepness of the main stream channel. A catchment with steep slopes delivers more sediments than a watershed in a flat landscape. The shape of a watershed may also affects the SDR: narrow catchments have high SDR's.

Traditionally the methods used to estimate the SDR are often data-driven. They require long periods of sediment yield records and precise measures of hillslope and plot erosion rates. New versions of the SDR were applied in single events erosion models like the MUSLE model (Williams and Berndt, 1977), (SWAT)(Arnold et al., 1996), WEPP (Ascough et al., 1997). The experimental results presented by Beuselinck et al. (2002)

showed that the SDR is dependent on flow discharge, sediment concentration, grain size distribution and slope.

2.3.3 Catchment scale erosion model using specific physical parameters

Physically based models were developed to predict spatial patterns of runoff and sediment yield over the land surface during individual rain events. They are based on mass conservation and energy conservation laws. To simulate the influence of land management practices over runoff and sediment transport, these models often include specific parameters or allow specific values of existing parameters describing roughness or soil infiltrability.

Almost all physically-based and process-based erosion models adopt the concept of transport capacity to distinguish between sediment transport and deposition (Sander et al., 2007). The sediment transport capacity T_c is defined as the maximum amount of sediment possibly carried by the flow (Foster, 1982), as a function of sediment size, flow velocity and turbulence conditions, among others. Sediment transport capacity is often derived from experimentations. For example Foster (1982) proposed that sediment transport capacity is a function of shear stress exerted by the flow on the bed:

$$T_c = \eta(\tau - \tau_c)^{kt} \tag{2.13}$$

where T_c is the transport capacity, η is the transport efficiency of sediment, kt is an exponent determined empirically and fixed at 1.5 after the work of Finkner et al. (1989), τ is the flow shear stress calculated as $\tau = V \cdot S$ (V being the flow velocity and S the bedslope) and τ_c is the critical shear stress over which detachment is initiated.

Vegetative filters reduce flow velocity, decreasing flow transport capacity. This principle is reproduced in physically-based erosion models by increasing roughness parameters, reducing flow velocity and decreasing flow transport capacity and thus promoting sediment deposition. The way a model applies this principle depends on the spatial description of processes. In a raster-based model one can give high values of roughness for a group of pixels to represent a vegetative filter: for example the model LISEM (De Roo et al., 1996b) offers the possibility to include grass strips by modifying physical parameters pertaining to the gridcell corresponding to the grass strips and bearing specific values of infiltrability and of the Manning coefficient. In the same way EUROSEM (Morgan et al., 1998b), KINEROS (Woolhiser et al., 1990), SHETRAN Ewen et al. (2000) and TOPOG Haskins and Davey (1991) propose modified values of the Manning coefficient and infiltrability to signal the existence of land management

practices on the catchment. Figure 2.6 shows values of the Manning coefficient for various vegetation covers in cited erosion models, compared to values for bare soils.

Vector models provide the option to include new surface objects with specific values of roughness coefficients to represent vegetative filters. The WEPP model (Laflen et al., 1997) allows the application of "impoundments", namely terraces, farm ponds and check dams. All have the same effect of reducing flow velocity, resulting in decreasing flow transport capacity and causing sediment to settle out of suspension. In these models, the use of these object is restricted to the channels, the sediment trapping capacity of each impoundment being function of its type and geometry, previously defined by the model user. The sediment trapping efficiency is calculated in function of particle size, Manning coefficient and peak discharge. For hillslopes WEPP integrates new values of the Manning coefficient and soil hydraulic conductivity specific to grassy areas: WEPP reproduces the expected effect of runoff reduction by increasing roughness and infiltrability.

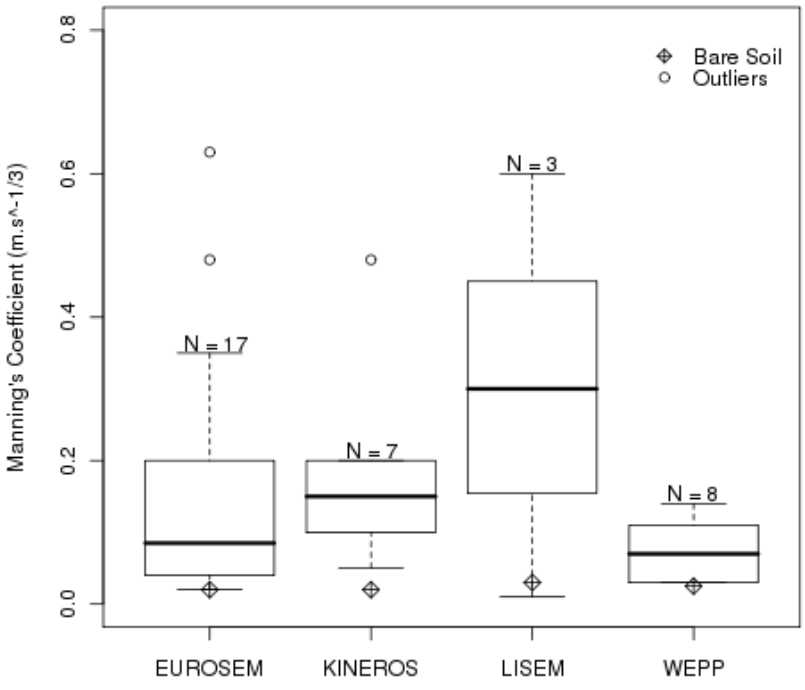

Figure 2.6: Boxplot of Manning's coefficient proposed to grass in erosion models

2.3.4 Comparison of sedimentological connectivity modelling approaches in catchment erosion models

Most erosion models listed in Table 2.3 use the USLE P-factor approach to deal with discontinuities provided by agricultural activities and land management practices in catchments. The P-factor associated to the C-factor in the USLE based models works as a connectivity factor that controls the transport of water and sediment from the source to the sink areas. The P-factor is a type of sediment transport efficiency empirically estimated by annual average measurements. With the RUSLE development the P-factor was revised and genericity was gained by taking into account new land management practices. The P-factor in the RUSLE is also obtained from experimental data, supplemented by analytical experiments (USDA, 1997) including observations of cause/effect relationships drawn from CREAMS model simulations. But the P-factor stays a hillslope or field scale factor addressing local connectivity, based on specific measurements. In particular, it does not integrate the effects of spatial distributions of land management practices on sediment removal for entire catchments composed of multiple (organised) entities. To integrate the distributed effects in the P-factor some models appealed to the concept of the SDR to moderate the predicted soil loss when upscaling.

The SDR is in itself an integration of catchment connectivity factors. There are many problems debated in literature about the SDR. Firstly, the SDR requires long periods of sediment yield records. Secondly, approaches based on the SDR do not allow to localise sediment sources (Bracken and Croke, 2007) which is a major drawback. Thirdly, as argumented by Parsons et al. (2004) the SDR is frequently used to correct overestimation of erosion at large scales, the SDR definition being however incompatible with process-based modelling.

Values for the SDR reported in literature range from less than 0.1 to almost 1 (Walling, 1983). As remarked by Graf (1988) and Wainwright et al. (2001), the SDR concept is ill-defined in the long-term because the sediment flux at the catchment outlet should match that from the hillslopes, otherwise catchments, would be progressively filling up with sediment, which is demonstrably false in most cases. Parsons et al. (2006) argued that most of the sediments transported by streams in the short term are delivered from the bed and banks of the channels, flushing the alluvial and colluvial deposits out of the catchment. Consequently, if sediment yield is to be related to an area, it should be the area that could potentially contribute to sediment yield to the channel over the period of measurement. It should not be the area of the entire catchment.

Spatially distributed physically based erosion models propose modified parameters of roughness and infiltrability for vegetated filters. Some of the models allow to spatiality distribute vegetated filters to study the effects on sediment trapping. The global sedimentological connectivity of the catchment is addressed by changing physical properties like roughness or infiltrability in order to represent land management practices. The problem is that equations in the model may be applied out of their domain of validity. For example, hydraulic equations often used in erosion models are not valid anymore when water height is equal to the surface roughness, which is debated by Lawrence (2000). She indeed recommended the use of different formulations for flow resistance according to relative submergence of the obstacles in the flow. Few models integrate the influence of the relative submergence of vegetation on values of the chosen friction coefficients (Wilson et al., 2005), the default option being wrongly assuming constant values for these coefficients.

Beside these modelling approachs Borselli et al. (2008) recently proposed a method to estimate a hydological and sedimentological connectivity index based on GIS parameterisation and field observations. This index could be used for parameterisation of spatially distributed erosion model.

2.4 Conclusion

Land management practices in agricultural catchments may affects runoff and sediment response by changing sedimentological connectivity. Walling et al. (1999) and Morgan (2005) among others, have shown that changing from natural vegetation to cultivation can increase soil erosion rates by an order of magnitude. Increasing soil erosion by rill development has a direct relationship with increased sedimentological connectivity. Ludwig et al. (1995) found that interactions between agricultural and topographic features resulted in a complex hydrological hillslope structure, which consisted of a runoff collector network composed of topographic or agricultural depressions. Land management practices have as objective to reduce runoff energy and volume by increases local infiltration and surface roughness. A good example of these land management practices are the vegetated filters. Theoretical aspects of vegetated filters confirm the complexity of vegetation-flow interaction. All theoretical studies converges to conclude that the effective roughness of a vegetated filter depends on the relative submergence of vegetation. The hydraulic resistance of vegetation decreases with increasing relative submergence. The hydraulic resistance of vegetation is linked to sediment transport capacity. Experimental aspects from literature of vegetated filters presented above

demonstrate that sediment trapping efficiency may be not completely derived from physical characteristics like width, slope or particle sediment size. Statistical tests from literature presented above demonstrate that trapping efficiency has no significant correlation with width and slope of vegetated filter. However, it was showed that efficiency is well correlated with flow discharge in according with the Deletic and Fletcher (2006); Sabbagh et al. (2009) works.

At the catchment scale, the spatial distribution of vegetated filters is one of the most important factor to determine catchment sedimentological connectivity. As showed by Lecomte (1999) the distributed organisation of grass strips in a catchment may have strong influences in the global sediment removal efficiency. Vegetated filters placed at the top of catchment have low impact in sediment removal, whereas when vegetated filters places downslope of agricultural fields in a progressive logic to the outlet, sediment removal is maximised. The use of experimentation to estimated the effect of spatial organisation in sediment exportation of erosion processes may be very expensive and difficult to apply, this is one reason for the development of distributed erosion models.

Several models propose to take into account the impact of land management practices in catchment sediment connectivity. Some models are based in the USLE P-factor to take into account the influences of land management practices in the sediment transport the catchment. However, P-factor of USLE acts only in sediment production and not in sediment transport. P-factor is not sensitive the location of the land management practices, it is a multiplicative factor on the USLE equation, if we place a vegetative filter at the top of a hillslope or at the end of a hillslope P-factor will have the same value. Other models uses the SDR approach to take into account the discontinuities the catchment. SDR is often calculated as a function of the catchment area (USDA, 1972). The limitation of these approaches (P-factor and SDR) is that they do not integrate the effects of spatial distribution of land management practices on sediment removal of the entire catchment. No information about sediment sources are given by these approaches. Thus we can conclude that these approaches may not give information about the optimisation of the spatial distribution of land management practices over the catchment scale.

The distributed physically based approaches propose to take into account the effects of spatial organisation of land management practices on sedimentological connectivity. They address sedimentological connectivity changing physical parameters such as: surface roughness and soil infiltrability. The advantage of this approach compared to the others is the spatialisation of the parameterisation.

The limitation is that changing physical parameters (roughness or infiltrability)

without observing the model equations validity domain may be dangerous. In fact, in this review we have identified a lack of an "intermediate" approach between very detailed descriptions of management practices not taking into account their distribution, and "black boxes" not offering sufficient understanding of the processes governing sediment filtration. A possible "intermediate" approach may be a coupling between specific management practices local models that are very detailed description of processes and physically based distributed erosion models. However, this intermediate approach should simplify the specific management practices equations to save the parameter parsimony principle and computation time.

Conclusion et conséquences pour les choix d'une modélisation

Synthèse sur les paramètres d'érodibilité

Il existe dans la littérature un grand nombre de données de référence pour les valeurs d'érodibilité du sol évaluées par des méthodes standard de type "parcelles de Wischmeier". C'est une raison majeure de l'emploi massif de cette méthode d'évaluation de l'érodibilité par la communauté scientifique. Cependant, cette méthode standard appliquée sur des parcelles de plusieurs m^2 ne permet pas de dissocier les processus relatifs à l'hydrologie, à l'érosion diffuse et à l'érosion linéaire. Ces méthodes sont en effet fortement influencées par les processus hydrologiques. Les sols sableux ont généralement une haute capacité d'infiltration et une faible transportabilité, ce qui résulte en un faible ruissellement, donc une faible érosion, et donc une faible érodibilité. Par conséquent, cette méthode de caractérisation de l'érodibilité ne semble pas judicieuse pour les modèles qui considèrent séparément les processus d'érosion diffuse et linéaire. Pour ces modèles, nous pensons que les méthodes locales de caractérisation de l'érodibilité diffuse -c'est à dire les tests d'impact de gouttes, de « splash cups » ou de stabilité structurale- sont préférables puisqu'ils permettent de paramétrer spécifiquement ce processus. Il serait dès lors intéressant de mener une étude comparative de ces différentes méthodes locales, mais le manque de données disponibles pour les méthodes splash cups et tests d'impact de gouttes ne l'a pas permis. Parmi ces tests locaux, la méthode de stabilité structurale du sol nous paraît l'approche à favoriser pour deux raisons principales. La première est l'existence, dans la littérature, d'un grand nombre de jeux de données pour les méthodes de stabilité structurale du sol normalisées (Kemper ou Le Bissonnais). La seconde est que cette méthode fournit également des informations sur la taille des particules susceptibles d'être transportées, taille qui conditionne les distances de transport des particules de sol.

La sensibilité des modèles d'érosion au paramètre d'érodibilité diffuse est fréquemment considérée comme faible à moyenne dans la littérature, en comparaison avec les paramètres hydrologiques telle que la conductivité hydraulique à saturation ou le potentiel d'entrée d'air du sol. Ces résultats méritent d'être approfondis car les tests de sensibilité généralement conduits dans la littérature sont souvent limités à des conditions hydrologiques fortes, voire extrême, alors que l'on sait que la sensibilité à un paramètre peut être fortement dépendante de ces conditions.

Synthèse sur l'effet des interfaces sur la connectivité sédimentologique

Dans les bassins versants agricoles les aménagements peuvent affecter les réponses hydrologiques et sédimentologiques en modifiant la connectivité du bassin versant. Morgan (2005) and Walling et al. (1999) ont montré que la disparition de la végétation naturelle au profit des cultures agricoles peut augmenter les taux d'érosion d'un ordre de grandeur.

Les pratiques et aménagements anti-érosifs ont pour objectif de réduire le ruissellement et l'érosion en augmentant l'infiltrabilité locale et la rugosité de la surface. Un des aménagements les plus répandus dans les milieux cultivés est le filtre végétal qui inclue les bandes enherbées, les haies et les talus. Plusieurs études théoriques et expérimentales à l'échelle locale ont confirmé la complexité de l'interaction entre le flux d'eau et la végétation. Les expériences avec des filtres végétaux ont démontré que la capacité de filtration d'une bande enherbée, par exemple, ne peut pas être complètement connue à partir de ses caractéristiques physiques (pente, largueur, densité). La capacité de filtration est aussi dépendante des conditions de flux à travers le filtre.

A l'échelle du bassin versant, la distribution spatiale des filtres végétaux devient un facteur très important pour déterminer la connectivité sédimentologique des bassins versants agricoles. Lecomte (1999) a démontré que l'organisation spatiale des bandes enherbées peut fortement influencer l'efficacité globale du filtrage des sédiments dans le bassin. Un filtre végétal placé dans les parcelles amont du bassin a un faible impact sur l'efficacité globale, tandis qu'un filtre placé en fonction des lignes d'écoulement peut largement améliorer l'efficacité globale.

Plusieurs modèles proposent de prendre en compte l'impact des aménagements sur le transport de sédiments d'une partie du bassin versant à un autre (connectivité sédimentologique). La plupart des modèles utilisent pour cela le P-facteur de l'équation universelle de perte en sol (USLE). Or, le P-facteur décrit seulement la production de

sédiments et non leur transport. De plus, il ne tient pas compte de la localisation spatiale de l'aménagement. D'autres modèles utilisent le SDR (*Sediment Delivery Ratio*) pour contrôler le transport de sédiments dans le bassin versant, mais cette approche n'intègre pas non plus les effets de la distribution spatiale des aménagements. Seuls quelques modèles distribués à base physique le permettent. La prise en compte des aménagements se fait alors en créant, dans la segmentation du bassin versant, des entités spatiales représentant ces aménagements sur lesquelles des valeurs particulières des paramètres physiques tels que la rugosité ou l'infiltrabilité sont affectées. Les principaux inconvénients de cette approche sont la surparamétrisation et le risque de sortir du domaine de validité des équations du modèle.

Dans cette synthèse bibliographique, nous avons identifié le manque d'une approche intermédiaire entre les descriptions très détaillées, mais très lourdes, des aménagements, qui sont donc difficilement applicables à l'échelle du bassin versant, et les modèles de "boîtes noires" basés sur le P-factor, qui ne prennent pas en considération leur disposition dans l'espace. Une possible approche intermédiaire pourrait être une combinaison entre les modèles locaux d'aménagements spécifiques (TRAVA, VFSMOD) et les modèles d'érosion distribués et à base physique. Cette approche intermédiaire consisterait à simplifier les équations des aménagements spécifiques pour en dégager des comportements fonctionnels basés sur un nombre limité de paramètres agissant au premier ordre. Ceci rendrait possible leur introduction en nombre non limité dans les modèles d'érosion distribués.

Conséquences pour les choix d'une modélisation

L'analyse bibliographique générale indique un certain nombre de consensus généraux et aussi des limites concernant les modèles d'érosion hydrique. Ces consensus indiquent que les modèles d'érosion hydrique doivent être basés sur un modèle hydrologique robuste. Pour tenir compte de la dynamique spatiale et temporelle, les modèles distribués à base physique semblent les plus adaptés, et pour bien représenter les processus d'érosion il semble nécessaire de séparer les mécanismes de détachement et de transport de particules, et notamment les processus d'érosion concentrée et d'érosion diffuse.

Pour le développement du modèle MHYDAS-Erosion, nous nous sommes appuyés sur ces consensus généraux et nous avons choisi d'utiliser un modèle hydrologique déjà développé et validé pour les échelles temporelle et spatiale qui nous préoccupent. Nous avons choisi de développer un modèle d'érosion distribué à base physique qui décrit séparément les processus d'érosion concentrée et diffuse. Nous nous appuyons pour

cela sur les équations et paramètres utilisés dans les modèles existants, en y introduisant des modifications concernant les deux questions explorées dans l'analyse bibliographique, à savoir une représentation des processus d'érosion diffuse à l'aide d'un paramètre d'érodibilité déduit de mesures de stabilité structurale, et une gestion de la connectivité sédimentologique permettant la prise en compte d'éléments anthropiques comme les bandes enherbées. Ces modifications constituent les principales originalités du modèle développé. Le modèle est structuré sous forme de modules implémentés au sein de la plate-forme de modélisation OpenFLUID ($http://www.umr-lisah.fr/openfluid/$) développée au LISAH, modules qui complètent le modèle hydrologique de base MHYDAS. Le format modulaire facilite l'implémentation de nouvelles fonctionnalités, d'autres processus érosifs ou de descriptions alternatives des mêmes processus. La stratégie de modélisation proposée par Refsgaard (1997) où chaque étape du processus est bien définie à partir un organigramme logique, a été suivie pour faciliter le processus de développement. La partie suivante expose les étapes de développement et de conceptualisation du modèle d'érosion développée dans le cadre de ce travail de thèse.

Part II

Modélisation

Introduction

Les modèles d'érosion distribués et à base physique consistent en un ensemble d'équations mathématiques permettant une représentation simplifiée du milieu naturel et des processus de détachement et de transport de sédiments dans le paysage. Il existe autant de modèles que de scientifique puisque chaque modèle correspond à une problématique donnée (Refsgaard, 1997). Beven (2000) rappelle les cinq étapes dans toute démarche de modélisation. La première étape pose le problème du choix du type de modèle et de représentation du système, la deuxième concerne le choix des équations pour représenter les processus, la troisième concerne la représentation des équations sous forme d'un code informatique, la quatrième concerne la paramétrisation et le calage du modèle, et la cinquième sa validation. Le passage d'une étape à la suivante n'est possible que sous certaines approximations. Par conséquent, les incertitudes sur les résultats finaux de la modélisation sont tributaires de toutes les approximations des étapes intermédiaires. Pour développer et appliquer une modélisation quelle qu'elle soit (dans notre cas à base physique), il est judicieux de suivre un protocole. Nous avons basé le notre sur celui de Refsgaard (1997), développé pour la modélisation hydrologique et adapté ici pour la modélisation de l'érosion figure II. Chaque étape sera expliquée en détail ci-dessous.

Protocole de modélisation

La définition de l'objectif

Dans le développement d'une modélisation, la définition de l'objectif doit être la première étape. Il s'agit de définir clairement si la modélisation est faite pour des fins prévisionnelles ou pour fournir une meilleur compréhension du phénomène à modéliser, car la définition de l'objectif a des conséquences sur la performance du modèle (Morgan, 2005). Une fois l'objectif bien connu, il est plus simple de choisir les moyens à employer (base physique, stochastique, empirique) pour résoudre le problème.

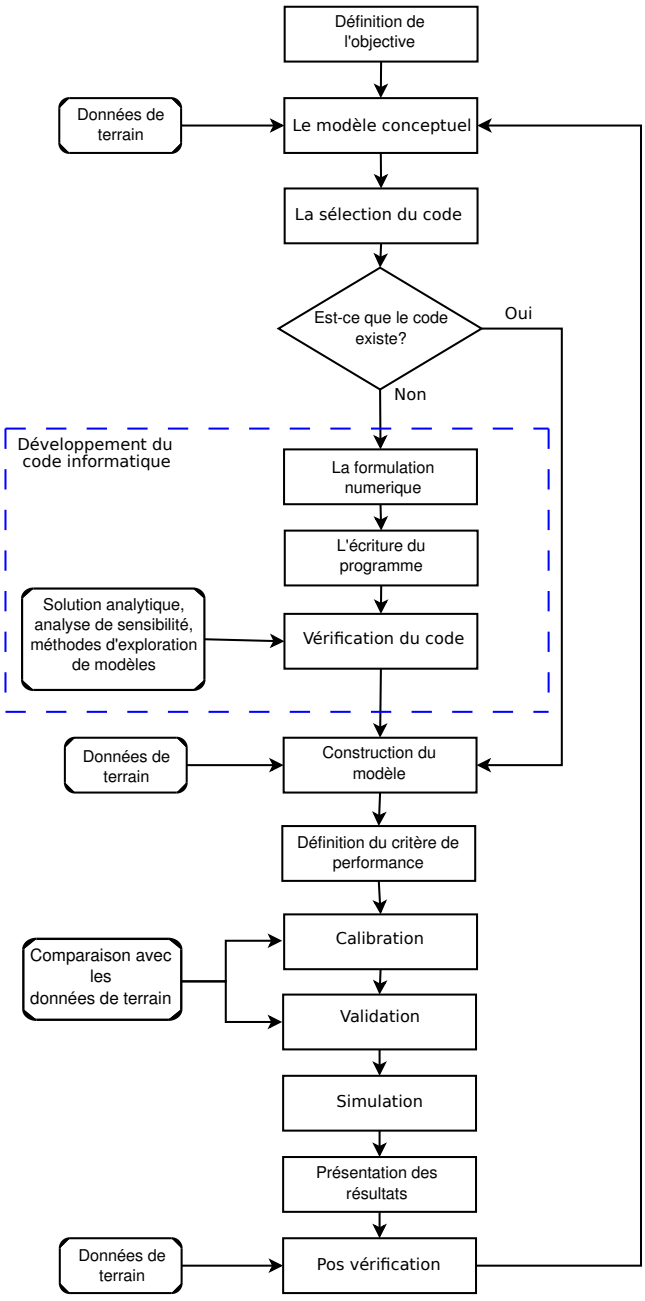

Figure II:Les étapes du processus de modélisation, adapté de Refsgaard (1997)

Le modèle conceptuel

En se référant à l'objectif de la modélisation et à l'analyse des résultats expérimentaux disponibles, le concepteur de la modélisation doit établir le modèle conceptuel. Le modèle conceptuel est développé en fonction de la perception qu'a le concepteur des principaux processus hydrologiques et d'érosion dans le bassin versant. Il intègre les simplifications jugées non abusives et utiles, au plan physique et mathématique, en particulier dans les résolutions numériques. Une méthode très utilisée est la construction d'un diagramme de boîtes où chaque boîte représente un processus, avec ses entrées et sorties ainsi que l'interaction avec les autres boîtes.

La sélection du code

Après avoir défini le modèle conceptuel, il est nécessaire de choisir un programme informatique pour résoudre le problème. Si le code de calcul existe il est nécessaire de bien s'assurer qu'il a été testé et vérifié pour les conditions d'utilisation spécifiques à la modélisation en question.

Si le code informatique n'existe pas il est nécessaire de le développer pour résoudre les équations du modèle mathématique numériquement. Le développement du code informatique peut être fait par étapes :

1. *La formulation numérique* - consiste a choisir la forme de solution la plus adaptée aux équations utilisées dans le modèle mathématique, ces solutions peuvent être de deux types : (i) solution analytique qui consiste à résoudre les équations "exactement" avec l'avantage d'une solution stable et robuste, mais avec l'inconvénient qu'une telle solution n'existe que pour des situations particulières, (ii) solution numérique qui consiste à résoudre les équations avec des approximations numériques (différences finies, volumes finis et éléments finis). L'avantage des solutions numériques par rapport aux solutions analytiques est que le numérique peut être appliqué à tous les cas possibles. Les inconvénients sont l'instabilité et le risque de non convergence, sans oublier le temps de calcul plus long;

2. *L'écriture du programme* - consiste à passer le code du langage humain au langage machine. Cette passage peut être fait en utilisent des langages intermédiaires tels que C^{++} ou FORTRAN qui après être compilés se transforment en langage machine. Le type de langage intermédiaire doit aussi être choisi en fonction de l'objectif final de la modélisation;

3. *La vérification du code* - consiste à comparer les résultats des solutions numériques avec des résultats analytiques et vice-versa. Une pratique répandue dans le domaine de l'hydrologie et de l'érosion est l'utilisation d'espaces virtuels tels que des bassins versants virtuels. Dans ces entités virtuelles, toutes les propriétés sont contrôlées et le nombre de paramètres ou de configurations paramétriques est limité. Une analyse de sensibilité et/ou l'application de méthodes d'exploration des modèles peuvent être très utiles à ce stade.

Le développement du modèle

Après avoir sélectionné ou développé le code informatique et avoir fait des mesures de terrain pour accéder aux valeurs des paramètres, il est temps de passer à la construction du modèle. Cette étape est celle du choix du type de discrétisation spatiale du bassin versant. Il faut aussi définir les conditions initiales et aux limites, c'est-à-dire déterminer le contour du domaine. Dans cette étape se fait également la paramétrisation du modèle, qui dans le cas des modélisations distribuées peut être facilitée par le recours à des outils de spatialisation du type Système d'Information Géographique.

La définition du critère de performance

Cette étape consiste a définir le critère de performance qui sera utilisé dans les étapes de calibration et validation du modèle. Pour définir le critère de performance, il faut faire un compromis entre le degré de précision voulu (connu à l'étape 1) et l'imprécision imposée par des observations de terrain. Comme montré par Nearing (2000) la définition du critère de performance doit prendre en compte la variabilité et l'incertitude intrinsèque des observations.

La calibration du modèle

Le calage consiste à sélectionner les paramètres d'un modèle de façon à ce que celui-ci simule le comportement hydrologique du bassin versant de la meilleure façon possible (Madsen, 2000). Il s'agit donc de rechercher le minimum d'une fonction mathématique reliant les données mesurées aux paramètres calculés. Mais le calage d'un modèle distribué pourrait être une histoire sans fin, où il y a toujours une possibilité d'amélioration (Refsgaard, 1997). Cette opération peut se faire manuellement, par essai et erreur ou automatiquement à partir d'algorithmes de recherche d'optimum (Ambroise, 1999). Le

calage devra commencer par la détermination du ou des critères d'adéquation du modèle et d'une méthode de recherche de l'optimum de la surface de réponse, lorsque de multiples paramètres sont impliqués.

De manière générale, le calage des modèles hydrologiques est problématique à cause de l'interdépendance et de la corrélation des paramètres entre eux, ce qui rend la surface de réponse discontinue, non dérivable, présentant plusieurs zones de convergence et des optima locaux (Beven and Binley, 1992a; Duan et al., 1992).

La validation du modèle

A l'issue du calage, il est nécessaire de vérifier la reproductibilité des résultats et la représentativité des paramètres calés. C'est l'opération de validation qui consiste à tester le modèle dans des conditions qui diffèrent du calage. (Klemes, 1986) propose un schéma hiérarchique en quatre points pour la validation des modèles : application du modèle à une série de données non utilisées pour le calage (Split sample test), transposition du modèle à d'autres zones géographiques (proxy-basin test), application du modèle au bassin versant de calage mais avec des données correspondant à un changement de l'occupation du sol ou du climat (differential split-sample test), transposition du modèle à d'autres zones climatiques (proxy-basin differential test). La validation peut porter soit sur le même type de variables et de critères que ceux qui ont servi au calage, c'est la validation mono-critère, soit sur d'autres variables et d'autres critères, c'est la validation multicritères. Il va de soi que les résultats de la validation seront tributaires de la qualité et du type de données utilisées pour le calage. Si la validation est faite sur des événements de faibles débits, la performance du modèle quant aux événements de fort débit peut être douteuse (Klemes, 1986).

La mise en place des simulations

Cette étape a pour but de vérifier la cohérence des prévisions faites par le modèle. Dans cette étape il est conseillé de faire une analyse de sensibilité du modèle aux paramètres d'entrée, afin d'identifier les paramètres les plus sensibles. Une autre analyse qui peut être très utile est l'étude de la propagation de l'incertitude d'entrée sur certains paramètres et son impact sur le résultat final du modèle.

La présentation des résultats

La présentation des résultats du modèle est une étape importante dans l'ensemble et elle doit faire référence à l'objectif. Aujourd'hui avec l'avancement technologique (Systèmes d'Information Géographique), des cartes peuvent être produites pour montrer par exemple la répartition des zones à haut risque d'érosion.

La post-vérification du modèle

La post-vérification est une autre possibilité de validation du modèle. Généralement elle est faite plusieurs années après l'étude de modélisation. Elle a pour but d'évaluer *a posteriori* les prédictions effectuées par le modèle lors de l'étape de simulation.

Dans le prochain chapitre nous allons brièvement rappeler les concepts du Modèle Hydrologique Distribué pour les AgroSystèmes MHYDAS ayant servi de support au développement du modèle d'érosion proposé dans le chapitre suivant de cette thèse.

Chapter 3

Le modèle hydrologique MHYDAS

Ce chapitre propose un bref rappel des concepts du modèle hydrologique distribué MHYDAS, modèle articulé autour de la segmentation de l'espace et des modules représentant les processus hydrologiques. Les processus présentés ici sont limités à ceux utilisés dans le modèle d'érosion MHYDAS-Erosion

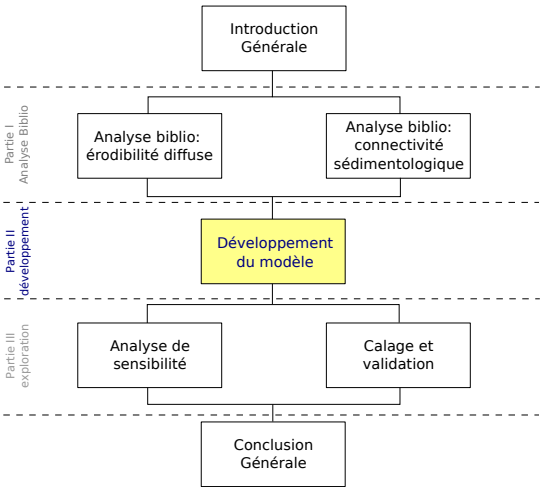

3.1 Rappel sur le modèle hydrologique MHYDAS

MHYDAS (Modélisation HYdrologique Distribuée des AgroSystèmes) n'est pas un modèle unique, mais une plate-forme de modélisation qui a été développée afin de comprendre et simuler les transferts d'eau et de polluants en milieu agricole. Sa structure modulaire permet à l'opérateur de choisir les options les plus appropriées à sa problématique. Nous limitons ici sa présentation à la version événementielle de crue, version la plus éprouvée ayant servie de base au développement de MHYDAS-Erosion.

3.1.1 Structure du modèle

MHYDAS est basé sur une segmentation de la surface du bassin versant en "unités de surface" (notées SU), une segmentation des nappes ou aquifères en "unités de nappes" (notées GU) et une segmentation du réseau hydrographique en tronçons (notés RS) figure 3.1. Une unité de nappe correspond à un groupe d'unités de surface. Chaque unité hydrologique est connectée soit à l'unité de surface située à l'aval si cette unité existe, soit à un tronçon du réseau hydrographique. Chaque unité hydrologique est aussi connectée à une unité de nappe. Chaque tronçon du réseau hydrographique est connecté à un tronçon aval et est connecté aussi à une unité de nappe. Le découpage en unités de surface et de nappes est effectué en mode vecteur, ce qui autorise la définition d'unités de formes très diverses. On peut ainsi représenter les discontinuités hydrologiques et la variabilité de l'occupation du sol en milieu agricole.

La Figure 3.2 illustre les principaux processus hydrologiques simulés dans MHYDAS. Sur chaque unité de surface (SU) la pluie est divisée en une partie qui s'infiltre et une partie qui ruisselle. L'eau s'infiltre verticalement dans la zone non-saturée pour atteindre la nappe. A la surface du sol, la partie non-infiltrée de la pluie est propagée sur les unités de surface et, *via* le réseau hydrographique, jusqu'à l'exutoire. Les processus d'échange nappe-rivière ainsi que la propagation du ruissellement à travers le réseau hydrographique sont pris en compte. Comme dans d'autres approches de modélisation (par exemple TOPMODEL ; Beven and Kirkby (1979)), on suppose que le toit de la nappe est parallèle à la surface du sol. Dans cette version de MHYDAS l'évaporation n'est pas prise en compte, la restriction à des événements de crue permettant de négliger ce processus en comparaison des autres processus.

Dans les parties suivantes, nous présentons la procédure de segmentation de l'espace, les processus hydrologiques représentés, les paramètres utilisés et les limites actuelles du modèle.

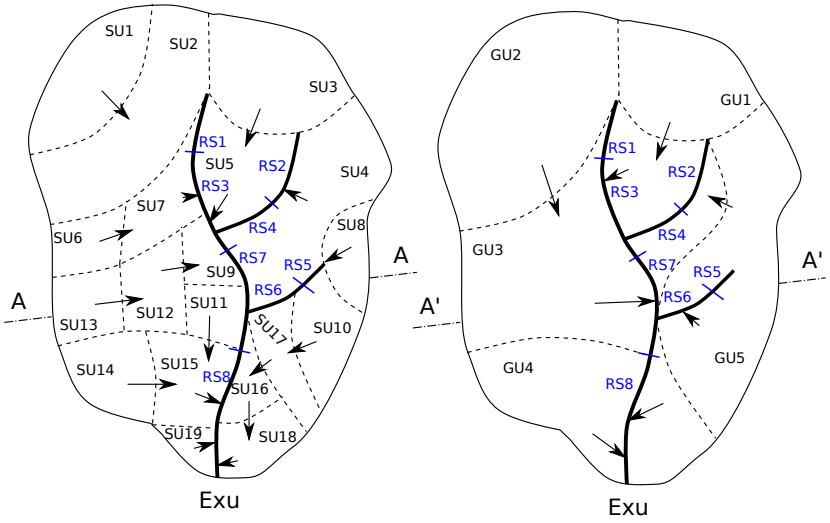

Figure 3.1: Exemple de découpage et de codage d'un bassin versant générique en unités de surface (SU), unités de nappes (GU) et tronçons de réseau hydrologique (RS).

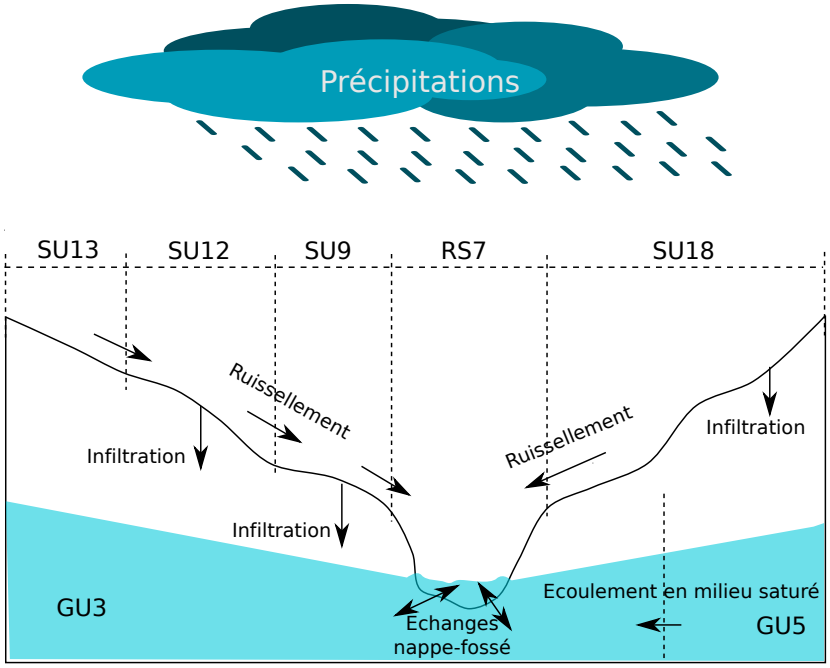

Figure 3.2: Processus hydrologiques représentés dans MHYDAS sur une coupe AA' de la Figure 3.1

3.1.2 Segmentation de l'espace

Le milieu agricole peut présenter de nombreuses discontinuités hydrologiques qui doivent apparaître dans le découpage de l'espace afin de pouvoir simuler la manière dont elles "interfèrent" dans le calcul hydrologique Gumiere et al. (2009c). Une procédure de segmentation de l'espace codée sous GRASS a été développée au sein du laboratoire LISAH (Lagacherie et al., 2009). La procédure comporte trois étapes :

1. Définition des "surfaces élémentaires";

2. Définition des contraintes et hiérarchisation des frontières des surfaces élémentaires;

3. Définition des "unités de surface".

La première étape consiste à définir des "surfaces élémentaires" en se basant sur les données cartographiques disponibles. La Figure 3.3 illustre un exemple exploitant les données de quatre cartes : limites du parcellaire, réseau hydrographique, carte des sols et MNT. Afin de réduire le nombre des surfaces élémentaires et par conséquent les temps de calcul du modèle, la procédure de segmentation de l'espace opèrent un regroupement des surfaces élémentaires pour définir des "unités de surface (SU)". Pour l'utilisation du modèle d'érosion nous avons choisi de garder une carte des SU la plus proche possible de la carte des parcelles agricoles, en privilégiant la cohérence physique des données.

La deuxième étape consiste à définir des contraintes pour former les frontières des surfaces élémentaires et ensuite les hiérarchiser. Une première contrainte définit une aire seuil minimale A_l pour toutes les unités de surface. Une seconde contrainte définit un "ordre d'importance" des frontières des surfaces élémentaires, imposé par l'opérateur en fonction des processus hydrologiques à modéliser.

Dans la troisième étape, les surfaces élémentaires sont regroupées en respectant les contraintes précédentes, ce qui définit les unités hydrologiques par une procédure itérative. Toutes les frontières des surfaces élémentaires ayant une aire inférieure à A_l sont identifiées. Tout d'abord, la frontière ayant l'ordre le moins important - si elle existe - est éliminée, et la surface élémentaire est accolée à sa voisine. Cette procédure est ensuite répétée pour toutes les frontières d'ordre d'importance supérieur. La procédure de regroupement est arrêtée lorsque la surface élémentaire est supérieure à A_l.

La Figure 3.3 montre les unités de surface obtenues par regroupement des surfaces élémentaires.

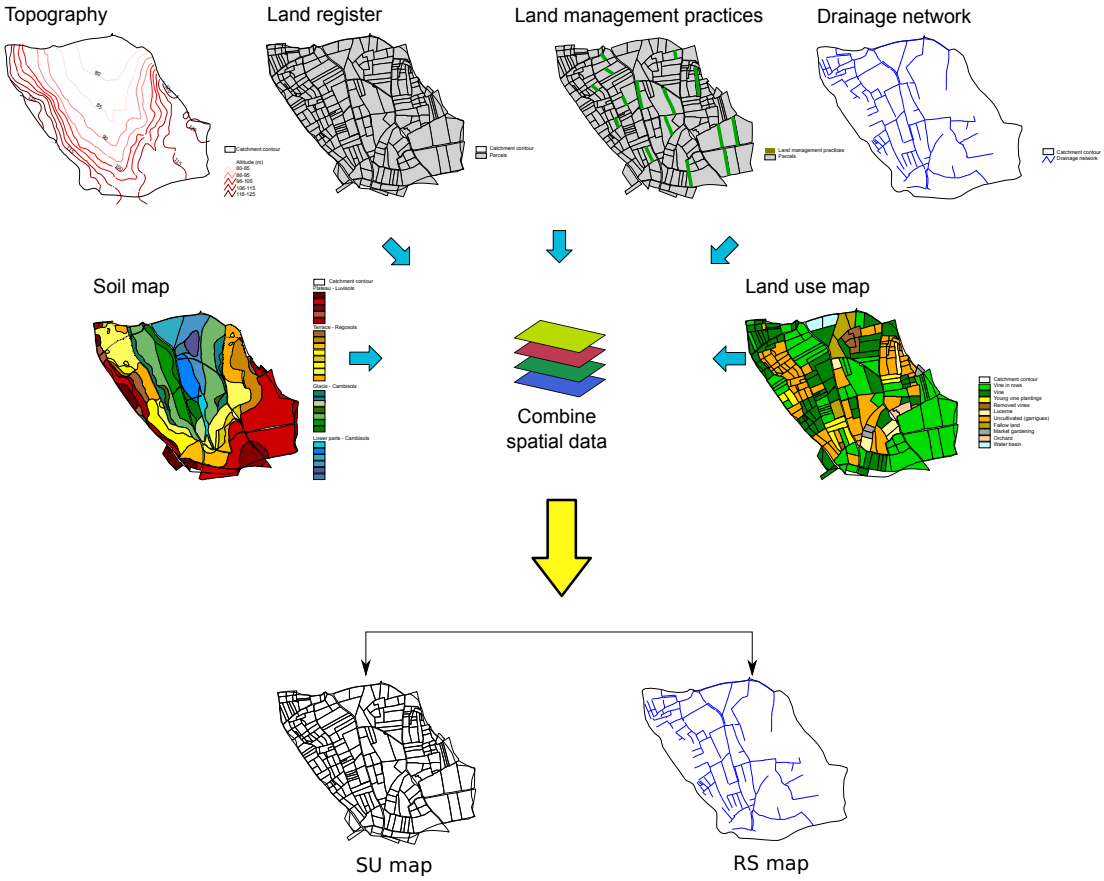

Figure 3.3: Processus de découpage de MHYDAS

La procédure de segmentation de la surface permet de définir les unités de surface, leurs caractéristiques géométriques (aire, pente, forme) ainsi que les liens topologiques entre elles et avec les tronçons du réseau hydrographique. Le découpage du milieu souterrain en unités de nappes est réalisé en dernier, de façon manuelle en se basant sur l'analyse des données piézométriques.

3.1.3 Processus hydrologique

Sur chaque unité de surface, la fonction de production de MHYDAS sépare la pluie en deux composantes, le ruissellement et l'infiltration. MHYDAS propose huit fonctions de production toutes basées sur des équations d'infiltration en une dimension sur la verticale :

- Cinq modèles à base physique : le modèle de Richards – 1D (Lehman and Ackerer, 1996; Richards, 1931), le modèle de Parlange and Haverkamp (1989), le modèle simplifié de Green and Ampt (1911) ou sa variante Morel-Seytoux (1978), le modèle de Philip (1957), et le modèle de Corradini et al. (1994, 1997). Ces modèles sont basés sur les équations de Richards ou leurs simplifications et par conséquent nécessitent une bonne connaissance des propriétés hydrodynamiques du sol et des conditions initiales d'humidité sur un profil vertical;

- Trois modèles basés sur une représentation simplifiée du milieu : un modèle à réservoir du type Diskin and Nazimov (1995) et les deux modèles empiriques de Horton (1933) et du *Soil Conservation Service* (USDA, 1972).

Ces modèles d'infiltration ne consommant pas beaucoup de temps de calcul sont bien adaptés pour simuler les flux d'eau aussi bien à l'échelle locale qu'à l'échelle du bassin versant. Cependant, ces modèles ne permettent pas la simulation des écoulements horizontaux dans le sol et notamment les mécanismes d'échanges nappe-rivière. A l'échelle du bassin versant, ces échanges sont pris en compte par un modèle empirique basé sur la loi de Darcy.

Pour ce travail, nous avons opté pour le modules d'infiltration de Morel-Seytoux (1978) qui est une solution analytique de l'équation d'infiltration. Cette approche a l'avantage d'être stable et robuste, sans requérir beaucoup de paramètres d'entrée. La partie suivante présente en détail les principaux processus hydrologiques : détermination du ruissellement (ou pluie efficace), ruissellement à la surface d'une unité hydrologique, échanges nappe-rivière, propagation *via* le réseau hydrographique.

3.1.3.1 Le calcul du ruissellement

Les fonctions de production (infiltration 1D) séparent la pluie qui tombe sur une unité de surface entre infiltration et pluie efficace (qui ruisselle). Ces fonctions de production diffèrent par le nombre de paramètres et la prise en compte de la condition initiale d'humidité. Sur chaque unité de surface, la pluie $P(t)$ est séparée en deux composantes,

l'infiltration $I(t)$ et le ruissellement $R(t)$.

$$P(t) = I(t) + R(t) \tag{3.1}$$

Le temps de flaquage (tp) ou "ponding time" (Morel-Seytoux and Khanji, 1974) est atteint lorsque la surface du sol atteint la saturation. Ce temps agit comme un seuil: avant le temps de flaquage, toute la pluie s'infiltre et le ruissellement est nul.

$$t \leq tp \Rightarrow I(t) = P(t) \; et \; R(t) = 0 \tag{3.2}$$

Après flaquage, et tant que la condition de saturation est vérifiée, le flux d'infiltration est égal à la capacité d'infiltration $f(t)$ $(m.s^{-1})$

$$t > tp \Rightarrow I(t) = f(t) \; et \; R(t) = P(t) - f(t) \tag{3.3}$$

La capacité d'infiltration $f(t)$, l'infiltration cumulée $F(t)(m)$ et le temps de flaquage tp peuvent être calculés pour chacune des huit fonctions de production. Nous présentons ci-dessous les caractéristiques du modèle de Morel-Seytoux.

Le modèle de Morel-Seytoux

Ce modèle est une adaptation de celui de Green and Ampt (1911). En effet, Morel-Seytoux and Khanji (1974) utilisent comme point de départ l'équation de Darcy (1856) et l'équation de continuité pour affirmer la nature physique de l'approximation de Green and Ampt (1911) supposant un front d'infiltration rectangulaire. Ils imposent pour cela des conditions aux limites qu'ils considèrent comme moins restrictives que celles de Richards (1931). Cependant, ils soulignent le fait que l'approximation de Green and Ampt (1911) néglige d'une part l'influence de la capillarité sur la forme du profil de la teneur en eau du sol, et d'autre part, suppose qu'il n'y a pas de flux simultané d'eau et d'air dans le profil (Morel-Seytoux and Khanji, 1974). A cet effet ils introduisent un coefficient de correction visqueuse (β) dont la valeur varie entre 1 et 1.7 (1.3 en général) (Morel-Seytoux, 1984).

Le modèle proposé initialement a aussi été modifié (Morel-Seytoux, 1978) pour tenir compte d'une pluviométrie variable dans le temps : les phénomènes de ruissellement ne pourront être observés avant que le stockage superficiel du sol ne soit satisfait et que l'on observe l'apparition de flaques (Morel-Seytoux, 1984). Par conséquent, ce modèle situe le début de l'infiltration maximale en fonction du temps de flaquage tp (ponding

time) : si $t < tp$ il y aura infiltration, si $t > tp$ il y aura ruissellement. Pour $t > tp$, $F(t)$ est calculé par :

$$F(t) - F_p - \left[S_f + \left(1 - \frac{1}{\beta}\right)\right] ln \left[\frac{S_f + F(t)}{S_f + Fp}\right] = \frac{K_s\,(t - t_p)}{\beta} \tag{3.4}$$

où S_f est donné par :

$$S_f = (\theta_s - \theta_i)\, H_c \left[1 - \frac{1}{3}\left(\frac{\theta_i - \theta_r}{\theta_s - \theta_r}\right)\right] \tag{3.5}$$

où $F_p\ (m)$ est l'infiltration cumulée à $t = t_p$, $Sf\ (m)$ est un facteur de stockage et de succion calculé à partir des propriétés hydrodynamiques du sol (Morel-Seytoux, 1978), $K_s\ (m.s^{-1})$ est la conductivité hydraulique à saturation, $H_c\ (m)$ la poussée capillaire, $\theta_s\ (m^3.m^{-3})$ la teneur en eau à saturation, $\theta_r\ (m^3.m^{-3})$ la teneur en eau résiduelle et $\theta_i\ (m^3.m^{-3})$ l'humidité initiale de la couche de surface. Le modèle de Morel-Seytoux (1978) a l'avantage de proposer une solution simple et physiquement valide au phénomène d'infiltration.

3.1.3.2 La propagation du ruissellement sur une unité de surface

La propagation du ruissellement R(t) sur une unité de surface est fonction de la distance $d\,(m)$ du centroïde de l'unité de surface vers le centroïde de l'objet aval (autre unité de surface SU ou tronçon de réseau hydrologique RS). Le ruissellement est propagé d'après le modèle de l'onde diffusante dans la résolution d'Hayami (Moussa, 1996).

$$Q(t) = \frac{d}{2\,(\pi D)^{1/2}} exp^{\frac{Cd}{2D}} \int_0^t R(t-\tau) A \frac{exp^{-\frac{Cd}{4D}\left(\frac{d}{C_\tau} + \frac{C_\tau}{d}\right)}}{\tau^{1/2}} d\tau$$

(3.6)

où $C\ (m.s^{-1})$ est la célérité et $D\ (m^2.s^{-1})$ la diffusivité. Ces deux paramètres sont fréquemment considérés constants ou liés à la rugosité de la surface et à la pente, en utilisant une relation du type Manning-Strickler :

$$C = C_u \sqrt{\frac{S}{S_n}\frac{n_m}{n}} \tag{3.7}$$

$$D = D_u\, \frac{S}{S_n}\frac{n_m}{n} \tag{3.8}$$

où n est le coefficient de rugosité de Manning-Strickler de la surface de l'unité de surface, n_m est la moyenne des coefficients de rugosité n des unités de surface, $S\,(m.m^{-1})$ est la pente moyenne de l'unité, $S_m\,(m.m^{-1})$ est la moyenne des pentes des unités de surface, $C_u\,(m.s^{-1})$ est le paramètre représentant la célérité moyenne de l'onde sur les unités de surface et $D_u\,(m^2.s^{-1})$ sa diffusivité moyenne sur les unités de surface.

En conséquence, pour chaque unité hydrologique, le couple (C, D) est défini uniquement en fonction de la pente, de la rugosité et des deux paramètres C_u et D_u. Ces deux derniers sont à considérer fixes ou à calibrer à l'échelle du bassin versant.

3.1.3.3 Les échanges nappe-tronçons de réseau hydrologique

Dans MHYDAS une unité de nappe (GU) est représentée par un réservoir défini comme étant un groupe d'unités de surface. Les échanges nappe-réseau hydrologique sont simulés par une simple relation de type Darcy. Chaque tronçon du réseau hydrographique est connecté à une unité de nappe.

Par convention $q_b(t)$ est le flux échangé, par unité de longueur du tronçon, entre le tronçon du réseau hydrologique et l'unité de nappe (Figure 3.4).

- si $qb(x,t) > 0$ il y a des apports latéraux (flux de l'aquifère vers le cours d'eau).
- si $qb(x,t) < 0$ il y a des pertes latérales (flux du cours d'eau vers l'aquifère).

Il est possible de distinguer deux cas :

Cas 1 - Le niveau de la nappe z'(t) est supérieur au fond du tronçon de réseau hydrologique (Figure 3.4). Dans ce cas, un drainage de la nappe est observé. L'eau peut s'écouler de la nappe vers le cours d'eau ou vice versa.

$$z_{ns}(t) = Zmax - z_n(t) \tag{3.9}$$

où $z_n(t)\,(m)$ est la hauteur entre le niveau de la nappe et le niveau du substratum imperméable à l'instant t, $z_{ns}(t)\,(m)$ est la hauteur entre la surface du sol et le niveau de la nappe à l'instant t, $Zmax\,(m)$ est le niveau du substratum imperméable par rapport à la surface du sol.

Considérons $Z_t\,(m)$ la profondeur du tronçon de réseau hydrologique. A un instant t, le flux va du cours d'eau vers la nappe ($qb(t) < 0$) si le niveau d'eau y(t) dans le cours d'eau est supérieur à $(Z_t - z_{ns}(t))$ et de la nappe vers le cours d'eau ($qb(t) > 0$) si $y(t) < (Z_t - z_{ns}(t))$. Dans ces deux situations nous avons :

$$z_{ns}(t) > Z_t \;\Rightarrow\; qb(t) = Ce_1\,[z_{ns}(t) - (Z_t - y(t))]\,L\,2\,y(t) + W \tag{3.10}$$

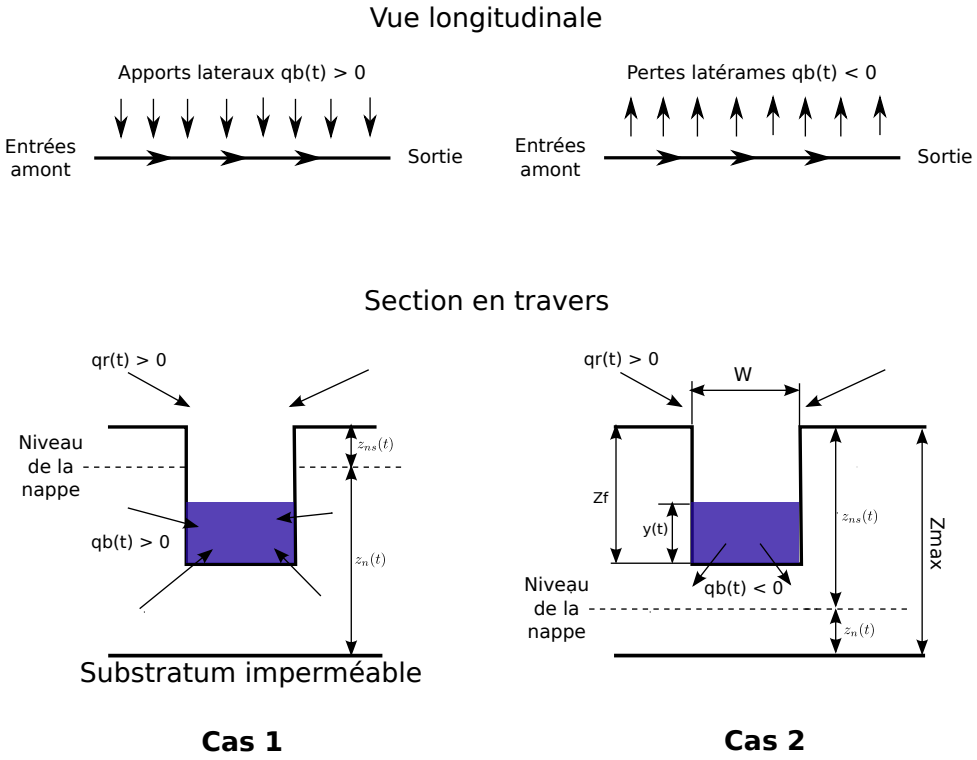

Figure 3.4: Echange nappe-tronçon de réseau hydrologique

où Ce_1 (s^{-1}) est un coefficient d'échange. L'indice "1" correspond à la première condition de la nappe, $L\,(m)$ est la longueur du tronçon de réseau hydrologique, $W\,(m)$ la largeur du tronçon de réseau hydrologique.

Cas 2 - Le niveau de la nappe $z(t)$ est inférieur au fond du tronçon de réseau hydrologique de profondeur Z_t (Figure 3.4). Dans ce cas il n'y a pas de drainage de la nappe vers le cours d'eau et on a uniquement une infiltration du cours d'eau vers la nappe.

$$z_{ns}(t) > Z_t \;\Rightarrow\; qb(t) = Ce_2\, y(t)\, L(2\, y(t) + W) \tag{3.11}$$

où Ce_2 (s^{-1}) est un coefficient d'échange. L'indice "2" correspond à la deuxième condition de niveau de la nappe.

Dans les deux cas, et après un pas de temps Δt, le nouveau niveau d'eau dans le réservoir correspondant à l'aquifère $(z_n(t + \Delta t))$ est calculé en utilisant une simple

équation de bilan de masse :

$$z_n(t+\Delta t) = z_n(t)\frac{qb(t)\Delta t}{A_{GU}(\eta-\theta_{GU})} \tag{3.12}$$

où A_{GU} (m^2) est l'aire de l'aquifère, Δt (s) est le pas de temps de calcul, η $(m^3.m^{-3})$ est la porosité de drainage de l'aquifère et θ_{GU} $(m^3.m^{-3})$ est la teneur en eau initiale de l'aquifère. Elle est obtenue en calculant la moyenne (pondérée par les surfaces) des teneurs en eau initiales mesures sur les profils des unités de surface qui compose l'unité souterraine (GU).

3.1.3.4 Propagation à travers le réseau hydrographique dans MHYDAS

La propagation de l'eau dans le réseau hydrographique débute dans les tronçons les plus en amont du bassin versant, puis continue le long du réseau hydrographique jusqu'à l'exutoire. A chaque noeud, les hydrogrammes amont sont additionnés et propagés vers l'aval en intégrant les apports latéraux. On distingue l'hydrogramme d'entrée, qui est la somme des hydrogrammes de sortie des tronçons amont, et l'hydrogramme d'apports, qui est la somme des apports latéraux provenant des unités de surface. La propagation d'onde dans un tronçon est calculée d'après l'équation de l'onde diffusante (Moussa and Bocquillon, 1996a,b).

$$\frac{\partial Q}{\partial t} + C\left(\frac{\partial Q}{\partial x} - q\right) - D\left(\frac{\partial^2 Q}{\partial x^2} - \frac{\partial q}{\partial x}\right) = 0 \tag{3.13}$$

où C $(m.s^{-1})$ est la célérité de l'onde, fonction du débit d'eau, D $(m^2.s^{-1})$ est la diffusivité de l'onde, également fonction du débit, $Q(x,t)$ $(m^3.s^{-1})$ est le débit dans la direction de l'écoulement, $q(x,t)$ $(m^2.s^{-1})$ sont les débits latéraux (apports si $q>0$ et pertes si $q<0$) par unité de longueur, t (s) est le temps et x (m) est la distance dans la direction du flux.

Le terme $q(t)$ représente la distribution latérale des apports ou pertes par unité de longueur. Il peut être scindé en deux :

$$q(t) = qr(t) + qb(t) \tag{3.14}$$

où qr $(m^2.s^{-1})$ est le débit d'apport latéral par unité de longueur du cours d'eau et qb $(m^2.s^{-1})$ est le flux d'échange entre le tronçon et la nappe par unité de longueur du tronçon.

MHYDAS propose deux solutions pour l'équation d'onde diffusante. La première est basée sur un schéma numérique aux différence finies (Moussa and Bocquillon, 1996a),

dans lequel la célérité C et la diffusivité D sont fonction du débit Q. La deuxième est la solution analytique de l'équation de diffusion proposée par (Moussa, 1996) où :

$$O(t) = \Phi(t) + (I(t) - \Phi(t)) * K(t) \tag{3.15}$$

Le symbole $(*)$ représente le produit de convolution. $I(t)$ et $O(t)$ sont respectivement l'hydrogramme d'entrée moins le débit de base et l'hydrogramme de sortie moins le débit de base. $K(t)$ est la fonction "noyau d'Hayami" définie par :

$$K(t) = \frac{L}{2(\pi D)^{1/2}} \frac{exp^{\frac{CL}{4D}\left(2-\frac{L}{C_t}-\frac{C_t}{L}\right)}}{t^{3/2}} \tag{3.16}$$

et

$$\Phi(t) = \frac{C}{L_i} \int_0^t (Q_a(\lambda) - Q_a(0))\, d\lambda \; et \; Q_a(t) = \int_0^L q(x,t)dx \tag{3.17}$$

La méthode de résolution d'Hayami suppose que la célérité C et la diffusivité D sont constantes sur un tronçon donné de longueur L. Cette solution a l'avantage d'être robuste et stable en comparaison des méthodes numériques. Le coefficients C et D sont calculés en fonction des caractéristiques géométriques du tronçon telle que la pente et la rugosité.

Chapter 4

MHYDAS-Erosion: A physically based spatially distributed erosion model for agricultural catchment application

À partir des conclusions des chapitres 1 et 2 sur le paramètre d'érodibilité diffuse et la connectivité sédimentologique, et du protocole de modélisation présenté comme introduction de la partie II de la thèse, nous avons développé un modèle distribué à base physique de l'érosion hydrique, qui peut être appliqué aux petits bassins versants agricoles. Ce chapitre présente le modèle développé dans cette thèse (MHYDAS-Erosion), avec les concepts pour la modélisation des processus érosifs, les paramètres et les limites d'application du modèle. Ce chapitre présente également une application du modèle au bassin versant de Roujan. Dans cette application nous avons comparé les hydrogrammes et sédigrammes de sortie du modèle avec ceux observés sur le terrain à différentes échelles du bassin versant : parcelle, sous-bassin et exutoire principal.

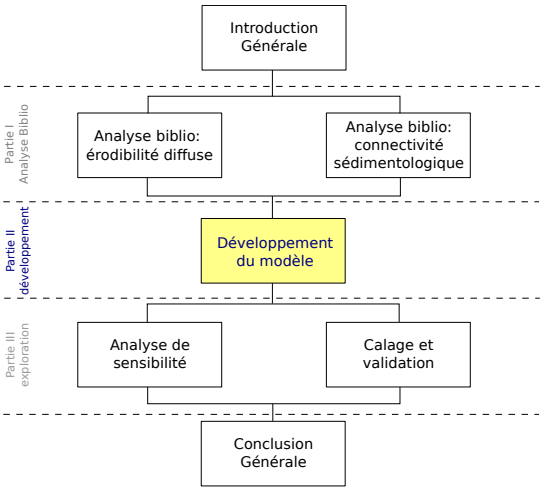

MHYDAS-Erosion: A physically based spatially distributed erosion model for agricultural catchment application [1]

Gumiere, S. J.; Davy, G.; Raclot, D.; Cheviron, B.; Louchart, X. & Le Bissonnais, Y. (article submitted to Journal of Soils and Sediments)

Abstract

In this study we developed a dynamic and distributed single-storm water erosion model called MHYDAS-Erosion able to simulate sediment transport, erosion and deposition by rill and interrill processes on small agricultural catchments. The water-sediment pathways used in MHYDAS-Erosion are determined by a process-oriented procedure defined and controlled by the user, which possibly includes the impact of land management practices on sedimentological connectivity in the catchment. Its originality relies on its capacity to integrate the dynamic effect of land management practices (vegetative filters typically), in order to improve the spatial and temporal modelling of within-catchment runoff and erosion patterns. The model was evaluated using water and sediment discharge measurements at three nested scales of a densely instrumented catchment (Roujan, OMERE Observatory, Southern France). Results of simulations have been found to be acceptable in comparaison with the observed hydrologic and sediment data at different scales. The sensibility of the model to change of the proportion of land management practices was demonstrated by testing two extreme scenarios of the Roujan catchment management with vegetative filters: 0 % on one hand and 100 % on the other hand.

4.1 Introduction

Distributed erosion models are intended to provide important informations about the effects of soil loss and sediment exportation or redistribution for agricultural and water quality concerns. Indications on spatial patterns of sediment sources and sinks are useful to managers, planners and policy-makers in soil conservation issues. Aiming at such predictive skills, several process-oriented and physically based erosion models have been developed. Models like, EUROSEM (European Soil Erosion Model) (Morgan et al., 1998b), KINEROS (Kinematic Erosion Simulation Model) (Woolhiser et al., 1990), CREAMS (Chemical Runoff and Erosion from Agricultural Management Systems) (Knisel, 1980a), WEPP (Water Erosion Prediction Project) (Ascough et al.,

[1] Silvio Jose Gumiere, Gregory Davy , Damien Raclot , Bruno Cheviron, Xavier Louchart and Yves Le Bissonnais. article submitted to *Journal of Soils and Sediments*

1997), LISEM (Limburg Soil Erosion Model) (De Roo et al., 1996b) and SWAT (Soil and Water Assessment Tool) (Arnold and Williams, 1995) estimate sediment concentration in flow and soil loss over different scales in the catchment. However, these present-day erosion models do not give completely satisfying results about soil losses and sediment concentration predictions.

Jetten et al. (2003, 1999) identified many reasons responsible for these limited performances. One of then is when parameters are held constant though describing dynamic phenomena, typically depending on rainfall intensity and duration. For example, the coherence of soil structure is affected by rainfall, resulting in crusting that changes surface roughness and topsoil infiltrability during a rainfall event. A further explanation cited by Jetten et al. (2003) is that the hydrological behaviour of a catchment may be different for medium and large rain events, the connectivity between objects depending on the available amount of water: some barriers constitute interfaces between landscape components that are normally not crossed by runoff but may be overflown in large rain events. Several studies report poor prediction quality for small rain events. However, as showed by Nearing (1998) and Jetten et al. (2003), many erosion models fail to predict soil losses in extreme events as well.

Tests with the MMF model (Morgan, 2001) gives values of Nash coefficients of 0.58 for annual runoff and 0.65 for annual soil loss. Hessel et al. (2006) evaluated the model LISEM in two East-African catchments and found values of Nash coefficient from -1.01 to 0.80. Kliment et al. (2008) tested annual runoff and annual sediment load simulated with models AnnAGNPS and SWAT. For AnnAGNPS the values of Nash coefficient were between -11.33 and -0.68 for annual runoff and between -62.79 and -0.13 for annual sediment load. For SWAT, results ranged from -5.99 to 0.70 for annual runoff and from -10.68 to 0.52 for annual sediment load. Jetten et al. (1999) pointed out that models may simulate values at the outlet well, but do not reproduce the spatial detail of within-basin runoff and erosion.

Almost all catchment-scale erosion models are based on the DEM (Digital Elevation Model) to define topology, *i.e.* potential water and sediment pathways through the catchment, but theses pathways do not only depend on topography and are influenced by many other factors. Bracken and Croke (2007) cited five other factors: climate, hillslope runoff potential, landscape position, delivery pathway and lateral buffering. However, as suggested by Gumiere et al. (2009c), the distributed effect of land management practices as well as vegetative filters, may be a key factor, in the case of agricultural catchments. Unfortunately, only few models describe the dynamic effect of land management practices on sedimentological connectivity at this scale.

The objective of this paper is to present a distributed water erosion model able to take into account the effect of such land management practices on sedimentological connectivity. The model is event-based and intended for small agricultural catchments. It is based on the acquired knowledge of process representation from present-day erosion modelling. Its originality relies on its capacity to integrate the dynamic effect of land management practices to improve the spatial and temporal modelling of within-catchment runoff and erosion. It can be used to evaluate the effect of the land management practices or to plan and optimize their set-up at catchment scale. Tests of the model were conducted in the Roujan catchment (Southern France) which is equipped with a network of automatic sediment samplers at nested scales.

4.2 Model Description

4.2.1 Model summary

MHYDAS-Erosion presented here is coupled to the pre-existing MHYDAS hydrological model (Moussa et al., 2002) that partitions rain between infiltration and runoff according to the method of Morel-Seytoux (1978) then analytically solve the one-dimensional Saint-Venant equations for concentrated flows in linear elements of the catchment (Moussa, 1996). Available runoff is thus derived from rain characteristics, saturated vertical hydraulic conductivity and initial water content. Flow depth and velocity are then obtained from discharge partition with the Manning formula, knowing the slope, shape and size of each reach segment draining a plot. The erosion module *a minima* requires a finer decomposition of flow regions into subsections of adaptable sizes representing rill and interrill areas associated with specific phenomenologies. Time steps fine enough to correctly track the fastest flow velocities expected were also redefined to ensure stability of the model according to the Courant-Friedrichs-Lewy (CFL) condition (Courant et al., 1928). MHYDAS-Erosion is a GIS vector-based model, allowing easy parameterisation and tests.

A structural difference exists between MHYDAS-Erosion and other catchment-scale water erosion models: topology (water-sediment pathways) is not a direct consequence of topography (DEM) but is determined by a process-oriented procedure defined and controlled by the user. This procedure was developed by Lagacherie et al. (2009) to possibly include the impact of (agricultural) discontinuities on water-sediment transport through the catchment. Depending on the hydrological and erosion processes retained, the user can even make abstraction of DEM and work with conceptual water-sediment pathways defined on purpose, for example virtual catchments. In addition, MHYDAS-

Erosion has an entirely devoted module that describes the spatial and temporal impact of land management practices onto water-sediment pathways. The next sections makes a more detailed description of these procedures.

4.2.2 Spatial segmentation

MHYDAS-Erosion uses the same spatial segmentation than the original MHYDAS. Where catchment is subdivided into homogeneous hydrological units "SU" for "surface units" and "RS" for "reach segments". These two constitutive elements were found necessary to take into account the variability and the discontinuities of the agricultural catchments, in a procedure extensively described by Moussa et al. (2002). SU are polygons that represent areas of surface units (e.g. agricultural plots) whereas RS are lines that represent concentrated flow (e.g. drainage channels and rivers). The procedure of subdivision developped by Lagacherie et al. (2009) consists in overlaying geographical information, such as location of the ditches, field limits, subcatchments, soil maps, land use, geographical localisation of land management practices and DEM. The choice among geographical inputs to use for segmentation is inferred by objectives of the study. Figure (4.1) shows the example of segmentation procedures used in MHYDAS-Erosion, leading to a selected spatial discretization of the catchment. From the objectives of the study, some limits or contours can be eliminated, for instance those that define very small areas. After this stage, all remaining units have the status of hydrological units. The topology and connectivity in the catchment may be constrained by lumping of input maps regarding predefined objectives. In this first approach, topology is fixed during rain events: flow paths stay unaffected by the governing hydrological conditions.

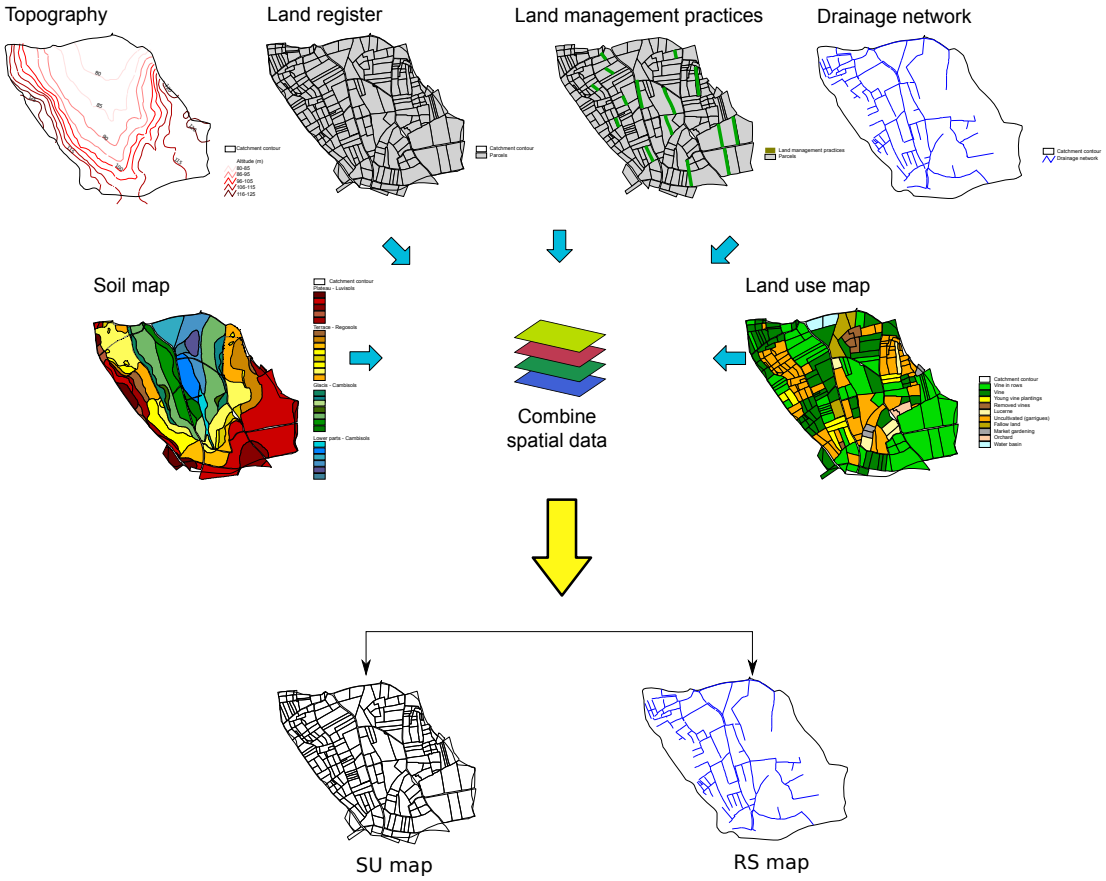

Figure 4.1: Segmentation processes of MHYDAS-Erosion

After segmentation, MHYDAS-Erosion divides each hydrological unit into "interrill" and "rill" areas associated with specific processes (Figure 4.2). Rainfall energy is the driving variable in interrill areas. Using the conceptualization made by Kinnell (2005), two processes are represented: raindrop detachment with transport by raindrop splash (RD-ST) and raindrop detachment with transport by raindrop-induced flow transport (RD-RIFT). Processes accounted for in rill areas are: raindrop detachment with transport by flow (RD-FT), flow detachment with transport by flow (FD-FT) (Kinnell, 2005) and sedimentation. Separate phenomenologies are described in rill and interrill areas from experimental observations but also trying to respect the domain of validity of mathematical formulations at our disposal in the context of this study. Interrill areas often do not have sufficient water heights for conventional flow equations to apply, whereas rill areas meet validity criteria more frequently.

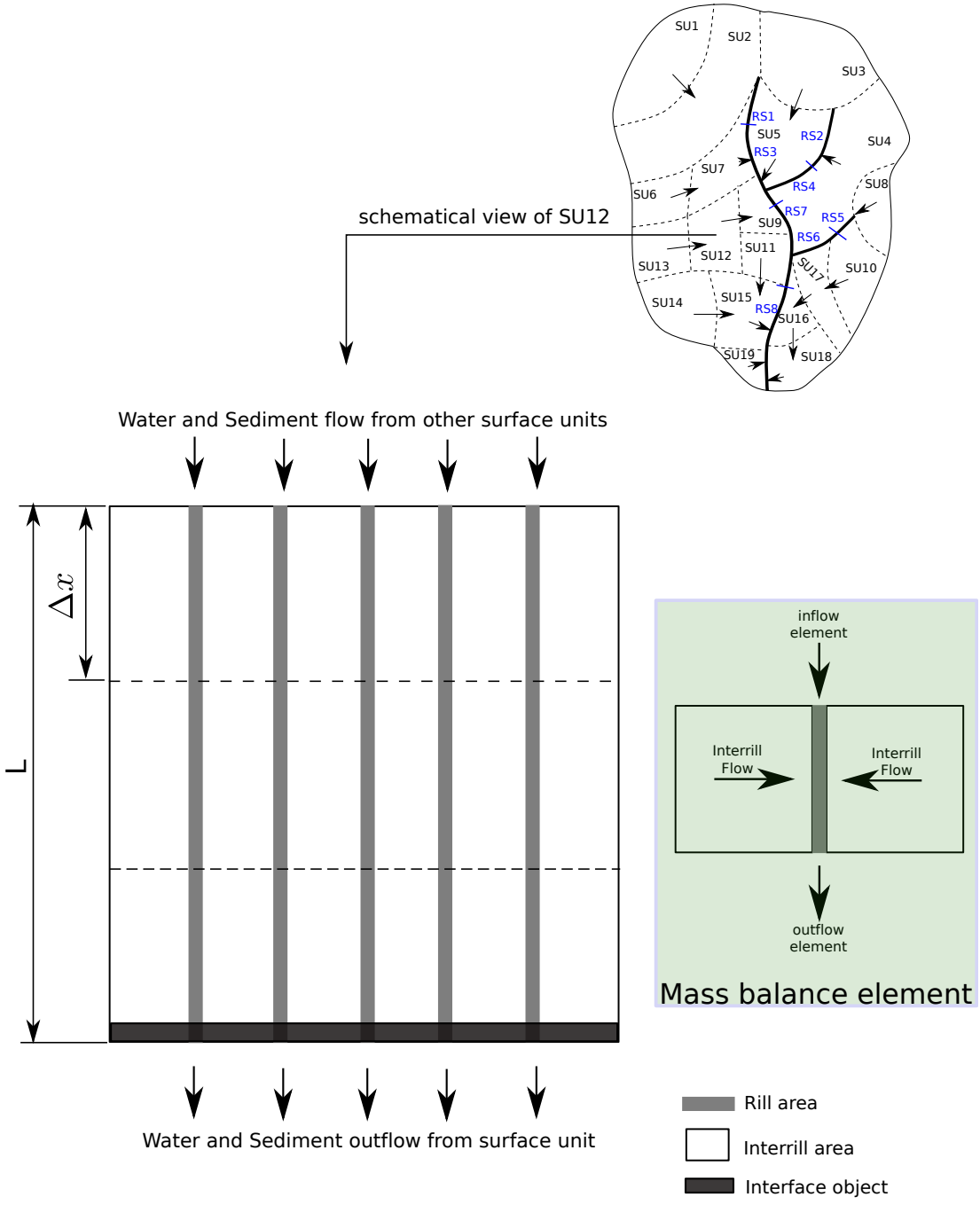

Figure 4.2: Segmentation of MHYDAS-Erosion, SU = surface unit, RS = reach segment, Δx = homogeneous slope elements, L is the length of a surface unit

4.2.3 Hydrological processes represented in the model

4.2.3.1 Rainfall-Runoff model

The model simulate the infiltration process, with the Morel-Seytoux (1978) equation, which is a modification of the Green and Ampt (1911) equation. The basic principle is the same, however, having realised that the Green and Ampt (1911) formulation neglects the influence of the capillary drive on the shape of the moisture profile and the simultaneous presence of water and air fluxes in the profile, a new viscous correction parameter (β) is introduced (Morel-Seytoux and Khanji, 1974). The value of this parameter varies usually between 1 and 1.7 with $\beta = 1.3$ in general (Morel-Seytoux, 1978).

The model is based on the ponding time concept, it needs to determine the ponding time $tp\,(s)$ after which runoff starts. if $t < tp$ infiltration occurs, else if $t > tp$ excess rainfall (runoff). For $t > tp$, $F(t)$ is calculated by:

$$F(t) - F_p - \left[S_f + \left(1 - \frac{1}{\beta}\right)\right] ln \left[\frac{S_f + F(t)}{S_f + Fp}\right] = \frac{K_s\,(t - t_p)}{\beta} \tag{4.1}$$

where S_f is given by:

$$S_f = (\theta_s - \theta_i)\, H_c \left[1 - \frac{1}{3}\left(\frac{\theta_i - \theta_r}{\theta_s - \theta_r}\right)\right] \tag{4.2}$$

where $F(t)\ (m)$ is the cumulative infiltration, $F_p\ (m)$ is the cumulative infiltration when ponding occurs $t = t_p$, $Sf\ (m)$ storage and suction factor (Morel-Seytoux, 1978), $K_s\ (m.s^{-1})$ is the hydraulic conductivity at natural saturation, $H_c\ (m)$ is the capillary height, $\theta_s\ (m^3.m^{-3})$ is the water content at natural saturation, $\theta_r\ (m^3.m^{-3})$ is the residual water content and $\theta_i\,(m^3.m^{-3})$ the water content at $t = 0$. The Morel-Seytoux (1978) model has the advantage to be a simple and physically validate solution to the infiltration problem (Moussa et al., 2002).

4.2.3.2 Transfert model in rill and reach elements

The dynamic modeling of one-dimensional gradually-varied and unsteady flows in open channels is realized, based on the system of Saint-Venant (1871) equations that are coupled hyperbolic equations of mass and momentum conservation with no analytical solution in the general case. Neglecting local inertia and convective terms leads to the diffusive wave formulation, whose justifications and domains of validity are detailed in

Moussa (1996):

$$\begin{cases} UH = q \\ \frac{\partial H}{\partial x} + (S - S_f) = 0 \end{cases} \tag{4.3}$$

where $U\,(m\,s^{-1})$ is double-averaged flow velocity, constant in time and over the entire flow depth $H\,(m)$, $q\,(m^2\,s^{-1})$ is unit flow discharge per meter width of the flow, $x\,(m)$ denotes streamwise direction, $S\,(-)$ is local bedslope in rills or reach segments of the channel network and $S_f\,(-)$ is local energy slope related to friction on the bed.

Total discharge $Q\,(m^3\,s^{-1})$ is obtained from q and flow width $w\,(m)$ with $Q = qw$. For simplicity the cross-sectional area $A\,(m2)$ of any concentrated flow is $A = Hw$ associated with rectangular shapes of rills and reach segments. Friction is expressed from the slope of the energy line by means of the Manning formula.

The problem of flow routing with lateral inflows was solved by Moussa (1996) requiring a modified form of the diffuse wave approximation in which celerity $C = \partial Q/\partial A\,(m\,s^{-1})$ and diffusivity $D = Q/2SH\,(m^2\,s^{-1})$ of the waves are functions of Q, following Chow et al. (1988). Simplifications previously made regarding flow characteristics resulted in constant values for C and D. Under the additional assumption of a semi-infinite channel as a downstream boundary condition the diffusive wave equation has an analytical solution parameterized by C and D, first described in Hayami (1951) then extended to situations with lateral inflows by Moussa (1996). This solution is preferred to numerical alternatives for its robustness and stability.

4.2.4 Erosion processes represented in the model

The erosion module is based on the mass conservation principle applied to sediment load proposed by Bennett (1974):

$$\frac{\partial(Hc)}{\partial t} + \frac{\partial(UHc)}{\partial x} = D_i + D_r - D_d \tag{4.4}$$

where $c\,(kg\,m^{-3})$ is sediment concentration, $t\,(s)$ is time, $D_i\,(kg\,m^{-2}\,s^{-1})$ is sediment inflow rate due to interrill erosion, $D_r\,(kg\,m^{-2}\,s^{-1})$ is sediment inflow rate due to rill erosion and $D_d\,(kg\,m^{-2}\,s^{-1})$ is sediment deposition rate, eventually coexisting with D_r.

Implicit validity conditions (and hypothesis made) are that all particles travel at the same velocity, which is the mean water velocity U. We thus consider only suspended load, ignoring bedload transport and particle dispersion. The latter assumption *a priori* discards the effects of strong turbulence with mixed flow lines causing particle redistribution. It is in accordance with the restrictive hypothesis of a gradually varied flow. The no-dispersion assumption also discards the possibility of high sediment loads for

which the water-sediment mixture should be modeled as a dispersed or dense-dispersed flow in a more complicated manner. We do not take into account bedload transport and only consider detachment, transport and deposition of the finest and easily suspended particles. This is equivalent to placing a limitation to the flow strength, depth, velocity and turbulence, which is again in coherence with the preceding regularity hypothesis made concerning flow characteristics: cascade, tumbling or river flow are not the scope of this study.

4.2.4.1 Soil detachment and transport by rainfall

Sediment inflow rate due to interrill erosion is the consequence of a multi-stage process described by Kinnell (2005) in which soil aggregates are broken by rainfall and eventually put into suspension before being transported by splash and/or in overland flow. The sediment inflow rate due to interrill erosion is calculated using the equation developed by Yan et al. (2008), where interrill erodibility is expressed by aggregate stability measurements (Gumiere et al., 2008; Le Bissonnais, 1996). The interrill detachment equation was developed empirically by Yan et al. (2008) and tested for ultisoils type in China:

$$d_i = 0.23\, A_s\, I^2\, S_{factor} \tag{4.5}$$

where A_s is the index of stability calculated from MWD measurements (Yan et al., 2008) and I is the rainfall intensity ($mm.h^{-1}$) and S_{factor} is the slope factor calculated by $(1.05 - 0.85\, exp^{-4sin\theta})$, where θ is the slope angle $(-)$.

The index of stability is based on the two proposed by Zhang and Horn (2001), the relative slaking index (RSI) and the relative mechanical breakdown index (RMI). The relationship between these indexes and MWD measurements is given by:

$$RSI = \frac{MWD_{SW} - MWD_{FW}}{MWD_{SW}} \tag{4.6}$$

$$RMI = \frac{MWD_{SW} - MWD_{WS}}{MWD_{SW}} \tag{4.7}$$

where MWD_{SW} is the mean weight diameter obtained by the slow-wetting treatment, MWD_{FW} is the mean weight diameter obtained by the fast-wetting treatment and MWD_{WS} is the mean weight diameter obtained by the stirring treatment. The index of stability A_s is derived from RSI and RMI values by the equation $A_s = RSI \times RMI$ (Yan et al., 2008).

The sediment inflow rate into rill due to interill erosion is then calculated by multiplying the interill detachment (equation 4.5) by a coefficient for efficiency of transport from interill to rill ($CETI$):

$$D_i = d_i \, CETI = 0.23 \, A_s \, I^2 \, S_{factor} \, CETI \tag{4.8}$$

$CETI$ is calculated from local runoff as:

$$CETI = CETI_{max} \, (1 - exp^{\alpha \, R}) \tag{4.9}$$

where $CETI_{max}$ is the maximum allowed value of CETI , α is an empirical exponent depending on roughness and R is the runoff amount in $mm.h^{-1}$.

In MHYDAS-Erosion we consider that water height on interrill areas is too shallow to apply transport equations used in hydraulics. The concept of $CETI$ was to introduced to describe the effect of the perpendicular roughness on interrill erosion contribution. $CETI_{max}$ values may vary in theory between 0 and 1, but experiments realized by Leguédois et al. (2005) and Nord (2005) gave values between 0.1 and 0.5 for five soil textures.

4.2.4.2 Soil detachment and transport by runoff

Sediment inflow rate due to rill erosion integrates two aspects in a single equation. When transport capacity of the flow exceeds sediment load, both particle detachment due to excess shear stress exerted by the flow and sediment transportation appear in the equation proposed by Foster et al. (1995) and further tested by Nord (2005):

$$D_r = K_r(\tau - \tau_c)(1 - \frac{q_s}{TC}) \tag{4.10}$$

where $K_r \, (s \, m^{-1})$ is rill erodibility (Nord, 2005), $\tau \, (Pa)$ is shear stress exerted on the bed by the flow, $\tau_c \, (Pa)$ is critical shear stress over which detachment is initiated, $q_s \, (kg \, m^{-1} \, s^{-1})$ is unit solid discharge by meter width of the flow calculated as $q_s = q \, c$ and $TC \, (kg \, m^{-1} \, s^{-1})$ is transport capacity measuring the ability of the flow to carry a sediment load.

TC was said to reach its maximum for pure water and to decrease with increasing sediment load. It has been empirically related to values of τ and τ_c by Foster (1982) in order to reduce the number of parameters implied:

$$TC = \eta \, (\tau - \tau_c)^{3/2} \tag{4.11}$$

where $\eta \, (m^{1/2} \, s2 \, kg^{-1/2})$ gives efficiency of the transport and the recommended value is $\eta = 0.04$.

MHYDAS-Erosion uses the transport capacity formulation established by Foster (1982), among many others available in the literature. This formulation was chosen because TC is expressed as a function of critical shear stress, which is a widely-used parameter (Knapen et al., 2007).

The critical shear stress is highly correlated with soil cohesion COH (Pa) though the latter is a tridimensional anisotropic soil characteristic. We then approximated τ_c to COH in the downstream direction (Nord, 2005). The hydrodynamic shear stress exerted on the bed is $\tau = \rho g H S$ where ρ $(kg\, m^{-3})$ is density of water and g $(m\, s^{-2})$ is gravitational acceleration. This expression rigorously holds under the assumptions of a uniform flow over a small slope approximated by its sine or tangent, when friction exerted by the bed on a given volume of fluid equals the streamwise component of the weight of the fluid. No contribution of suspended particles is integrated in the description of the hydrodynamic shear stress or detachment capacity of the flow: abrasion is not considered.

When $q_s > TC$ a part of the material transported by the flow is deposited on the bed. Deposition happens as detailed in Nord (2005) after initial works by Hairsine and Rose (1992) and Foster et al. (1995):

$$D_d = \frac{v_s}{q} \left(q_s - TC\right) \tag{4.12}$$

where v_s $(m\, s^{-1})$ is the settling velocity defined by Soulsby (1997).

Settling velocity is said to apply over a wide range of concentrations up to $c = 100\, g\, L^{-1}$:

$$v_s = \frac{\nu}{d_s} \left[\sqrt{10.362 + 1.049 \left(1 - c_{vol}\right)^{4.7} d_{s*}3} - 10.36\right] \tag{4.13}$$

where ν $(m2\, s^{-1})$ is kinematic viscosity of water, d_s (m) is diameter of the particles, c_{vol} $(-)$ is their volumetric concentration in the flow and d_{s*} $(-)$ is their adimensional sedimentological diameter.

The adimensional sedimentological diameter is taken from Julien (1998):

$$d_{s*} = d_s \left[\frac{\left(\rho_s/\rho - 1\right) g}{\nu 2}\right] \tag{4.14}$$

where ρ_s $(kg\, m^{-3})$ is density of the particles.

4.2.4.3 Sedimentological connectivity

The model has a module devoted to the sedimentological connectivity between pairs of catchment components (SU-SU, SU-RS and RS-RS). The sedimentological connectivity module is inspired by the typology developed by Harvey (2001), listing the three types of

connections between catchment objects as (i) coupled, (ii) not coupled, (iii) dis-coupled and (iv) re-coupled (add by the authors):

i coupled, when landscape units have free transmission of matter and energy (sediment, water) between two catchment components (hillslope-channel, channel-channel);

ii not coupled, when landscape units show no linkages between catchment components (bench terraces, barriers, vegetation etc);

iii dis-coupled, when landscape units were previously coupled, but for some reason became disconnected, often as a result of sediment deposition processes (alluvial fans, floodplains);

iv re-coupled, when landscape units were previously disconnected, but for some reason they became connected, often as result of over-bank barriers or saturation sediment trapping capacity.

According to Fryirs et al. (2007); Harvey (2001), time-variable connectivity is influenced by rain and runoff intensity, initial moisture conditions, vegetation type and localizationa and catchment location. The spatial scale for connectivity in the model is only the local scale, involving hillslopes-channels and channels-channels connections. The time scale is that of pluviometric events. In this first version of MHYDAS-Erosion, only vegetated filters are tested regarding local sedimentological connectivity. This approach is based on flume experiments by Deletic (2001) and Deletic and Fletcher (2006). Artificial grass was used to filter water mixed with natural sediment particle of $d_{50} = 50\mu m$ diameter. Deletic (2001) used slopes of 2 and 7% for three different grass densities, defined as the cross-section of flow not blocked by the grass blades, fixed at 0.6, 0.67 and 0.75 $m.m^{-1}$. Sediment trapping efficiency (T_r) was defined as a function of the adimensional particle fall number (N_f) (Fig. 4.3).

As voiced by Deletic (2005) the cross-correlation coefficient between measured and calculated trapping efficiencies reached $R^2 = 0.85$, which is acceptable. Observing Fig.4.3. there is a high scattering of measured data around the calculated line for smallest sediment size fractions. According to Deletic (2005) the high dispersion is due to measurement errors, as "the concentration of particles below $5.8\mu m$ was very small and therefore difficult to measure accuratel".

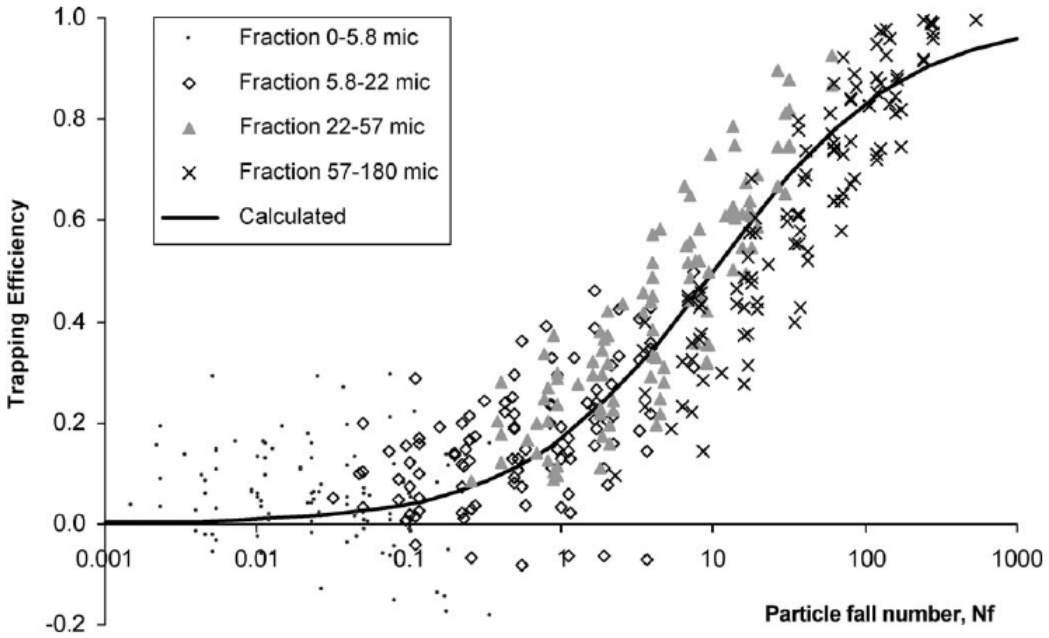

Figure 4.3: Sediment trapping efficiency as a function of the adimensional particle fall number N_f for four sediment size fractions, from: Deletic (2005)

The sediment trapping efficiency T_r is calculated with the equation proposed by Deletic (2005):

$$T_r = \frac{N_f^{0.69}}{N_f^{0.69} + 4.95} \tag{4.15}$$

where

$$N_f = \frac{l \cdot V_s}{h \cdot V} \tag{4.16}$$

where l is the grass strip length (m), V_s is Stokes velocity for settling of sediment particles $(m.s^{-1})$, V is the mean flow velocity between grass blades $(m.s^{-1})$. Mean flow and settling velocities in the model are calculated as:

$$V = \frac{q}{B_0 \cdot h} \tag{4.17}$$

and

$$V_s = \frac{g}{18\mu}(\rho_s - \rho)d_s^2 \tag{4.18}$$

where B_0 is grass density, μ is dynamic viscosity of water $(kg.s^{-1}.m^{-1})$, ρ is water density $(kg.m^{-3})$, ρ_s is sediment particle density $(kg.m^{-3})$ and d_s is particle diameter (m).

In MHYDAS-Erosion, T_r is calculated for each time step, thus sediment trapping efficiency is time-dependent. Parameters B_0 and l are estimated from field observations and may be spatially-distributed on the catchment. As argued by Deletic (2001) and Deletic (2005), the approach based in the particle fall number is only valid for low sediment concentrations that do not influence sediment deposition. The choice of relatively simple efficiency functions is a compromise between model objectives and (code) complexity.

4.2.5 Numerical methods

The hydrological and erosion equations are solved independently within *a priori* fixed time step. Sediment concentration is supposed not to affect water flow behaviour Bennett (1974). At a given time step, hydrological variables q_i^t, v_i^t and h_i^t (unit flow discharge, flow velocity and water height respectively) are calculated by the hydrological module MHYDAS. The analytical solutions of infiltration and excess infiltration equations proposed by Morel-Seytoux (1984) and the analytical solution of the kinetic flow equation proposed by Hayami (1951), are found. As debated by Moussa (1996), analytical solutions are preferred to numerical schemes to preserve stability and convergence of the results.

Output hydrological variables become input variables for MHYDAS-Erosion. Mass balance equations (Eq. 4.4) are solved at each time step using a backward explicit finite difference scheme. The volumetric concentration of suspended sediment in flow at $t + \Delta t$ is calculated using values of q, v, h and c at time step t.

$$c_i^{-t+\Delta t} = c_i^t + \left(\frac{\partial c_i}{\partial t}\right)^t \Delta t \tag{4.19}$$

where

$$\begin{aligned}\left(\frac{\partial c_i}{\partial t}\right)^t &= \frac{1}{h_i^t}\left[\left(\frac{\partial h_i}{\partial t}\right) + \frac{(q_y)_i^t - (q_y)_{i-1}^t}{\Delta x}\right] \\ &- \frac{1}{h_i^t}\left[(q_y)_i^t \frac{c_i^t - c_{i-1}^t}{\Delta x}\right] + \frac{1}{h_i^t}\left[\frac{\left(D_{i_i}^t + D_{r_i}^t + D_{d_i}^t\right)}{\rho_s}\right]\end{aligned} \tag{4.20}$$

where c_i^t $(m^3.m^{-3})$ is the volumetric sediment concentration in flow at the i^{th} space step and t^{th} time step, q $(m^2.s)$ is the unit flow discharge , x (m) is downslope distance, D_i $(kg.s^{-1})$ and D_r $(kg.s^{-1})$ are respectively the interrill and rill contribution and D_d $(kg.s^{-1})$ is the sediment deposition.

In the same way the trapping efficiency T_r is calculated using as input, hydrological variable calculated previously. Sediment discharge flowing between two hydrological objects (SU or RS) is filtered using T_r at the t^{th} time step, calculated by:

$$T_r^t = \frac{(N_f^t)^{0.69}}{(N_f^t)^{0.69} + 4.95} \tag{4.21}$$

4.3 Model Testing

4.3.1 Test procedure

The evaluation tests of the model were performed at the Roujan catchment described in detail in the next section. The first step was a manual calibration of the model relying on water and sediment discharge data obtained from automatic samplers at several places in the catchment. The model was calibrated for hydrology using the hydrographs at three measurement points associated with successive scale inclusions: in a plot, then in the sub-catchment including the plot, then at the outlet of the catchment including the sub-catchment. Once the hydrological parameters estimated, the erosion parameters were then calibrated using the measured sedigraphs at the same points. The objective criteria for calibration were the Nash-Sutcliffe Efficiency and Root Mean Square Error.

The second step was to test the model response to spatial organizations of land management practices, which are essentially grass strips at the Roujan catchment, placed between agricultural plots and drainage channels or between agricultural plots. Tests included: (i) the reference scenario, where the localization and number of grass strips was measured from field observation, (ii) a scenario where zero grass strip exist at the catchment and (iii) a scenario where 100% of agricultural plots have a grass strip.

4.3.2 Study area

MHYDAS-Erosion is evaluated on a small agricultural catchment called Roujan catchment (43.300 N, 3.190 E, area = 0.91 km^2), which is a densely instrumented catchment included in the experimental research observatory called OMERE (Mediterranean Observatory of Rural Environmental and Water). It is located in Southern France, 60 km West of Montpellier and has a Mediterranean climate. The catchment is equiped with hydro-meteorological measurement devices since 1992: a meteorological station, rain gauges, stream flow recorders, automatic sediment samplers, Venturi channels. The catchment has seven points of automatic sediment concentration sampling, dispatched as shown in figure 4.4. The localization of land management practices as well their

characteristics were measured *in situ*. We found that only 22% of agricultural plots bear a land management practice, they are shown in figure 4.4.

Annual rainfall varies between 500 and 1400 mm, in a bimodal temporal distribution with two major rainy periods, one in spring and the other in autumn. Rainfall is usually of high intensity and short duration. The mean annual temperature is about $14°C$ and the mean annual Penman evapotranspiration is 1090 mm. Soils of the catchment have developed from marine, lacustrine or fluvial sediments (Moussa et al., 2002). The catchment is mainly covered by vineyards and divided into 237 agricultural plots. Agricultural plots areas vary between 320 and 22 427 m^2. A survey (Moussa et al., 2002) identified two main treatments against weeding. In the first one, herbicides are applied over the whole field without any tillage. In the second one, soil is tilled with a rotovator between vine rows one to three times during the growing period, between March and July. The drainage network is formed by man-made ditches and generally follows the limits of agricultural plots. The total length of the ditch network is 11 069 m.

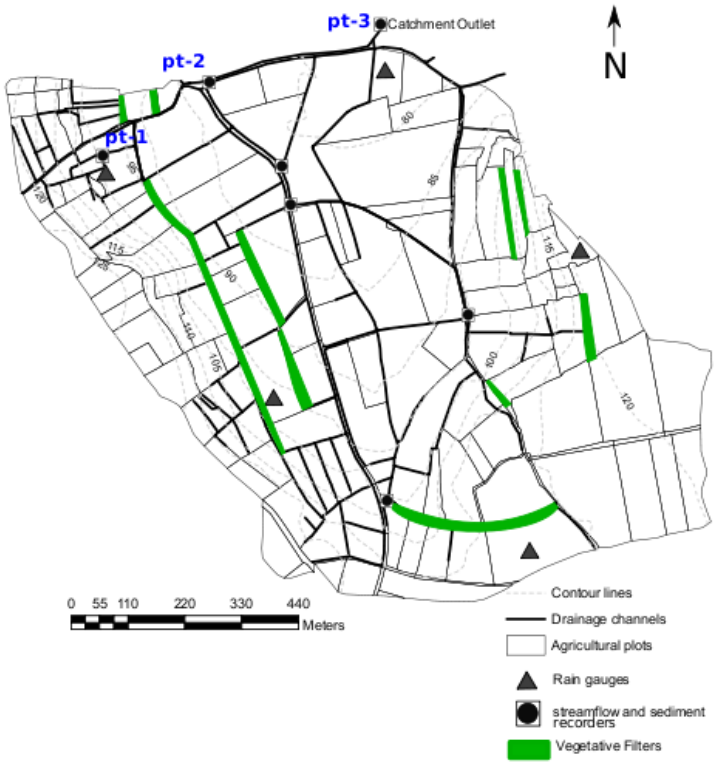

Figure 4.4: Meteo-Hydro-sedimentological equipments of Roujan agricultural catchment

4.3.3 Statistical evaluation

The statistical evaluation criteria used in this work were Root Mean Square Error ($RMSE$) and Nash-Sutcliffe Efficiency, (E_{NS}). These criteria were calculated as functions of time for each tested rainfall event. The root mean square error is an index of the variance between simulated and observed values expressed by:

$$RMSE = \sqrt{\frac{1}{n}\sum_{i=1}^{n}(Y_i - \hat{Y}_i)^2} \tag{4.22}$$

where Y_i is the observed value, $\hat{Y}_i$ is the simulated (predicted) value and n is the sample size. The $RMSE$ has the same units than the observed and simulated values. Generally higher $RMSE$ values indicate poor performances of the model.

The Nash-Sutcliffe Efficiency (E_{NS}) is the measure of overall fit between observed and simulated values, which ranges from $-\infty$ to 1. Values near one indicate better performances of the model. Nash-Sutcliffe Efficiency (E_{NS}) can be calculated by:

$$E_{NS} = \frac{\sum_{i=1}^{n}(Y_i - \hat{Y}_i)^2}{\sum_{i=1}^{n}(Y_i - \bar{Y})^2} \tag{4.23}$$

where Y_i is the observed value, $\hat{Y}_i$ the simulated value, n the sample size and $\bar{Y}$ the mean of the observed values.

4.3.4 Model parameterisation

Almost all input parameters were obtained from field observations. As MHYDAS-Erosion takes into account many spatially-distributed erosion processes, each input parameter may also be spatially distributed among homogeneous surface units. Model parameterisation was constrained by land-use data: values of Manning's roughness coefficient, soil cohesion, soil aggregate stability, interrill erodibility and rill erodibility were attributed from land-use and soil maps. The saturated hydraulic conductivity was measured *in situ* from rainfall simulations, for each combination of land-use and soil type. The initial soil moisture in surface layers was deducted from antecedent rainfall events.

Because of spatial and temporal variability of the parameters, we performed a manual calibration. Based on sensitivity analyses presented in Cheviron et al. (2009b) we identified the key parameters for calibration, saturated soil hydraulic conductivity for hydrology, rill and interrill erodibilities, $CETI_{max}$ and soil cohesion for erosion processes. The numerical values for each parameter were first estimated from measurements, then multiplied by a "calibration factor". Ranges scanned during calibration

were checked for physical coherence and to avoid equifinality. Table 4.1 shows the calibrated parameters with their tolerated ranges for each land use. Very detailed multiscale and multi-event parameterisation and calibration procedures for MHYDAS-Erosion is presented in Gumiere et al. (2009a).

Table 4.1: Input parameters for MHYDAS-Erosion

Input parameter	**Reference value**	**Unit**	**Calibration parameter**
n	$0.01 - 0.035$	$s.m^{-1/3}$	-
ks	$1.10^{-8} - 1.10^{-5}$	$m.s^{-1}$	+
θ_i	$0.05 - 0.35$	$m^3.m^{-3}$	-
θ_r	0.44	$m^3.m^{-3}$	-
θ_s	0.05	$m^3.m^{-3}$	-
β	1.3	-	-
K	$0.01 - 1.0$	-	+
$\%cover$	$0 - 100$	-	-
$Nrill$	$1 - 50$	-	-
D_{50}	100.10^{-6}	m	-
COH	$0 - 100$	Pa	+
$CETI_{max}$	$0 - 1$	-	+

To evaluate the influence of land management practices on model responses, we performed two virtual tests with 0 % and 100 % of agricultural plots bearing vegetated filters that we compared to the real situation (22 % of agricultural plots bearing vegetated filters). The grass strips characteristics like grass density, strip width and slope were obtained from field observations for the real case. For the virtual tests, we maintained the same distribution of each characteristic and we used the same calibrated parameters than in the real test.

4.4 Results and discussion

In this section we discuss model evaluation, illustrated with results obtained from one typical Mediterranean rainfall event (Jul.10, 2007). Its duration is 3 hours, with an average rainfall intensity of 12 mm.h^{-1}, recorded with a 5-minute time step and its 5 minutes maximum intensity is 73.3 $mm.h^{-1}$. It is a typical Mediterranean event, short

but with a clear peak in intensity.

Figure 4.5 shows the hydrographs and sedigraphs for three points in the catchment after calibration. On Fig.4.5 and Table 4.2 the plot scale has the best Nash coefficient for hydrology (0.73). For erosion the best Nash coefficient (0.92) was obtained at the outlet of the catchment.

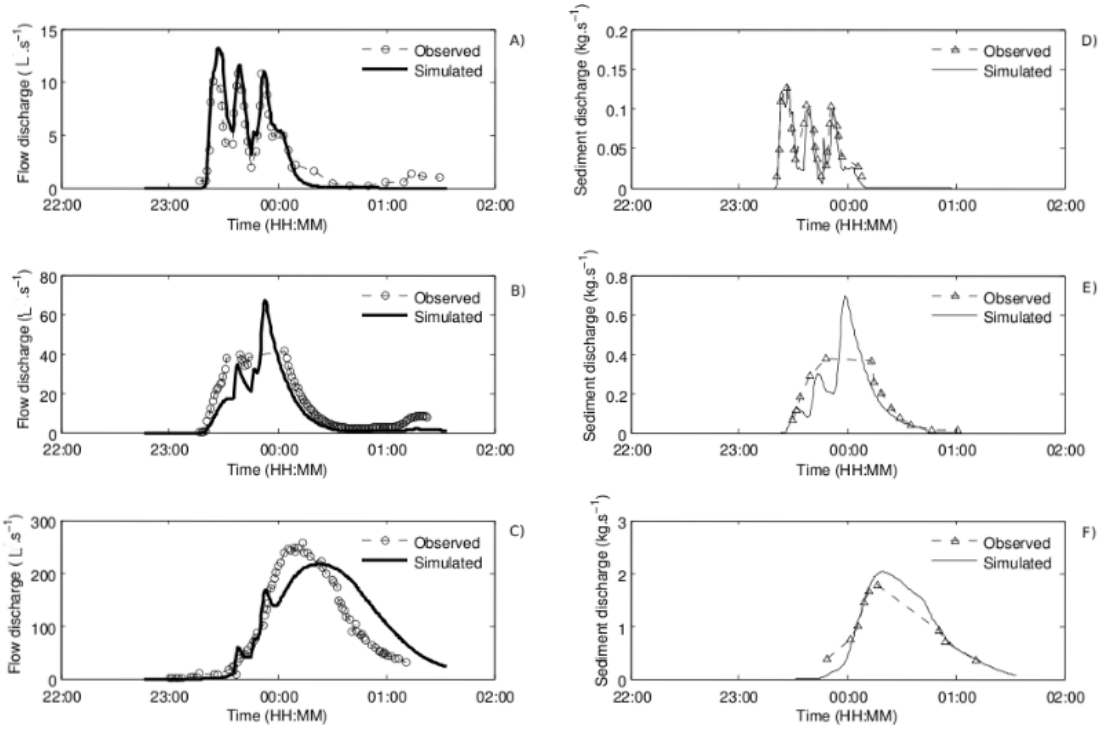

Figure 4.5: Simulated and observed hydrographs and sedigraphs for Jul.10, 2007 rainfall event. A) observed and simulated hydrographs at point 1 (agricultural plot scale); B) observed and simulated hydrographs at point 2 (sub-catchment scale); C) observed and simulated hydrographs at point 3 (outlet of the catchment); D) observed and simulated sedigraphs at point 1 (agricultural plot scale); E) observed and simulated sedigraphs at point 2 (sub-catchment scale); F) observed and simulated sedigraphs at point 3 (outlet of the catchment).

Results in Fig.(4.5) show that the model has fairly simulated the observed hydrographs and sedigraphs at the three measurement points. The values of Nash-Sutcliffe efficiency and the Root Mean Square Error at these points are given in Table 4.2. For hydrology, the Nash-Sutcliffe efficiency ranges from 0.67 to 0.73 with an average value of 0.70 when including the three scales. For erosion, the Nash-Sutcliffe efficiency

ranges from 0.50 to 0.92 with an average value of 0.67 when including the three scales. These values meet requirements made by Nearing (2000) for calibrated erosion models ($efficiency > 0.60$).

Table 4.2: Summary of model efficiency

Measure Point	**Hydrology**		**Erosion**	
	Nash coef.	RMSE ($L.s^{-1}$)	Nash coef.	RMSE ($kg.s^{-1}$)
Point 1	0.73	1.77	0.60	0.02
Point 2	0.69	6.36	0.50	0.08
Point 3	0.67	47.77	0.92	0.13

From Table 4.3 one observes that total sediment outflow has been simulated with a difference of -0.66% to 16.00% to observed values, peak sediment outflow rate with a difference of -13.48% to 72.00%, total flow discharge with a difference of -0.43% to 25.83%, and peak flow discharge with a difference of-15.57% to 62.39%. The poorest fit is for peak sediment outflow rate at the outlet of the sub-catchment. It should be noted that hydrology at this point is poorly simulated in terms of peak discharge, yielding a plausible explanation to the degraded quality of erosion results. More precisely, the hydrological module generates a peak (Fig.4.5 B) that does not exist in observed data. As erosion variables are calculated from and after hydrological ones, any error on hydrology is transmitted into the erosion module. Another possible explanation is a possible measurement error around the peak discharge. That could be caused by overflowing the Venturi channel at this point.

Results for spatial distributions of land management practices are shown in Fig4.6. Scenario 1 simulates the case when 0% of agricultural plots bear a grass strip. Scenario 2 is the real percentage of grass strips in the Roujan catchment, obtained from field observations. Scenario 3 simulates the case when 100% of agricultural plots bear a grass

Table 4.3: Model results for tested events in the Roujan catchment

Measure Point	**Total sediment outflow**			**Peak sediment outflow rate**			**Total flow discharge**			**Peak flow discharge**		
	Obs. (kg)	Sim.	Diff. (%)	Obs. ($kg.s^{-}1$)	Sim. ($kg.s^{-}1$)	Diff. (%)	Obs. (m^3)	Sim. (m^3)	Diff. (%)	Obs. ($L.s^{-}1$)	Sim. ($L.s^{-}1$)	Diff. (%)
Point 1	147.46	146.42	-0.66	0.13	0.13	0.00	20.9	21.66	3.63	10.8	13.04	24.07
Point 2	1140.53	970.46	-14.91	0.40	0.69	72.5	75.81	95.41	25.85	41.35	67.15	62.39
Point 3	5078.00	5890.00	16.00	1.78	2.02	-13.48	904.34	900.44	-0.43	256.8	216.8	-15.57

Diff = Difference = $\frac{(simulated - observed)}{observed} \cdot 100$

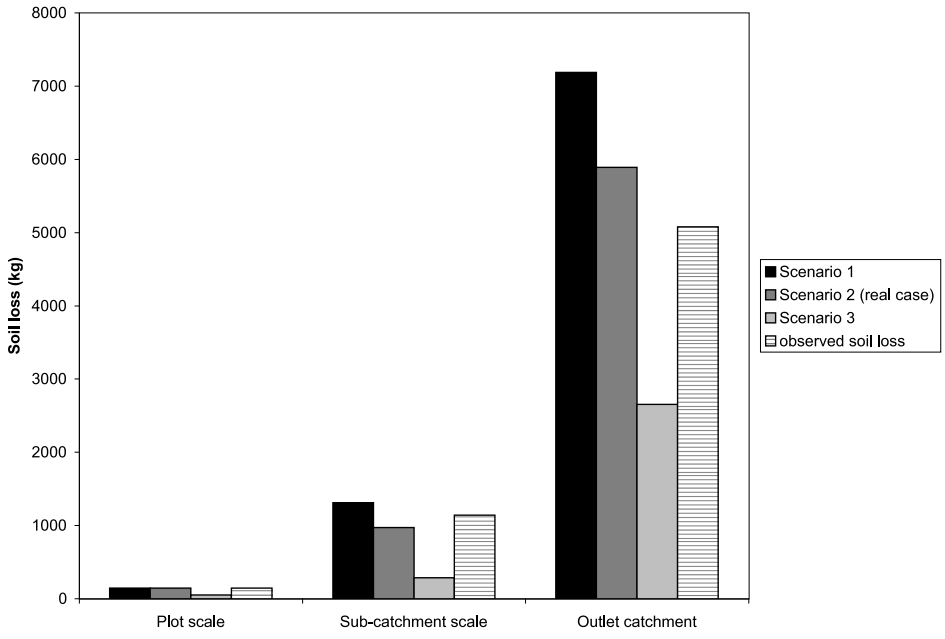

Figure 4.6: Scenarios for spatial distributions of land management practices

strip. In Fig.4.6, soil loss decreases at all scales for scenario 3, by 65% for agricultural plot scale, 62% for sub-catchment scale and 45% at the outlet of the catchment, when compared to scenario 1. Scenario 2 provides a reduction of 26% at the sub-catchment scale and 18% at the outlet of the catchment, still in comparison with scenario 1. The objective was here to identify the sensitivity trends of MHYDAS-Erosion when varying spatial distributions of land management practices, reduced here to grass strips. From results exposed here, MHYDAS-Erosion is able to simulate the spatial and temporal dynamics of sediment in a small-scale agricultural catchment. The three scales involved confirm that the model is able to provide distributed information about soil loss and sediment discharge patterns in the catchment, at least whenever sufficient data are available. Scenarios of land management practices have shown that the model may be used to understand and provide information about the impact of these practices on effective sedimentological connectivity.

4.5 Conclusion

In this study, a distributed water erosion model has been exposed. The developed model is suitable for small agricultural catchments (surface about 1 km^2), event-based erosion and sediment outflow simulations. Tests results have showed that the model can simulate the temporal dynamic of water and sediment outflow in a distributed way, given information about sediment sources and sinks within the catchment. The comparison between observed and simulated hydrographs and sedigraphs showed that the model produces reasonable results in estimation of sediment and water outflow for the three tested scale (agricultural plot, sub-catchment and catchment). The model response to the influence of land management practices were as expected. When percentage of grass strips increases soil loss decreases. The model showed a strong dependence of land management practices exemplified here as grass strips. The sedimentological connectivity represented in the model seem provide better results related to total sediment outflow. The model gives distributed information about erosion and sediment flow into the catchment, it can give information about the impact of land management practices in the sedimentological connectivity. With this model it is possible to test different spatial organizations of land management practices. That can provide important information to planners and decision-makers about agricultural catchment management. Not all described problems related to water erosion modeling were fixed with MHYDAS-Erosion development, its far from this. We will cite some of model limitations: The number of rill on agricultural plots is defined *a priori* as in the WEPP model, the model does not take into account the surface evolution and crusting effects during the rainfall event, the influence of land management practices is only taken into account for sedimentological connectivity, as all distributed erosion model parametrization is time onerous. But as voiced by Boardman (2006), "we should not be disappointed by modeling performance [and limitations] models are still developing and unsatisfactory results [and limitations] may indicate which aspects of models are most in need of further development". The next steps of this work are to include effects of land management practices over hydrological variables and to quantify the sensibility of MHYDAS-Erosion to the spatial distribution of land management practices.

Part III

Analyse de sensibilité et exploration du modèle

Introduction

Les modèles d'érosion hydrique contiennent deux types d'incertitudes : l'incertitude structurelle, liée de la description approximative et inexacte de la réalité par des équations (différentielles par exemple), et l'incertitude contextuelle, qui résulte des erreurs dans l'estimation des valeurs numériques des paramètres et qui englobe aussi les imperfections dans la collecte des données expérimentales utilisées (Nearing, 2000; Nearing et al., 1999). En fait, les valeurs exactes des paramètres d'entrée d'un modèle ne sont jamais connues, et pourtant très souvent elles influencent significativement les prédictions du modèle, même si celui-ci est correct du point de vue physico-mathématique. Ainsi, selon Saltelli et al. (1999), il est impératif pour le modélisateur de chercher à savoir comment le fonctionnement d'un modèle dépend de ses paramètres d'entrée. Cette recherche de la compréhension du comportement d'un modèle vis-à-vis de ses paramètres, de la cohérence entre le modèle et le système qu'il représente et de la manière dont ses différentes parties interagissent, ne peut se faire que par le biais d'une analyse de sensibilité du modèle, qu'il soit numérique ou autre (Saltelli et al., 1999). Il existe différents formalismes d'analyse de sensibilité qui peuvent être utilisés en fonction de l'objectif poursuivi et du type de modèle à examiner. Les trois principales écoles sont : l'analyse de sensibilité locale (*local sensivity analysis*), globale (*global sensivity analysis*) ou reposant sur des techniques d'exploration de l'espace des paramètres (*screening designs*). L'analyse de sensibilité locale s'attache à déterminer comment le modèle réagit à une variation de ses paramètres d'entrée, au voisinage d'une configuration paramétrique donnée. Il faut pour cela calculer les dérivées partielles des fonctions de sortie par rapport aux paramètres d'entrée. Ces calculs se font numériquement, en faisant varier les entrées du modèle dans un intervalle très restreint autour d'une valeur nominale. Un cas particulier très utilisé est l'approche "One-Factor-At-A-Time" (OAT), dans laquelle un seul paramètre varie à la fois, tous les autres étant maintenus constants. Généralement, quand on applique cette méthode, les relations entre les entrées et les sorties sont supposées être linéaires, pourvu que l'intervalle de variation soit

assez restreint.

L'analyse de sensibilité globale est une méthode quantitative basée sur l'estimation de la contribution de chaque paramètre d'entrée d'un modèle à la variance observée dans les sorties. Elle étudie aussi l'interaction entre ces différentes variables d'entrée (Ratto et al., 2001; Soutter and Musy, 1999). On peut recourir alors à la méthode de *Monte Carlo*, à celle de la surface de réponse (*Response Surface Methodology*) ou bien à la méthode FAST reposant sur l'analyse de Fourier (*Fourrier Amplitude Sensivity Test*).Ces techniques s'affranchissent des hypothèses classiques de linéarité que supposent les principes de régression et de corrélation entre les paramètres. Les méthodes (*Screening Designs*) d'exploration privilégiée (ou orientée) de l'espace des paramètres sont les plus adaptables. Leur but est d'isoler les paramètres les plus importants parmi de nombreux autres pouvant affecter une sortie particulière d'un modèle donné (Nearing et al., 1990). Le *Screening Design* est très efficace quand le modèle à analyser a un nombre considérable de paramètres d'entrée.

Dans le domaine de l'érosion, des études ont montré que les résultats des modèles en termes de perte en sol sont très sensibles aux paramètres hydrologiques. Nearing et al. (1990),Veihe and Quinton (2000) et De Roo et al. (1996a) ont montré que les sorties de perte en terre des modèle WEPP, EUROSEM et LISEM respectivement sont très sensibles en particulier à la conductivité hydraulique à saturation du sol. Plus encore, il semble y avoir un consensus général dans les études de sensibilité des modèles d'érosion qui confirme la grande sensibilité aux paramètres hydrologiques. Gumiere et al. (2009b) ont suggéré que cette propension à être sensible au paramètre hydrologique est liée à la configuration de l'analyse de sensibilité, souvent effectuée pour des précipitations intenses. Il est alors nécessaire de développer une procédure qui permette de séparer la sensibilité aux conditions hydrologiques (flux et paramètres) de la sensibilité aux paramètres spécifiques de l'érosion. Les deux chapitres à venir présentent une procédure d'analyse de sensibilité local des modèles d'érosion distribués, pour différentes échelles de processus, ainsi que son application à quatre différents modèles d'érosion.

Un des principaux intérêts de la modélisation distribuée de l'érosion hydrique au niveau du bassin versant, est d'aider à la décision sur l'emplacement optimal des pratiques et des aménagements anti-érosifs, pour une meilleure gestion de la productivité agricole et de la conservation des sols. Pour cela, il faut avant tout, que le modèle utilisé soit sensible à la distribution spatiale des aménagements. La troisième partie présente également la sensibilité du modèle développé à la distribution des aménagements sur le bassin versant. En utilisant la méthode de méta-modèle pour distribuer les aménagements sur le bassin versant, nous avons calculé les indices de sensibilité à

la distribution des aménagements et à la densité des aménagements. Ce travail a pour objectif de compléter l'analyse d'exploration du modèle MHYDAS-Erosion.

Chapter 5

Sensitivity analysis of distributed erosion models - I. Framework

Nous avons développé un cadre théorique pour l'analyse de sensibilité des modèles distribués, qui s'appuie sur un jeu réduit de configurations paramétriques pour s'affranchir au maximum de l'influence des paramètres hydrologiques et faciliter la comparaison entre les différents modèles d'érosion. Ce cadre théorique introduit les notions de penteéquivalente et d'érodibilité équivalente comme paramètres constitutifs communs à tous les modèles. Les résultats de perte en sol sont testés dans plusieurs conditions combinées de pluie et de ruissellement. Dans ce chapitre la sensibilité des modèles est calculée sous forme de dérivées directionnelles discrètes, associées à des déplacements librement choisis dans l'espace des paramètres.

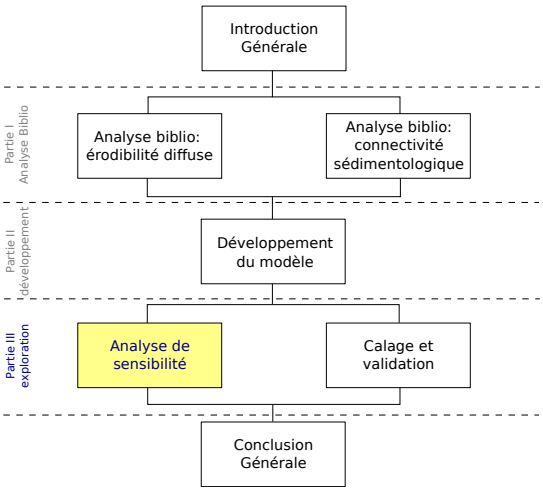

Sensitivity analysis of distributed erosion models - I. Framework [1]

Cheviron, B.; Gumiere, S.J.; Le Bissonnais Y.; Moussa, R. & Raclot, D. (article acepted with major revision required in Water Resource Research)

Abstract

We introduce the (P, R, p) procedure for analysis of distributed erosion models, evaluating separate sensitivities to input fluxes (precipitations P), to the propensity of soil to surface flow (runoff conditions R) and to specific erosion properties (descriptive parameters p). For genericity and easier comparisons between models, super-parameters of "equivalent slope" and "equivalent erodibility" are assembled from innate descriptive parameters: parameterization is reduced to four coded integers that are arguments of the soil loss function. Directional sensitivities are calculated in a deterministic way, associated with any selected displacement in parameter space. In this multi-stage and risk-orientated procedure, special emphasis is placed on trajectories from best-case towards worst-case scenarios, involving *one-at-a-time* variations and Latin Hypercube samples. Sensitivity maps are produced in the super-parameter plane, tracing risk isovalues, estimating the relative importance of the equivalent parameters and of their spatial distributions.

5.1 Introduction and scope

New insights on the topic of climate change urge research on erosion, especially in regions that have been identified as vulnerable to sharpened or more frequent natural events. Although different concepts appear in models pertaining to different scales, all water erosion models address potential damages caused by rain and runoff. Soil loss results are nevertheless conditioned by slopes and by soil erodibility encountered along flow paths. Regarding phenomenology and parameter requirements, erosion models integrate specific processes, one step further in complexity but far less studied than the hydrological descriptions on which they necessarily rely and strongly depend. Sensitivity analysis conducted on erosion models lack an explicit and generic framework to estimate the relative importance of hydrological and erosion factors or categories of factors.

[1] Cheviron, B.; Gumiere, S.J.; Le Bissonnais Y.; Moussa, R. & Raclot, D. Sensitivity analysis of distributed erosion models - I. Framework, 2009, article acepted with major revision required in Water Resource Research

Hydrological parameters cited as crucial to soil losses are the saturated hydraulic conductivity of surface layers in WEPP (Nearing et al., 1990), LISEM (De Roo et al., 1996b) and EUROSEM (Veihe and Quinton, 2000), friction coefficients responsible for flow retardation in PSEM-2D (Nord, 2005) or net capillary drive (Veihe and Quinton, 2000) in small-scale physics based models. At medium scales, sensitivity to runoff and antecedent rain are used in STREAM (Cerdan et al., 2002) to qualify the influence of hydrological factors. At larger scales, surface crusting and percentage of vegetation cover control the effect of input fluxes on soil losses in PESERA (Gobin et al., 2004; Kirkby et al., 2008), while MESALES (Le Bissonnais et al., 2002) resorts to surface crusting and land use as indicators of runoff conditions. Parameter sets associated with optimum transmission of input fluxes render soils more prone to simulated erosion, but particle detachment still depends on values of a different set of specific erosion parame! ters. For example, key erosion parameters are soil erodibility in MESALES and PESERA, sensitivity to diffuse erosion and soil cohesion in STREAM, sediment size in EUROSEM, soil cohesion and rill erodibility in PSEM-2D and again rill erodibility in LISEM.

Only partial sensitivity results are available in literature on erosion models, for the relative importance of hydrological and specific erosion parameters has not been tested yet. The actual consensus is that models are more sensitive to hydrological conditions than to speficic erosion parameters, but Gumiere et al. (2009d) suggested that reported sensitivity indexes may be influenced by test configurations, almost always involving strong input fluxes. Investigation procedures combining widely-varied rain intensities, runoff conditions and erosion parameters are therefore needed.

In a unified description, a causal link exists between the input flux, precipitations P, the transmitted flux, obtained from runoff conditions R, and the resulting soil loss, calculated from specific erosion properties p. A three-category (P,R,p) sensitivity analysis procedure seems therefore possible and appropriate to most erosion models, its effectiveness being to discriminate between the effects of "control" hydrological factors (P,R) and "descriptive" erosion parameters (p). Focusing on erosion processes, one may wish to estimate the sensitivity to parameters of the p category for varied (P,R) combinations representing as many water excess conditions.

To reach a satisfying level of genericity and meet the claimed objectives, the (P,R,p) framework should certainly refer to literature to:

1.1 - exploit at best the identified structural similarities between the very different pairs of hydrology-erosion models, to ensure a wide applicability of the procedure,

1.2 - define its position in the world of sensitivity analysis, as a deterministic multi-local procedure resorting to a combination of methods to gain sensitivity results from selected parameter arrangements,

1.3 - prove its usefulness in erosion modelling, through specific and argumented choices for sensitivity measurement and representation, relying on common calculation devices,

1.4 - place emphasis on simple tests to measure the sensitivity of an erosion model to spatial distributions of its descriptive parameters,

5.1.1 Position regarding hydrology-erosion models

Sufficient complexity of underlying hydrological models is a prerequisite to accurate erosion modelling, at the risk of degraded performances due to overparameterization (Beven, 1989), especially for models involving spatially-distributed parameters (Beven, 1993). Additional uncertainties arise when only few measured data are available, increasing equifinality thus weakening the physical meaning of parameters, as discussed by de Marsily (1994) then Beven et al. (2001) from a theoretical point of view. While intended to describe a wide set of often non-observable events, the construction of a model is a deterministic process that relies on a limited series of scenarios and choices. It requires *a minima* identification of the flow chart and slopes of the system, plus knowledge about the nature and range of intensity of its driving mechanisms at the nominal scale of the model. The existence of scale effects (Blöschl and Sivapalan, 1995) and the lack of a well-established rule to perform scale aggregations (Sivapalan, 2003) both question the compatibility of different models when reaching the limit between different scales (Blöschl, 2001).

Owing to the interdependence with hydrology (Merritt et al., 2003) and to intrinsic strong measurement errors (Nearing, 2000; Nearing et al., 1999), several obstacles prevent high-performance erosion modelling and *in situ* evaluation of the models (Boardman, 2006). As a major concern regarding land management, Jetten et al. (2003, 1999) pointed out poor predictions of the spatial pattern of soil losses. They also reported the scale-dependence of computed soil loss to the resolution grid used, but suggested that precision could be gained from an adequate confinement of phenomena in certain cells (Jetten et al., 2005).

All mentioned elements plead in favour of a deterministic procedure involving a reduced number of descriptive parameters, whose values would be distributed on a fixed topology and tested under the widest expected range of precipitation intensities.

The number of cells in the discretization grid should be high enough to induce noticeable distribution effects through clearly-contrasted parametric configurations. On the other hand, the number of cells should be small enough to induce few equifinality and facilitate interpretation. To decrease the number of erosion parameters without disregrading specificities of each model or losing generality, one may constitue groups of parameters, thus reducing the parameterization to the two necessary components of any erosion model, the "equivalent slope" and "equivalent erodibility". The former super-parameter should thus integrate all relief or Digital Elevation Model information. The latter should bear information relative to rill (Knapen et al., 2007) and interrill erodibility (Gumiere et al., 2009d) as a whole or separately dealt with (Bryan, 1976, 2000; Sheridan et al., 2000; Wischmeier and Smith, 1978), as in physics-based models where distinct parameter sets may be used to constitute an "equivalent rill erodibility" and an "equivalent interrill erodibility". Whatever their nominal scales, the described procedure places all models on the same starting line before the final stage of sensitivity analysis begins, which is an indirect way of studying scale issues: searching for sensitivity trends associated with the nominal scales of models under examination.

5.1.2 Position regarding sensitivity analysis practices

Regarding sensitivity analysis practices (Frey and Patil, 2002; Pappenberger et al., 2008; Saltelli et al., 2000), the (P,R,p) framework is a multi-stage procedure combining *one-at-a-time* variations and Latin-Hypercube sampling techniques (McKay et al., 1979). It performs a partial screening of the parameter space which originates in the method exposed by Morris (1991), adapted by van Griensven et al. (2006), also used by Mulungu and Munishi (2007) then renewed and improved by Campolongo et al. (2007). The advantages of using combined methods as a surrogate to their respective limitations have been advocated by Kleijnen and Helton (1999) and Frey and Patil (2002).

Our scope is to obtain sensitivity estimations near certain nodes in the parameter space, for selected realisations of the (P,R,$\bar{p}$) triplet, where $\bar{p}$ accounts for hypercube combinations of p values forming the super-parameters of "equivalent slope" and "equivalent erodibility". Relevant values of the $\bar{p}$ parameters are sorted after initial *one-at-a-time* variations in the individual p parameters, then variations in values of $\bar{p}$ are tested together (hypercubes) or separately (*one-at-a-time*) for different values of (P,R). From its construction and roles played by (P,R) on one side, p or $\bar{p}$ on the other side, our procedure falls in the multilocal rather than in the global sensitivity analysis classification. Deterministic and local sensitivity information is seeked, so we leave aside the intensive but "blind" Monte-Carlo screenings (Sieber and Uhlenbrook, 2005)

or variance-based sensitivity estimations (Castaings et al., 2007; Hier-Majumder et al., 2006; Tang et al., 2006) eventually resorting to Sobol (1993) algorithms or conducted with the Fourier Amplitude Sensitivity Test (Crosetto and Tarantola, 2001; Helton, 1993). These discarded methods yield statistical results and perform well in verifications of model structure when no prior knowledge on the models is available. On the contrary, the (P,R,p) framework is progressively executed from successive sensitivity results inferring priviledged scenarios. As explained by Saltelli et al. (2004) and Pappenberger et al. (2008), sensitivity results may also depend on the way the analysis method is formulated. Hypothesis of uniform distribution of parameter values similar to these formulated by Beven and Binley (1992b) are nevertheless expected to reduce dis! crepancies between results of the deterministic and probabilistic methods, judging from studies conducted in other research domains (Kamboj et al., 2005; Mitchell and Campbell, 2001).

5.1.3 Position regarding sensitivity measure and representation

The choice of a sensitivity measure is constrained by that of a sensitivity analysis procedure. Local deterministic schemes incline to intuitive definitions of sensitivity (Lions, 1968), relying on first-order Taylor developments, *i.e.* the linear hypothesis. These first-order local sensitivities (Saltelli et al., 2000) simply approximate sensitivity as the proportionality between output and input variation, in absolute or relative form. This measure was termed "elementary effect" by Morris (1991). It applies for displacements in parameter space involving variations in a single parameter or in two at once (Campolongo and Braddock, 1999), provided input variations are not to narrow, causing roundoff or "divide by zero" errors, or not too big, breaking the linear hypothesis (Cacuci and D'Auria, 2006) when confronted to non-linear behaviour of the model.

When two or more parameters are varied at the same time, it becomes a challenge to identify the individual contribution of each parameter to the output variation. The classical probabilistic answer in global (non-point) methods is to measure linear and higher-order sensitivities as the mean elementary effect and its standard deviation. The latter estimates correlations and interactions between parameters, providing the non-diagonal values in sensitivity matrixes, see Ronen (1988) for example. But as stated by Saltelli et al. (2004) and Ionescu-Bujor and Cacuci (2004), the identification of high-order effects is doubtful unless additional assumptions are available regarding pairs of non-independent parameters. A convincing example is given by Knight and Shiono (1996) scrutating complex interactions between parameters associated to channel and floodplain friction.

In the (P,R,p) procedure, deterministic and multilocal sensitivity calculations are possible, starting from the nodes of interest in parameter space. Additional assumptions are also available to indicate relevant directions for these multiple calculations, including combined parameter variations towards best-case or worst-case scenarios. The underlying concept and calculation device is that of the Gâteaux directional derivatives (Gâteaux, 1913). It pertains in analysis of non-linear discrete systems (Cacuci, 1981, 2003) and generalizes the concept of "elementary effect" to any displacement in parameter space.

5.1.4 Sensitivity to spatial distributions of parameters

Again, the purpose here is not to test the sensitivity of a model to every spatial distribution of its descriptive parameters or super-parameters, ignoring previous knowledge on the model behaviour (Lilburne and Tarantola, 2009). The analysis rather involves a limited number of very different and contrasted spatial distributions of parameter values, associated with expected noticeable effects on the soil loss results. The sensitivity to spatial distributions is the retained measure of these effects, which the reader may compare to other deterministic techniques listed in Turanyi and Rabitz (2000), yielding so-called "distributed sensitivities". As any spatial distribution can be seen as a disturbance of spatial homogeneity, the natural sensitivity measure should make reference to the result obtained in a spatially-homogeneous configuration.

We propose here a sensitivity analysis framework relying on a multi-stage procedure especially designed for distributed erosion models. This procedure discriminates between sensitivity effects due to hydrological factors and specific erosion properties. It resorts to deterministic multilocal sensitivity calculations in which erosion parameters are tested one- or many-at-a-time for a wide set of combined rain intensities and runoff conditions. A combination of sensitivity analysis techniques is used but this paper does not aim at any theoretical novelty. We rather focus on easy-to-apply sensitivity measures allowing comparisons between models pertaining at different scales and appealing to different concepts. Emphasis is placed on the estimation of the sensitivity of a model to spatial distributions of its parameters, which is calculated and illustrated from selected contrasted configurations. All tests were performed on the OpenFluid (2009) platform, a sofware environment for modelling fluxes in landscapes.

5.2 Materials and methods

5.2.1 Virtual Catchment

In the (P,R,p) procedure, the virtual catchment is the topographical entity on which soil loss and sensitivity calculations are performed. Its principal features are shown Fig.5.1. Its topology is fixed. Flow paths stay unaffected by the driving rain conditions and are the only connectivity lines between cells in the catchment, regarding hydrological and sedimentological processes. If not bridged by a flow line, two adjacent cells have no interactions. For simplicity, all cells are abusively represented by squares but their length and width may vary, if distance to the drainage line or streamwise distance has to be introduced to fit requirements of a given model. Conversely, the surface of the elements should be kept constant, in accordance with the nominal spatial scale of the model.

Only spatially-homogeneous values of the hydrological factors accounting for precipitations P and runoff conditions R are considered here. Asymmetry is thus provided by the flow network. This very simple nine-cell setting introduces differences between the five equivalent upstream cells (1, 2, 3, 6, 9) and higher-order cells (4, 5, 8, 7), sorted here by increasing numbers of drained cells. Five different levels of flow aggregation exist thus in the virtual catchment, tested for multiple pairs of hydrological conditions (P,R). A wide data set of local (cell) and global (virtual catchment) soil loss results is thus created. It spans over the entire phenomenological range of the model, from very weak erosion in upstream cells under low water-excess conditions to very strong erosion in downstream cells under high water-excess conditions.

The same number of data set entries could have been obtained from a more complicated flow chart involving a higher number of cells and less pairs of (P,R) values, but would have represented a different variety in situations. We preferred testing more (P,R) values on a reduced 3×3 setting for graphical simplicity and to better analyse the contribution of interrill (or diffuse) erosion. When separately computed in a model, interrill erosion does not depend on flow aggregations but is governed by local rain intensity, thus is better studied when considering more P values.

The advantages of more complex flow networks *a priori* remains that of more diverse patterns of flow aggregations or embranchments, occuring at more varied positions along the linear network, this time concerning rill (linear) erosion. But even with the simple 3×3 setting, the virtual catchment partly remedies the expected drawbacks: flow aggregations are made in two different manners, either streamwise ($1 \rightarrow 4$) or by embranchments ($2\&3 \rightarrow 5$, $5\&6\&9 \rightarrow 8$, $4\&8 \rightarrow 7$). The (P,R,p) procedure tests the

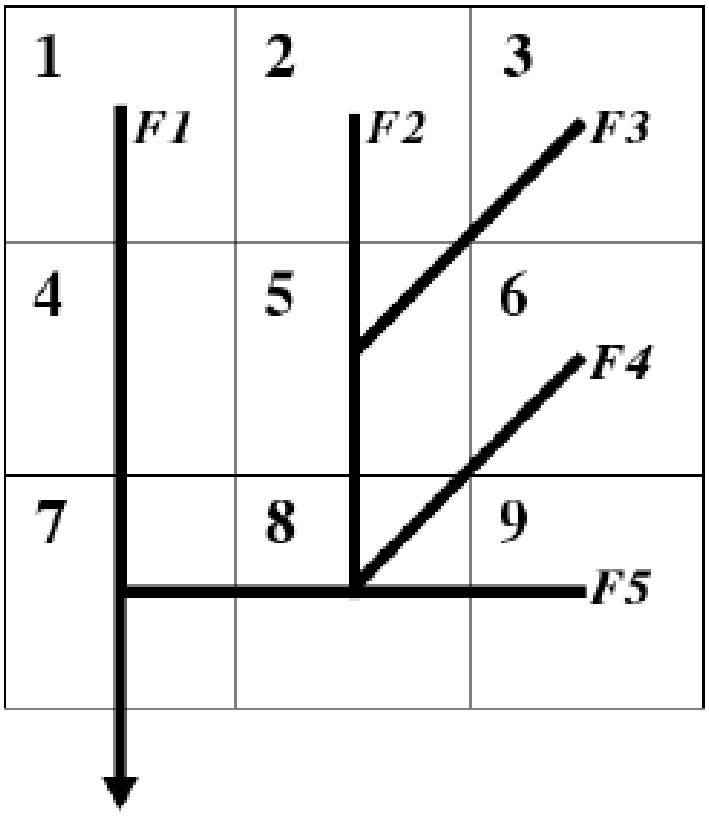

Figure 5.1: Layout and connectivity in the virtual catchment between surface units numbered 1 to 9. The one-way downstream hydrological and sedimentological connectivity is indicated by flow lines numbered *F1* to *F5*.

way a model performs these aggregations at different flow strengths, depending on their position in the network and on the imposed (P,R) values.

As we focus on the role played by specific erosion parameters, both spatially-homogeneous and distributed configurations of the descriptive parameters p are tested. In the former case, asymmetry is only due to the flow chart, five different and increasing soil loss results are expected at the outlet of cells (1,4,5,8,7), involving four aggregations, for any pair of (P,R) values. In the latter case, heterogeneity in values of p between cells is superimposed to assymetry created by the flow chart.

5.2.2 Classification of the parameters

The (P,R,p) procedure distinguishes between the P, R and p categories on phenomenological criteria. Input fluxes given as rain intensities are termed "precipitations" and placed in the P category. Parameters describing slope or taking part in the definition of an "equivalent erodibility" fall in the p category. The remaining parameters, neither directly related to erosion processes nor being input fluxes, are termed "runoff conditions", coded R. Though this definition aims at unambiguously discriminating between R and p parameters, it is adaptable to specificities of any model. A general strategy regarding parameterization of all compared models is nevertheless intended and wishable. If for example a given parameter switches from the p to the R category when testing a different model, the corresponding sensitivity is recorded as a sensitivity to R and not anymore to p values, which complicates comparative analyses.

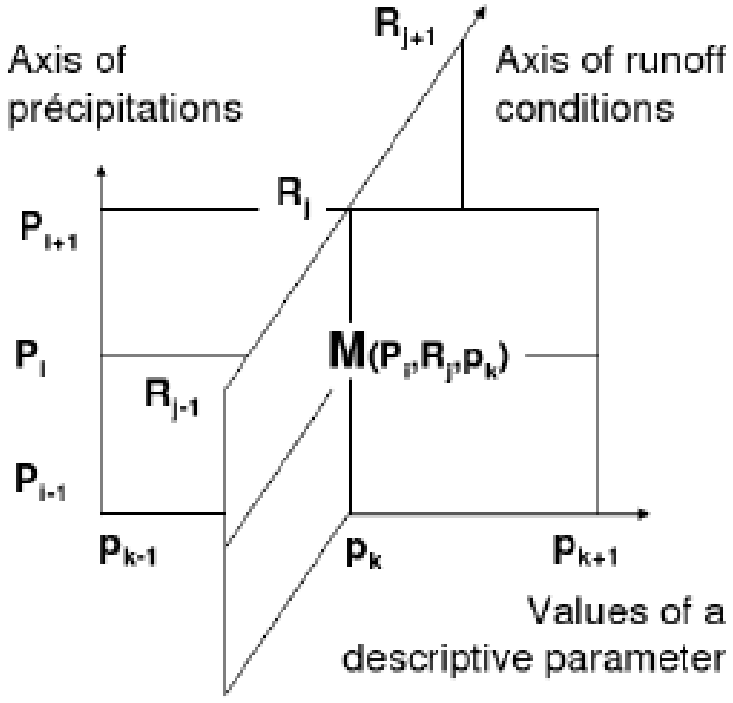

Figure 5.2: Model response M in the first stage of the (P,R,p) procedure. Unit increments separate consecutive values of P, R and p on each axis.

As parameters are dispatched into three independent categories without interac-

tions, these categories may be seen on Fig.5.2 as orthogonal axis bearing values of P, R and p. The gradation along each axis is made of unit increments: the range of variation for "real" P, R and p values is reduced to a certain number of segments of unit length. As references to a central point in parameter space are made, an odd number of values should preferentially be used in each category, finding the same number of values on both sides of the central position on each axis. Depending on allowances of each model or on user-defined options a different number of P and R conditions may be tested, but further steps in the procedure impose the same number of values for all parameters in the p category. The (P,R,p) procedure requires at least three values for P and R but needs at least five for p.

In an event-based erosion model, one may thus have five rain intensities corresponding to precipitations of 20, 35, 50, 65 and 80 $\mathrm{mm\,h^{-1}}$ coded 1, 2, 3, 4 and 5 as P values. In a large-scale model, if rain intensities appear as a monthly average with a given standard deviation and additional information on the number of rainy days, the user must create undoubtedly "increasing" P conditions. This operation requires a minimum knowledge of the model as well as clear modelling objectives. The simplest way to achieve the choice in P values is to freeze all R and p values before testing combinations of parameters intended to form the P values, then to sort these P values by increasing calculated soil losses.

The problem is similar in the definition of runoff conditions. Let us consider for illustration a process-based model where runoff is governed by the saturated hydraulic conductivity K_s and initial water content θ_i of the top soil layers. If three values are available for each, the natural choice to form R values is to combine K_s and θ_i in increasingly favourable runoff conditions $R = 1\,(K_s\,\mathrm{max}, \theta_i\,\mathrm{min})$, $R = 2\,(K_s\,\mathrm{median}, \theta_i\,\mathrm{median})$ and $R = 3\,(K_s\,\mathrm{min}, \theta_i\,\mathrm{max})$.

5.2.3 Spatial distributions of the parameters

Parameters of the p category should not raise definition issues, as they are tested for themselves though in various spatial patterns, either homogeneous (A) or distributed (B). In A configurations, the tested parameter has the same value in all cells and at least five levels of values are needed: five is the minimum to correctly draw the form of the model response in *one-at-a-time* variations.

When designing B configurations, we opted for a limited number of contrasted configurations, in terms of spatial distributions and parameter values involved, as can be seen on Fig.5.3. Several arguments explain this choice:

- the deterministic logic followed throughout this study appeals to a small number

of easily identifiable cases and results,

- only limited-precision data are available in hydrology or erosion science, pleading for tests involving contrasted data that could be related to field conditions,

- these sensitivity tests do not aim at complete examination of a model, rather at identifying its behaviour in the more or less risky situations present among the proposed heterogenous settings.

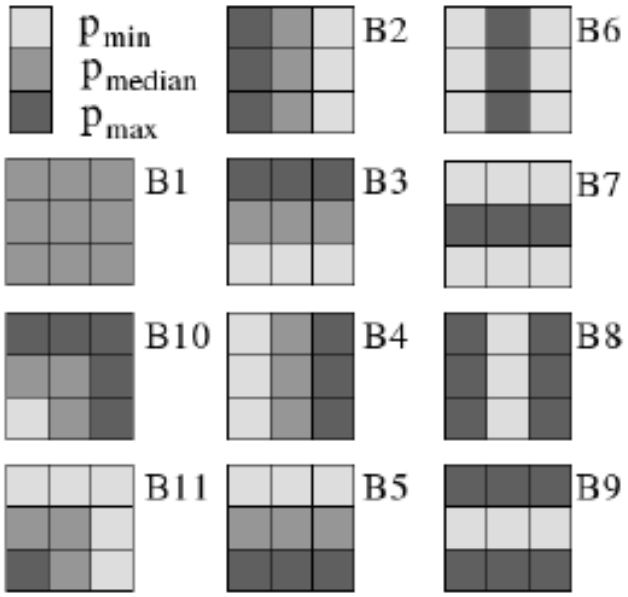

Figure 5.3: Spatially-distributed B configurations used in testing specific erosion parameters. Light, median and dark grey cells receive values respectively associated with minimum, median and maximum soil loss.

For comparison purposes between homogeneous and distributed settings, configuration $B1$ was chosen identical to the median A case: when compared to $B1$, other B configurations could also be compared to any of the A cases. We then imposed three very different and simple patterns:

- the first sub-family of B configurations includes *B2* to *B5* and simulates a gradation of values by stripes, involving only the minimal, median and maximal values among the eleven allowed values,

- the second sub-family includes *B6* to *B9* where a stripe of maximal values is placed between two stripes of minimal values or vice versa,
- the last sub-family (*B10*,*B11*) proposes gradations of values approximately superimposed to the flow chart.

5.2.4 Resolution scheme

The predefined parametric configurations can be processed in the model under control of the SENSAN (Doherty, 2004) sensitivity analysis tool as depicted in Fig.5.4. A line in the parameter variation file contains all user-defined values of the tested descriptive parameter in the nine cells of the virtual catchment, as well as indications of the P and R values. Consequently, the parameter variation files has as many lines as the number of parametric configurations to be tested. Once numerical and graphical post-treatments have been completed and the parameter variation file has been entirely read, SENSAN's execution normally terminates. To keep it running on several parameter files in a row, *i.e.* for each descriptive parameter, we used additional automation scripts.

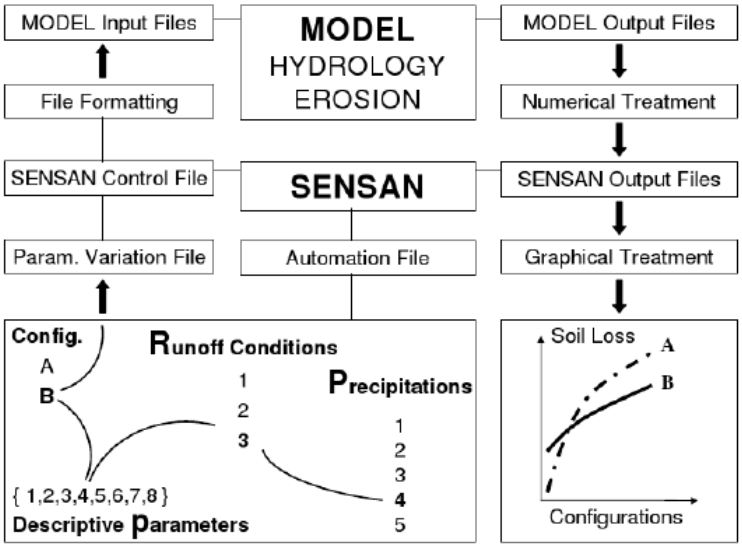

Figure 5.4: Resolution scheme proposing a coupling between the tested model, the sensitivity analysis tool and auxiliary programs involved in post-treatments. Represented here in bold is the run series for the fourth precipitation value ($P = 4$) in strong runoff conditions ($R = 3$) where the tested parameter (fourth among eight p parameters) takes spatially-distributed values in the set of B configurations.

5.2.5 Sensitivity calculations

When considering a single parameter, the intuitive definition of sensitivity is a first-order approximation:

$$M(p) - M(p_0) = \left.\frac{\partial M}{\partial p}\right|_{p_0} (p - p_0) = [S^*]\,(p - p_0) \tag{5.1}$$

where $M(p)$ is the output obtained from a certain p parameter value, $M(p_0)$ is the output obtained from the p_0 starting parameter value. $[S^*]$ is the local sensitivity of the model, accounting for the derivative of $M(p)$ with respect to p and calculated at p_0. In this formulation, $[S^*]$ is implicitly constant on $[p_0, p]$, which questions the relevant size of the $[p_0, p]$ interval, especially for models associated with local non-linear behaviours or threshold effects.

According to the previous developments:

$$M(\vec{p})_{P,R} - M(\vec{p_0})_{P,R} = [S^*]_{P,R}\,(\vec{\delta p}) \tag{5.2}$$

where model outputs and the associated sensitivity calculation hold for the given (P, R) values and for any (sufficiently small) $\vec{\delta p} = \vec{p} - \vec{p_0}$ displacement in parameter space involving one or more descriptive parameters.

Using unit increments as gradations of the axis of p values and only taking discrete values of p as multiples of the unit increments, $[S^*]_{P,R}$ is *de facto* estimated as an approximate Gâteaux directional derivative (Behmardi and Nayeri, 2008; Cacuci, 2003; Gâteaux, 1913):

$$[S^*]_{P,R} = \frac{M(\vec{p_0} + \lambda\vec{\delta p})_{P,R} - M(\vec{p_0})_{P,R}}{\lambda} \tag{5.3}$$

where λ is a (sufficiently small) real number and $\vec{\delta p}$ has not to be small anymore, provided $\vec{p_0} + \vec{\delta p}$ is a point still inside or at least on the boundaries of the parameter space. Note that if n descriptive parameters are involved, they are the n components of $\vec{p} = (p_1, p_2, .., p_n)$.

In such conditions, $[S^*]_{P,R}$ should be termed "sensitivity at $\vec{p_0}$ in the direction of $\vec{\delta p}$". More than a formal remark, it refers to a crucial property of the Gâteaux derivative. We make use of it when directing the $\vec{\delta p}$ increment from any chosen point towards points corresponding to best-case or worst-case scenarios, *i.e.* points located at the "hyper-corners" of the parameter space, corresponding to minimum or maximum values of P, R and $\vec{p}$ at-a-time.

To achieve complete generality of sensitivity calculations, one has indeed to consider the local model response as a function $M(P, R, \vec{p})$ where $\vec{p}$ accounts for the fact that

several p parameters may be varied at-a-time. Using entire values for P and R on unit-gradated axis, we may calculate sensitivities with the formalism inherited from the Gâteaux derivative for changes in P or R values, or in both P and R values, or even in P, R and $\vec{p}$ values at-a-time.

5.2.6 Sensitivity to spatial distributions

The previous sensitivity calculations refer to spatially-homogenous p_0 and p values for variations in a single descriptive parameter. They appeal to $\vec{p_0}$ and $\vec{p}$ for spatially-homogeneous variations in multiple descriptive parameters. But such scalar or vectorial quantities have no equivalent when considering spatial distributions which need a specific sensitivity measure.

We define the $E(B_i)$ efficiency of a B_i configuration as:

$$E(B_i)_{P,R} = \frac{M(B_i)_{P,R}}{M(B_1)_{P,R}},\ \forall i \in \{1,..,11\} \tag{5.4}$$

where $M(B_i)_{P,R}$ is soil loss obtained in the B_i configuration for a given pair of (P,R) hydrological conditions and $M(B_1)$ is that obtained in the median homogeneous case.

Accordingly, we define the $[S_B]$ sensitivity of a model to the eleven spatial distributions as the simplest measure of dispersion of the eleven soil loss results:

$$[S_B]_{P,R} = \max[E(B_i)_{P,R}] - \min[E(B_i)_{P,R}],\ \forall i \in \{1,..,11\} \tag{5.5}$$

where the sensitivity of $[S_B]$ to displacements along the P and R axis may also be studied with the formalism inherited from the Gâteaux directional derivative.

5.2.7 Sensitivity to flow aggregations

Asymmetry in the flow chart of Fig.5.1 was intended to create heterogeneity in soil loss results between cells, even for spatially-homogeneous values of the descriptive parameters. The nine-cell virtual catchment exhibits five flow aggregation levels, associated with positions of the cells in the network. Flow aggregations occur either in a streamwise (or longitudinal) manner or by embranchments, with lateral inflows. The purpose of this section is to scrutate the behaviour of a model at the nodes of the flow network, under varied (P,R) hydrological conditions, for spatially-homogeneous p values. Do flow aggregations have a linear effect on soil loss? Is this effect affected by the hydrological conditions, and how? What are the sensitivity trends?

These issues should be addressed in sensitivity analysis because they refer to constitutive elements of a model, to its inner structure. The sensitivity to flow aggregations

is certainly not disconnected from the sensitivity of a model to its parameters: its analysis is rather a complementary approach. In the virtual catchment, such an analysis requires soil loss results at the outlet of the involved cells (1,4,5,8,7) to be recorded, whereas other sensitivity results concern soil losses at the global outlet. As any network integrates both longitudinal and lateral flow aggregations: results obtained in our very simple pattern (but for many hydrological conditions) may be extrapolated to much more complicated patterns. They may also be extrapolated to other water-excess conditions, once known sensitivity trends appearing with varied (P,R) values.

The model response is $M(P, R, \vec{p})$ and we consider here the spatially-homogeneous case for hydrological conditions (P, R) and all descriptive parameters contained in $\vec{p}$. Changing variables, we introduce $M(X, \vec{p})$ where X is an unknown function $X(P, R)$ representing the amount of water flowing out of a given cell. Consequently, X depends on local (P, R) values in a cell as well as on the inflow provided by immediate upstream cells. X can therefore be expressed as a function of the local runoff x and the incoming upstream flow y. With these notations X becomes $X(x, y)$.

For illustration, let us describe flow aggregation between cells 1 and 4:

- For example, soil loss at the outlet of cell 1 is $M(X_1, \vec{p})$ with indicial notation $X_1(x_1, y_1)$ for local cell values. But no incoming upstream flow y_1 must be considered as cell 1 itself is an upstream cell. We may thus express soil loss at the outlet of cell 1 as $M(x_1, \vec{p})$.

- Passing downstream to the next cell, soil loss at the outlet of cell 4 is $M(X_4, \vec{p})$, with $X_4(x_4, y_4)$ and $y_4 = x_1$. We may now write $M(x_4, x_1, \vec{p})$. Introducing $\delta x = x_4 - x_1$, we use the equivalent expression $M(\delta x, \vec{p})$ which relates soil loss at the outlet of cell 4 to the streamwise flow aggregation δx between cells 1 and 4.

- It is then possible to test the sensitivity of this quantity to different levels of P, R and p by comparing $M(\delta x, \vec{p})$ with $\delta M = M(X_4, \vec{p}) - M(X_1, \vec{p})$. The same calculation pertains for lateral aggregations.

5.2.8 Stages of the procedure

5.2.8.1 Objectives

This section deals with construction of the multi-stage (P,R,p) procedure, describing a progressive and orientated exploration of parameter space. A combination of *one-at-a-time* and Latin-Hypercube sampling methods is applied, which reduces the parameterization to super-parameters accounting for "equivalent slope" ($\bar{p_s}$) and "equivalent

erodibility" ($\bar{p_e}$). These essential components of any erosion model are then tested individually and together to yield final sensitivity results prone to graphical representation. The following paragraphs enumerate the stages of the procedure for spatially-homogeneous configurations of the descriptive p parameters. A last item indicates adaptations to the case of spatially-distributed p values.

5.2.8.2 Preliminary stage

The already-described preliminary stage is the univoque classification of fluxes and parameters into the P,R and p categories. A further sub-division of the p category is needed for models that distinguish between linear and diffuse erosion processes, before building the "equivalent erodibility" from the "equivalent linear erodibility" and "equivalent diffuse erodibility". If a parameter is called in both erosion processes, the best solution whenever possible is to separately test its values in both processes for example under to different names. When no distinction exists between linear and diffuse erosion, for example in regional-scale models, the procedure simply aims at building an "equivalent erodibility".

5.2.8.3 Individual one-at-a-time tests

Figure 5.5 depicts the situation where candidate descriptive parameters of the model are erodibility, rooting depth and soil texture. *One-at-a-time* tests are performed on each of them under three combinations of P and R values, namely the less, median and most prone to soil loss. These tests involve at least five parameter values covering the entire nominal range of variation. Useful representations of the results are "spider diagrams" plotting the relative ouput variation in y-ordinate versus the relative input variation in x-ordinate, the centre of the diagram being the (0,0) reference point. When testing a parameter, all others are held at their reference (median) values.

If the model is proven to be insensitive to a candidate parameter under varied hydrological conditions, this parameter is excluded from the procedure. We discard the pathologic case where a parameter has no influence if tested alone but a strong influence if tested in correlation with some other parameters. The choice we make here is coherent with the fact that prior knowledge is available on tested models. Moreover, such problematic behaviours should have been removed or smoothened during construction of the models. On the contrary, threshold phenomena in tested models were correctly addressed by the procedure, which is a major concern in erosion modelling.

If the model is sensitive to a candidate parameter, the sign of the sensitivity is checked for: is it a positive one, an increase in parameter value causing an increase in

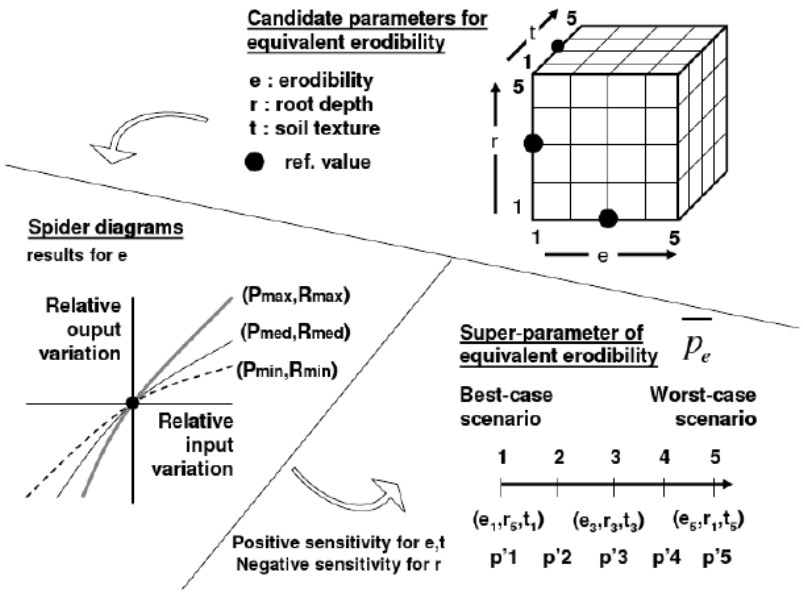

Figure 5.5: Candidate p parameters are extracted from the innate parameterization of the model, tested individually then gathered to create a set of as many p' values. These combinations are sorted by increasing soil loss order and represent values of the super-parameter $\bar{p_e}$ termed "equivalent erodibility".

model response, or a negative one? For parameters showing a negative sensitivity, the list of values is re-sorted in opposite order, so that progressing inside this list finally gives increasing soil loss values. In the chosen example, erodibility values are certainly already sorted in the right order, whereas rooting depth values probably need re-sorting. The trend is *a priori* uncertain for soil texture values and may even depend on (P, R) conditions.

5.2.8.4 Rules to form super-parameters

In the next step, super-parameters are formed by assembling values of each of the retained candidate parameters into increasing p' values. Figure 5 shows five tested values coded 1 to 5 for erodibility (e_1 to e_5), rooting depth (r_1 to r_5) and soil texture (t_1 to t_5). In addition, soil texture was supposed here to have a positive sensitivity. Then five combinations of values are available to form the "equivalent erodibility", which are (e_1, r_5, t_1), (e_2, r_4, t_2), (e_3, r_3, t_3), (e_4, r_2, t_4) and (e_5, r_1, t_5) in increasing soil loss order. Depending on specificities of the models, at least two super-parameters are built: "equivalent slope" ($\bar{p_s}$) and "equivalent erodibility" ($\bar{p_e}$). The latter is sub-

divided into "equivalent linear erodibility" and "equivalent diffuse erodibility" only in process-based models.

Through options retained in the construction of super-parameters, the procedure follows an imaginary line between best-case and worst-case scenarios. This strategy of an orientated exploration must be related to what is expected from erosion models: understanding of the key aspects of the problem for disaster prevention. Consequently a similar but enriched approach is maintained in exploration of super-parameter space, where trajectories are still centered on the best-case-worst-case axis.

5.2.8.5 Exploration of super-parameter space

Shown in Fig.5.6 is the coverage of super-parameter space from values of the equivalent slope $\bar{p_s}$ and equivalent erodibility $\bar{p_e}$. The minimum grid of five by five values is presented in the background. Two types of explorations are clearly visible, involving *one-at-a-time* (OAT) displacements between black disks and Latin-Hypercube (LH) samples between white disks. The first diagonal is the axis linking the best-case to the worst-case scenarios, for any given (P,R) conditions. The second diagonal is a transverse axis of lesser importance but whose points are needed to complete sensitivity maps in the $(\bar{p_s}, \bar{p_e})$ plane.

All sensitivity calculations resort to Eq.5.3. The default algorithms perform sensitivity calculations between two successive points on the OAT or LH axis. They could be easily extended to displacements between any two disks but were found sufficient to obtain relevant sensitivity information in the $(\bar{p_s}, \bar{p_e})$ plane. As the general expression for soil loss is $M(P, R, \bar{p_s}, \bar{p_e})$, local sensitivity results are available for variations in P, R, $\bar{p_s}$, $\bar{p_e}$ and for any displacement involving one or more arguments of the M function.

5.2.8.6 Adaptations for spatially-distributed configurations

Figure 5.7 is the adaptation of Fig.5.5 to the case of spatially-distributed parameters. Each one of the candidate descriptive parameters takes the eleven spatial distributions of Fig.5.3. All configurations are then sorted by increasing efficiencies relative to the reference configuration *B1*. In this example, the less productive configuration for e is *B3* and the most productive is *B8*. *B1* is near the beginning of the list, which means that many spatially-distributed configurations yield more soil loss than the median homogeneous case. Depending on models and hydrological conditions, the position of *B1* in the list may drastically vary between simulations.

Gathering results for all descriptive parameters, *B'* values are assembled exactly like *p'* values. If *B3*, *B6* and *B9* are the less productive configurations for e, r and

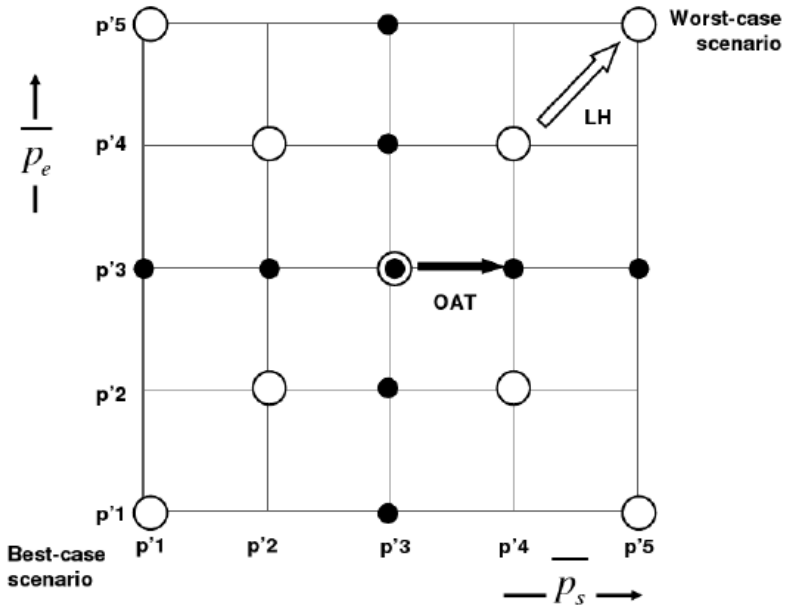

Figure 5.6: Exploration of super-parameter space involving *one-at-a-time* (OAT, black disks) and Latin-Hypercube (LH, white disks) displacements in values of the "equivalent slope" $\bar{p_s}$ and "equivalent erodibility" $\bar{p_e}$.

t respectively, then B'1 is the combination (e_{B3}, r_{B6}, t_{B9}) representing the lesser risk among tested spatial distributions of the super-parameter $\bar{p_e}$. At the other end of the list, in the fictitious situation of Fig.5.7 the higher risk *B'11* is reached when parameters e, r and t take the *B8*, *B5* and *B6* patterns, respectively. The logic is still to draw the line from best-case to worst-case scenarios, for each of the super-parameters $\bar{p_s}$ and $\bar{p_e}$, then for both.

Figure 5.8 is the adaptation of Fig.5.6 and describes how *B'* values associated with $\bar{p_s}$ and $\bar{p_e}$ are managed into OAT and LH samples. In the suggested exploration of super-parameter space, *B'6* plays the role of the median *p'3* value in Fig.6. Again, the diagonal of primary interest joins the $(B'1, B'1)$ and $(B'11, B'11)$ points at the lower left and upper right of the ($\bar{p_s}$,$\bar{p_e}$) plane. Directional sensitivity calculations along OAT and LH axis allow comparisons between relative importance of the $\bar{p_s}$ and $\bar{p_e}$ parameters. Sensitivity maps discussed in the next section plot this information obtained from both model responses (black and white disks) and sensitivity calculations (displacements between disks).

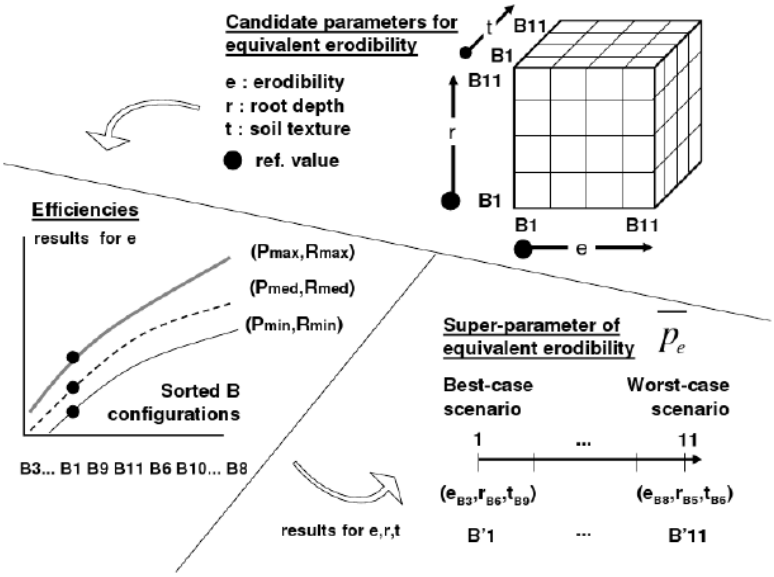

Figure 5.7: Spatial distributions of the candidate p parameters are tested individually then gathered to create a set of as many B' values. These combinations are sorted by increasing soil loss order and represent distributed values of the super-parameter $\bar{p_e}$ termed "equivalent erodibility".

5.3 Results and representation

5.3.1 Spatially-homogeneous configurations

In the final stages of the (P,R,p) procedure, the innate parameterization of the tested model has been altered at the benefit of a $M(P,R,\bar{p}$ description where M is model response, P accounts for rain intensity, R for runoff conditions and $\bar{p}$ is the set of two super-parameters $\bar{p_s}$ ("equivalent slope") and $\bar{p_e}$ ("equivalent erodibility"). Like P and R values, both $\bar{p_s}$ and $\bar{p_e}$ values are coded into unit increments and termed p' values along the corresponding axis (Fig.5.5).

Though p' is used as descriptor on both axis, the notation is unambiguous once specified the displacement in super-parameter space (Fig.5.6) and the general notation $M(P,R,p')$ is kept for simplicity. For a vertical displacement along black disks, p' in the preceding expression represents points on the line ($\bar{p_s} = 3, p' = \bar{p_e} = 1$ to 5). For a horizontal displacement between black disks, p' is ($p' = \bar{p_s} = 1$ to $5, \bar{p_e} = 3$). On the first diagonal p' is indeed ($p' = \bar{p_s} = \bar{p_e} = 1$ to 5) and on the second diagonal it is ($\bar{p_s} = 1$ to $5, p' = \bar{p_e} = 6 - \bar{p_s}$). In all cases, only one parameter is needed to describe the

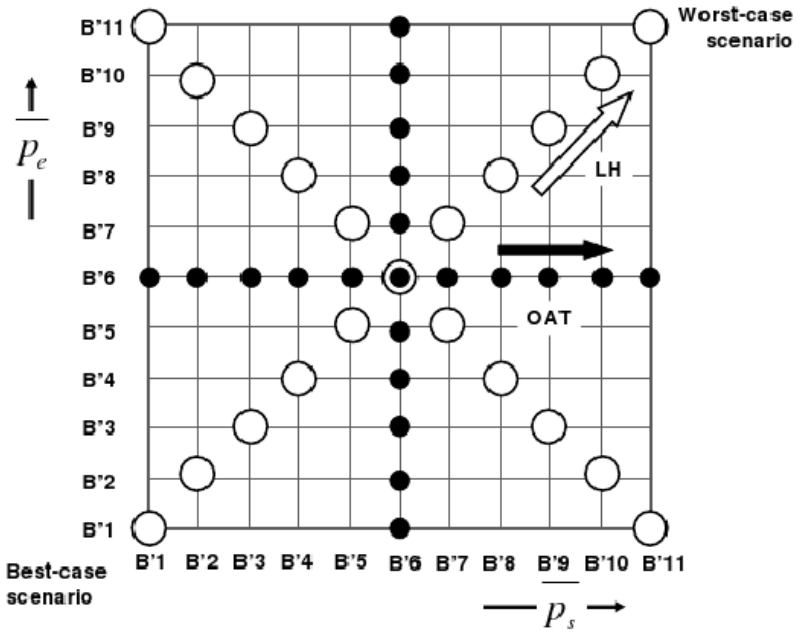

Figure 5.8: Exploration of super-parameter space involving *one-at-a-time* (OAT, black disks) and Latin-Hypercube (LH, white disks) displacements in distributed configurations of the "equivalent slope" $\bar{p_s}$ and "equivalent erodibility" $\bar{p_e}$.

displacement, which makes the general $M(P, R, p')$ notation valid and not confusing.

The retained description involves four quantities: the problem has four dimensions but only a planar representation allows sufficiently detailed information to be plotted. Figure 5.9 indicates how dimensionality may be reduced by placing on the x-ordinate the arguments of the M function and on the y-ordinate its values. The arguments are sorted by increasing P, R and p' values. The same device pertains for representation of the effects of flow aggregations on soil loss, replacing p' by sorted $\vec{p}$ values.

A complete model response is shown in Fig.5.10a. It was obtained from early tests performed during development of the physics-based erosion model relying on the existing hydrological module "MHYDAS"(Moussa et al., 2002). In MHYDAS-Erosion (Gumiere et al., 2009c), the slope parameter is identical to the "equivalent slope"(p=p'). Precipitation intensities $P1$ to $P5$ were 20, 35, 50, 65 and 80 mm h^{-1} during two hours. Runoff conditions $R1$ to $R5$ were formed from combinations of saturated hydraulic conductivity and initial surface water content. Eleven slope values $p1$ to $p11$ between 1% and 30% were available, so that model response is plotted from $5 \times 5 \times 11 = 275$ points. Apart for slight anomalies in the $(P1, R3)$ and $(P2, R2)$ hydrological conditions and a

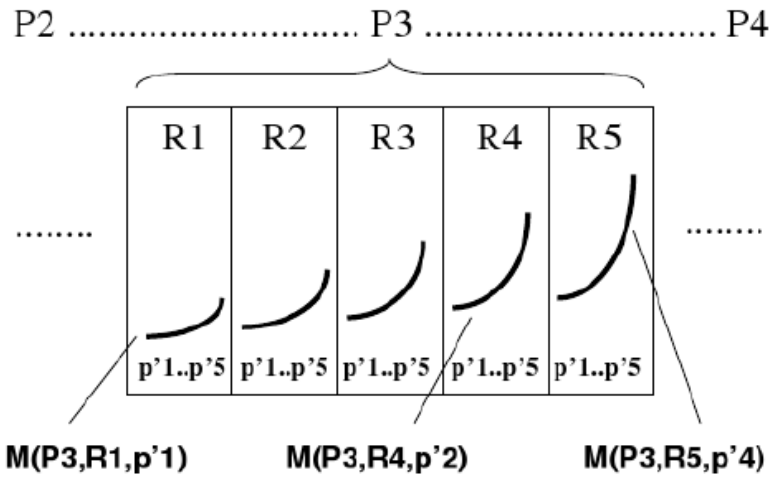

Figure 5.9: 2-D representation of the 4-D problem in (M,P,R,p') used for spatially-homogeneous parametric configurations: P,R and p' values are placed on the x-ordinate and only M appears in y-ordinate.

low point in the $(P4, R1)$ series, the expected "triple" soil loss increase for increasing values of P, R and p is correctly simulated.

Multilocal sensitivity results (Fig.5.10b) also depend on P, R, and p' values. They are represented using the same graphical device than for model responses, which helps composing a dashboard that summarizes a model's behaviour, as illustrated by Fig.5.10 seen as a whole. Directional sensitivities G_p, G_P and G_R are approximate Gâteaux derivatives calculated from Eq.5.3, involving separate unit increments in p, P and R. They give sensitivity results as absolute algebraic variations in the same unit than the model response, which is part of their relevancy and facilitates analysis. We also proposed representing G_p before G_P and G_R for an easier eye-interpretation, especially comparison between magnitudes of the function and its derivatives.

Lacking points in the curves of Fig.5.10b are consequences of the "positive unit increment" option used to calculate sensitivities. For example, sensitivity results $G_P(P, R, p)$ represented in the $P4$ column address variations from $M(P4, R, p)$ to $M(P5, R, p)$ and no such results are given for variations from $P5$ to $P6$ because $P6$ does not exist. The same applies here when values $p = 10$ and $R = 4$ are reached.

Sensitivity results show here noticeably high points in the G_p curve corresponding to transitions between the first (1%) and second (3%) slope values which resulted in threshold effects, more pronounced for median (P, R) values near the middle of the

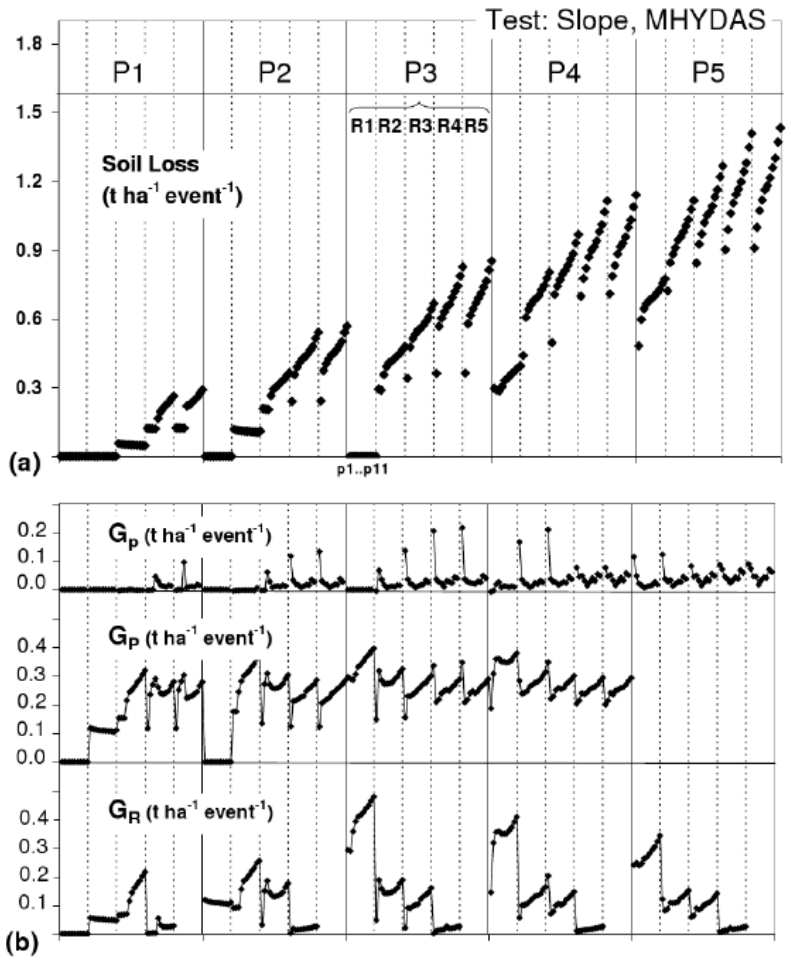

Figure 5.10: Dashboard used to represent soil loss results (a) and directional sensitivities (b) of a model when dealing with spatially-homogeneous parameters. Eleven values of the slope parameter were tested with other descriptive parameters all held at their reference spatially-homogeneous values. G_p, G_P and G_R are Gâteaux derivatives indicating variations in model response for unit increments along the axis of p, P and R values. These results were obtained during development of the physics-based erosion model "MHYDAS-Erosion".

curve. The G_P curve rises with increasing (P, R) conditions then stabilizes, indicating a near-linear effect of P values for high water excess conditions. The sensitivity to an increase in runoff conditions is somewhat different. Whatever the P value, G_R strongly decreases when R is augmented, the effect being again more pronounced for median P

values. A brief overview on model responses and sensitivity results indicates that the model has no diverging behaviour or redhibitory drawbacks.

5.3.2 Spatially-distributed configurations

Figure 5.9 is easily adaptable to the case of spatially-distributed parameters, where $B'1$ to $B'11$ play the same role as $p'1$ to $p'5$. The expression for model response $M(P, R, B')$ and associated local sensitivities are univoque and hold only when accompanied by indications on the trajectory in super-parameter space (Fig.5.8), either vertical, horizontal or diagonal.

Figure 5.11 shows a dashboard obtained from tests with spatially-distributed values of the descriptive parameters, during development of MHYDAS-Erosion. The "equivalent erodibility" super-parameter integrates soil cohesion in rills, rill erodibility, Manning coefficient, sediment size, streamwise length of a plot, number of rills, interrill erodibility and a coefficient accounting for efficiency of interrill transport. From preliminary individual *one-at-a-time* tests the number of rills was found by far the most sensitive parameter and strongly influences the overall sensitivity results. In such a case, the most productive spatial configurations are always the same when increasing (P, R) values, which would not be true for models governed by many parameters of varying sensitivity.

The S_B sensitivity measure (Eq.5.3) reports the dispersion of model responses obtained from all configuration, normalized by the response in the reference configuration. Consequently, S_B is not B'-dependent and has a unique value for the set of eleven B' configurations under given (P, R) conditions.

A clear convergence is visible when increasing water-excess conditions, which indicates that the model has a controlled behaviour when applied to very risky situations. The asymptotic S_B value is high, of the same order of soil loss results, which is another cornerstone of the analysis. As S_B shows signs of convergence, values of G_P and G_R come close to zero, reporting progressively smaller changes of S_B with increments of P and R values.

5.3.3 Sensitivity maps

A more focussed representation is sensitivity maps. They do not allow showing results for the entire set of P, R and p' or B' values but target the behaviour of a model in the $(\bar{p_s}, \bar{p_e})$ plane, *i.e.* when confronting values of the "equivalent slope" and "equivalent erodibility". Figure 5.12 illustrates the case of a model whose responses are classes of

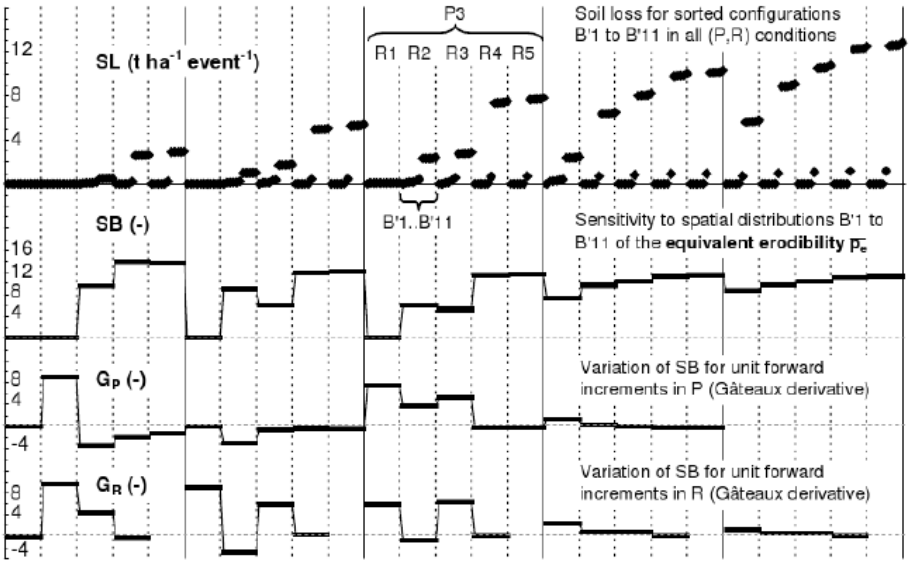

Figure 5.11: Dashboard used to represent soil loss results and multilocal sensitivity of a model when dealing with spatially-distributed super-parameters. Tested here were the spatially-distributed configurations *B'1* to *B'11* of the equivalent erodibility $\bar{p_e}$, sorted by increasing model responses. These results were obtained during development of the physics-based erosion model "MHYDAS-Erosion".

risks regarding erosion damages. The corresponding integer values are placed at the nodes of super-parameter space and curves of isovalues yield a clearly-understandable result, but it should be kept in mind that this decription only holds for a given set of (P, R) values.

In the retained example, $\bar{p_e}$ dominates over $\bar{p_s}$ as curves of isovalues tend to be parallel to the x-axis but hypercube effects are non-negligible, both near best-case and worst-case scenarios. Isovalues slightly resemble circles centered on the lower left and upper right of the graph and asymmetry exists between results on the vertical and horizontal OAT axis. Strictly speaking, segments of high sensitivity are identified when crossing several isovalues in a small displacement on any one of the four sensitivity axis: other results appeal to interpolation methods and to minimal prior knowledge on the behaviour of the model.

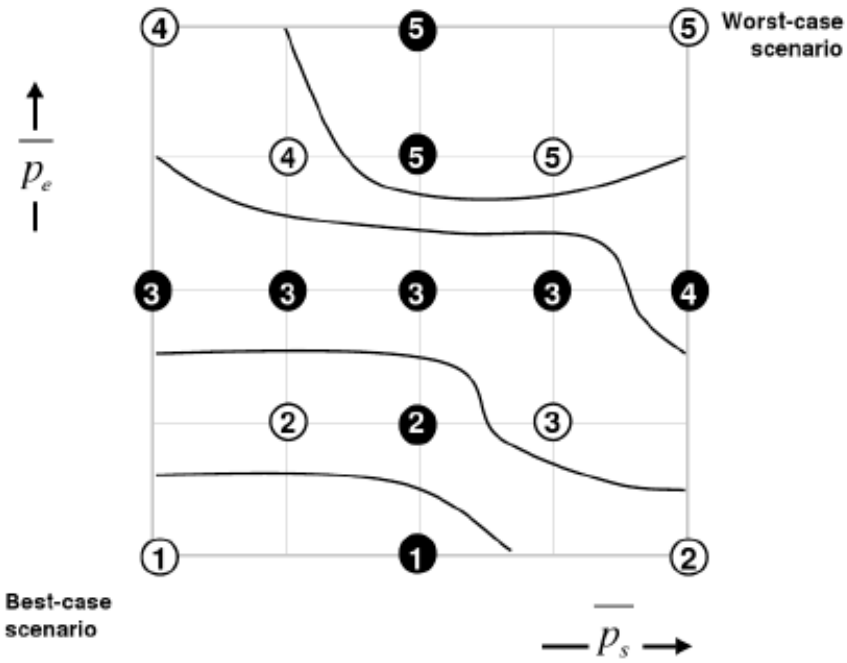

Figure 5.12: Sensitivity map obtained in the final stage of the analysis, describing the behaviour of a model for confronted values of its two super-parameters of "equivalent slope" $\bar{p_s}$ and "equivalent erodibility" $\bar{p_e}$. This representation pertains to spatially-homogeneous or distributed cases and holds for given (P,R) hydrological conditions. Model responses are localized by integers (for example risk classes) and allow tracing curves of isovalues. Regions of high sensitivity are identified by close isovalues.

5.4 Conclusion

The formal and theoretical work presented here aims at establishing a framework suitable for sensitivity analysis of spatially-distributed models and graphical representation of the results. It relies on the causal link existing between hydrology and erosion. This link is exploited in the (P, R, p) procedure distinguishing between input fluxes (precipitations P), propensity to surface flows (runoff conditions R) and specific erosion processes (descriptive parameters p). The latter convert driving phenomena into particle detachment and soil loss, expressed as the discrete non-linear model response $M(P, R, p)$.

As many descriptive parameters may be included in the innate parameterization of the model, the relevant general form is $M(P, R, \vec{p})$ where $\vec{p}$ is the vector whose compo-

nents are the spatially-homogenous parameter values on the nine-cell virtual catchment designed for the simulations. When spatially-distributed values of the descriptive parameters are considered, the model response is termed $M(P, R, B)$ where B refers to any of the eleven very contrasted configurations used to produce significant deterministic results.

To reach sufficient genericity and allow further comparisons between models on a common basis, the dimensionality of parameter space is reduced as super-parameters accounting for "equivalent slope" (p_s) and "equivalent erodibility" (p_e) are obtained from selected combinations of all intrinsic parameters. These super-parameters are tested *one-at-a-time* then together, resorting to Latin Hypercube samples, in both spatially-homogeneous and distributed cases.

At this stage, model responses are transformed into $M(P, R, p')$ and $M(P, R, B')$, where p' and B' respectively are spatially-homogeneous and distributed values of the super-parameters sorted by increasing soil loss. Throughout its successive developments, the deterministic sensitivity estimation procedure always relies on a limited series of cases, orientated from best-case to worst-case scenarios and not aiming at a thorough or novel screening method.

Directional sensitivity calculations are performed: the evolution of model responses is followed for any displacement in super-parameter space involving variations in one or more arguments of the M function. The S_B sensitivity of a model to the tested spatial distributions of its descriptive parameters is defined and its evolution also tracked for variations in the driving (P, R) hydrological conditions. For given (P, R) conditions, sensitivity maps are plotted in the $\bar{p_s}, \bar{p_e}$ plane to estimate relative importance of the "equivalent slope" and "equivalent erodibility".

Finally, the (P, R, p) procedure yields multilocal and risk-orientated deterministic sensitivity results, together with facilities for graphical representations. Its application to comparisons between four erosion models pertaining at different scales and appealing to different concepts is part II. of this paper.

Chapter 6

A framework for sensitivity analysis of distributed physics based erosion models II: Application to four Distributed Erosion Models

Nous appliquons ici le formalisme précédemment mis au point pour l'analyse de sensibilité des modèles d'érosion à paramètres spatialement distribués. Quatre modèles utilisés dans le projet MESO-EROS21 ont été choisis pour cette illustration comparative: MHYDAS-Erosion, STREAM, PESERA et MESALES, qui présentent des caractéristiques et des échelles d'application très différentes. La procédure (P, R, p) décompose leur paramétrisation de manière à bien séparer les paramètres liés aux flux d'entrée (précipitations P), ceux à la manière dont ces flux sont transmis (conditions de ruissellement R) et enfin ceux qui sont spécifiques à la modélisation de l'érosion (paramètres descriptifs p).

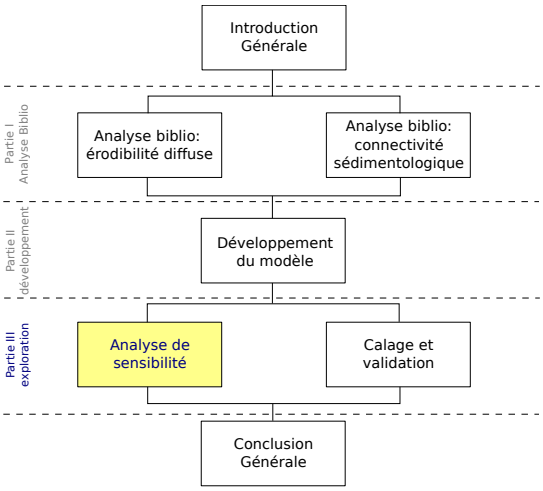

A framework for sensitivity analysis of distributed physics based erosion models II: application to four distributed erosion models[1]

Cheviron, B. ; Gumiere, S. J. ; Le Bissonnais, Y.; Desprats, J. F.; Cerdan, O. ; Darboux, F. ; Couturier, A. ; Raclot, D. (article in prep. to Water Resource Research)

Abstract

Following the framework established in Part I. of this paper, we compared four distributed erosion models (MHYDAS-Erosion, STREAM, PESERA, MESALES) by investigating their sensitivities to input fluxes, hydrological sub-models and specific erosion parameters gathered into equivalent slope and equivalent erodibility. Tests involved multiple combinations of rain intensities and runoff conditions in addition to selected screenings of the equivalent parameter space, resorting both to one-at-a-time displacements and to Latin-Hypercube samples. Sensitivity to spatial distributions of erosion parameters was calculated as an indice of numrical spreadth of soil loss results, obtained at the outlet of a nine-cell virtual catchment endowed with a fixed flow chart. Equivalent erodibility proved to be the key parameter in innate parameterization of the models. Domineering sensitivity effects were obtained and measured in tests appealing to both parameters, with comparable magnitude in spatially-homogeneous or distributed settings.

6.1 Introduction

Scenarios of climate change applied to the Mediterranean ring indicate high and increasing erosion risk: sparse vegetation, low structural stability and intense rainstorms render soils especially prone to degradation and loss of fertility in Northern Africa and Southern Europe. This study is a contribution to the MESOEROS21 project which focuses on erosion issues in connection with climatic and land use hypothesis for the 21st century. We debate here theoretical aspects of erosion modelling through a cross-scale sensitivity analysis and comparison of four models, following the framework presented in part I. of this paper (Cheviron et al., 2009a). The retained models are all resorted to for soil loss predictions at different spatial and temporal scales, on experimental sites, instrumented catchments or entire regions included in the project.

[1]Cheviron, Bruno ; Gumiere, Silvio Jose ; Le Bissonnais, Yves; Desprats, Jean François; Cerdan, Olivier; Darboux, Frédéric ; Couturier, Alain; Raclot, Damien. article in prep to Water Resource Research

Very different concepts underly models intended for different scales, the general trend being a progressively more refined description when smaller spatial extensions and time intervals are considered. In MHYDAS-Erosion (Gumiere et al., 2009a), these dimensions are reduced to the elementary size of the event: a single and spatially-homogeneous rain falls on a small agricultural catchment. Physical processes in detachment, transport and deposition of particles are described with the level of detail allowed by the pre-existing MHYDAS hydrological model (Moussa et al., 2002), where flow routing is computed from solutions of the one-dimensional Saint-Venant equations (Moussa, 1996; Moussa and Bocquillon, 1996b). At intermediate spatial scales and for a succession of rain events, the semi-empirical STREAM model (Cerdan et al., 2002) calculates water and sediment fluxes from surface sealing, land cover, digital elevation models and flow charts in agricultural catchments. It was built to work on a limited number of easily measured field parameters and designed for land management purposes. At larger scales, the PESERA model (Gobin et al., 2004; Kirkby et al., 2008) relies on monthly statistical climatic data, integrates evolutive land cover scenarios eventually associated with cropping seasons. It belongs to the "simplified physics-based" category of erosion models in the classification by Merritt et al. (2003). For equally large scales, the expert model MESALES (Le Bissonnais et al., 2002) uses a decision tree to combine values of crusting, slope, erodibility, land use and rain inputs into discrete classes of erosion risks. A conversion is then possible into continuous soil losses values in tons per hectare and per year.

A set of sensitive erosion parameters may certainly be inferred from physical understanding of the phenomena, choices in their description and objectives prevailing in construction of the models. Routine checks for consistency, coherence or convergence also yield occasional sensitivity results, at the expected limitations of these indications being too few, scattered, *i.e.* obtained from too distant points in parameter space, or isolated, *i.e.* not comprised in a screening scheme, thus unexploitable as such. In addition, as water erosion strongly depends on hydrology, elements of the hydrological description must appear in the parameter space of erosion models. Confronting the arguments above, any relevant analysis of erosion models should (i) rely on a sufficient number of points in parameter space, (ii) organize these points in a dense enough network, (iii) perform a justified exploration of the network, and (iv) consider testing hydrological conditions with the same care and wide range than specific erosion parameters. The first three items refer to screening strategies but the fourth points at a seemingly recurrent lack in analyses of erosion models.

For example, recent literature reviews (Gumiere et al., 2009c; Knapen et al., 2007)

report a possible higher sensitivity of erosion results on hydrological parameters than on specific erosion parameters, not without warning that examinations are often conducted under high rain intensities. Only few hydrological conditions have been tested in studies of WEPP (Nearing et al., 1990), LISEM (De Roo et al., 1996a), EUROSEM (Veihe and Quinton, 2000) or PSEM-2D (Nord, 2005) whereas these models all identified a major infuence of hydrological conditions on erosion results. One may also remark that no formal attempt was made to discriminate between the effects of hydrological conditions and those of specific erosion parameters on soil loss results.

In the framework for sensitivity analysis defended in part I. of this paper we introduced such a separation by exploiting the causal link between hydrology and erosion in structure and behaviour of the models, aiming at a unified description that would hold beyond major differences between models. As the upstream section of a model we identified the input flux, precipitations P and the transmitted flux, obtained from runoff conditions R, which signal the propensity of soil to runoff. Specific erosion properties p come next, in a logical and chronological sense, to determine the calculated soil loss. A three-category (P,R,p) sensitivity analysis procedure was therefore found possible and appropriate to most erosion models, its effectiveness being to discriminate between the effects of "control" hydrological factors (P,R) and "descriptive" erosion parameters (p). Focusing on erosion processes, one may wish to estimate the sensitivity to parameters of the p category for varied (P,R) combinations, representing as many water excess conditions. To facilitate a simple and clear comparison between models, we dispatched parameters of the p category into sub-categories $\bar{p_s}$ and $\bar{p_e}$ accounting for equivalent slope and equivalent erodibility, respectively. The same formalism applies whether equivalent slopes or erodibilities take spatially homogeneous or spatially-distributed values.

A point in parameter space is localized by its four coordinates $(P, R, \bar{p_s}, \bar{p_e})$ and corresponding model results read $M(P, R, \bar{p_s}, \bar{p_e})$. Among numerous methods and indicators available (Frey and Patil, 2002; Pappenberger et al., 2008; Saltelli et al., 2000; Van Griensven et al., 2006), we chose to express sensitivity as the deterministic δM variation associated to any selected displacement in parameter space, which makes it a multilocal function $G(P, R, \bar{p_s}, \bar{p_e})$. The underlying concept and calculation device is that of the Gâteaux directional derivatives (Gâteaux, 1913). It pertains in analysis of non-linear discrete systems (Cacuci, 1981, 2003) and generalizes the concept of "elementary effect" to any displacement in parameter space involving one or more of the P, R, $\bar{p_s}$ and $\bar{p_e}$ quantities.

Comparisons between models of different nominal scales indirectly question the exis-

tence and characterization of scale effects (Blöschl and Sivapalan, 1995), the possibility to perform scale aggregations (Sivapalan, 2003) and the compatibility of different approaches when upscaling (Blöschl, 2001). Validity of the comparison between models is ensured by using the same framework and the same physical support, a nine-cell virtual catchment with a fixed flow chart. Elements of a scale analysis may be found by confronting results of the event-based models (MHYDAS-Erosion, STREAM) with these of the regional ones (PESERA, MESALES), the former giving soil loss results in tons per hectare and per event and the latter in tons per hectare and per year. A simple connection between scales could be obtained by simulating as many events as needed for the soil loss results to be the same, then to vary $\bar{p_s}$ and $\bar{p_e}$ to record the transmission of sensitivity between scales, at least in the studied models.

6.2 Materials and methods

6.2.1 Models

MHYDAS is a runoff-rainfall model developed by the LISAH-INRA laboratory at Montpellier, France, to study the effects of agricultural management on the hydrological behaviour of a farmed catchment during rain events (Moussa et al., 2002). It relies on the one-dimensional description of flow routing in connected reach segments by means of the diffusive wave approximation of the Saint-Venant equations, as solved by (Moussa, 1996; Moussa and Bocquillon, 1996b). The MHYDAS-Erosion module (Gumiere et al., 2009a,d) was added recently to the OpenFluid (2009) development platform, a sofware environment for modelling fluxes in landscapes supporting improvements made to MHYDAS in surface-groundwater exchanges, water balance or pollutant fate and transport. MHYDAS-Erosion is a small-scale physics-based model with dedicated parameter sets for concentrated and diffuse erosion processes, the former located in rills, the latter on interrills. This event-based model was intended for small Mediterranean catchments, as indicated by its typology and parameterization where the number of rills and plot length (or streamwise distance) are key parameters. Sensitivity tests on MHYDAS-Erosion were automated as indicated in part I.(chapter 5) of this paper thanks to a resolution scheme centered on the SENSAN software (Doherty, 2004).

STREAM was developed by the INRA laboratory at Orléans, France, from early works on the respective effects of slope and tillage directions on runoff (Souchère et al., 1998). It grew into an event-based spatially-distributed erosion model (Cerdan et al., 2002) with both expert and empirical inputs in the determination of its few innate

parameters. It was conceived for agricultural management purposes and its parameterization is directly acquainted from field observations. Whereas MHYDAS-Erosion updates erosion calculations at each time step, STREAM yields cumulative results for concentrated and diffuse erosion over the entire duration of an event. The model has been recently described and succesfully tested in three completely different contexts (Northern France, Belgium, Southern France). Automation of tests performed on STREAM was made in an *ad hoc* procedure, for the model could not be ran under the command line: Geographical Information Systems would not fit in a resolution scheme commanded by SENSAN.

PESERA is a coarse-scale model developed at Leeds University, United Kingdom (Gobin et al., 2004; Kirkby et al., 2008), intended for erosion risk assessment across Europe, relying on a refined meteorological sub-model and on simplified physics-based equations for erosion. It was designed to estimate long-term average erosion rates in replacement of the Universal Soil Loss Equation (USLE) less suitable for European conditions than for North-American ones and not compatible with higher resolution data. A classical use of PESERA involves a resolution grid of one kilometer, soil data taken from the European Soil Database, land cover data from CORINE land cover, climate data from the MARS project and a Digital Elevation Model. An evaluation of PESERA by Licciardello et al. (2009) in contrasting contexts revealed that variability between the investigated land uses and climate conditions was well captured, whereas absolute rates were strongly underestimated. Soil erodibility factor was identified as the key descriptive parameter. This finding was confirmed by *one-at-a-time* sensitivity tests conducted on each parameter of each model as preliminary steps for the present study. The heart of PESERA being a series of three small executable files, the model could be ran without difficulty within the intended resolution scheme.

MESALES (Le Bissonnais et al., 2002) was developed by the INRA laboratory at Orléans, France, to assess soil erosion risk at the European scale. It is one of the thematic applications based on the Soil Geographical Data Base of Europe. It should be considered as an intermediate step towards a "state-of-the-art erosion modelling at the European scale", subsequent to the work of Van der Knijff et al. (2000) and prior to the initiation of the PESERA project. MESALES uses expert-defined rules to combine factors influencing erosion, attributing priviledged influences to land cover and crust formation onto results expressed in five classes of erosion risks. A classical use of MESALES requires CORINE land cover data, soil crusting susceptibility, soil erodibility obtained from pedotransfer rules, a Digital Elevation Model and meteorological data at one km pixel size. Relying on a Geographical Information System, MESALES could

not be automated and was ran by hand.

6.2.2 Virtual Catchment and Parameterization

In the (P,R,p) procedure, the virtual catchment is the topographical entity on which soil loss and sensitivity calculations are performed. Its features appear Fig.6.1. Its topology is fixed. Flow paths stay unaffected by the driving rain conditions, they are the only connectivity lines between cells in the catchment, regarding hydrological and sedimentological processes. If not bridged by a flow line, two adjacent cells have no interactions. For simplicity, all cells are abusively represented by squares but their length and width may vary, if distance to the drainage line or streamwise distance has to be tested as requirement of a given model. Conversely, the surface of the elements must be kept constant and in accordance with the nominal spatial scale of models.

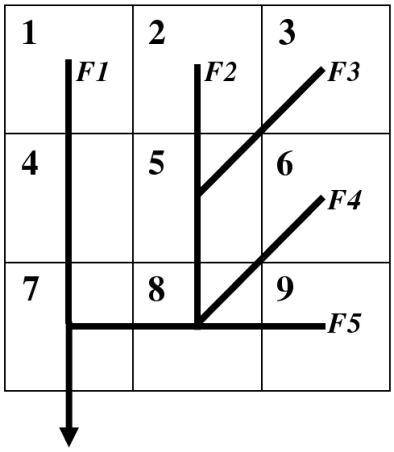

Figure 6.1: Layout and connectivity in the virtual catchment between surface units numbered 1 to 9. The one-way downstream hydrological and sedimentological connectivity is indicated by flow lines numbered *F1* to *F5*.

Only spatially-homogeneous values of the hydrological factors accounting for precipitations P and runoff conditions R were considered here, to facilitate interpretation. As we focus on the role played by specific erosion parameters, both spatially-homogeneous and distributed configurations of the descriptive parameters p are tested. Preliminary attempts with spatial distributions in all categories at once were discarded for they created too much equifinality in soil loss results at the outlet. They are nevertheless useful when intending a cell-by-cell analysis, providing diversity in the situations with far less redundancy.

In spatially-homogeneous A configurations, a tested parameter has the same value in all cells but a progressive gradation of values is considered. If for example three values (p_1, p_2, p_3) are involved, they are previously sorted in phenomenological order regarding soil loss results, so that p_1 has a low contribution (or efficiency), p_2 a median one and p_3 a high one. When designing spatially-distributed B configurations, we opted for a limited number of contrasted configurations, in terms of spatial distributions and parameter values involved, as can be seen on Fig.6.2. B configurations consist in patches of elementary homogeneous cells of low, median and high efficiency superimposed to the flow chart.

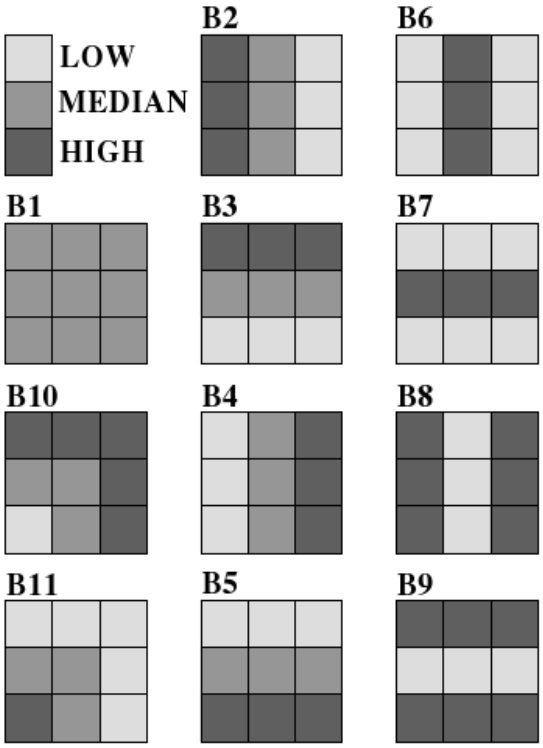

Figure 6.2: Spatially-distributed B configurations. Light, median and dark grey cells receive values of erosion parameters associated with low, median and high efficiency regarding soil loss.

Whereas A configurations provide a simple understanding of sensitivity trends under various (P, R) conditions, B configurations reveal how these trends are affected by the imposed spatial distributions of descriptive parameters. It is therefore a cornerstone of the analysis to compare results obtained in A and B settings for a given model and between models. To facilitate such investigations, configuration $B1$ was chosen identical

to the median (or reference) A case. An interesting opening is the comparison between dispersions in soil loss values obtained in A and B configurations, involving the most and less efficient configuration of each.

6.2.3 Equivalent Parameters

Besides common patterns for topography, topology and spatial distributions of the (P, R, p) entries, a reliable comparison between models requires definition and coding of equivalent (P, R, p) entries. As units to (P, R, p) values differ between models, no straightforward numerical comparison could be planned. For each model, we opted for a paving of the entire nominal range of each P, R and p axis into unit increments, converting values of dissimilar nature into comparable adimensional entries. In this typology, $P1$ figures the lowest precipitation value, $R1$ the runoff condition of lowest efficiency and $p1$ the set of erosion parameters of lowest efficiency, too. Depending on the models and situations tested, P values found themselves between $P1$ and a maximum of $P5$, R values between $R1$ and a maximum of $R5$, p values between $p1$ and a maximum of $p11$. Parameters of the p category are attributed to the $\bar{p_s}$ and $\bar{p_e}$ sub-categories. Figure 6.3 gives an overview of innate parameters of each model confronted in the definition of equivalent $(P, R, \bar{p_s}, \bar{p_e})$ parameterizations.

For either A or B configurations, tests on MHYDAS-Erosion involved five P, five R, eleven $\bar{p_s}$ and eleven $\bar{p_e}$ values. Precipitation intensities were $P1 = 20$, $P2 = 35$, $P3 = 50$, $P4 = 65$ and $P5 = 80\,\mathrm{mm\,h^{-1}}$. Runoff conditions were formed by (K_s, θ_i) combinations of saturated hydraulic conductivity and initial surface water content values, from $R1$ given as $(K_s = 37\,\mathrm{mm\,h^{-1}}, \theta_i = 0.02)$ to $R5$ given as $(K_s = 0.1\,\mathrm{mm\,h^{-1}}, \theta_i = 0.40)$ in increasing efficiency order. Slope values were taken between 1 for the less and 30% for the most productive one. The efficiency of the group of parameters constituting the equivalent erodibility was influenced by parameters accounting for the number of rills, interrill erodibility, cohesion in rills and rill rugosity for low to median (P, R) conditions, then totally controlled (with exponential effects) by parameters accounting for the number of rills and plot length (streamwise distance) for high (P, R) conditions.

Tests on STREAM involved five P and three R values. Precipitation intensities were chosen to match these tested for MHYDAS-Erosion and runoff conditions were formed by combinations of antecedent rain values in $\mathrm{mm\,h^{-1}}$ and classes of sensitivity to runoff. Increasing R conditions were obtained from pairs of increasing antecedent rain values and classes of sensitivity to runoff. Equivalent slope values from 1 to 30% were produced by creating the adequate Digital Elevation Model required by STREAM, but only $\bar{p_s}$ values corresponding to 1, 3, 10 and 30% were tested in A configurations.

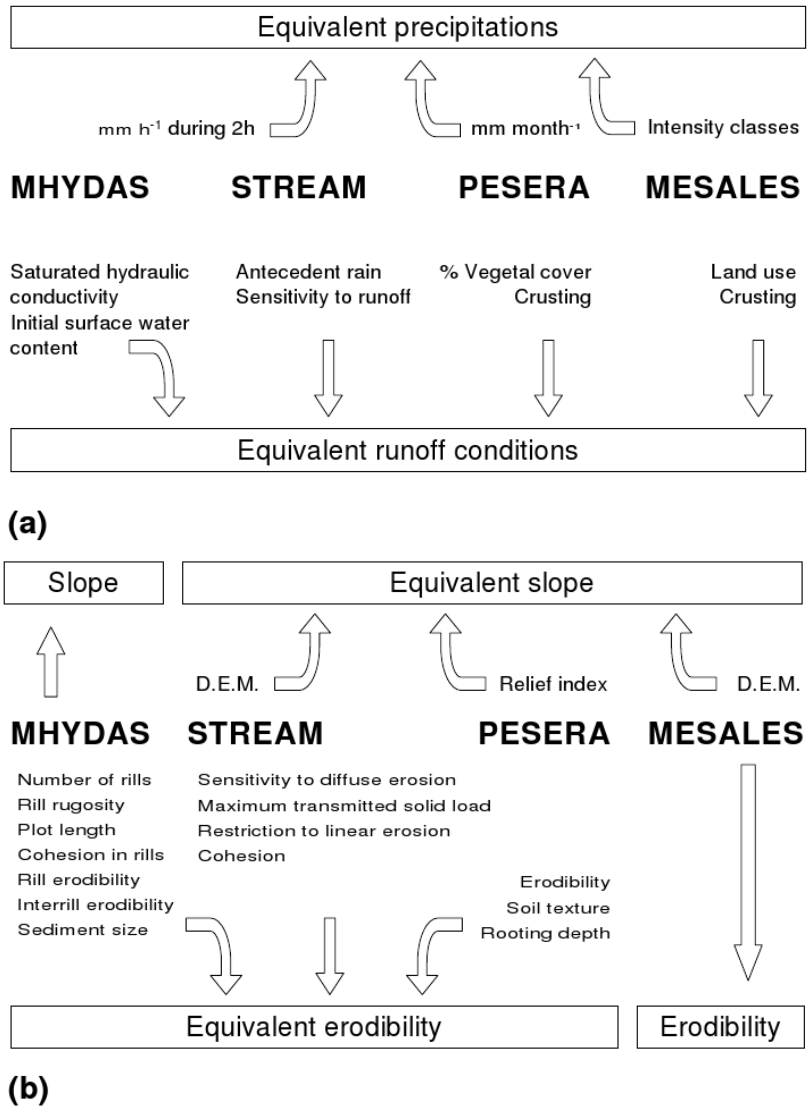

Figure 6.3: Innate entries of each model chosen for definition of equivalent control hydrological conditions (a) and equivalent "descriptive" parameters of slope and erodibility (b). Slope appears as such in the innate parameterization of MHYDAS-Erosion, as for erodibility in MESALES.

Five out of the possible eleven values of $\bar{p_e}$ were tested in A configurations, none of the constitutive elements of equivalent erodibility showing a domineering influence.

Tests on PESERA involved six P values but only five appear in reresentation of the results, corresponding to precipitation intensities of 35, 55, 75, 95 and 115mm month^{-1}.

In its meteorological parameterization, PESERA also includes a number of rainy days per month and a coefficient of rainfall variation accounting for fluctuation in intensity of the precipitations. The influences of these parameters were separately tested in one-at-a-time procedures but found to be of secondary order relative to the monthly precipitation value: these parameters were kept at their recommended default values. Annual sine temperature variations were treated the same way. Detailed results for these "frozen" parameters are nevertheless available on demand for further studies. Increasing runoff conditions were thought of as combinations of decreasing percentage of vegetal cover with increasing soil crusting values, yielding five R values. The less efficient one has 100% surface cover and $1mm$ crusting, the most efficient one has a bare soil with $5mm$ crusting. Eleven equivalent slopes from 1 to 30% were produced resorting to the same subterfuge as for STREAM, feeding PESERA with the adequate relief index required. Equivalent erodibility was strongly dominated by the innate erodibility parameter. Parameters accounting for soil texture and rooting depth playing secondary though non-negligible roles, especially in low (P, R) conditions.

MESALES was tested under five increasing classes of precipitation intensities. The difficulty was to find three unambiguously increasing runoff conditions. The only way to perform a (P, R, p) analysis of MESALES and to ensure comparison with other models was to define runoff conditions as the combination of a given land use and a given crusting value. The first argument of the combination prevents continuity in the description of runoff conditions. We had to choose very contrasted land uses to create a progression between R values, which involved testing almost all nine land use classes listed in MESALES. As for PESERA, the corresponding dataset is available for further studies. $R1$ was finally defined as a forest with class one crusting, $R2$ as an arable land with class three crusting and $R3$ as vineyards with class five crusting. The same strategy as for STREAM and PESERA was used to simulate the intended slopes from Digital Elevation Model requirements. Erodibility and equivalent erodibility are strictly identical in MESALES.

6.2.4 Screening and Sensitivity Indices

Figure 6.4a indicates explorations of the $(\bar{p_s}, \bar{p_e})$ plane when dealing with A configurations. Four trajectories are followed, involving *one-at-a-time* (OAT) or Latin-Hypercube (LH) displacements, flagged with small black and big white disks, respectively. Along the vertical sequence of black disks, increasingly efficient configurations of the equivalent erodibility are tested whereas equivalent slope is held at its median values, which is noted $OAT\,A(\bar{p_e})$. Roles are exchanged when considering the horizontal

sequence of black disks, indicated as $OAT\ A(\bar{p_s})$. Along the first diagonal, conjunct increasing values of $\bar{p_s}$ and $\bar{p_e}$ are tested, noted $LH\ A(\bar{p_s}, \bar{p_e})$. Along the second diagonal, $\bar{p_s}$ is augmented while $\bar{p_e}$ is decreased. Such a representation holds for given (P, R) conditions. If soil loss values $M(P, R, \bar{p_s}, \bar{p_e})$ are placed on the occupied nodes of the grid, then selected displacements $OAT\ A(\bar{p_s})$, $OAT\ A(\bar{p_e})$ or $LH\ A(\bar{p_s}, \bar{p_e})$ result in variations in M associated with sensitivities $G(P, R, p)$.

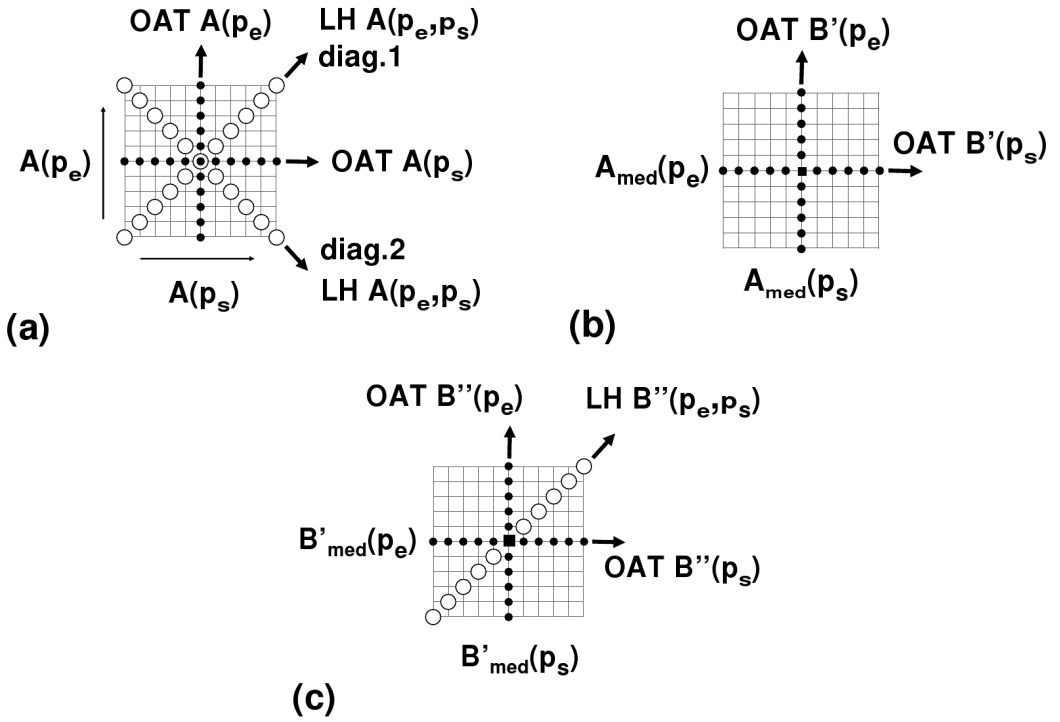

Figure 6.4: Screening stages and strategies.

The vertical sequence of black disks in Fig. 6.4b indicates tests performed with spatially-distributed B configurations of $\bar{p_e}$ while $\bar{p_s}$ is held at its median value in all cells. As soil loss results are sorted by increasingly efficient B configurations, the test is noted $OAT\ B'(\bar{p_e})$ instead of $OAT\ B(\bar{p_e})$. The same applies for the horizontal sequence of black disks when exchanging roles between $\bar{p_s}$ and $\bar{p_e}$. These sequences were abusively placed perpendicular one to the other as the central point bears a non-unique value. This artefact was proven useful to represent the relative effects of distributions in equivalent slope and equivalent erodibility.

Figure 6.4c goes one step further in analysis of the influence of spatial distributions of the equivalent parameters. The vertical sequence of black disks corresponds to the test of spatial distributions of $\bar{p_e}$ while $\bar{p_s}$ is held at its median-efficiency distributed configuration. Spatially-distributed configurations of $\bar{p_e}$ are again sorted by increasing efficiency, then termed $OAT\ B''(\bar{p_e})$. The same applies for the horizontal sequence of black disks when exchanging roles between $\bar{p_s}$ and $\bar{p_e}$. The $LH\ B''(\bar{p_s}, \bar{p_e})$ test involves conjunct increasingly efficient spatial distributions $B'(\bar{p_s})$ and $B'(\bar{p_e})$. In cases where soil loss results were not monotonously increasing along the first diagonal, they were re-sorted to fulfill this requirement. The abusive graphical representation was used as in Fig. 6.4b, this time to compare the magnitude of values obtained in the three different directions.

6.3 Results and Discussion

6.3.1 Spatially-homogeneous Configurations

6.3.1.1 MHYDAS-Erosion

Soil loss is expressed as the model response $M(P, R, p)$ or equivalently as $M(P, R, \bar{p_s}, \bar{p_e})$ where either $\bar{p_s}$ or $\bar{p_e}$ or both are varied, in addition to P and R. When both $\bar{p_s}$ and $\bar{p_e}$ are varied, they are varied together in a Latin-Hypercube screening, leaving only three degrees of freedom: P, R and $\bar{p_s}$ or $\bar{p_e}$, let us use the generic term p. The representation problem *a priori* has four dimensions, M, P, R and p. We opted for a graphical option placing ordonated values of P, R and p on the x-ordinate and plotting M as the y-ordinate, thus reducing the problem to two dimensions.

Figure 6.5a exemplifies this representation, which is maintained throughout the rest of the paper. Soil loss values obtained with MHYDAS-Erosion are plotted for all (P, R) conditions and the eleven p values involved in $OAT\ A(\bar{p_s})$, $OAT\ A(\bar{p_e})$ and $LH\ A(\bar{p_s}, \bar{p_e})$ on the first diagonal of Fig. 6.4a. If one takes a close look at the $(P3, R2)$ condition

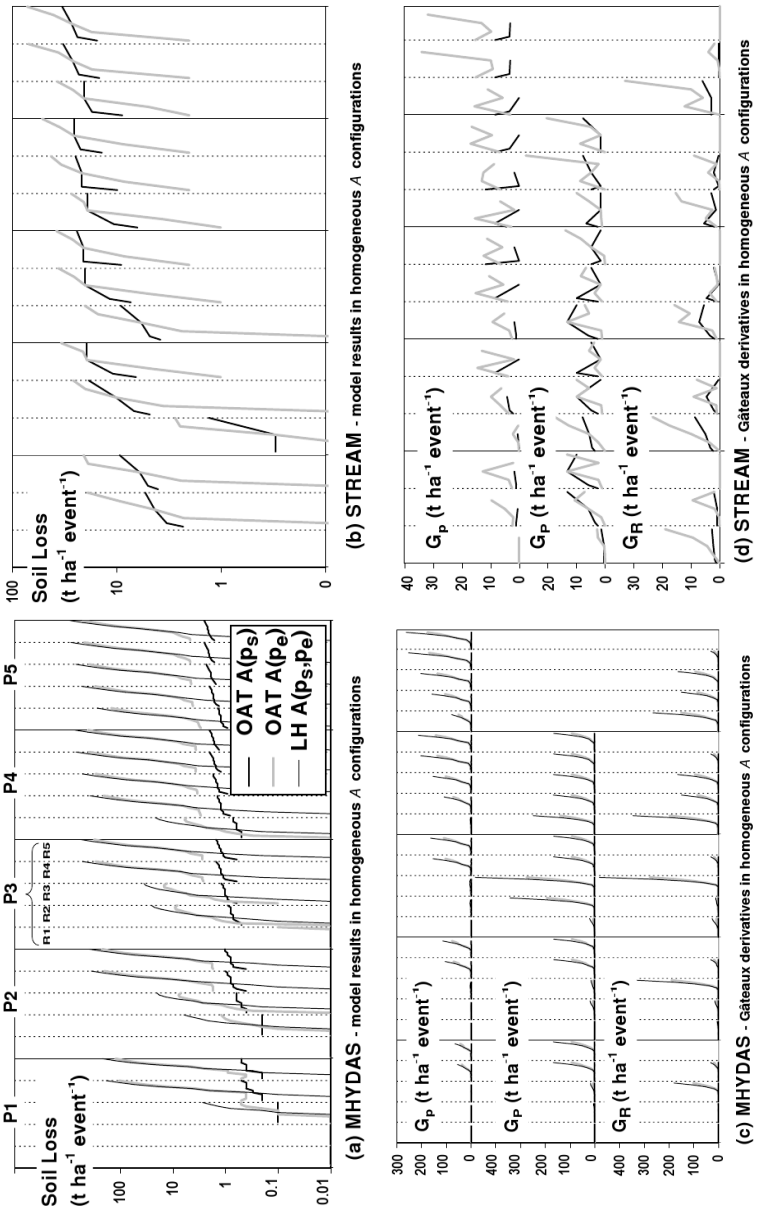

Figure 6.5: Dashboards representing soil loss and sensitivity results for MHYDAS-Erosion (a,b) and STREAM (b,d) under all combinations of Precipations P and Runoff conditions R, for *one-at-a-time* (OAT) and Latin-Hypercube (LH) screenings involving equivalent slope $\bar{p_s}$ and erodibility $\bar{p_e}$.

one observes a slowly increasing soil loss response of about 1 tons ha^{-1} event^{-1} when testing increasing slopes for median erodibility in all cells as $OAT\ A(\bar{p_s})$. In the same

column, soil loss varies more drastically for increasing erodibilities and median slopes in $OAT\ A(\bar{p_e})$. The variation is even more spectacular when increasing both equivalent parameters at once in $LH\ A(\bar{p_s}, \bar{p_e})$.

A dashboard is constituted by placing Fig. 6.5c under Fig. 6.5a, so that soil loss variations and the associated sensitivities are placed in the same column spanning over both figures. In Fig. 6.5c, G_p indicates the variation in soil loss caused by a unit increase in p, G_P the variation caused by a unit increase in P and G_R the variation caused by a unit increase in R. As for soil loss values in Fig. 6.5a, the Gâteaux derivatives G_p, G_P and G_R are available in columns corresponding to pairs of (P, R) conditions whereas progression of the results inside a column corresponds to a screening strategy.

Soil loss results in Fig. 6.5a show a wide dispersion over several orders of magnitude, with much more sensitivity to $\bar{p_e}$ than to $\bar{p_s}$. Hypercube tests indicate an even wider spreadth of values. Values are driven near zero by the influence of low slopes in combined low values, then stretched up to high values under exponential influences of factors taking part in the definition of equivalent erodibility, previously cited as the number of rills and streamwise distance. Several sensitivity trends clearly appear in Fig. 6.5c. The first indication is that values of the derivatives are almost of the same order of magnitude than these of soil loss results, indicating a very dynamic response of the model. The global trend in G_p curves indicate an increase in sensitivity of the model to variation in descriptive parameter values p for increasing (P, R) conditions. The G_P curves indicate a maximal sensitivity to variations in P values in the middle range of (P, R) conditions, certainly targetting the heart of the nominal range of the model. The sensitivity to P values stabilizes then for increasing water excess conditions. The same behaviour is observed for G_R.

6.3.1.2 STREAM

As no hypercube tests were performed for STREAM, only two soil loss curves are visible on Fig. 6.5b. One easily observes the intersection between curves, corresponding to the central point of the screening diagram Fig. 6.4a. Each column of Fig. 6.5b therefore bears a small spider diagram. Soil loss values are far less dispersed than for MHYDAS-Erosion, though exhibiting comparable orders of magnitude: STREAM has a less dynamic answer to parameter variations. Little change exists between dotted columns corresponding to increased R conditions inside the same P value, except for weaker precipitations values where R conditions take a dominant importance. Tests performed on equivalent erodibility show a stronger sensitivity than to slope variation, with a smoother behaviour and no sharp inflection points indicating threshold effects.

The order of magnitude of the derivatives in Fig. 6.5d is inferior to that of the soil loss results, to some punctual exceptions: G_p values for equivalent erodibility become high for high (P, R) conditions, as in the beginning of an exponential behaviour that should have been tested further. The same trends are visible on G_P and G_R curves. Other less remarkable features are high values of G_P and G_R corresponding to the appearance of non-zero responses for low (P, R) conditions.

6.3.1.3 PESERA

Figure 6.6a shows very smooth soil loss results over several orders of magnitude. Spider diagrams inside dotted columns show steeper response curves for hypercube screenings and *one-at-a-time* tests on equivalent erodibility than for *one-at-a-time* tests on equivalent slope. There is nevertheless less difference between steepness of curves than between orders of magnitudes. The increase in R conditions is clearly traduced on the results between adjacent dotted columns for a given P value. On the contrary, little difference appears between results obtained for successive P values. As for MHYDAS-Erosion, values of the derivatives in Fig. 6.6c are high compared to soil loss values. G_p exhibits a "triple increase" in sensitivity with increasing P, R and p values, accelerating into a seemingly exponential behaviour for highest (P, R) conditions. On the contrary, curves for G_P and G_R quickly reach a stable and auto-reproduced pattern for median then high (P, R) conditions. Notice that the sixth P condition tested for PESERA ($P = 135\,\mathrm{mm\,h^{-1}}$) was used to trace the rightmost part of the G_P curve.

6.3.1.4 MESALES

To allow comparisons with other models, classes or erosion risks obtained as MESALES outputs have been converted into values in $\mathrm{tons\,ha^{-1}\,yr^{-1}}$. Class one was equated to 0.5, class two to 2, class three to 6.5, class four to 20 and class five to $50\,\mathrm{tons\,ha^{-1}\,yr^{-1}}$. As for PESERA, soil loss results were obtained cell by cell, as the flow chart imposed in Fig. 6.1 was not compatible with requirements of these models. Soil loss values presented here are averages over the nine-cell catchment.

One observes in Fig. 6.6b that *one-at-a-time* screenings were not performed for precipitations $P2$ and $P4$, where responses to hypercube screenings are present to ensure sufficient continuity of the representation with increasing (P, R) conditions. As previously discussed, a specific difficulty with MESALES was to choose increasing R conditions, which could not be made in a continuous way for different R conditions are associated with different land uses of specific properties. The problem seems to be overcome here, as the expected trend of an increase is visible between adjacent

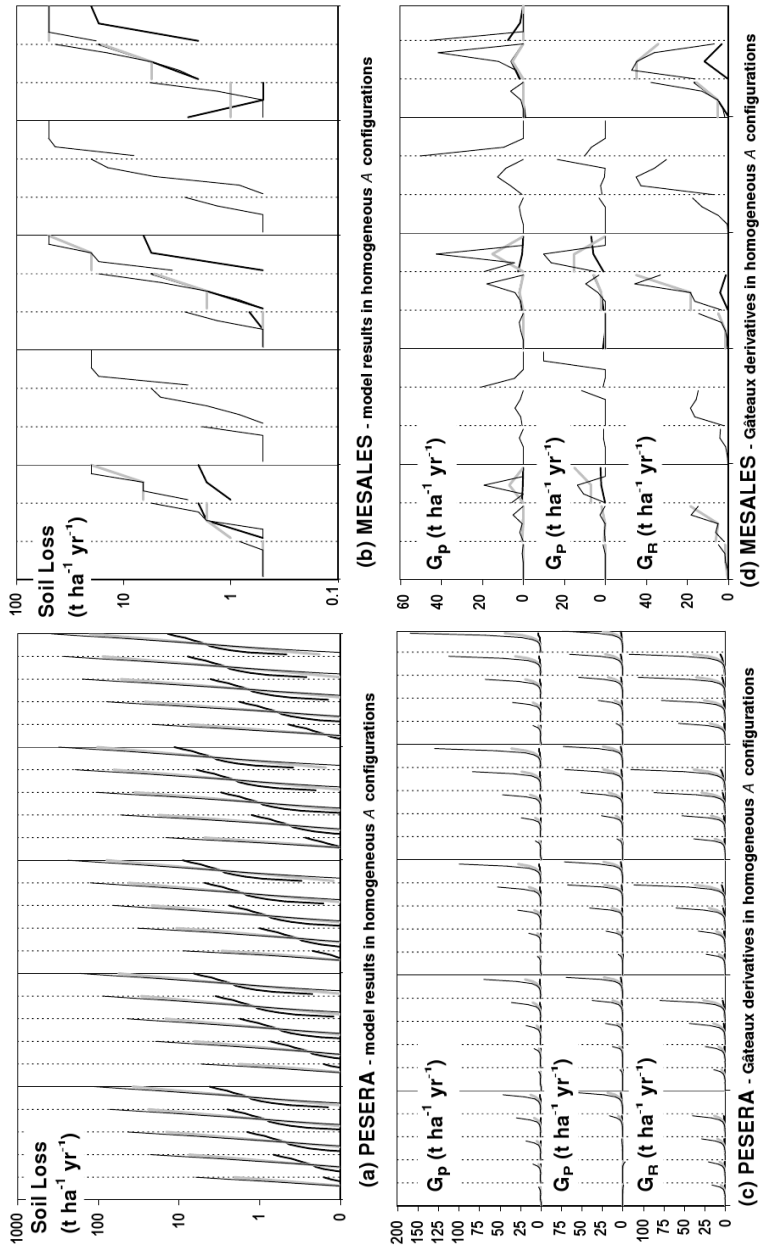

Figure 6.6: Dashboards representing soil loss and sensitivity results for PESERA (a,b) and MESALES (b,d) under all combinations of Precipations P and Runoff conditions R, for *one-at-a-time* (OAT) and Latin-Hypercube (LH) screenings involving equivalent slope $\bar{p_s}$ and erodibility $\bar{p_e}$.

dotted columns for a given P value. Soil loss results also exhibit the expected increase with increasing P conditions, though bounded values are reached in stronger (P, R) conditions. As these values correspond to class five results, they would have been higher when using a different conversion table. The reader may notice an irrealistic decrease in model response when testing the equivalent slope under $(P5, R1)$ conditions. This aspect is currently under examination, meaning either an incoherence in the decision tree or misplaced simulation results. General trends appearing Fig. 6.6d indicate that model derivatives G_p and G_R have higher absolute values than G_P, allowing hypothesis of a stronger sensitivity to p and R values, especially in high (P, R) conditions. In such conditions, the derivatives become non-negligible relative to model responses, signaling a more dynamic behaviour of the model.

6.3.1.5 Sensitivity Maps

We traced the sensitivity maps of Fig. 6.7 to focus on the relative importance of equivalent slope and equivalent erodibility for each model under increasing (P, R) conditions. These maps were plotted from data gathered in the four screenings described Fig. 6.4a. Each line of three figures corresponds to a single model, namely MHYDAS-Erosion, STREAM, PESERA then MESALES. Both P and R conditions increase when going from the left to the right column of figures, except for MESALES which was mapped in its median runoff condition but for increasing precipitations. From left to right the conditions read $(P2, R2)$, $(P3, R3)$ and $(P5, R5)$ for MHYDAS-Erosion, $(P2, R1)$, $(P3, R2)$ and $(P5, R3)$ for STREAM, $(P1, R1)$, $(P3, R3)$ and $(P5, R5)$ for PESERA, $(P1, R2)$, $(P3, R2)$ and $(P5, R2)$ for MESALES.

From orientation of isovalues as well as labels placed on them, almost all figures exhibit the same sensitivity trend, in which equivalent erodibility dominates over equivalent slope, whereas combined effects are even more stronger, stretching values to the upper right corner of each plot. Fig. 6.7l for MESALES is an exception, in which equvalent slope regains a first-order influence under high precipitation values. Fig. 6.7b for MHYDAS-Erosion shows an isle of high soil loss values for median to low slopes confronted with high equivalent erodibilities, which we relate to small irregularities already observed in sensitivity tests on the slope parameters for moderate precipitation conditions. Isovalues of Fig. 6.7d, e, f for STREAM were not extrapolated to points where no data were available, in absence of Latin-Hypercube screening on diagonals.

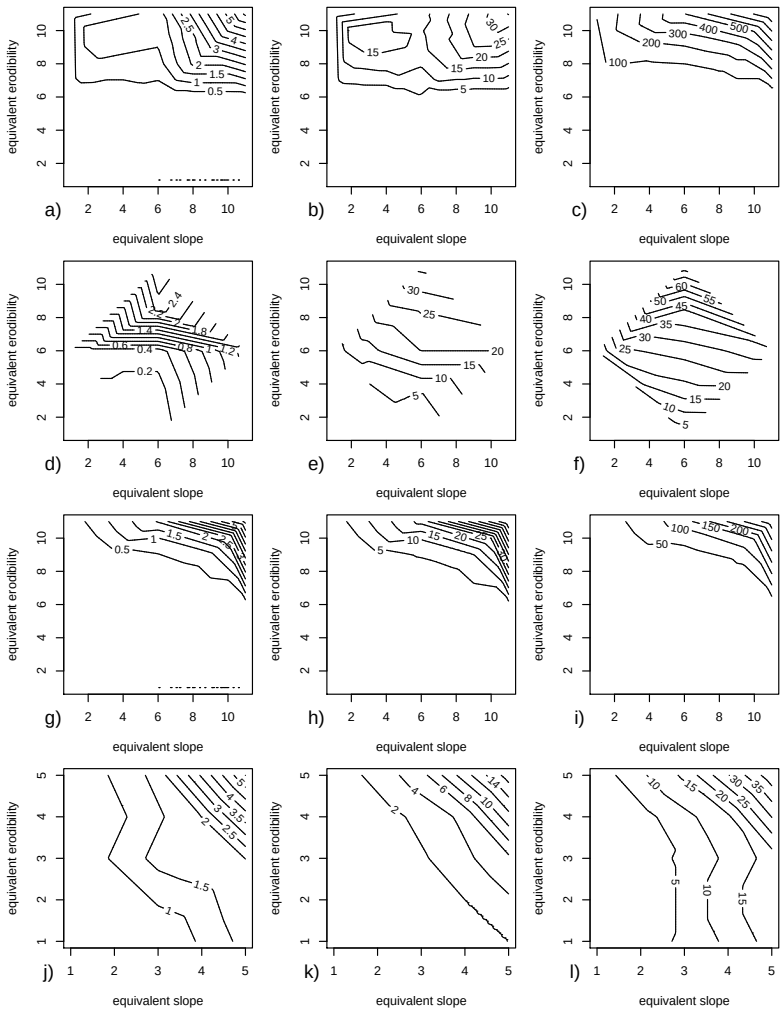

Figure 6.7: Sensitivity maps for MHYDAS-Erosion (a,b,c), STREAM (d,e,f), PESERA (g,h,i) and MESALES (j,k,l) in spatially-homogeneous configurations. Precipitations and runoff conditions increase from left to right for each model, except for MESALES mapped in a median runoff condition but for increasing precipitations. Soil loss isovalues are labeled in tons ha^{-1} $event^{-1}$ for MHYDAS-Erosion and STREAM, in tons ha^{-1} yr^{-1} for PESERA and MESALES.

6.3.2 Spatially-distributed Configurations

6.3.2.1 MHYDAS-Erosion

A clear discrepancy in magnitude of the results is observed between spatially-distributed configurations of equivalent slope and equivalent erodibility on Fig. 6.8a. The increase

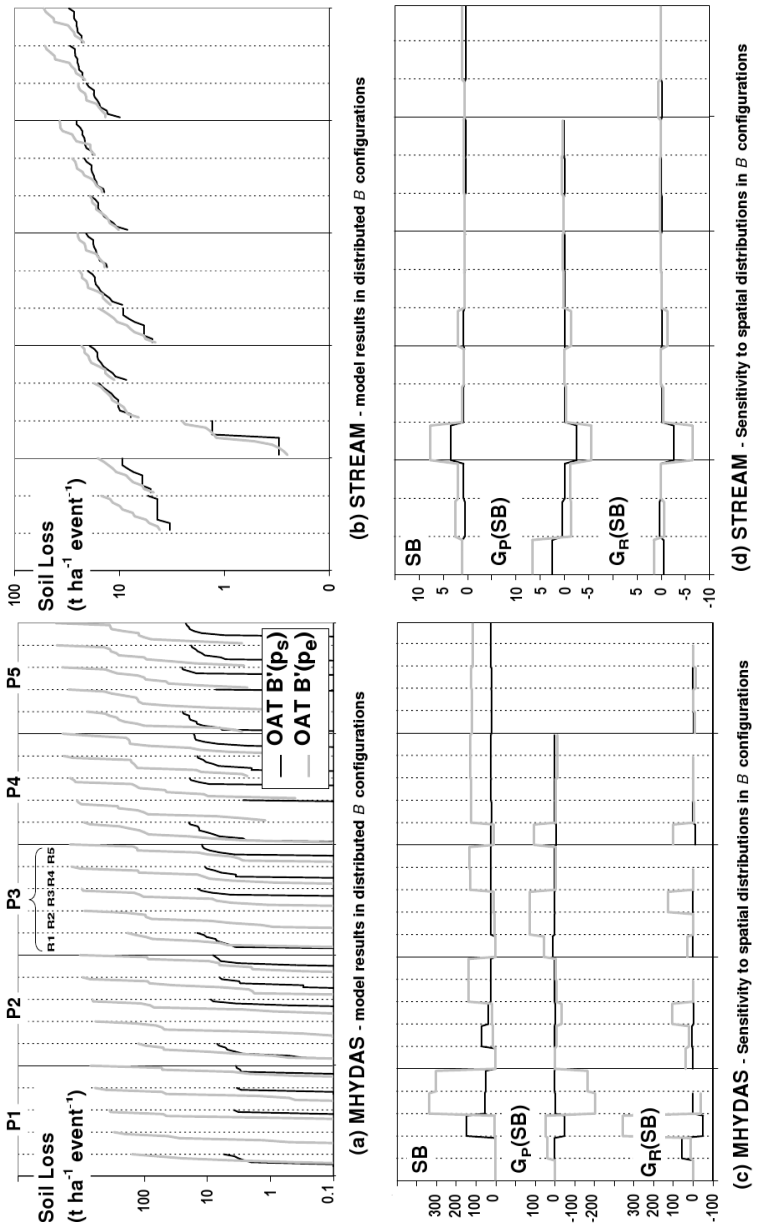

Figure 6.8: Dashboards representing soil loss, dispersion SB and variations in SB for MHYDAS-Erosion (a,b) and STREAM (b,d) under all combinations of Precipations P and Runoff conditions R, for *one-at-a-time* (OAT) and Latin-Hypercube (LH) screenings involving equivalent slope $\bar{p_s}$ and erodibility $\bar{p_e}$.

in soil loss results with increasing R and P values is less evident for $\bar{p_e}$ and becomes even untrue for $\bar{p_s}$. A possible interpretation is that the effect of spatial distributions of

$\bar{p_s}$ overcompensates the effect of an increase in runoff conditions. All results are nevertheless higher than in spatially-homogeneous configurations, especially for "favourable" spatial patterns of the equivalent erodibility, associated with $B2$, $B10$, $B8$ and $B7$ configurations.

The sensitivity of a model to the Bi spatial distributions of its parameters may be calculated from the dispersion of the results, *i.e.* as the normalized S_B spreadth:

$$[S_B]_{P,R} = \frac{\max[M(P,R,Bi)] - \min[M(P,R,Bi)]}{M(P,R,B1)} \tag{6.1}$$

This quantity is plotted for MHYDAS-Erosion in Fig. 6.8c, together with its derivatives $G_P(SB)$ and $G_R(SB)$. An asymptotic regime seems to be reached when advancing towards the right of Fig. 6.8c, as S_B stabilizes to a high value and derivatives progressively tend to zero.

6.3.2.2 STREAM

Soil loss results for STREAM in Fig. 6.8b resemble these of Fig. 6.5b with less dispersion and discrepancies between curves associated to $\bar{p_s}$ and $\bar{p_e}$. Depending on the (P,R) conditions, the most productive configurations were $B1$ or $B2$ for equivalent slope and $B9$ or $B2$ for equivalent erodibility. Whereas soil loss values are about one order of magnitude lower than these of MHYDAS-Erosion, values of S_B for STREAM are negligible compared to these of MHYDAS-Erosion, except for low water-excess conditions on the left of Fig. 6.5d.

6.3.2.3 PESERA

Soil loss results for PESERA in Fig. 6.9a show six discrete levels of values inside any dotted column, as equal results are obtained from subfamilies of B configurations, namely $B1$, $B11$, $B6$ and $B7$, $B2$ to $B5$, $B10$, $B8$ and $B9$ in increasing efficiency order for $\bar{p_e}$. This order is almost the same for $\bar{p_s}$, for which $B11$ comes before $B1$. These discrete levels are a consequence of the fact that the imposed flow chart is not relevant and not taken into account by the model. Soil loss values are only dependent on the cell values of equivalent parameters, not on the connectivity between cells.

The order of magnitude of soil loss results obtained in spatially-distributed configurations is somewhat inferior to that obtained from spatially-homogeneous settings, whereas about the same difference exist in relative extension of results associated to equivalent slope and equivalent erodibility, at the aadvantage of the latter. Figure 6.9c indicates a perfectly clear trend in terms of dispersion of the results. S_B decreases with

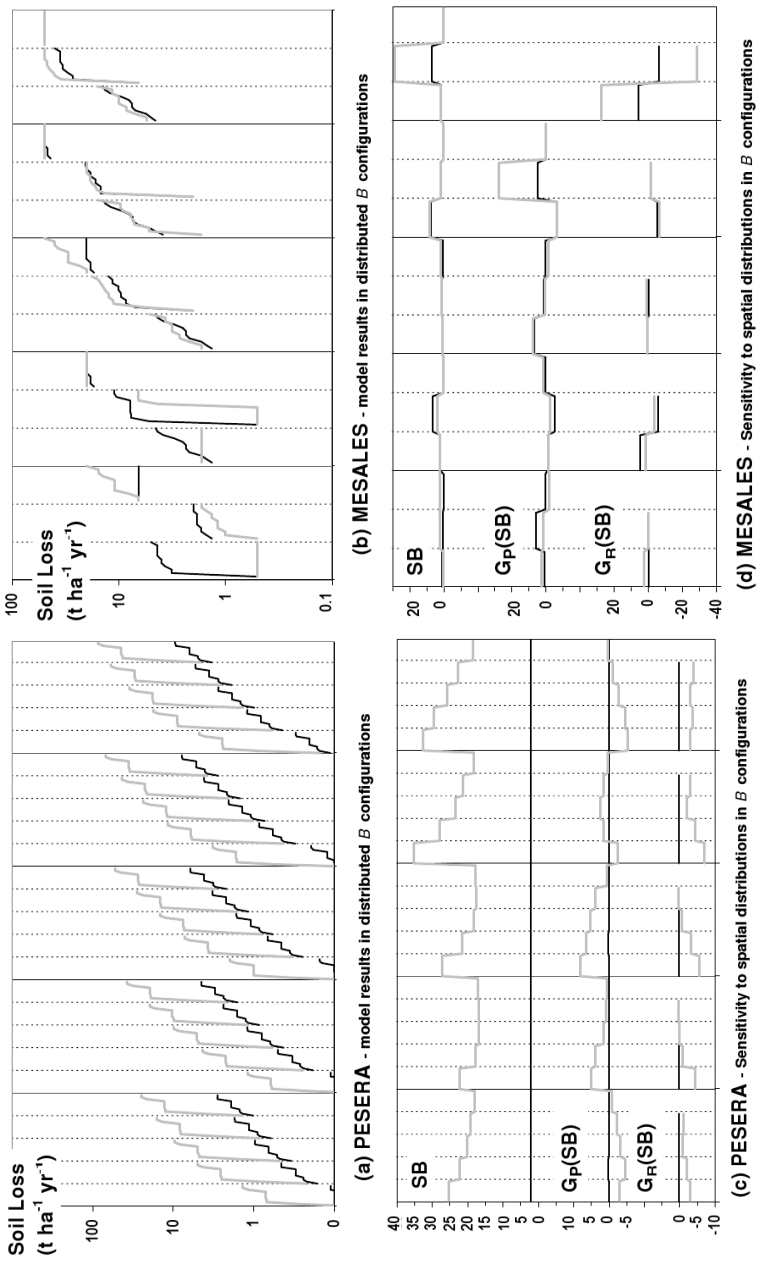

Figure 6.9: Dashboards representing soil loss, dispersion SB and variations in SB for PESERA (a,b) and MESALES (b,d) under all combinations of Precipations P and Runoff conditions R, for *one-at-a-time* (OAT) and Latin-Hypercube (LH) screenings involving equivalent slope $\bar{p_s}$ and erodibility $\bar{p_e}$.

increasing R conditions, *i.e.* with reduced percentage of vegetal cover and increased crusting, and the decrease in S_B tends to be more spectacular for higher values of P. Values of S_B range between 20 and 40, which is non-negligible before calculated soil losses on the one hand and places PESERA between STREAM and MHYDAS-Erosion regarding S_B values on the other hand.

6.3.2.4 MESALES

MESALES shows very comparable features in terms of magnitude of soil loss results (Fig. 6.9b) and sensitivity trends (Fig. 6.9d) in spatially-distributed than in spatially-homogeneous settings. The progression in numerical values is even smoother according to P and R conditions than it was in Fig. 6.6b. As for PESERA, one observes discrete levels of values inside dotted columns, though less clearly because of the conversion of classes of results into continuous values, which adds smoothing post-treatments. Configurations $B1$ and $B3$ are the less efficient when testing $\bar{p_s}$, the most efficient ones being $B6$ and $B9$. Concerning $\bar{p_e}$, the less efficient one are $B1$ and $B7$, whereas the most efficient ones are $B10$ and $B5$. Values of S_B are weak but become non-negligible in certain circumstances, again involving strong P values and median R values, corresponding to changes in land use for middle-range contributing land uses.

6.3.2.5 Sensitivity Maps

Sensitivity maps obtained from tests involving spatially-distributed configurations are placed in Fig. 6.10 and organized as in Fig. 6.7. These maps were plotted from data gathered in screenings described Fig. 6.4b and c. Each line of three figures corresponds to a single model, namely MHYDAS-Erosion, STREAM, PESERA then MESALES. Both P and R conditions increase when going from the left to the right column of figures, except for MESALES which was mapped in its median runoff condition but for increasing precipitations. From left to right the conditions read $(P2, R2)$, $(P3, R3)$ and $(P5, R5)$ for MHYDAS-Erosion, $(P2, R1)$, $(P3, R2)$ and $(P5, R3)$ for STREAM, $(P1, R1)$, $(P3, R3)$ and $(P5, R5)$ for PESERA, $(P1, R2)$, $(P3, R2)$ and $(P5, R2)$ for MESALES. The same pairs of (P, R) conditions were used as in Fig. 6.7 to facilitate comparisons. Screenings and representation facilities of Fig. 6.4c were used when available, *i.e.* for all models but STREAM, whose maps were plotted from screenings described in Fig. 6.4b.

As (P, R) conditions stregthen (Fig. 6.10a, b, c), MHYDAS-Erosion evolves from a situation where equivalent erodibility dominates to a situation where combined spatially-distributed effects gain more importance. A comparable behaviour is suspected for

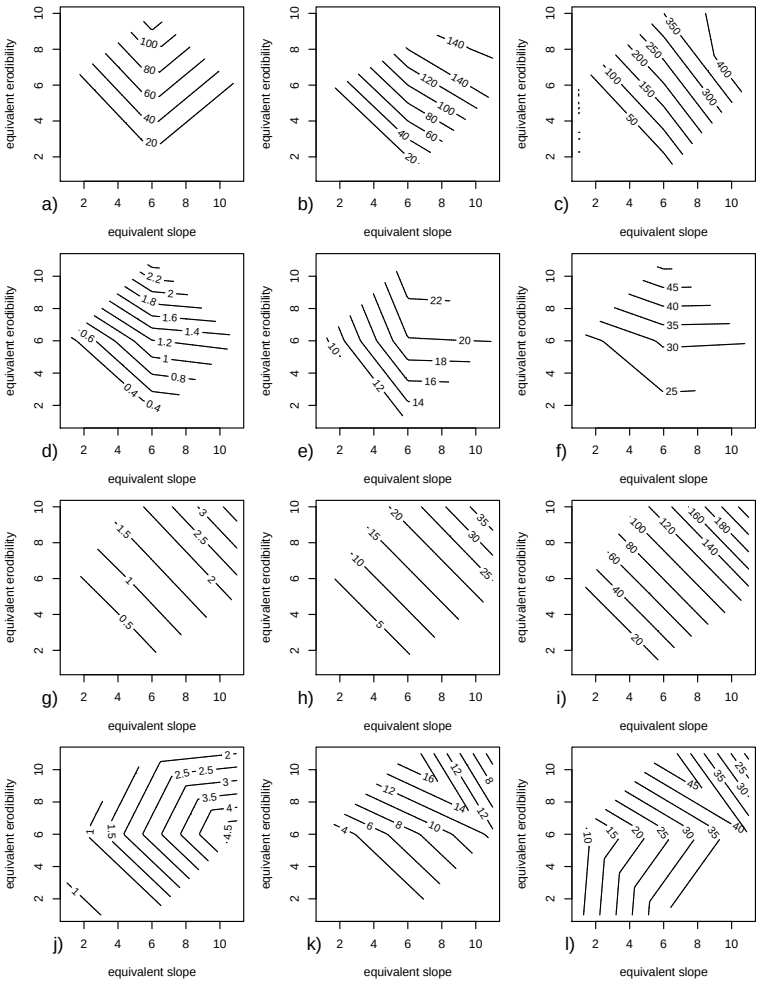

Figure 6.10: Sensitivity maps for MHYDAS-Erosion (a,b,c), STREAM (d,e,f), PESERA (g,h,i) and MESALES (j,k,l) in spatially-distributed configurations. Precipitations and runoff conditions increase from left to right for each model, except for MESALES mapped in a median runoff condition but for increasing precipitations. Soil loss isovalues are labeled in tons ha^{-1} $event^{-1}$ for MHYDAS-Erosion and STREAM, in tons ha^{-1} yr^{-1} for PESERA and MESALES.

STREAM (Fig. 6.10d, e, f) but could not be proven. For PESERA (Fig. 6.10g, h, i), soil loss values are stretched along the diagonal, indicating domineering combined effects whatever the (P, R) conditions considered. For MESALES (Fig. 6.10j, k, l), in a constant R condition corresponding to arable lands with median crusting, the maps are first dominated by equivalent slope effects, then by both equivalent erodibility and

equivalent slope, combined distributed values resulting in non-crucial effects, which is somewhat surprising and needs further investigations.

6.3.3 Summary of Comparative Results

Dispersion results have been placed in Table 6.1, involving all types of screenings performed in this study (Fig. 6.4), given here for selected (P, R) conditions. Dispersion indices in spatially-homogeneous are calculated on the model of Eq. 6.1, as:

$$[S_A]_{P,R} = \frac{[M(P, R, A_{max})] - [M(P, R, A_{min})]}{M(P, R, A_{med})} \tag{6.2}$$

where A_{med} simply denotes the case where all parameters have their median values in each cell. The equivalence between A_{med} and $B1$ makes all dispersion indices comparable.

Table 6.1 exhibits similarities between MHYDAS-Erosion and PESERA, associated with strong dispersion indices, whereas STREAM and MESALES show results more confined near reference values. A possible manner to step further into the analysis would be to calculate indices of the form S_B/S_A which would erase the reported differences between pairs of models.

General trends between models and reported hydrological conditions are that dispersion indices are higher when testing equivalent erodibility than when testing equivalent slope, and even higher when testing both. Highest sensitivities obtained when testing equivalent parameters in spatially-homogeneous settings result in highest sensitivities to spatial distributions.

Table 6.1: Dispersion results obtained for all screenings (Fig. 6.4) involving equivalent slope and/or equivalent erodibility under selected pairs of (P, R) precipitations and runoff conditions.

Screening	$P_{min}R_{min}$	$P_{min}R_{med}$	$P_{min}R_{max}$	$P_{med}R_{min}$	$P_{med}R_{med}$	$P_{med}R_{max}$	$P_{max}R_{min}$	$P_{max}R_{med}$	$P_{max}R_{max}$
MHYDAS-Erosion									
OAT $A(\bar{p}_s)$	-	-0.2	0.7	-	0.6	0.7	0.4	0.4	0.4
OAT $A(\bar{p}_e)$	-	9.1	13.9	-	5.4	12.0	8.7	10.6	11.5
LH $A(\bar{p}_s, \bar{p}_e)$	-	36.9	85.0	-	6.4	54.1	47.5	47.7	46.0
OAT $B'(\bar{p}_s)$	-	54.6	1.6	-	2.2	1.2	4.3	1.9	1.2
OAT $B'(\bar{p}_e)$	-	10.1	324.0	-	24.0	150.0	159.7	146.5	133.5
OAT $B"(\bar{p}_s)$	-	145.1	49.3	-	23.0	22.8	19.7	22.1	24.6
OAT $B"(\bar{p}_e)$	-	5128.0	325.2	-	153.7	154.1	139.8	152.8	142.5
LH $B"(\bar{p}_s, \bar{p}_e)$	-	105.9	239.6	-	20.8	160.0	131.1	152.9	127.8
STREAM									
OAT $A(\bar{p}_s)$	-	0.7	0.9	0.9	0.6	0.7	0.6	0.7	0.7
OAT $A(\bar{p}_e)$	-	4.4	3.4	3.5	1.8	1.7	1.7	2.6	2.6
OAT $B'(\bar{p}_s)$	-	0.5	0.7	0.7	0.5	0.4	0.5	0.3	0.3
OAT $B'(\bar{p}_e)$	-	2.5	1.9	1.9	0.6	0.5	0.5	1.1	1.1
PESERA									
OAT $A(\bar{p}_s)$	2.9	2.9	2.9	2.9	2.9	2.9	2.9	2.9	2.9
OAT $A(\bar{p}_e)$	37.7	30.0	26.7	40.6	27.3	26.4	48.7	38.6	27.7
LH $A(\bar{p}_s, \bar{p}_e)$	113.3	90.0	80.3	121.9	82.0	79.3	146.3	115.9	83.2
OAT $B'(\bar{p}_s)$	2.0	2.0	2.0	2.0	2.0	2.0	2.0	2.0	2.0
OAT $B'(\bar{p}_e)$	25.2	20.0	17.9	27.1	18.2	17.7	32.5	25.8	18.5
OAT $B"(\bar{p}_s)$	38.1	30.3	27.1	41.0	27.7	26.8	49.1	39.0	28.1
OAT $B"(\bar{p}_e)$	39.0	31.0	27.7	42.0	28.3	37.3	50.4	40.0	28.7
LH $B"(\bar{p}_s, \bar{p}_e)$	104.5	82.9	74.1	112.5	75.6	73.3	134.3	107.0	76.8
MESALES									
OAT $A(\bar{p}_s)$	0.0	0.9	0.9	0.3	3.0	1.1	-4.0	2.7	1.1
OAT $A(\bar{p}_e)$	0.0	0.7	2.1	0.0	2.1	1.5	0.0	1.9	0.0
LH $A(\bar{p}_s, \bar{p}_e)$	0.0	2.3	0.6	0.0	1.4	1.0	0.0	1.2	0.6
OAT $B'(\bar{p}_s)$	1.0	0.4	0.0	0.8	0.9	0.2	1.2	6.7	0.0
OAT $B'(\bar{p}_e)$	0.0	2.3	2.1	0.7	0.9	1.5	1.6	28.9	0.0
LH $B"(\bar{p}_s, \bar{p}_e)$	0.0	3.0	1.4	0.9	0.9	1.0	0.7	0.6	0.0

6.4 Conclusion

We exploited here the formal and theoretical work presented in the part I. paper (chapter 5) to perform a comparative sensitivity analysis of four very different distributed erosion models: MHYDAS-Erosion, STREAM, PESERA and MESALES. Relying on phenomenological arguments and causal links in the internal structure of models, they could be discomposed by means of the (P, R, p) procedure into parameters accounting for fluxes (precipitations P), propensity to surface flows (runoff conditions R) and specific erosion processes (descriptives parameters p). The model response took thus the general form $M(P, R, p)$, representing soil losses expressed in tons ha^{-1} event^{-1} for event-based models MHYDAS-Erosion and STREAM, and in tons ha^{-1} yr^{-1} for regional-scale models PESERA and MESALES.

Comparisons between models were made possible by the common coding of P and R arguments as unit increments along their respective axis. Descriptive parameter values were dispatched into constitutive subcategories of equivalent slope $\bar{p_s}$ and equivalent erodibility $\bar{p_e}$, which was found as the ultimate possible reduction in dimensionality of the problem. Spatially-homogeneous configurations of $\bar{p_s}$ and $\bar{p_e}$ were first examined to gain understanding of models behaviour and sensitivity trends. Tests were performed under varied combinations of (P, R) conditions figuring as many water-excess situations, imposed to a nine-cell virtual catchment endowed with a fixed flow chart. Spatially-distributed configurations of the equivalent parameters were considered then: the effect of spatial distributions was measured as the dispersion caused on soil loss results.

The analysis targetted soil loss results obtained at the outlet of the virtual catchment but could have involved a cell-by-cell procedure. Screening methods used to explore the equivalent parameter space resorted to both *one-at-time* displacements and Latin-Hypercube samples between discrete values of $\bar{p_s}$ and $\bar{p_e}$. Sensitivity was calculated as a deterministic, multilocal and directional quantity $G(P, R, \bar{p_s}, \bar{p_e})$ termed Gâteaux derivative but expressed in the same units as model outputs. The G function indicates local sensitivity of the model for any displacement in one or many of its arguments starting from a given position in parameter space.

A major finding was that equivalent erodibility plays a dominant role over equivalent slope in innate parameterization of the models, though sensitivity trends may differ under varied hydrological (P, R) conditions. The latter remark points out at the interest and relevancy of performing a separation between what is down to hydrology and what is specific to erosion in erosion models. Soil loss results were of the same order of magnitude when testing spatially-homogeneous or distributed configurations of

equivalent slope and equivalent erodibility. Combined tests involving both parameters had a domineering effect on soil loss results, especially in spatially-distributed configurations and for models found to be sensitive to spatial distributions of their parameters (MHYDAS-Erosion and PESERA).

Chapter 7

Sensibility analyses of a Water Erosion Model to the Spatial Distribution of Land Management Practices

Les modèles distribués d'érosion hydrique peuvent a priori être utilisés pour aider à localiser l'implantation des aménagements dans les bassins versants agricoles. Pour atteindre cet objectif les modèles doivent être capable de reproduire l'impact des aménagements sur le transport de sédiments à l'intérieur du bassin versant. En d'autres termes, il faut que le modèle en question soit sensible à la distribution spatiale des aménagements. Ce chapitre a pour objectif d'évaluer la sensibilité du modèle développé dans cette thèse (MHYDAS-Erosion) à la distribution spatiale des aménagements. Ce travail d'exploration du modèle a été appliqué au bassin versant de Roujan. En utilisant un méta-modèle pour déterminer la distribution des aménagements sur le bassin versant de Roujan nous avons calculé des indices de sensibilité globale à partir de la méthode de Sobol.

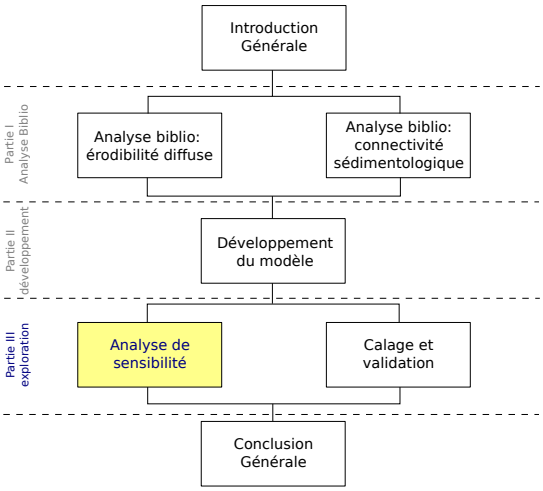

Sensibility analyses of a Water Erosion Model to the Spatial Distribution of Land Management Practices [1]

Gumiere, S.J.; Bailly, J. S.; Cheviron, B. ; Raclot, D.& Le Bissonnais, Y. (Article in prep.)

7.1 Introduction

The spatial distribution of land management practices in an agricultural catchment determines the capacity of any given part of the catchment to reduce or increase the global sedimentological connectivity (Cammeraat and Imeson, 1999; Fitzjohn et al., 1998). Fryirs et al. (2007) in a work on large-scale systems proposed that the effects of buffers in catchments depends on their scale and on the localization of sediment conveyance channels.

Distributed erosion models may be used to provide information to help farmers, managers, planners and policy makers in order to predict or explain how local land management practices (LMP) can impact soil erosion and sediment transport (Boardman, 2006). To reach this goal, distributed erosion model should be able to re-transcript any variation in LMP spatial distribution inside catchment.

Lecomte (1999), using the model STREAM, showed that a change in spatial distributions of grass strips over catchment has more impacts on total runoff and sediment trapping than a variation in size of the grass strips staying in the same position.

In this work we propose to make a sensitivity analyses of the model to the LMP spatial distribution. Sensitivity analyses includes the set of methods that aim to measure how uncertainty in model predictions is determined by uncertainty in model inputs (Saltelli et al., 1999). In case of spatially distributed and physically based models, the sensitivity analysis is also used for assessing the rationality of the model, to provide insight into the overall physical system that the simulation model represents, and to help identify research needs (Nearing et al., 1990).

Sensitivity analyses methods are generally categorized into two main groups: local methods and global methods (Saltelli et al., 2004, 1999). Differential analysis and nominal range methods are the most used local parameter sensitivity analysis methods (Frey and Patil, 2002; Helton, 1993). Differential analysis calculates partial derivatives of the model output with respect to the imposed perturbation of the model input. The

[1] Silvio Jose Gumiere, Jean-Stephane Bailly , Bruno Cheviron, Damien Raclot and Yves Le Bissonnais, Article in prep.

derivative values are themselves the measure of sensitivity. Nominal range method calculate the percentage variation of outputs due to the change of model input relative to nominal (reference) values. The percentage variation is the sensitivity value of the corresponding input parameter. The disadvantage of local sensitivity analysis methods is their incapability to account for model input parameters interactions, that may causing mis-estimation of the real value of model sensitivity. Moreover, these methods are dissuaded when models are complex and non linear. In that case, global sensitivity methods analysis are more suitable.

There are several global sensitivity analysis methods such as regional sensitivity analysis (RSA) (Young, 1978),variance based methods (Saltelli et al., 2000) and regression based approaches (Spear et al., 1994). Global methods attempt to explore the full parameter space within predefine feasible parameter ranges.

Among the global methods the Sobol sensitivity method is normally suitable when crossing effects between input parameters exist (Saltelli, 2002). When having spatially distributed factors, the Sobol sensitivity analyses however present computing limitations due to the way the numerous spatially distributed model factors are considered (Lilburne and Tarantola, 2009). That's why strategies to model the uncertainty in the spatial distribution of original factors, corresponding to uncertainty in LMP spatial distribution, has to be proposed. A strategy could be to model the LMP spatial distribution using few parameters, in order to reduce dimensionality (meta-modeling) (Marrel et al., 2008).

In this study, a sensitivity analysis of the MHYDAS-EROSION (Gumiere et al., 2009d) spatially distributed and physically based model to the LMP spatial distribution is performed using the Sobol method. The LMP upstream-downstream distribution is modeled and simulated through a stochastic model defined along a specific upstream-dowstream catchment location index and controlled by a set of three parameters (upstream-dowstream LMP gradient, LMP density overall catchment and a smooth parameter). The Sobol sensitivity indices are calculated for these three parameters using replications of Latin hypercube sampling in their finite range of uncertainties.

7.2 Material and Methods

7.2.1 Study site

The study area is located in the small agricultural catchment called Roujan (43.300 N, 3.190 E , area = 0.91 km^2). The Roujan catchment is an experimental catchment belonging to the OMERE long-term hydro-meteorological Observatory (http://www.umr-

lisah.fr/omere). Located in Southern France, 60 km west of Montpellier (Figure 7.1), catchment has a Mediterranean climate. The catchment is densely instrumented with hydro-meteorological equipments since 1992. Seven measurements points of runoff equipped with automatic sediment samplers are placed into Roujan catchment, as shown in figure 7.1. For this study we have chosen to use six of them i.e. five sub-catchments outlets and the main catchment outlet. The single field measurement point was excluded of this analyse, because its response to the LMP will be binary (it is composed by only one agricultural field). Approximately twenty percent of agricultural fields have a vegetated filter downstream, we consider that these vegetated filters acts as a grass strip filtering de sediment pass through.

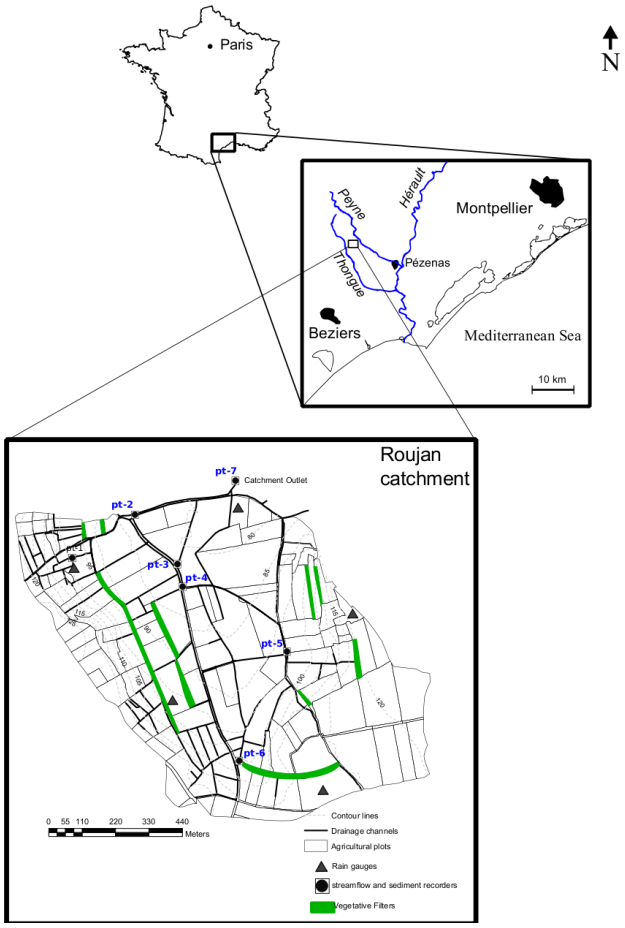

Figure 7.1: Measurement dispositives of Roujan catchment, France, and its LMPs localisation

Annual rainfall varies between 500 and 1400 mm, showing a bimodal temporal distribution with two major rainy periods, one in spring and another in autumn. Rainfall is usually of high intensity and short duration. The mean annual temperature is about $14°C$ and the mean annual Penman evapotranspiration is 1090 mm. The soils of the catchment developed from marine, lacustrine or fluvial sediments (Moussa et al., 2002). The catchment is mainly covered by vineyards and is divided into 237 agricultural plots. Agricultural plots area varies between 320 and 22 427 m^2. The drainage network is very dense and formed by man-made ditches, it generally follows agricultural plot limits. The total length of the ditch network is 11 069 m. The catchment is organized into four geomorphological and topographical domains: a depression with a minimum elevation of 75 m at the outlet (0.12 km^2), a glacis, which is an extension of the depression (0.24 km^2), terraces where slopes can reach 20% (0.30 km^2) and a plateau that peaks at 125 m (0.25 km^2).

7.2.2 The erosion model

MHYDAS-Erosion (Gumiere et al., 2009d) distributed water erosion model tested here is coupled to MHYDAS hydrological model (Moussa et al., 2002) that partitions rain between infiltration and runoff according to the model of Morel-Seytoux (1978) then analytically solve the one-dimensional Saint-Venant equations for concentrated flows in linear elements of the catchment (Moussa, 1996; Moussa and Bocquillon, 1996a). Available runoff is thus derived from saturated vertical hydraulic conductivity and initial water content. Flow depth and velocity are then obtained from discharge partition with the Manning formula, from known slope and width of each reach segment draining a plot. The erosion module *a minima* requires a finer decomposition of flow regions into subsections of adaptable sizes representing rill and interrill areas associated with different phenomenologies (see chapter 4, figure 4.2). Time steps fine enough to correctly track the fastest flow velocities expected were also redefined to ensure stability of the model according to the Courant-Friedrichs-Lewy condition (Courant et al., 1928). MHYDAS-Erosion is a GIS vector based model, that allow easy parameterisation.

The model has been designed to simulate runoff and erosion processes from single rainfall event in agricultural catchment. MHYDAS-Erosion is based on a catchment spatial segmentation where agricultural fields are represented by homogeneous polygons called surface units (SU) and drainage channel network system is represented by a series of interconnected reach segments (RS). A semi-automatic GIS vector based procedure (Lagacherie et al., 2009) allows easy segmentation and next easy parameterisation of the hydrological objects. Processes incorporated into the model are rainfall, infiltration,

overland flow, channel flow, soil detachment by rainfall, soil detachment by overland flow, soil detachment by channel flow. The model has a module to describe the influence of land management practices on sedimentological connectivity. In the first version of MHYDAS-Erosion, the land management practices are limited to vegetative filters located between two SU or between one SU and one RS. Table 7.1 shows the input parameters and description used to simulation with MHYDAS-Erosion.

Table 7.1: Input parameters for MHYDAS-Erosion

Parameter	Description	unit
surface unit (SU)		
k_s	saturated hydraulic conductivity	$m.s^{-1}$
β	correction factor Morel-Seytoux	-
hc	capillarity potential	m
n_{su}	SU Manning coefficient	$m.s^{-}1/3$
k	index of interrill erodibility	-
kr	rill erodibility for SU	$s.m^{-1}$
$CETI_{max}$	interrill to rill transport coefficient	-
COH_{su}	soil cohesion	Pa
N_{rill}	number of rills	-
W	rill width	m
LMP_{code}	identification of LMP	-
channels (RS)		
Ce	infiltration channel coefficient	$m.s^{-1}$
n_{rs}	RS Manning coefficient	$m.s^{-}1/3$
kr_{rs}	channel erodibility	$s.m^{-1}$
COH_{rs}	channel soil cohesion	Pa

The sedimentological connectivity module of MHYDAS-Erosion controls the sediment transfer between two hydrological objects ($SU \rightarrow SU$, $SU \rightarrow RS$ and $RS \rightarrow RS$). This version of MHYDAS-Erosion takes account only LMPs classified as vegetated filters (grass strips, vegetated water ways, riparian zones etc). The parameter LMP_{code} define to MHYDAS-Erosion which type of LMP is applied to the hydrological object (SU or RS). For example, when $LMP_{code} = 0$ no LMP is applied to the hydrological object and when $LMP_{code} = 1$ a LMP of the type grass strip is applied to the SU. For this sensitivity analyses we limit LMP as a grass strip, only applied to the SU (surface unit).

In MHYDAS-Erosion the sediment filtration provided by a grass strip is based on flume experiments by Deletic (2001) and Deletic and Fletcher (2006). Where sediment trapping efficiency (T_r) was defined as a function of the adimensional particle fall number (N_f) (see Chapter 4, figure 4.3). The sediment trapping efficiency T_r is calculated with the equation proposed by Deletic (2005):

$$T_r = \frac{N_f^{0.69}}{N_f^{0.69} + 4.95} \tag{7.1}$$

where

$$N_f = \frac{l \cdot V_s}{h \cdot V} \tag{7.2}$$

where l is the grass strip length (m), V_s is Stokes velocity for settling of sediment particles ($m.s^{-1}$), V is the mean flow velocity between grass blades ($m.s^{-1}$). Mean flow and settling velocities in the model are calculated as:

$$V = \frac{q}{B_0 \cdot h} \tag{7.3}$$

and

$$V_s = \frac{g}{18\mu}(\rho_s - \rho)d_s^2 \tag{7.4}$$

where B_0 is grass density, μ is dynamic viscosity of water ($kg.s^{-1}.m^{-1}$), ρ is water density ($kg.m^{-3}$), ρ_s is sediment particle density ($kg.m^{-3}$) and d_s is particle diameter (m). Deletic (2005) showed that the cross-correlation coefficient between measured and calculated trapping efficiencies reached $R^2 = 0.85$, which is acceptable. In MHYDAS-Erosion, T_r is calculated for each time step, thus sediment trapping efficiency is time-dependent. Parameters B_0 and l are estimated from field observations and may be spatially-distributed on the catchment. For this test we have adopted B_0 and l constants for all grass strips (LMP) of Roujan catchment, its values are 0.5 and 2 (m) respectively.

7.2.3 Sensitivity analysis procedure

The developed procedure for the MHYDAS-EROSION sensitivity analysis to LMP spatial distribution can be decomposed in three sequential steps. In a first step, a stochastic model of LMP upstream-downstream distribution is developed. The stochastic model simulate the LMP upstream-downstream distribution over catchment. In a second step, a framework to link stochastic model outputs (LMP upstream-downstream distribution) with MHYDAS-Erosion is proposed. In the third and last step, the principles of global sensitivity Sobol indices calculation based on random input-output set is exposed.

7.2.3.1 Stochastic model of LMP upstream-downstream distribution

The transfer of water and sediment in MHYDAS-Erosion is based on a processes oriented topology where each hydrological object (SU and RS) is linked to an upstream-downstream order. The flux of water and sediment from a surface unit can not be divided, but a surface unit can receive water and sediment discharge from one or more than one hydrological object. Consequently, the inner MHYDAS-Erosion topology of catchment corresponds to a directed tree shown by the network on figure 7.2A for the Roujan catchment.

The directed tree graph resuming catchment spatial structure can be projected in geographical space or other user-defined spaces. In figure 7.2B, we chose to represent the Roujan catchment directed tree along an ordinate corresponding to the distance of each hydrological objects centroid to catchment outlet, distance computed along the network. Further, this ordinate denoted h is chosen as the upstream-downstream location index for LMP distribution. The catchment configuration is thus resumed along this h axis.

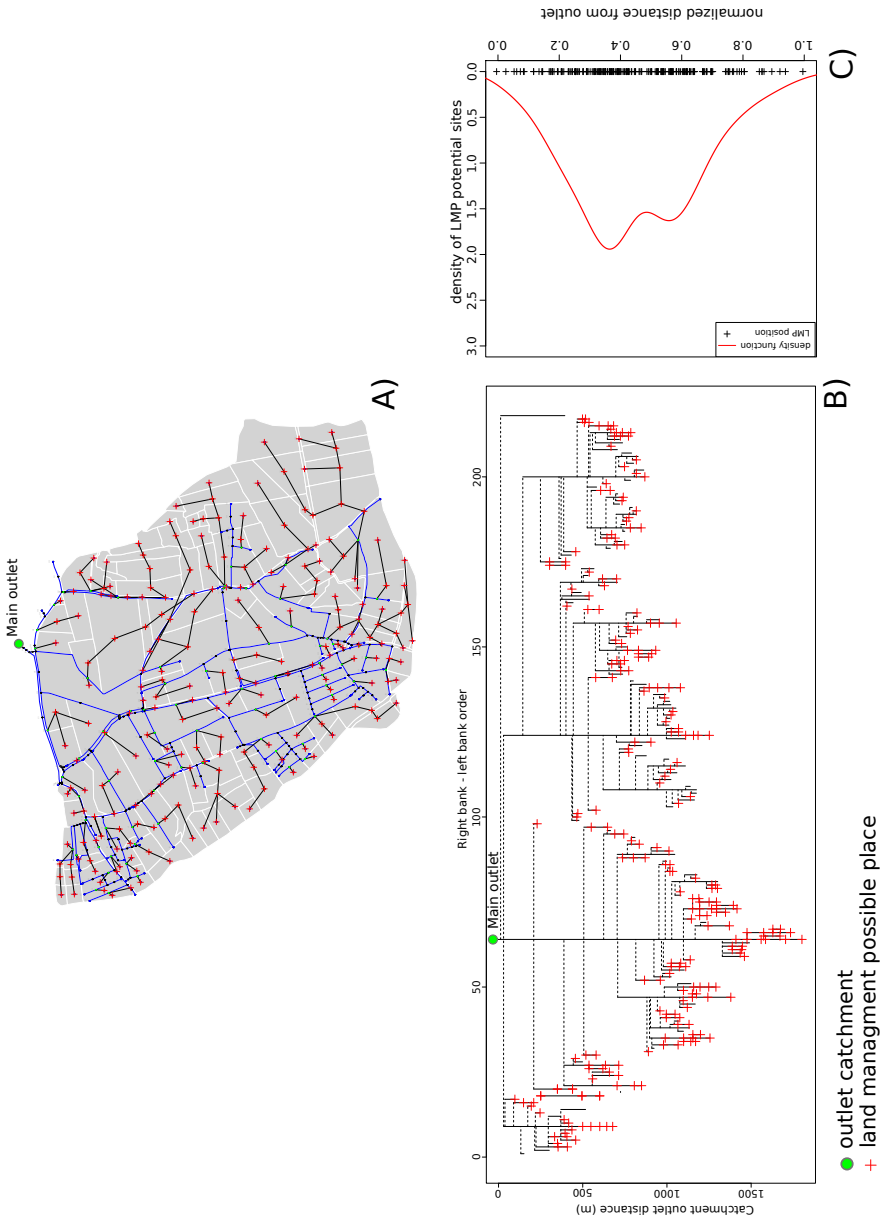

Figure 7.2: Schematic view of localisation of land management practices over Roujan catchment, A) Catchment topology representation, B) Catchment represented as a directed tree with the potential sites of LMPs and C) Probability density function of LMPs potential sites

LMP potential sites of the catchment graph can be identified by the nodes ("+" symbol in figure 7.2B. Two types of connection are possible, a SU to SU edge and a SU

to RS edge where water and sediment flow are discharged. For this sensitivity analysis we have chosen to apply LMPs only for SU, so only connections between $SU \rightarrow SU$ and $SU \rightarrow RS$ will be affected. The LMP here is exemplified as a grass strip applied at the downslope of the SU, for simplicity we have chosen to make grass strip parameters (B_0 and l) constants for all SU. The figure 7.2B shows the potential site to apply a LMP in the chosen topological space. Figure 7.2C shows the LMP potential site (points) projected along the h axis and a resulting kernel smoothed density probability function (line).

Firstly, the h index is transformed for convenience into the normalized x index ranging from 0 to 1:

$$x = \frac{h}{\max(h)} \tag{7.5}$$

In order to model contrasted LMP upstream-downstream configurations, we have proposed a linear upstream-downstream probability function $g(x)$. That is defined for any location x through:

$$g(x) = \left(\frac{1+p}{2}\right) - (p * x) \tag{7.6}$$

where p is the upstream-dowstream LMP gradient, ranging from -1 to 1. When $p = 0$, potential sites of LMP have same probability to be selected, whatever x value is. When $p = -1$ upstream potential sites of LMP are more probable to be selected, than downstream potential sites and conversely, when $p = 1$ downstream potential sites of LMP are more probable than upstream potential sites.

In order to amplify the contrast between LMP upstream-downstream configuration, and to avoid the effect of intrinsic LMPs potential sites probability function of the catchment figure 7.2C. We have defined a non-uniform distribution of the potential LMP along the upstream-downstream location index x, the $f(x)$ upstream-downstream function is defined from $g(x)$ through:

$$f(x) = \frac{\frac{g(x)}{l(x,bw)}}{\max\left(\frac{g(x)}{l(x,bw)}\right)} \tag{7.7}$$

where $l(x, bw)$ denotes the potential LMP non parametric kernel density function along the x axis (Silverman, 1986) (figure 7.2C). For a given catchment, this empirical function is estimated from potential LMP locations along the x axis. The bw parameter is the smooth parameter (bandwidth) of the $l(x)$ kernel density function. The stochastic

model $d(x)$ is thus defined to describe the LMP upstream-downstream location over the catchment. This model corresponds to a probability density function with two parameters p and bw defined by:

$$d(x) = \frac{f(x)}{\int_0^1 f(x)dx} \tag{7.8}$$

For LMP simulation, we need to define the number of LMPs that will be placed over the catchment. So we have added the LMP density r ranged from 0 to 1. It is defined as the number of LMP that will be applied by the number of LMP potential sites of the catchment. In fact, r just controls the repetition of sampling in the $d(x)$ function up to obtain the desired amount of simulated LMP overall catchment.

Finally the position of LMPs overall catchment is function of the three parameters (r, p and bw) which define the stochastique model. Figure 7.3 shows mean upstream-downstream position of LMPs calculated within stochastic model.

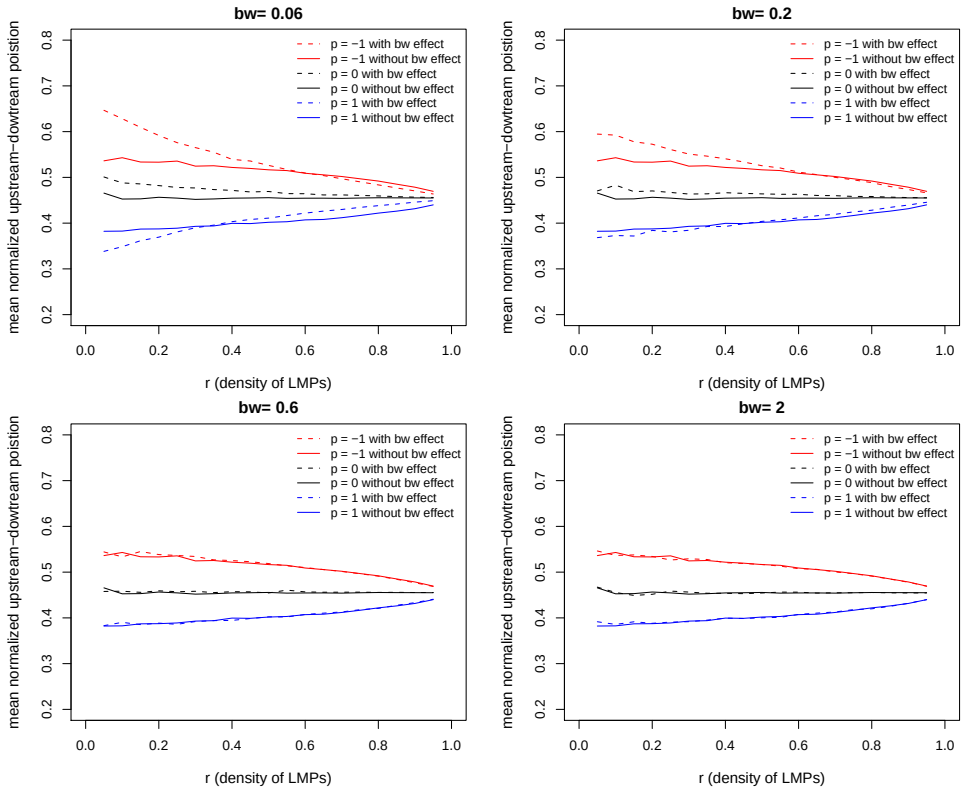

Figure 7.3: Mean normalized distance of LMPs in function of r, p and bw variation

It is observed from figure 7.3 that for $bw = 0.02$ mean upstream-downstream position of LMPs are more contrasted than those where $bw = 2$. It is equally observed the effect of p variation, when $p = 1$ upstream positions are more probable and when $p = -1$ downstream positions became more probable.

7.2.3.2 A framework to link stochastic model to MHYDAS-Erosion

Only the three parameters which define the stochastic model were used to the sensitivity analyses. The sensitivity of MHYDAS-Erosion to the others inputs parameters have been tested by Cheviron et al. (2009b). For this test all model input parameters have been considered spatially constant for all hydrological objects (SU and RS).

We used the SENSAN software (Doherty, 2004) to predefine parameter sets for MHYDAS-Erosion and to automate MHYDAS-Erosion runs until all parameter sets have been tested. SENSAN is the direct mode of the inverse parameter estimation PEST tool. It acts as a master model to any slave model to which it is linked, provided the communication between them is possible through input and output ASCII files. Figure 7.4 shows the overall coupling between stochastic model, SENSAN and MHYDAS-Erosion for the sensitivity analysis.

Based on the Latin hypercube sampling (LSH) of the three tested parameters (r, p and bw) the LMP stochastique model generate LMP position over all catchment. In fact, the LMP stochastic model output is a set of LMP_{code} that indicate whether the SU has a LMP or whether it has not, for each of 237 surface unities of Roujan catchment. One thousand simulations with MHYDAS-Erosion were made using fixed rainfall characteristics to ensure that parameter sensitivity had stabilized. A constant 60 $mm.h^{-1}$ during 4 h storm event with a delayed pattern was used for all the simulations. After one thousand MHYDAS-Erosion runs, first order and total Sobol sensitivity indices were calculated using the R-CRAN software sensitivity package.

7.2.3.3 Principles of global sensitivity Sobol indices calculation

For this work we have chosen the Sobol method described in Saltelli et al. (2000); Sobol (1993). Sobol method is variance-based global sensitivity analysis method based global sensitivity analysis methods based on "Total Sensitivity Indices" (TSI) that take into account interaction parameters effects. The TSI of a model parameter is defined as the sum of all the sensitivity indices involving that parameter. The TSI includes both the main effect as well as interaction effects Saltelli et al. (2000). For example, if a model have three parameters A, B and C, the TSI of parameter A is given by $S(A) + S(AB) + S(ABC)$, where $S(x)$ is the sensitivity index of x. $S(A)$ refers to the

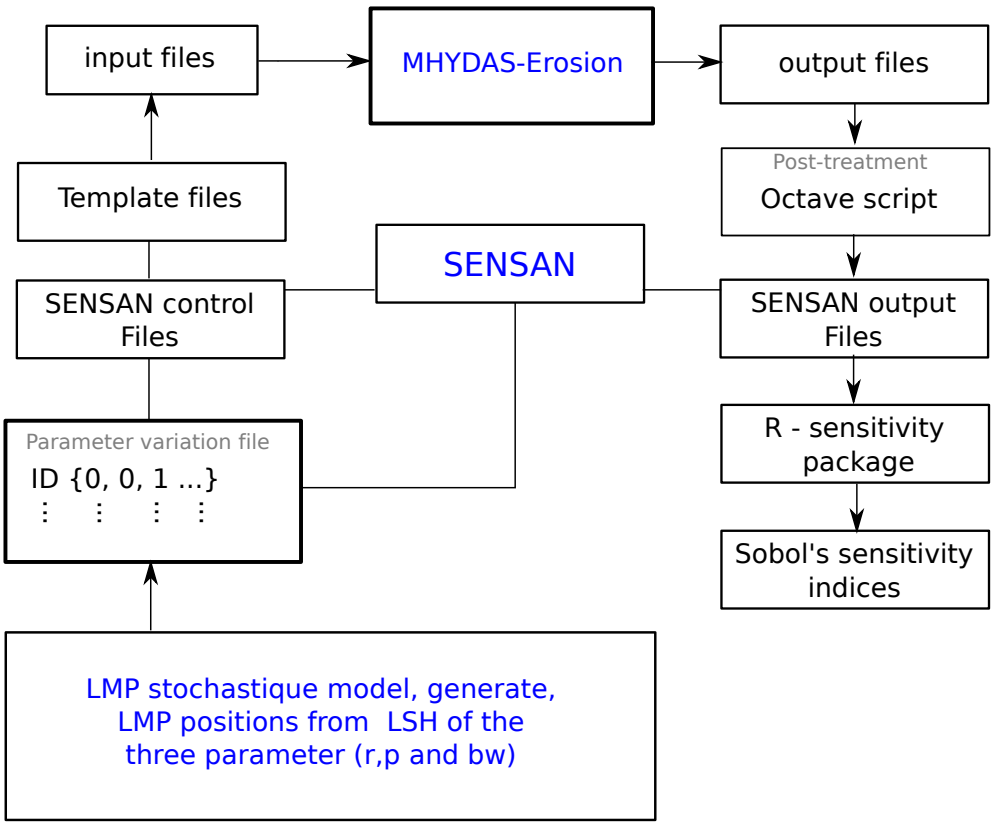

Figure 7.4: SENSAN scheme

main effect of A. $S(AB)$ refers to the interaction effect between A and B. $S(ABC)$ refers to the interaction effect between A, B, and C.

The Sobol method decomposes the output variability into all its possible sources, based on the high dimensional representation of the model. The high dimensional model representation consist in a decomposition of the model output as a superposition of orthogonal functions of increasing dimensionality and mean equal zero.

$$y = f_0 + \sum_{i=1}^{n} f_i(x_i) + \sum_{i=1}^{n} \sum_{j=i+1}^{n} f_{ij}(x_i, x_j) + ... + f_{1...n}(x_{1...n}) \tag{7.9}$$

where y is the model output, f_0 is the mean value of the model output, f_i is the main effect of the i^{th} input parameter, f_{ij} is the interaction effect between the input parameter i and j and so on for the higher order indexes. Based on the high dimensional model representation and the premise that all input parameters are statistically independent,

the model output variance can be decomposed as:

$$Var(y) = \sum_{i=1}^{n} Var(f_i) + \sum_{i=1}^{n} \sum_{j=i+1}^{n} Var(f_{ij}) + ... + Var(f_{1...n}) \tag{7.10}$$

Defining Sobol sensitivity indexes as:

$$S_i \equiv \frac{Var(f_i)}{Var(y)}, \; S_{ij} \equiv \frac{Var(f_{ij})}{Var(y)}, \; ... \, S_{1...n} \equiv \frac{Var(f_{1...n})}{Var(y)} \tag{7.11}$$

The advantage of Sobol method is to provide information about the influence of input including additive, nonlinear or with interactions effects. Furthermore, Sobol method can be smoothly applied to categorical variables without re-scaling. In this work we have used the R-CRAN package "sensitivity". In the next section we will test the sensitivity of the model output soil loss related to the three input parameters used for the LMP stochastic model to generate LMP location.

7.3 Results

7.3.1 Model response to upstream-downstream position

From one thousand simulations using the set of LMP_{code} generated by the LMP stochastic model and a constant 60 $mm.h^{-1}$ during 4 h storm event with a delayed pattern. Normalized soil loss results were simulated with MHYDAS-Erosion for the six sediment measurement points retained in Roujan catchment. We have adopted to use normalized soil loss for easy comparison between scales. Normalized soil loss (NSL) is calculated for each measurement point with: $NSL = \frac{E_i - min(E)}{max(E) - min(E)}$ where E_i (kg) is the soil loss in a measurement point for the i^{th} simulation and E is the vector with all simulated erosion values. In figure 7.5 simulated normalized soil losses responses to p, r and bw parameters variation are shown for the 6 measurements points of Roujan catchment.

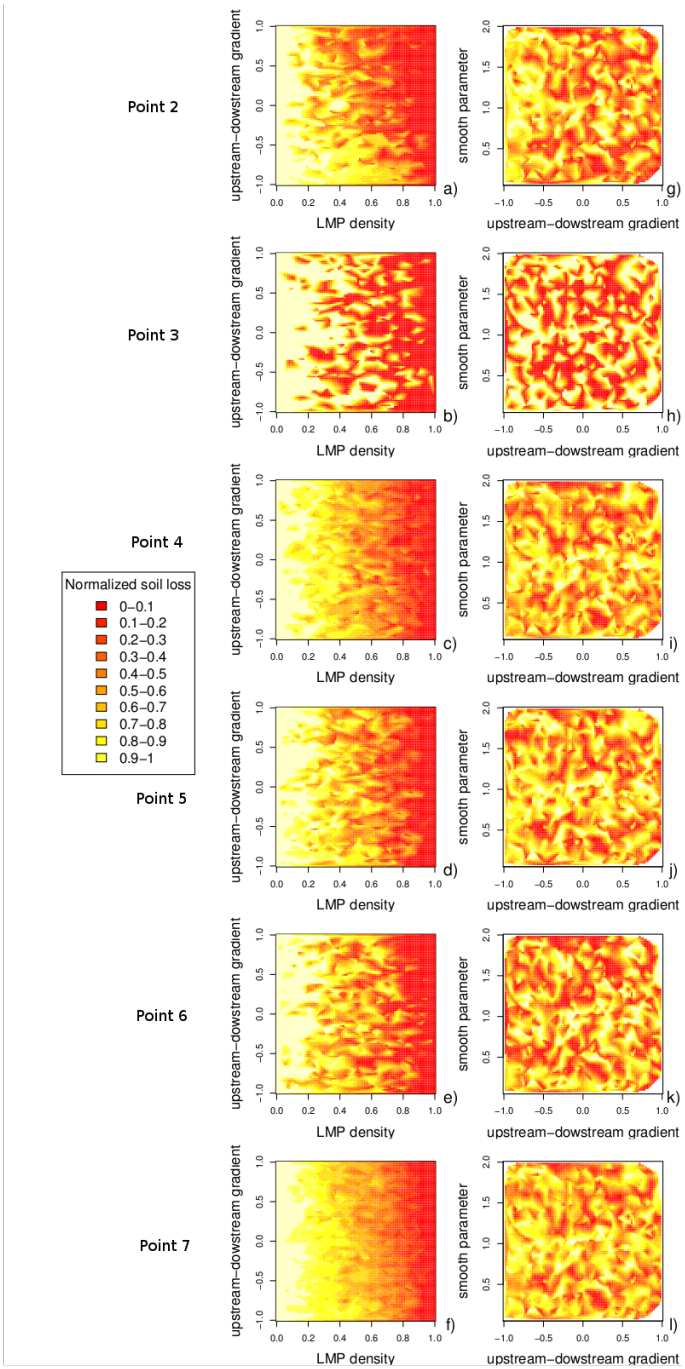

Figure 7.5: Color maps of normalized soil loss responses to the three parameters variation

From a qualitative point of view, figure 7.5a to f shows that LMP density (r) has more impact over simulated soil loss than the other two parameter upstream-downstream gradient (p) and smooth parameter (bw). However, figure 7.5 shows that with a same LMP density over the catchment, different values of normalized soil loss are possible. That means that the upstream-downstream of LMPs position overall catchment has influences on the soil loss model response. With a same LMP density (r value constant), normalized soil loss changes in function of upstream-downstream gradient (p) values. Normalized soil loss of the outlet measurement point seems to be not influenced by p values than other measurement points. No tendencies in simulated normalized soil loss is observed from figure 7.5g to l. This results confirm that LMP density (r) is the more important parameter. Measurement point of the catchment outlet 7.5f seems to respond differently to the upstream-downstream of LMPs position than other points. It can be explained by the presence of a very dense drainage network that limits the effect of the p parameter at the Roujan catchment outlet (point 7) as no LMP is applied on the drainage channels.

7.3.2 Sobol's sensitivity indices results

In figure 7.6 are shown Sobol total and 1 st order sensitivity indices, related to the three input parameters and the physical output NSL for sub-catchments and catchment scales of Roujan. As expected, the highest sensitivity indices are found for LMP density (r). This results indicates that LMP density is the predominant parameter influencing soil loss simulated by MHYDAS-Erosion in Roujan compared to the two others tested parameters for all scales of the catchment. The other input parameters p and bw have a smaller, but non null influence on the physical model output variation. The numerical values of the Sobol indices are shown in Table 7.2. The maximum 1 st order index is found for the outlet measurement point for the r parameter, the values of 1 st order index r parameter is 0.73 twice superior to the other parameters average values, showing that r explain in average 73% of the variance simulated normalized soil loss for overall catchment.

Total Sobol sensitivity indices give information about interaction input between parameters. By considering the total effect sensitivity indices (Table 7.2), a very slight increase in the absolute values with respect to the 1 st order sensitivity indices is detected for catchment measure point 4 and 7 (increase of 0.15 to point 4 and 0.03 to point 7) related to LMP density (r). This implies that few interaction is revealed by the analysis of the physical output normalized soil loss. However, for the other measurement points a significant increase is observed. The greatest increase from 1

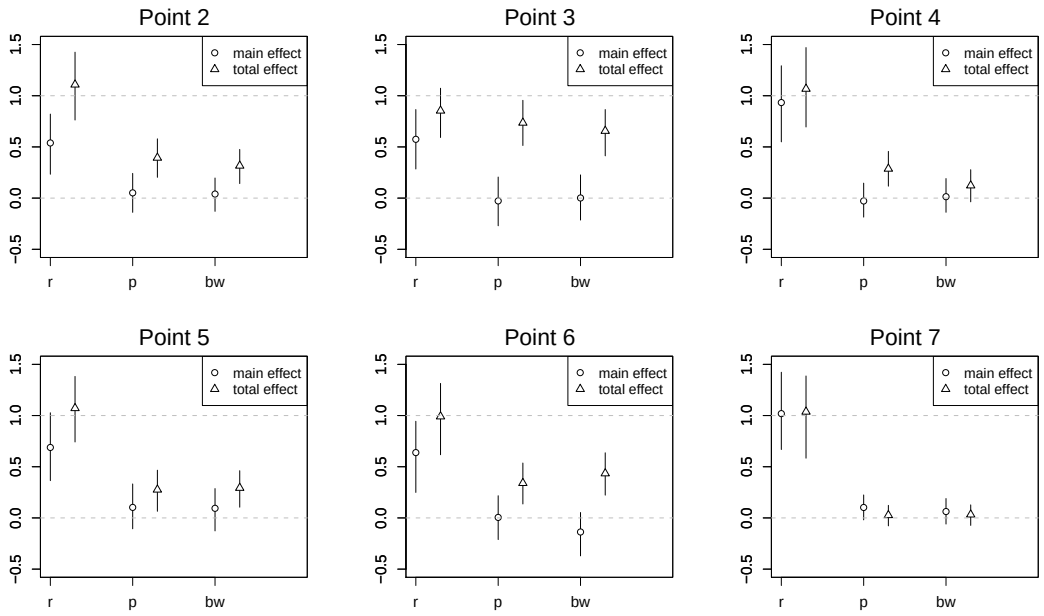

Figure 7.6: total and 1 st order Sobol's sensitivity indices

Table 7.2: Sobol sensitivity indices

Parameters →	r			p			bw		
Points	1 st (S_i)	total(S_T)	$S_T - S_i$	1 st(S_i)	total(S_T)	$S_T - S_i$	1 st (S_i)	total (S_T)	$S_T - S_i$
2	0.54	1.10	0.56	0.052	0.39	0.34	0.04	0.32	0.28
3	0.58	0.85	0.27	-0.015	0.73	0.75	0.005	0.65	0.65
4	0.93	1.08	0.15	-0.03	0.29	0.32	0.01	0.12	0.11
5	0.68	1.07	0.39	0.09	0.28	0.19	0.05	0.29	0.24
6	0.65	0.99	0.34	0.01	0.34	0.33	-0.13	0.43	0.56
7	1.02	1.05	0.03	0.10	0.03	-0.07	0.06	0.04	-0.02
mean	0.73	1.02	0.29	0.03	0.03	0.31	0.01	0.31	0.3
std	0.2	0.09	0.19	0.05	0.23	0.26	0.07	0.22	0.26
CV	0.27	0.09	0.64	1.58	0.66	0.86	12.01	0.71	0.85

st to total sensitivity indices is found for the upstream-dowstream LMP gradient (p) at the catchment measure point 3, showing a high interaction of this input parameter with the others.

7.4 Discussion and Conclusion

The proposed sensitivity analysis can be considered as a framework to study model behaviour to both LMPs density and LMPs spatial distribution through an original upstream-downstream distribution parameter. Based on Sobol sensitivity analysis methods, the method provides information about model sensitivity to both input parameters variation and its interactions. In the case studied, we may conclude that simulated soil loss from MHYDAS-Erosion is more sensitive to the LMP density (r) than upstream-dowstream LMP gradient (p) and smooth parameter (bw). This hierarchy can be evaluated through the 1 st order Sobol indices which show that 73% of simulated soil loss is explained by the r (LMP density) in average for all point measurements. On the tested case, the surface response of normalized soil loss have shown that the upstream-dowstream LMP gradient (p) is a not the preponderant sensitive parameter. It however significantly affects MHYDAS-erosion output as different values of normalized soil loss are possible for a given values of LMP density (r) when upstream-dowstream LMP gradient (p) varies. It confirms that the efficiency of LMPs is linked to their location within the catchment. Therefore, their layout must be properly addressed. Such conclusions must be considered with caution as they are limited to the tested case : with the Roujan catchment, with a given model parameterisation, with a unique rainfall events and initial conditions. However the proposed method is generic and can be easily extended to any catchment and configurations to refine and generalize the conclusions. Futur works will focus on this task. Based on these results we may also conclude that MHYDAS-Erosion is adapted to take into account the spatial organization effects of LMP in the sub-catchment and catchment scales. It can be used as a toolbox for optimization LMP application into agricultural catchments.

Chapter 8

Multi-scale Calibration and Validation of a Distributed Water Erosion Model: Application in a Mediterranean Vineyards Catchment

Les modèles distribués ont une forte propension à l'équifinalité, c'est à dire qu'ils présentent le risque de donner les bons résultats pour de mauvaises raisons. Pour pouvoir réduire ce risque d'équifinalité, nous avons utilisé une procédure automatique de calage multi-échelle, s'appuyant sur des connaissances d'expert pour vérifier la cohérence entre la valeur des paramètres et les conditions observées sur le terrain. Ce chapitre présente cette procédure de calage multi échelle appliquée au bassin versant de Roujan, qui possède 7 sites de mesure du débit et des MES répartis au sein du bassin versant.

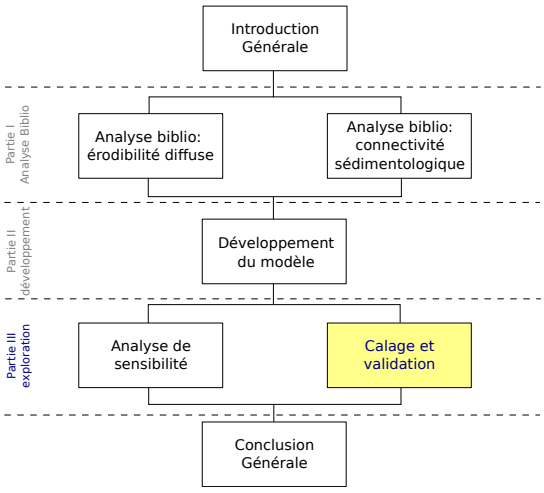

Multi-scale Calibration and Validation of a Distributed Water Erosion Model: Application in a Mediterranean Vineyards Catchment [1]

Gumiere, S.J.; Delattre, L.; Cheviron, B. ; Slimane, A. B.; Raclot, D.& Le Bissonnais, Y. (Article in prep.)

8.1 Introduction

Coupled hydrological and erosion models address damages caused by runoff, depending on rain intensity, soil properties and vegetal cover. Boardman (2006) suggested that only distributed models could possibly quantify areas on which erosion rates exceed some risk threshold, estimate erosion rates in locations where no observable data are available or predict erosion rates under evolutive land use and climate. Distributed information about erosion processes and risks is required for managers, planners and policy-makers to test spatial hypothesis implied in predictive scenarios (Beven, 1989; de Vente and Poesen, 2005).

Simulations with the MMF model (Morgan, 2001) gave values of Nash coefficients of 0.58 for annual runoff and 0.65 for annual soil loss. Hessel et al. (2006) evaluated the model LISEM in two East-African catchments and found values from -1.01 to 0.80. Kliment et al. (2008) simulated annual runoff and annual sediment load with models AnnAGNPS and SWAT. For AnnAGNPS the values of Nash coefficient were between -11.33 and -0.68 for annual runoff and between -62.79 and -0.13 for annual sediment load. For SWAT, results ranged from -5.99 to 0.70 for annual runoff and from -10.68 to 0.52 for annual sediment load. However, these effectivenesses are questionable when referring to the variability of measured data established by Nearing (2000), which should be taken into account to achieve a reliable model evaluation. Even though, these model results are helpful to understand model behaviours and may also be used with caution in erosion risk previsions. Results are most of the time available at the outlet of the catchment, where models perform well, whereas they often fail completely to reproduce the spatial pattern of within-basin runoff and erosion (Jetten et al., 1999). One common form of equifinality is to end up with the right result for the wrong reason, and non-uniqueness of parameterisation is a known problem in spatially-distributed erosion modelling (Brazier et al., 2000). In a test of a physically-based erosion model (LISEM) using field data from an extreme rainfall event, Takken et al. (1999) established that erosion rates were strongly overpredicted from densely-vegetated fields. Validation of models using

[1] Silvio Jose Gumiere, Laurence Delattre, Bruno Cheviron, Damien Raclot, Abir Ben Slimane and Yves Le Bissonnais. Article in prep.

sole outlet data are not reliable: the behaviour of spatially-distributed models is fully described and understandable when evaluated using spatially-distributed data (Takken et al., 1999).

The Roujan (Southern France) experimental catchment has spatially-distributed measurement points for sediment discharge and water runoff fluxes. In addition, it is situated in the Mediterranean ring especially prone to water erosion because of intense seasonal rainfalls and agricultural practices like vineyards on slopes, almost bare soils, abandonment of traditional conservation techniques and tillage along the major slope (Le Bissonnais et al., 2002). Moreover, long term climate change in this region is expected to accentuate the contrast between dry and hot summers and rainy intermediate seasons. This trend could increase the vulnerability to water erosion and have important economic and environmental consequences (Citeau et al., 2008).

The objectives of this work are to present a multi-scale calibration and validation procedure and a model evaluation for a spatially-distributed and event-based water erosion model, named MHYDAS-Erosion. We used spatially-distributed data of sediment discharge and runoff, collected under entities of three different scales in the Roujan catchment. Calibrations have been achieved using the open-source software PEST (Model-Independent Parameter Estimation and Uncertainty Analysis) developed by Doherty (2004).

8.2 Material and Methods

8.2.1 Study site

The study area is located in the small catchment called Roujan (43.300 N, 3.190 E , area = 0.91 km^2). The Roujan catchment is an experimental catchment belonging to the OMERE long-term hydro-meteorological Observatory (http://www.umr-lisah.fr/omere). Located in Southern France, 60 km west of Montpellier (Figure 8.1), catchment has a Mediterranean climate. The catchment is densely instrumented with hydro-meteorological equipments since 1992. Seven measurements points of runoff equipped with automatic sediment samplers are placed into Roujan catchment, as shown in figure 8.1. Approximately twenty percent of agricultural fields are has a vegetated filter downstream, we consider that these vegetated filters acts as a grass strip filtering de sediment pass through.

Vineyards cover about 60% of the area of this basin, divided into more than 230 field entities (Moussa et al., 2002). Two main soil management approaches to weeding were identified : chemical weeding or mechanical weeding by superficial tillage (Raclot

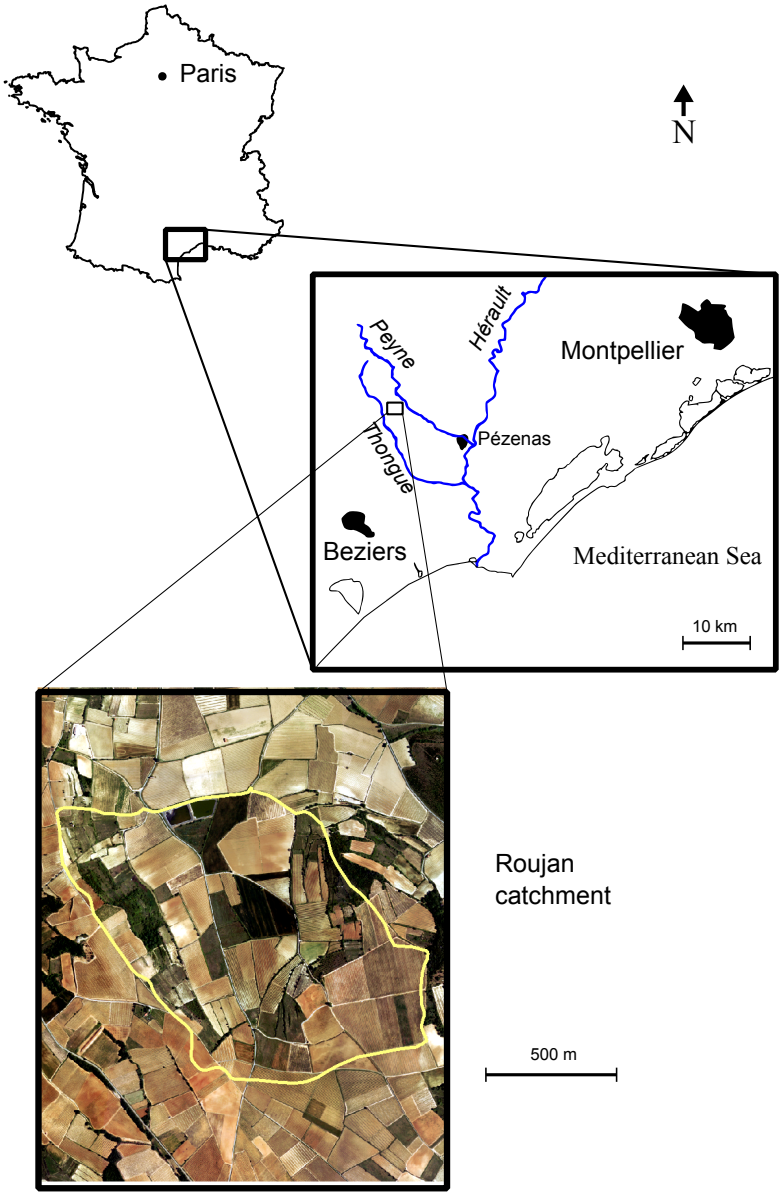

Figure 8.1: Roujan catchment, France

et al., 2009).The ditch network follows the plot margins and has a total length of 11069 m. Ditches are of variable forms and sizes.

The climate is Mediterranean with a long dry season and an average annual temperature of $14°C$. Annual rainfall varies between 500 and 1400 mm (Moussa et al., 2002) with a mean of 650 mm. Precipitations occur essentially in the form of brief and intense storms in spring or autumn and result in predominant hortonian runoff as-

sociated with small response-times throughout the basin. Enhanced by pedo-climatic conditions, overland flow explains indeed 80% of the peak discharge (Moussa et al., 2002). The runoff coefficient for the entire basin varies from 0 to 68% in the first 30 to 60 minutes after rainfall is initiated (Moussa et al., 2002) and runoff volume was estimated to about 70% of the rain volume on a non-tilled plot. Ditches play a major role in guiding the flow towards the outlet. Though event-dominated, the hydrological behaviour of the basin has seasonal characteristics.

8.2.1.1 The measurement devices

The catchment is instrumented with hydro-meteorological equipments since 1992 (meteorological station, rain gauges, streamflow recorders, piezometers, tensio-neutronic sites, automatic sediment samplers, Venturi channels). Figure 8.2 shows the localization of some measurement devices.

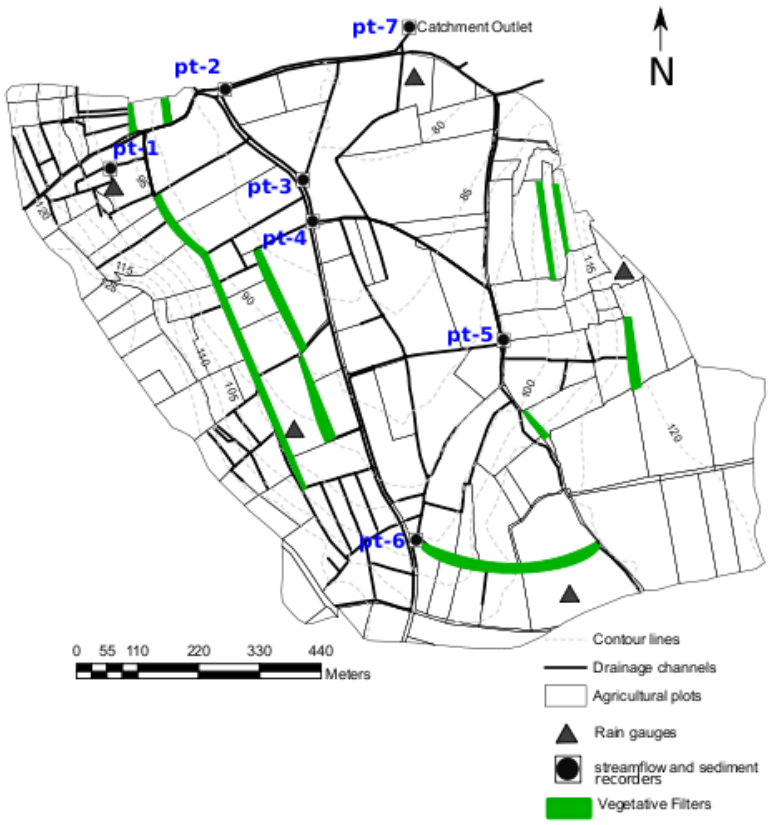

Figure 8.2: Meteo-Hydro-sedimentological devices of Roujan agricultural catchment

The tipping bucket rain gauges system allows recording every 5 minutes. The outflow is measured from depth gauges set up in Venturi channels and recorded every 5 minutes or every 10 minutes if the variation in height between two recordings is less than 10 mm. Measurement of the quantity of suspended material is done thanks to automatic sediment samplers collecting small liquid volumes at determined water height, immediately upstream the Venturi channel. The choice of water heights used in collecting loaded water is function of the drainage area and its observed hydrological behaviour. The samplings continue with one sampling every 30 mm variation during flood then decrease of water height.

Global sampling systems put each sample in the same recipient to form an average concentration in suspended materials during an event. Sequential sampling systems put each sample in a separate recipient to monitor the evolution of the instantaneous concentration during the event. The samples are filtered at 0.45 μm, then dried at $105°C$ during 48h and finally weighted in order to get the mass concentration of suspended materials.

8.2.2 Rainfall events

Eleven rainfall events over the 2005-2007 period have been chosen. These events were chosen for calibration an validation procedures. They last from 2 h 10min to 1day 16h 10 min for total rain amounts varying from 20 mm to 92 mm. Sub-catchments and catchment lag times are short, generally inferior to 30 minutes. Table 8.1 shows the principal characteristics of retained rainfall events.

Table 8.1: Main rainfall characteristics for calibration and validation events, C^a corresponds to calibration events, I_{mean} is the mean rainfall intensity, I_{max} is the maximum rainfall intensity and IPA5 is an index of antecedent rainfall events

	Date $(yyyy-mm-dd)$	Season (min)	Duration (mm)	Total rainfall $(mm.h^{-1})$	I_{mean} $(mm.h^{-1})$	I_{max}	C^a	IPA5
1	2007-06-10	spring	170	33	11.65	48.96	X	19.88
2	2007-06-06	spring	130	32	14.77	64.32	X	0.00
3	2007-03-31	spring	740	24	1.95	13.68		0.00
4	2006-10-18	autumn	230	22	5.74	18.72	X	0.36
5	2006-01-15	winter	1075	20	1.12	10.56	X	0.00
6	2005-11-12	autumn	1810	92	3.05	37.44	X	2.96
7	2005-10-18	autumn	965	47	2.92	24.60	X	52.54
8	2006-09-13	summer	620	44	4.26	48.72		0.00
9	2006-10-11	autumn	805	35	2.61	123.6		0.00
10	2007-02-17	winter	955	46	2.89	11.28		2.04
11	2007-05-03	spring	1335	33	2.89	8.70	X	16.76

We performed a PCA (Principal Component Analysis) using as factors the total amount of rain, maximum intensity and effective duration of rainfall. Seven calibration rainfall events were chosen (2007-06-10, 2007-06-06, 2006-10-18, 2006-01-15, 2005-11-12, 2005-10-18, 2007-05-03) and the four remaining events (2007-03-31, 2006-09-13, 2006-10-11, 2007-02-17) were used in validation procedures. . From de PCA analysis (figure 8.3) it can be seen that rainfall events 2005-11-12 (6) and 2006-10-11 (9) are out-group.

The 2005-11-12 rainfall event has the bigest duration and rainfall amount. And the 2006-10-11 has the greatest maximum intensity. Both 2005-11-12 and 2006-10-11 are different from the others rainfall events.

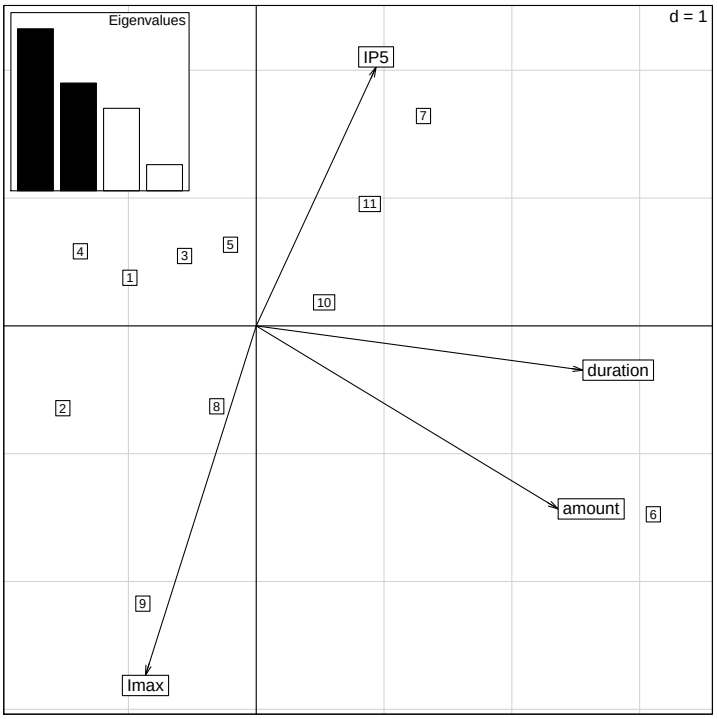

Figure 8.3: Principal component analysis of the eleven rainfall events where: IP5 is the five days anteriors rainfall events, duration is the time to rainfall beging to the end of event, Imax is the maximum rainfall intensity during the event

8.2.3 Model description

The distributed water erosion model (MHYDAS-Erosion) tested here is coupled to an underlying pre-existing hydrological model (MHYDAS), presented by (Moussa et al., 2002). MHYDAS partitions rain between infiltration and runoff according to the method of Morel-Seytoux (1978) then analytically solve the one-dimensional Saint-Venant equations for concentrated flows in linear elements of the catchment (Moussa, 1996; Moussa and Bocquillon, 1996a). Available runoff is thus derived from saturated vertical hydraulic conductivity and initial water content. Flow depth and velocity are then obtained from discharge partition with the Manning formula, from known slope and width of each reach segment draining a plot. The erosion module *a minima* requires a finer decomposition of flow regions into subsections of adaptable sizes representing rill and interrill areas associated with different phenomenologies. Time steps fine enough to correctly track the fastest flow velocities expected were also redefined to ensure stability of the model, with respect to the Courant-Friedrichs-Lewy (CFL) condition

(Courant et al., 1928). MHYDAS-Erosion is a Geographical Information System (GIS) vector-based model that allows easy parameterisation.

The model has been designed to simulate runoff and erosion processes from single (isolated) rainfall events in an agricultural catchment. MHYDAS-Erosion (Gumiere et al., 2009d) is based on the spatial segmentation of a catchment where agricultural fields are represented by homogeneous polygons called surface units (SU) and river systems are represented by interconnected lines forming a drainage channel network called reach segments (RS). Segmentation is accomplished by a semi-automatic procedure resorting to expert knowledge, maps and field observations. Processes incorporated into the model are rainfall, infiltration, overland flow, channel flow, soil detachment by rainfall, soil detachment by overland flow and soil detachment by channel flow. The model integrates a module to describe the influence of land management practices on sedimentological connectivity. In the first version of MHYDAS-Erosion, the land management practices are limited to vegetative filters located between two SU or between one SU and one RS. Table 8.2 shows the input parameters and description used to simulation with MHYDAS-Erosion.

Table 8.2: input parameters for MHYDAS-Erosion

Parameter	Description	unit
surface unit (SU)		
k_s	saturated hydraulic conductivity	$m.s^{-1}$
β	correction factor Morel-Seytoux	-
hc	capillarity potential	m
n_{su}	SU Manning coefficient	$m.s^{-}1/3$
k	index of interrill erodibility	-
kr	rill erodibility for SU	$s.m^{-1}$
$CETI_{max}$	interrill to rill transport coefficient	-
COH_{su}	soil cohesion	Pa
N_{rill}	number of rills	-
W	rill width	m
LMP_{code}	identification of LMP	-
channels (RS)		
Ce	infiltration channel coefficient	$m.s^{-1}$
n_{rs}	RS Manning coefficient	$m.s^{-}1/3$
kr_{rs}	channel erodibility	$s.m^{-1}$
COH_{rs}	channel soil cohesion	Pa

8.2.4 Model calibration and validation procedure

8.2.4.1 Calibration parameters

In order to avoid or at least diminish equifinality (Brazier et al., 2000), we reduced the number of calibration parameters, based on a previous sensitivity analyses of the model (Cheviron et al., 2009b). Considering the dependence of erosion processes on hydrological processes, we calibrated hydrology first and erosion then. In fact, in MHYDAS-Erosion as well as most erosion models, erosion variables are calculated using previously calculated hydrological variables . The influence of error from hydrological output has been pointed out by Wainwright and Parsons (1998), whose demonstrated that estimations of flow depth is a critical variable to erosion estimations. The flow depth at any location will depend on the prediction of infiltration rate, resistance to flow and flow routing causing hyper-sensitivity of modeled erosion processes to the before calculated hydrological outputs. Thus, we have chosen to calibrate the hydrological outputs at best in order to avoid the part of erosion error caused by hydrology misrepresentation, and focuse the analysis on error caused by erosion representation.

Hydrological parameters chosen for calibration saturated hydraulic conductivity (k_s), which is the most sensitive hydrological parameter of MHYDAS-Erosion, and Ce which is an equivalent infiltrability parameter, it describes transfers between ditches and groundwater units. Values of k_s were divided into four classes attributed to the hydrological units according to reported land uses. To prevent equifinality each class value for k_s is linked to the reference value k_{s1}: $k_{s2} = 1.1\ k_{s1}$, $k_{s3} = 1.7\ k_{s1}$. The given initial values for each k_s class related to a given land use are $k_{s0} = 5.5\ 10^{-8}$ for roads and impermeable surfaces, $k_{s1} = 5.5\ 10^{-7}$ for tillage vineyards, $k_{s2} = 1.1\ 10^{-7}$ for non-tillage vineyards and annual crops and $k_{s3} = 2.2\ 10^{-6}$ for forests, fallows and scrublands. The reference value adopted to Ce is $1.2\ 10^{-3}$.

Erosion parameters chosen for calibration were interrill erodibility (k) [1], rill erodibility (kr), soil cohesion (COH) and the maximum value of the coefficient for efficiency of interrill transport ($CETI_{max}$). Initial (*i.e.* starting) values used in calibration of erosion parameters were obtained from land use reports (table 8.3). Ditches are considered homogeneous over the catchment. The initial values of the ditches calibration erosion parameters were $COH = 10$ and $kr = 5.0\ 10^{-5}$.

[1] ici (k) est utilisé en dehors du significat dans la nomenclature

Table 8.3: Calibration parameters for erosion processes

	Initial value and unit	Land use
k_0	0.001 (−)	Roads
k_1	0.7 (−)	Non-grassed vineyards and annual crops
k_2	0.5 (−)	Fallows, scrulands, forests and grassed areas
$CETI_{max\,0}$	0.25 (−)	Roads
$CETI_{max\,1}$	0.06 (−)	tillage vineyards and annual crops
$CETI_{max\,2}$	0.12 (−)	non-tillage vineyards
$CETI_{max\,3}$	0.01 (−)	Fallows, scrublands, forests and grassed areas
COH_0	100 (Pa)	Roads
COH_1	2 (Pa)	Sand, loamy sand, sandy loam
COH_2	3 (Pa)	Loam, silt loam, sandy clay loam
COH_3	10 (Pa)	Clay loam, silty clay
kr_0	$1.0\,10^{-9}$ $(s.m^{-1})$	Roads
kr_1	0.1 $s.m^{-1}$	Sand, loamy sand, sandy loam
kr_2	0.01 $s.m^{-1}$	Loam, silt loam, sandy clay loam
kr_3	0.005 $s.m^{-1}$	Clay loam, silty clay

8.2.4.2 Automatic calibration procedure with PEST

We used the PEST software (Doherty, 2004) to calibrate parameter sets for MHYDAS-Erosion. PEST is a non-linear parameter estimation software that uses the Gauss-Marquardt-Levenberg (Marquardt, 1963) algorithm with an iterative process. At the beginning of each iteration the relationship between model parameters and model-generated observations is linearised by formulating it as a Taylor expansion about the currently best parameter set, hence the derivatives of all observations with respect to all parameters must be calculated. This linearised problem is then solved for a better parameter set, and the new parameters tested by running the model again, under user-defined options. By comparing parameter changes and objective function improvement achieved through the current iteration with those achieved in previous iterations, PEST can tell whether it is worth undertaking another optimisation iteration, if so the whole process is repeated. It acts as a master model to any slave model to which it is linked, provided the communication between them is possible through input and output ASCII files (figure 8.4).

The calibration procedure is made of two steps. It starts with the calibration of the total flow discharge from the agricultural field scale, *i.e.* over the entire basin. In fact, the agricultural field scale is a kind of"learning stage" where the optimum value of k_{s1} is obtained for a specific land use. We then relied on literature and expert opinion to determine the multiplicative factors between the different k_s values corresponding

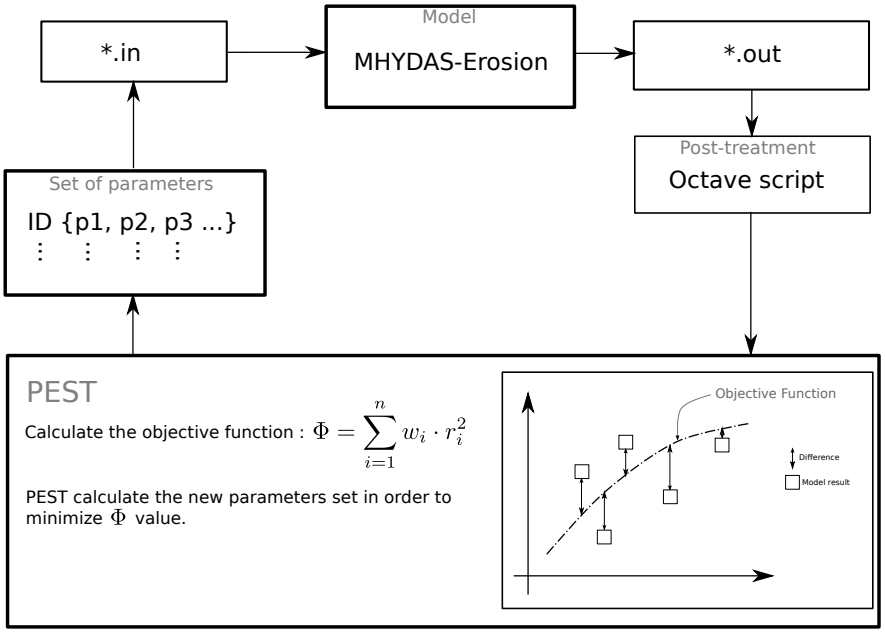

Figure 8.4: Flowchart of PEST

to different land uses. In this case study, k_{s1} corresponds to vineyards with chemical tillage that favours crusting formation and decreases infiltrability (Le Bissonnais and Singer, 1992). The $k_{s2} = 1.1 k_{s1}$ values corresponds to vineyards with mechanical tillage or to annual crops, that favours infiltration. The $k_{s3} = 1.7\ k_{s1}$ corresponds to forests and natural vegetation. In the second step, the multi-scale calibration is applied using the seven measurement points. The multi-scale calibration procedure consists in fixing the k_s values obtained during the first step and varying Ce values. The aim is to reach the minimum difference between observed and simulated flow discharge for each measurement point simultaneously.

Erosion parameters were calibrated the in same way, using agricultural field scale as a "learning stage" Values of k_1, $CETI_{max\,1}$, COH_1 and kr_1 were first calibrated with total sediment discharge values from the agricultural field scale, then multiplying factors were introduced with reference to known land uses. At the end of calibration procedures, a set of erosion parameters was defined. Validation procedures adopted in this case-study consisted in identifying an average erosion parameter set including k_1, $CETI_{max\,1}$, COH_1 and kr_1 for the seven calibration events (table 8.4). The model was then ran for the four validation events with the average parameter set: total soil loss simulated for each rainfall event at each measurement point were compared with observed values.

8.3 Results

In table 8.4 calibrated values of the hydrological and erosion parameters for the eleven rainfall events are shown, it can be observed that k_{s1} values have a coefficient of variation (CV) of 1.05. These values are coherent with those found in others works at the Roujan catchment (Chahinian et al., 2006a,b; Moussa et al., 2002). The variation coefficient of Ce values is 2.03. We calibrated k_s and Ce for all rainfall events because of the high sensitivity of the model to these parameters (Cheviron et al., 2009a,b), which also have a high spatial variability (Gumiere et al., 2007). As shown by the coefficients of variation, the widest adjustments were made on Ce, showing a higher dependence of MHYDAS-Erosion on this parameter than on k_s.

Table 8.4: Hydrological and erosion calibrated input parameters

Events	Hydrology		Erosion					
	k_{s1} $(m.s^{-1})$	Ce $(m.s^{-1})$	$CETI_{max}$	kr_{RS} $(s\,m^{-1})$	COH_{RS} (Pa)	k	COH_{SU}	kr_{SU}
1	$5.18\,10^{-6}$	$5.49\,10^{-7}$	0.35	$1.11\,10^{-3}$	7.35	0.5	2.0	0.01
2	$5.10\,10^{-6}$	$6.10\,10^{-8}$	0.27	$2.61\,10^{-3}$	7.18	0.5	2.0	0.01
3	$5.49\,10^{-7}$	$1.15\,10^{-3}$	-	-	-	-	-	-
4	$1.61\,10^{-6}$	$6.10\,10^{-8}$	0.73	$1.66\,10^{-5}$	8.53	0.5	2.0	0.01
5	$1.47\,10^{-5}$	$1.65\,10^{-6}$	0.19	$5.56\,10^{-6}$	10.06	0.5	2.0	0.01
6	$1.27\,10^{-6}$	$4.45\,10^{-4}$	0.27	$5.56\,10^{-8}$	150.00	0.5	2.0	0.01
7	$9.42\,10^{-7}$	$1.49\,10^{-3}$	0.15	$5.00\,10^{-5}$	7.64	0.5	2.0	0.01
8	$5.50\,10^{-8}$	$1.42\,10^{-2}$	-	-	-	-	-	-
9	$1.02\,10^{-6}$	$1.73\,10^{-3}$	-	-	-	-	-	-
10	$6.37\,10^{-7}$	$1.34\,10^{-3}$	-	-	-	-	-	-
11	$6.30\,10^{-7}$	$1.89\,10^{-3}$	0.26	$5.00\,10^{-5}$	7.64	0.5	2.0	0.01
average	$2.88\,10^{-6}$	$2.02\,10^{-3}$	0.32	$5.49\,10^{-4}$	28.3	0.5	2.00	0.01
std	$4.30\,10^{-6}$	$4.11\,10^{-3}$	0.19	$9.95\,10^{-4}$	53.7	0.0	0.0	0.0
CV	1.05	2.03	0.61	1.81	0.13	0.0	0.0	0.0

Concerning erosion parameters, only $CETI_{max}$, kr_{RS} and COH_{RS} had their values adjusted during the seven calibration events. Calibrated values for erosion parameters are shown in table 8.4. It can be observed that $CETI_{max}$ has a variation coefficient of 0.61. Values of kr_{RS} have a variation coefficient of 1.81. And values of COH_{RS} have a variation coefficient of 0.13. Though freely adjustable, parameters k, COH and kr remained at their reference value. From the coefficients of variation, rill erodibility in linear elements (kr_{RS}) was the most affected parameter.

Results for calibration and validation of MHYDAS-Erosion are summarized in Table 8.5. In order to compare values of total flow discharge and total sediment discharge at different scales, we represented the results in relative form, dividing the total flow discharge and the total sediment discharge by the contributing surfaces.

Table 8.5: Hydrology and erosion results for calibration and validation procedures.

Date	Rainfall		Total discharge ($m^3.ha^{-1}$)			Total sediment discharge ($kg.ha^{-1}$)		
	(mm)		Obs.	Sim.	Diff.	Obs.	Sim.	Diff.
Calibration		*Point*						
2007-06-10	33	1	141.29	141.29	0	1431.35	1431.35	0
		2	9.61	7.72	1.89	82.15	147.71	65.56
		3	0.33	0.00	0.33	2.06	0.00	2.06
		4	11.42	3.49	7.93	246.31	50.07	196.23
		5	21.28	3.63	17.65	165.88	100.95	64.93
		6	10.00	6.15	3.85	86.59	215.26	128.67
		7	9.97	4.40	5.58	42.77	42.77	0
2007-06-06	32	1	77.68	77.74	0.06	634.19	634.19	0
		2	2.50	3.86	1.37	14.92	88.34	73.42
		3	0.00	0.00	0	0.00	0.00	0
		4	5.90	1.70	4.2	149.17	27.76	121.41
		5	36.60	1.72	34.88	260.68	54.73	205.96
		6	10.02	2.92	7.1	97.86	104.91	7.05
		7	2.81	2.20	0.61	21.28	21.28	0
2006-10-18	22	1	91.55	91.55	0	385.74	385.74	0
		2	12.59	3.57	9.02	35.14	2.26	32.88
		3	0.59	0.00	0.59	0.42	0.00	0.42
		4	5.60	1.40	4.19	4.32	13.36	9.04
		5	2.03	1.41	0.62	0.51	11.85	11.34
		6	7.92	2.37	5.55	145.16	18.53	126.63
		7	1.62	1.29	0.32	1.91	2.45	0.55
2006-01-15	20	1	22.06	22.06	0	24.26	24.26	0
		2	4.96	1.71	3.25	0.00	0.09	0.09
		3	0.62	0.00	0.62	0.00	0.00	0
		4	0.39	0.90	0.51	0.00	0.29	0.29
		5	13.80	0.94	12.85	0.00	1.99	1.99
		6	9.82	1.59	8.23	1.68	1.53	0.16
		7	9.24	1.22	8.02	0.00	0.05	0.05
2005-11-12	92	1	480.65	480.65	0	926.52	926.52	0
		2	58.23	64.52	6.29	100.86	402.57	301.7
		3	26.61	38.20	11.59	7.46	0.09	7.37
		4	56.05	57.21	1.16	36.35	1601.75	1565.4
		5	198.21	65.00	133.21	138.75	1990.81	1852.06
		6	39.31	126.91	87.6	13.14	4610.22	4597.08
		7	51.09	51.09	0	2.66	1200.03	1197.37
2005-10-18	47	1	262.13	262.13	0	114.32	114.32	0
		2	15.97	32.84	16.87	20.87	7.03	13.84
		3	3.11	16.37	13.27	0.32	0.00	0.32
		4	9.86	20.89	11.04	1.89	3.29	1.4
		5	22.85	27.99	5.14	2.26	15.75	13.49
		6	10.90	45.81	34.91	3.25	17.07	13.82
		7	5.42	5.42	0	0.00	0.00	0
2007-05-03	33	1	122.13	122.13	0	53.48	53.48	0
		2	0.00	0.17	0.17	0.07	0.00	0.07
		3	8.15	8.63	0.48	0.00	0.00	0
		4	0.16	1.48	1.31	0.00	0.48	0.48
		5	1.83	2.75	0.92	0.09	0.00	0.09
		6	1.47	3.12	1.65	0.24	0.00	0.24
		7	0.12	0.12	0	0.00	0.00	0
Validation		*Point*						
2007-03-31	24	1	0.22	0.22	0	138.32	92.20	46.12
		2	0.56	2.34	1.78	0.43	12.06	11.63
		3	0.88	2.16	1.28	0.00	0.13	0.13
		4	0.01	1.32	1.31	0.00	7.13	7.13
		5	0.00	0.64	0.64	0.00	44.14	44.14
		6	1.74	3.29	1.55	0.00	44.35	44.35
		7	106.13	106.13	0	0.00	0.06	0.06
2006-09-13	44	1	0.18	0.18	0	1590.32	1320.00	270.32
		2	2.67	0.00	2.67	18.99	416.61	397.62
		3	2.35	8.33	5.98	0.00	0.00	0
		4	0.14	0.96	0.83	0.00	24.77	24.77
		5	0.00	0.00	0	7.40	233.32	225.91
		6	7.34	12.14	4.8	10.79	0.00	10.79
		7	494.97	416.26	78.71	0.00	3.09	3.08
2006-10-11	35	1	8.35	8.35	0	5272.32	5652.48	380.16
		2	19.23	166.05	146.81	19.41	4900.70	4881.28
		3	6.93	92.87	85.95	12.68	120.23	107.55
		4	30.49	78.90	48.41	2.12	3254.36	3252.23
		5	6.10	45.13	39.04	14.81	4376.27	4361.46
		6	2.60	121.66	119.06	1287.22	8081.06	6793.84
		7	289.68	289.68	0	40.27	279.16	238.89
2007-02-17	46	1	0.12	0.12	0	288.13	94.92	193.21
		2	3.83	3.91	0.09	2.26	20.13	17.87
		3	3.21	3.20	0.01	0.00	0.00	0
		4	0.66	1.67	1.02	0.00	10.10	10.1
		5	0.00	0.61	0.61	0.47	55.38	54.91
		6	7.65	4.39	3.25	2.21	84.18	81.97
		7	183.10	183.10	0	0.00	1.40	1.4

From table 8.5 total flow discharge has been simulated with an average difference of 9.49 $m^3.ha^{-1}$ whatever the scale. The maximum value of the difference between observed and simulated flow discharges is 146.81 $m^3.ha^{-1}$. It was obtained at point

2 (sub-catchment scale) for the rainfall event of 2006-10-11. The minimum value of the difference is 0.00 $m^3.ha^{-1}$, often found at point 1 and 7 (agricultural field and outlet catchment scale) because objective function is calculated for these points in the calibration procedure. Figure 8.5 shows a scatter diagram for observed and simulated total flow discharges using all measurement points and all rainfall events.

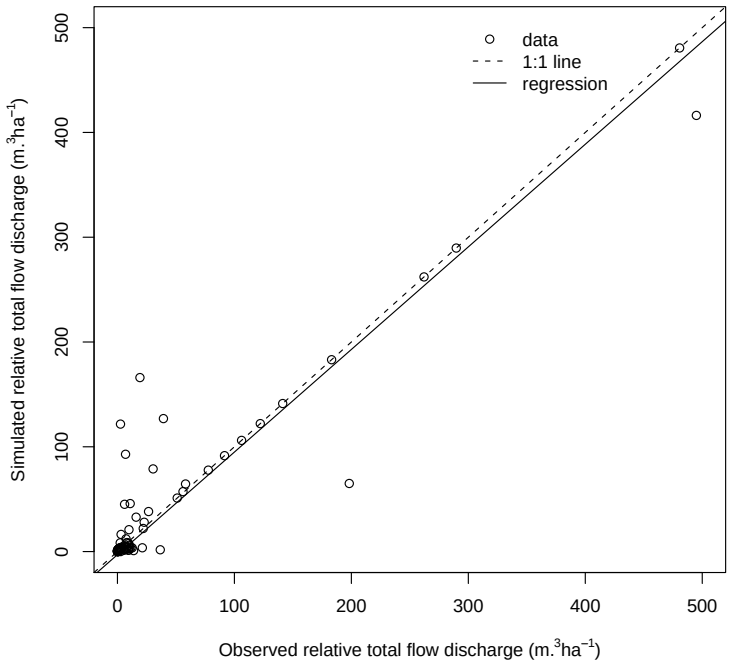

Figure 8.5: hydrology results

The commonly-used statistical R^2 value for total flow discharge is 0.94 with 95% confidence. Dispersion observed in figure 8.5 is associated to the worse simulation points, while most data are grouped near 0 to 50 $m^3.ha^{-1}$ showing that for these rainfall events a weak-moderate runoff coefficient of 1.0 to 10% .

From figure 8.6 calibration results indicates that the median difference between simulated and observed discharge is lower than 10 $m^3.ha^{-1}$. The biggest difference between simulated and observed discharge occurs at measurement points 5 and 6, for sub-catchment scales. A probable explanation is the discontinuous presence of exfiltration phenomenona, merely witnessed in autumn or winter and associated with high watertable levels (Chahinian et al., 2006a). Previous studies at the Roujan catchment

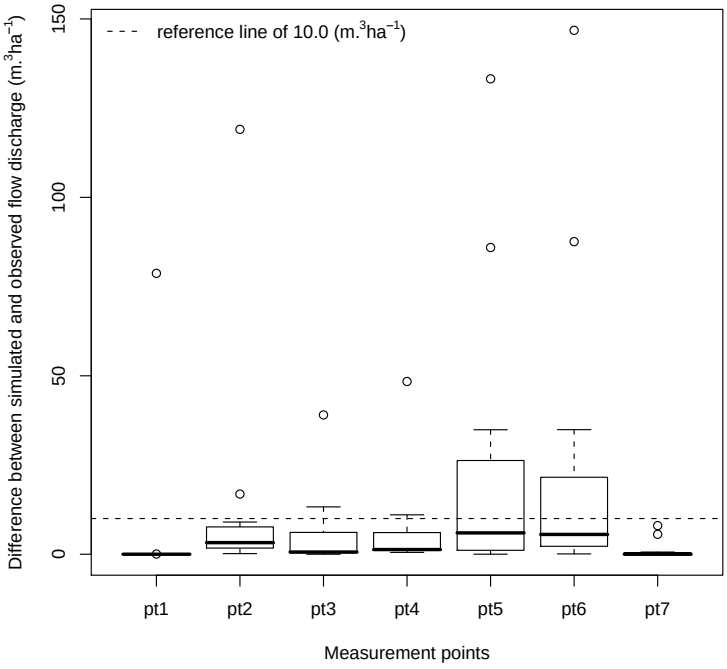

Figure 8.6: analysis hydro

have shown that exfiltrations may represent up to 100% of total discharge at the outlet catchment (Chahinian, 2004) under certain circumstances. In this study, we only take into account runoff production by hortonian processes and ignore return flow processes from the subsurface. The worth calibration results were found for the middle autumn event (2005-11-12), where water table is normally high compared to the other seasons.

All scales considered, table 8.5 shows that total sediment discharge has been simulated within an average difference of 216 $kg.ha^{-1}$ (0.2 $ton.ha^{-1}$). The maximum value of the difference between observed and simulated sediment discharge is 4597.08 $kg.ha^{-1}$, again obtained at point 6 (sub-catchment scale) and for the biggest rainfall event (2005-11-12). The minimum value of the difference is 0.00 $kg.ha^{-1}$ often found at point 1 and 7 (agricultural field and outlet catchment scale) because objective function is calculated for these points in the calibration procedure. Figure 8.7 shows a scatter diagram for observed and simulated total sediment discharge using all measurement points and the seven rainfall events.

For total sediment discharge the R^2 value is 0.74 with 95% confidence. Some data

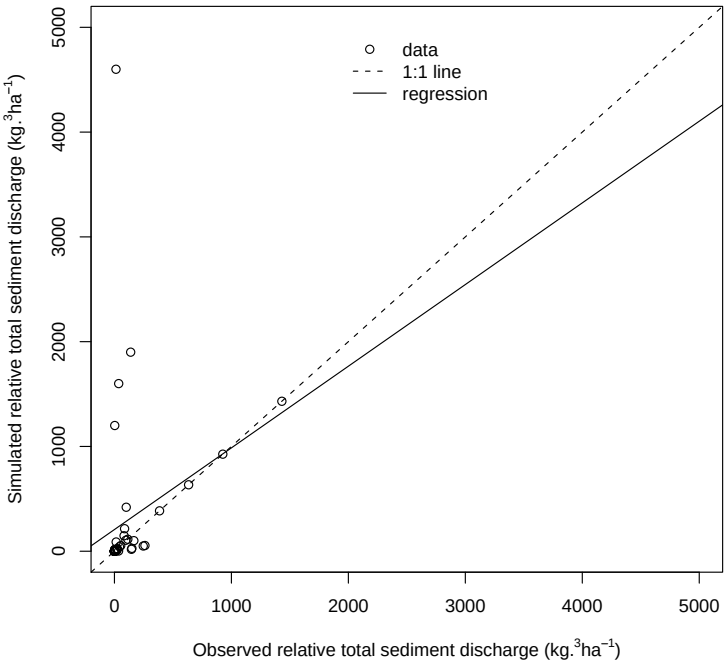

Figure 8.7: erosion results

dispersion is observed in figure 8.7, related to bad simulation points. Data are grouped between 0 and 150 $kg.ha^{-1}$, explained by the weak erosivity of recorded rainfall events during the 2005-2007 period. Figure 8.8 shows a boxplot for the difference between simulated and observed total sediment discharge.

Figure 8.8 shows the difference between simulated and observed total sediment discharge for calibration rainfall events, except event 6. The biggest differences between simulated and observed values are found at points 4, 5 and 6. They may be explained by the fact that we did not use spatially-distributed rain values, for simplicity and in absence of clear decision rules to do so. Meanwhile, differences of about 20-30% in rainfall amount have been recorded between the five rain gauges distributed over the catchment. Beside this, the exfiltration phenomenon may also affect sediment discharge values.

For validation rainfall events table 8.5 shows that total sediment discharge has been simulated within an average difference of 766.46 $kg.ha^{-1}$, all scales considered. The maximum value of the difference between observed and simulated sediment discharge

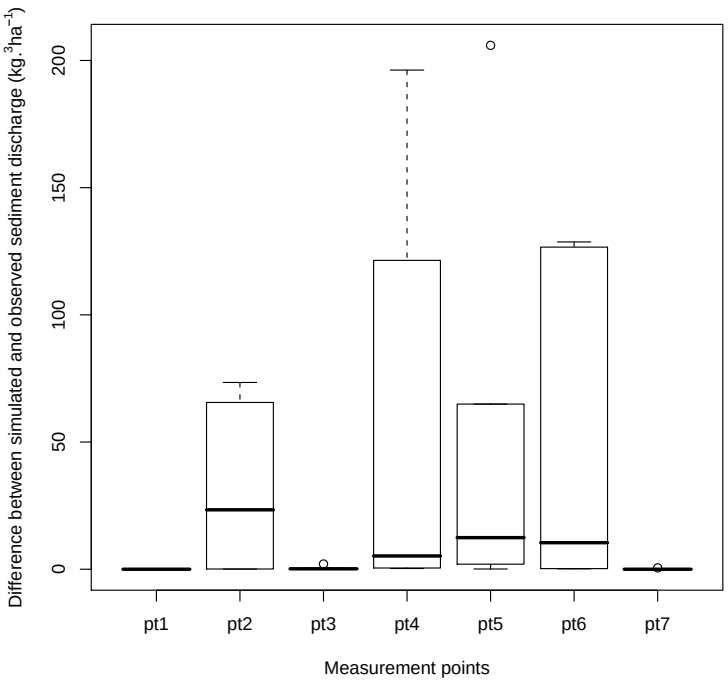

Figure 8.8: analysis erosion

is 6793.84 $kg.ha^{-1}$, at the point 6 (sub-catchment scale) for the event 2006-10-11. The minimum value of the difference is 0.00 $kg.ha^{-1}$ often found at points 1, 3 and 7 (agricultural field, sub-catchment and outlet catchment scale). Figure 8.9 shows the difference between simulated and observed total sediment discharge for validation rainfall events. In figure 8.9 all median values of measurement points are inferior of 500 $kg.ha^{-1}$ (0.5 $ton.ha^{-1}$).

The figure 8.10 shows the boxplot of the difference between simulated and observed sediment discharge without the 2006-10-11 rainfall event. In fact, the 2006-10-11 rainfall event is an average rainfall event with a very low sediment discharge in comparison with other average rainfall events. Table 8.1 indicates for this event the highest I_{max} (123.6 $mm.h^{-1}$), which is approximately 4 times the average I_{max} when considering all rainfall events.

Validation results have shown that the model satisfyingly simulates total sediment discharge and total flow discharge at all measurement points over the Roujan catchment, except for the 2006-10-11 rainfall event. The average difference between simulated and

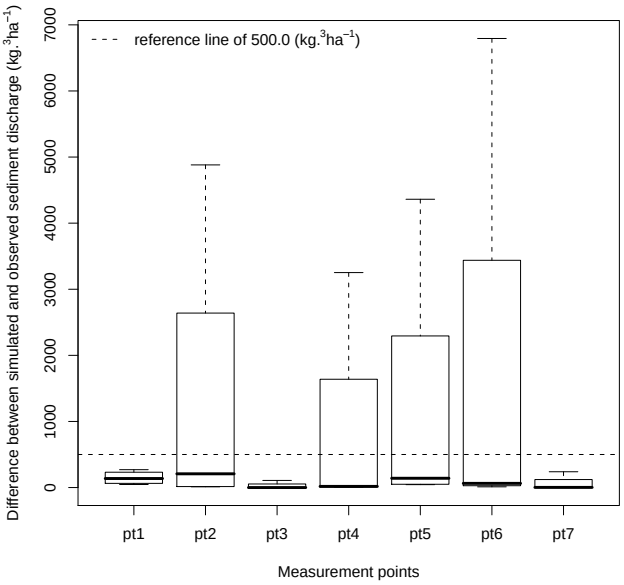

Figure 8.9: results validation erosion

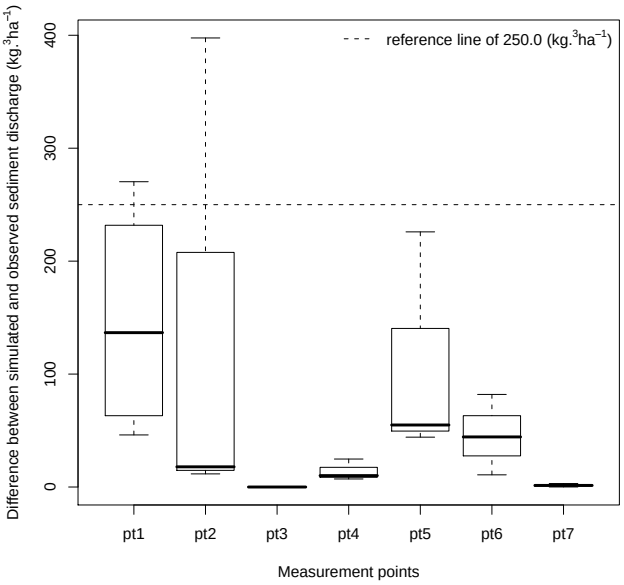

Figure 8.10: results validation erosion without event 9

observed total sediment discharge for 2006-10-11 rainfall event is 2859.3 $kg.ha^{-1}$, *i.e.* ten times the acceptable limit. We have noted that discrepancies between observed and simulated values are generally higher at measurement points associated with sub-catchment scales, where the hydrological error is somehow transmitted into erosion modelling.

8.4 Discussion and Conclusion

Model validation not only includes comparisons between observed and simulated data. During calibration and validation procedures the coherence of the underlying mathematical model is also questioned in a interactive and dynamic process. At this stage, it is checked if assumed model description of the reality is acceptable and if the model adequately represents the essential features and behaviour of the real system (De Roo and Jetten, 1999). The existence of distributed data about flow and sediment discharge at the Roujan catchment was crucial to the multi-scale calibration and validation procedures. Takken et al. (1999) suggested that validations of models using outlet data alone were not reliable because the behaviour of spatially-distributed models could only be understood when evaluated using spatially-distributed data. Distributed models are strongly prone to equifinality (Brazier et al., 2000). However, the calibration procedure followed in this study was intended to reduce this risk. Expert knowledge in linking physical parameters to land uses was associated to an automatic calibration procedure using the PEST software. Acceptable results were obtained in terms of parameter values, identification of their physical meaning and coherence. However, some limitations have been identified too, and could be remedied for in more detailed studies involving (i) spatially-distributed rainfall on the catchment, (ii) a description of groundwater exfiltration and (iii) spatially-distributed properties of the ditches over the catchment. Nevertheless, a richer parameterisation would reactivate the risk of equifinality unless precise informations are available. A large difference between observed and simulated total sediment discharge values is observed for two out of the eleven rainfall events. In fact, both 2005-11-12 (6) and 2006-10-11 (9) rainfall events can be considered out-group from PCA analysis figure 8.3. The particularity of 2005-11-12 (6) is the duration and the total amount of rain. The 2005-11-12 rainfall event has a duration of 30 h with a relatively low mean intensity of 3.05 $mm.h^{-1}$, but a short high intensity period is observed with a 5 minutes maximum intensity of 38 $mm.h^{-1}$. The model apparently has a problem to reproduce total sediment discharge for this rainfall event conditions. For this rainfall event the model over predict total sediment discharge for all catchment

measurement points, except for plot scale. This result could be an overestimation of interrill detachment rate simulated by the model, for the period with low rainfall intensity. The consequences of interrill detachment overestimation may be less visible for shorter rainfall events. But in the case of a large rainfall events the effects may be more perceptible, as well as 2005-11-12 rainfall event. We also may not exclude that for complex rainfall events, as well as 2005-11-12 the measurement error may be elevate.

Validation results have shown that the distributed water erosion model (MHYDAS-Erosion) seems to be able to reproduce total sediment discharge and total flow discharge in a spatially-distributed way. Except for one rainfall event (2006-10-11 (9)). It can be explained because the 2006-10-11 event is also an out-group event from PCA analysis (figure 8.3). An other explanation is for high intensity rainfall events (as well as 2006-10-11), the transport from sediment sources to the outlet in the model, may be faster compared to the real world. In fact, more studies may be done with these kind of rainfall events to understand model behaviour. However, hydrological and erosive phenomena were simulated with acceptable precision at the three intricate scales accounting for the catchment, sub-catchment and plot scales. It is important to note that calibration and validation may respect the principle of the unity of place (de Marsily, 1994). Thus, the application of this model to another catchment would certainly need specific calibration.

Chapter 9

Conclusion Générale, Réflexions et Perspectives

9.1 Introduction

L'érosion hydrique résulte de l'interaction complexe d'une multitude de processus relatifs au détachement et au transport des particules de sol sous l'action mécanique de l'eau. Étant donnée son importance sur les plans socio-économique et environnemental, l'érosion a été étudiée ces derniers années par différentes disciplines qui incluent : la géomorphologie, l'agronomie, l'hydrologie, l'hydraulique et la mécanique des fluides. Chaque domaine a abordé les processus d'érosion selon sa propre conception de la réalité, son échelle et ses outils d'analyse. Il en a résulté une connaissance plus riche et diversifiée de ces processus. Les nombreuses données expérimentales de terrain et de laboratoire ont amélioré la compréhension et la distinction des processus qui composent l'érosion hydrique. Cela a servi non seulement de base au développement des modèles d'érosion, mais aussi à la paramétrisation des équations qui composent les modèles. Cependant, les modèles d'érosion hydrique à l'échelle de petits bassins versants ne sont pas encore suffisamment performants pour reproduire de manière satisfaisante la dynamique spatiale et temporelle de processus érosifs.

Des nombreux travaux d'évaluation de modèles d'érosion ont été conduits et leurs conclusions ont été publiées à la suite des ateliers organisés par le réseau érosion du programme GCTE (Global Change Terrestrial Ecosystem) à Oxford (Boardman and Favis-Mortlock, 1998; Favis-Mortlock, 1998; Nearing and Nicks, 1998) et Utrecht (Folly et al., 1999; Jetten et al., 2003, 1999; Takken et al., 1999). Nous en rappelons ici les principales conclusions :

- La calibration est toujours indispensable pour les modèles actuels d'érosion;
- Le ruissellement est toujours mieux simulé que la perte en sol;
- Les résultats de ruissellement et d'érosion sont généralement mieux simulés à long-terme qu'à l'échelle événementielle;
- L'évaluation des modèles a plutôt été focalisée sur des modèles de simulation continue que sur les modèles événementiels;
- La familiarité de l'utilisateur avec le modèle utilisé se révèle un facteur important à prendre en compte pour la performance des modèles, mais difficile à quantifier;
- Il y a beaucoup de facteurs et de processus qui sont mal décrits et pris en compte dans les modèles. Par exemple, le processus de formation de croûte superficielle ou l'influence des pierres à la surface du sol;
- Beaucoup de tests ont été basés sur l'échelle parcellaire, mais il est clair que la variabilité spatiale est un facteur important à l'échelle du bassin versant;
- La plupart des modèles d'érosion supposent que le ruissellement est généré seulement par le processus Hortonien, tandis que dans la réalité une grande part de l'écoulement superficiel peut provenir de pluies de faible intensité sur sol saturé;
- Les modèles événementiels sont très sensibles aux conditions initiales, en général très difficiles à déterminer;
- Les paramètres d'entrée des modèles ont une variabilité spatiale et temporelle qui vient s'ajouter à l'incertitude intrinsèque de leur mesure;
- Le fonctionnement d'un bassin versant peut être différent selon l'intensité des événements pluviométriques;
- Certains facteurs du modèle sont considérés comme constants pendant la durée de l'événement, alors qu'ils ont un comportement dynamique.

Toutes ces conclusions montrent que la modélisation de l'érosion hydrique, quelque soit l'échelle d'espace et de temps considéré, est encore en phase de développement. Beaucoup d'études semblent nécessaires pour résoudre les problèmes évoqués ci-dessus. Cette thèse avait pour objectif de contribuer à une réflexion sur la modélisation de l'érosion hydrique à l'échelle des petits bassins versants agricoles et sur les limites

actuelles identifiées. Un modèle d'érosion a été développé à partir de cette réflexion en cherchant à résoudre certains de ces problèmes.

D'autres questions scientifiques ont émergé pendant et à la suite du développement du modèle d'érosion. Des questions qui concernent la paramétrisation, l'analyse de sensibilité du modèle par rapport à l'incertitude des paramètres d'entrée et aussi sur l'utilisation des modèles d'une manière générale. Dans les sections suivantes nous essayons de conclure d'une manière synthétique sur chaque partie de la thèse, en finissant par une réflexion sur la modélisation en général et la présentation de perspectives pour de futurs travaux.

9.2 Conclusion sur la conceptualisation et le développement de la modélisation de l'érosion

9.2.1 L'érodibilité interrill (érosion diffuse)

Le premier chapitre est une analyse bibliographique sur les paramètres d'érodibilité utilisés dans les modèles d'érosion. Il fait aussi allusion à la sensibilité des modèles à base physique au paramètre d'érosion diffuse. Nous avons choisi d'approfondir cette question parce que ce processus est souvent négligé, probablement sous-estimé dans l'étude de l'érosion du fait du caractère insidieux et peu spectaculaire de l'érosion diffuse en comparaison de l'érosion ravinaire largement étudiée (Knapen et al., 2007). Cette analyse bibliographique nous amène à aux conclusions suivantes :

- Il y a un grand nombre de données de référence pour les valeurs d'érodibilité "globale" du sol dans la littérature, en particulier issues des méthodes standards de type "parcelles de Wischmeier", qui pour cette raison est la méthode la plus utilisée;

- Les méthodes de mesure de l'érodibilité des sols sur des parcelles standardisées sont fortement influencées par les processus hydrologiques. Les sols sableux ont généralement une haute capacité d'infiltration et une faible transportabilité, ce qui résulte en un faible ruissellement donc une faible érosion;

- L'utilisation d'un seul paramètre d'érodibilité pour décrire différents processus d'érosion tel que les processus d'érosion linéaire et diffuse est fortement déconseillée pour des modèles à base physique qui font une distinction explicite entre les processus;

- Quelque soit la méthode utilisée pour déterminer l'érodibilité du sol, l'utilisation de méthodes de mesures directes est préférable, lorsque cela est possible, à l'utilisation de fonction de pédotransfert;

- Les méthodes de mesure de la stabilité structurale du sol peuvent être bien adaptées pour la paramétrisation de l'érodibilité diffuse dans des modèles à base physique, parce que, en plus de la mesure de résistance du sol à un agent érosif, elle donne des informations sur la transportabilité des particules.

- L'érosion diffuse ne dépend cependant pas uniquement de l'érodibilité diffuse, mais aussi de l'état de surface du sol, qui est en particulier déterminé par les pratiques culturales, et qui influence le transfert des sédiments détachés par la pluie.

- La sensibilité des modèles d'érosion au paramètre d'érodibilité diffuse est fréquemment considérée comme faible à moyenne dans la littérature, en comparaison avec les paramètres hydrologiques telle que la conductivité hydraulique à saturation ou le potentiel d'entrée d'air du sol. Ces résultats peuvent être liés à la construction des tests de sensibilité qui utilisent le plus souvent des pluies fortes et cette sensibilité est en réalité probablement plus importante dans le cas de pluies d'intensité faible ou modérée.

9.2.2 Connectivité sedimentologique

Le deuxième chapitre est une analyse bibliographique sur l'impact des aménagements sur la connectivité sédimentologique des bassins versants agricoles et aussi sur la façon dont les modèles d'érosion prennent ces aménagements en compte dans la modélisation. Les principaux résultats de cette analyse bibliographique sont les suivants :

- Dans les bassins versants agricoles, les pratiques et aménagements peuvent affecter les réponses hydrologiques et sédimentologiques en modifiant la connectivité du bassin versant. Walling et al. (1999) et Morgan (2005) ont montré que la disparition de la végétation naturelle au profit des cultures agricoles peut augmenter les taux d'érosion d'un ordre de grandeur. De nombreux résultats indiquent des effets similaires lorque les bordures végétales des parcelles cultivées (haies, talus...) sont supprimés (Cammeraat and Imeson, 1999; Fitzjohn et al., 1998).

- Les expériences avec des filtres végétaux ont démontré que la capacité de filtrage d'une bande enherbée, par exemple, ne peut pas être complètement connue à

partir de ses caractéristiques physiques (pente, largueur, densité de végétation). La capacité de filtrage est aussi dépendante de la condition de flux à travers le filtre;

- Plusieurs études théoriques et expérimentales à l'échelle locale ont confirmé la complexité de l'interaction entre le flux d'eau et la végétation;

- A l'échelle du bassin versant, la distribution spatiale des filtres végétaux devient un facteur très important pour déterminer la connectivité sédimentologique des bassins versants agricoles. L'organisation spatiale des bandes enherbées peut fortement influencer l'efficacité globale du filtrage des sédiments dans le bassin;

- La plupart des modèles utilisent le P-facteur de l'équation universelle de perte en sol (USLE) pour prendre en compte l'impact des aménagements sur le transport de sédiment;

- Il manque une approche intermédiaire entre les descriptions très détaillées des aménagements, qui ne prennent pas en considération leur distribution spatiale, et les modèles de type "boîte noire" basés sur le P-factor.

9.2.3 Développement de la modélisation

L'analyse bibliographique a indiqué que les modèles d'érosion hydrique doivent être basés sur un modèle hydrologique robuste. Pour tenir compte de la dynamique spatiale et temporelle, les modèles distribués à base physique sont les plus adaptés, et pour bien représenter les processus d'érosion il est nécessaire de séparer les mécanismes de détachement et de transport de particule (par exemple l'érosion concentrée et diffuse).

En analysant les conclusions des études sur l'évaluation des modèles d'érosion et les conclusions de nos deux analyses bibliographiques, nous avons proposé dans cette thèse un modèle d'érosion hydrique distribué et à base physique à l'échelle des petits bassins versants cultivés. Nous avons en particulier essayé de lever deux points de blocage constamment cités dans les études d'évaluation de modèle. Le premier concerne la paramétrisation de l'érosion diffuse. Nous avons choisi d'utiliser la mesure de MWD (*Mean Weight Diameter*) comme paramètre d'érodibilité diffuse en utilisent une fonction proposé par Yan et al. (2008) et d'introduire un coefficient d'efficacité du transfert dans la zone d'écoulement diffus (CETI). Cette approche nous a permis de relier les paramètres d'érodibilité aux caractéristiques du sol, mais aussi à l'occupation du sol qui influence fortement l'érosion diffuse, facilitant ainsi la paramétrisation du modèle. Le

second concerne la modélisation de l'impact des aménagements sur la connectivité sédimentologique du bassin versant. En milieux agricoles, la connectivité sédimentologique est en effet contrôlée par l'existence des éléments du paysage installés par l'homme afin de maîtriser le transfert d'eau et de sédiments d'une partie du bassin à l'autre.

Dans le chapitre 4, le modèle développé au cours de cette thèse est présenté. MHYDAS-Erosion est un modèle d'érosion hydrique distribué à base physique qui est capable de prendre en compte l'influence des aménagements sur la connectivité sédimentologique des bassins versants cultivés. L'hydrologie utilisé pour calculer les processus d'érosion est celle du modèle hydrologique MHYDAS (Moussa et al., 2002). Dans MHYDAS l'infiltration est calculée à l'aide du modèle de Morel-Seytoux et le ruissellement comme le transfert d'eau dans le réseau de fossé est calculé en utilisant l'onde diffusante résolue par la méthode d'Hayami. L'érosion est calculée à partir de l'équation de conservation de la masse de sédiment en suspension (Bennett, 1974).

Les comparaisons entre les hydrogrammes et turbidigrammes observés et simulés ont démontré que le modèle développé reproduit raisonnablement la dynamique spatiale et temporelle du débit et du flux de sédiments à différentes échelles du bassin versant. Avec le développement du module de connectivité sédimentologique il a été possible de prendre en compte l'impact des aménagements sur le transport de sédiments dans le bassin versant. Les résultats obtenus avec l'utilisation du module de connectivité sédimentologique ont été plus proches des valeurs de flux de sédiment observé que ceux obtenus sans utiliser ce module.

Une autre conclusion que nous pouvons retirer est relative au couplage de la modélisation de l'érosion avec l'hydrologie : en partant d'une base hydrologique solide, telle que celle du modèle hydrologique MHYDAS (Moussa et al., 2002), nous pouvons réduire certains des problèmes de modélisation qui sont normalement liés à l'hydrologie, par exemple la paramétrisation, la représentation des processus, l'instabilité des solutions numériques, etc. Néanmoins, nous restons en partie contraints par les choix conceptuels qui ont été fait pour le développement du modèle hydrologique. L'influence de la concentration de sédiment sur la viscosité de l'eau, lorsqu'elle dépasse le limite de 100 $g.L^{-1}$, n'est par exemple pas prise en compte, l'utilisation de l'équation de Manning afin d'estimer l'épaisseur de la lame d'eau et sa vitesse en zone d'écoulement diffus reste également discutable.

Avec le développement du modèle MHYDAS-Erosion, il est clair que nous n'avons pas réussi à résoudre l'ensemble des problèmes liés à la modélisation, loin de là. Par exemple, l'hydrologie n'est pas calculée spécifiquement pour les processus d'érosion, et les interactions entre érosion et hydrologie ne sont pas prises en compte. Par ailleurs, le

ruissellement est toujours généré uniquement par des processus hortonien. Une autre difficulté concerne le nombre de rigoles potentielles sur les parcelles agricoles, qui doit être défini à l'avance. Il reste encore à intégrer la dynamique intra-événementielle d'évolution des états de surface et son influence sur l'infiltrabilité et l'érodibilité. Un autre facteur limitant est l'utilisation de l'équation de Bennett, pour le transport de sédiments, qui décrit uniquement les transports en suspension en ignorant les transports par charriage. Tous ces aspects devraient faire l'objet de recherches complémentaires. L'un des principaux points positifs par rapport à notre objectif initial, est que MHYDAS-Erosion peut donner des informations distribuées sur l'érosion et le transport de sédiment et qu'il peut tenir compte de l'impact des aménagements sur la connectivité sédimentologique du bassin versant.

9.3 Conclusion sur l'analyse de sensibilité et l'analyse exploratoire du modèle

9.3.1 L'analyse de sensibilité

9.3.1.1 Cadre pour l'analyse de sensibilité, développement et application

Dans le chapitre 5, nous avons développé un cadre théorique pour l'analyse de sensibilité des modèles distribués appliqué à un bassin virtuel. Ce cadre théorique s'appuie sur un jeu réduit de configurations paramétriques pour s'affranchir au maximum de l'influence des paramètres hydrologiques et faciliter la comparaison entre les différents modèles d'érosion. Ce cadre théorique introduit les notions de pente équivalente et d'érodibilité équivalente comme paramètres constitutifs communs à tous les modèles.

L'application du formalisme d'analyse de sensibilité présenté dans le chapitre 5 à quatre modèles d'érosion à paramètres distribués a permis de mettre en évidence l'importance dominante des paramètres décrivant l'érodibilité par rapport à ceux qui décrivent la pente. Ce résultat reste vrai, que l'on considère des paramètres spatialement distribués, ou que leurs valeurs soient homogènes, mais des nuances apparaissent avec les variations de conditions hydrologiques. Ceci apporte la démonstration de l'intérêt d'une analyse séparée des parties "hydrologie" et "érosion" des modèles.

L'analyse de sensibilité a ciblé les résultats simulés de perte en terre à l'exutoire du bassin virtuel. Nous avons utilisé les *Screening methods* pour explorer l'espace des paramètres équivalents. La sensibilité des modèles a été calculé d'une manière déterministe et multi-locale en utilisant les dérivées directionnelles de Gâteaux.

Les situations les plus sensibles sont celles où les paramètres de pente et d'érodibilité

sont testés en même temps. Pour les modèles répondant bien à la distribution des paramètres (MHYDAS et PESERA), le fait de distribuer à la fois la pente et l'érodibilité conduit à des effets multiplicatifs. Dans la majorité des cas, les résultats de perte en sol obtenus dans les configurations homogènes ou spatialement distribuées restent du même ordre de grandeur.

9.3.1.2 Sensibilité de MHYDAS-Erosion à la position amont-aval des aménagements

Dans le chapitre 7, nous avons fait une analyse exploratoire du modèle MHYDAS-Erosion particulière aux effets des aménagements sur le transport de sédiments. Cette analyse a consisté à faire varier l'emplacement des aménagements au sein du bassin versant en regardant les effets sur l'érosion simulée en 6 différents points du bassin versant de Roujan. Afin de simuler les emplacements des aménagements au sein de Roujan, nous avons développé un modèle stochastique qui génère des emplacements en fonction de trois paramètres (la densité des aménagements au sein du bassin (r), le gradient de position amont-aval (p) et un paramètre de lissage (bw)).

Les résultats de cette analyse ont démontré que la densité des aménagements au sein du bassin est le paramètre le plus influent sur la perte en terre simulée par le modèle dans les 6 points du bassin. Cependant, nous avons noté à partir des surfaces de réponses, que le gradient de position amont-aval peut aussi influencer les résultats simulés de perte en terre. Cela veux dire que le modèle développé est capable de répondre au changement de position des aménagement au sein du bassin versant.

Dans ce chapitre nous avons également analysé la sensibilité du modèle d'érosion au trois paramètre (la densité des aménagements au sein du bassin (r), le gradient de position amont-aval (p) et un paramètre de lisage (bw)), en utilisant la méthode de Sobol. Les résultats de l'analyse de sensibilité ont confirmé les constatations faites précédemment. Le modèle est plus sensible au paramètre de densité des aménagements, en effet, 73% de la variance de la perte en terre simulée par le modèle est due à ce paramètre.

9.3.2 Calage et validation

La validation d'un modèle n'est pas seulement la comparaison entre les résultats simulés et observés. Dans les procédures de calage et de validation nous testons la cohérence du modèle mathématique et de la structure logique du code informatique. Dans cette étape, nous vérifions si les hypothèses qui ont été faites à partir de l'observation du monde

réel et inclus dans le modèle sont acceptables ou non. Nous vérifions aussi si le modèle en question arrive à bien représenter les principaux processus et le comportement du système réel.

La disponibilité des mesures de sédiments en suspension en différents points du bassin versant de Roujan a été cruciale pour la procédure de calage et de validation multi-échelle. En fait, comme cela a été suggéré par Takken et al. (1999), la validation des modèles distribués en observant seulement les mesures à l'exutoire n'est pas recommandée. Car au delà de la paramétrisation distribuée du modèle , il est encore plus important que le modèle puisse fournir des résultats distribués sur l'érosion et les pertes en terre, en particulier dans l'optique d'une utilisation pour simuler des scénarios d'aménagements anti-érosifs. Il est en effet impossible d'assurer que le modèle donne des résultats acceptables seulement à partir d'une confrontation des résultats à l'exutoire.

Les modèles distribués ont notamment la propension à l'équifinalité (Brazier et al., 2000). Nous avons cependant cherché à réduire le risque d'équifinalité en utilisant des connaissances expertes dans la relation entre les paramètres physiques et l'occupation du sol avec une procédure automatique qui utilise le logiciel PEST. A travers ce couplage entre connaissance et procédure automatique, nous avons réussi à produire des résultats acceptables pour différentes échelles du bassin versant de Roujan.

9.4 Réflexions

La modélisation distribuée à base physique de l'érosion hydrique est en elle même un sujet très complexe, qui demande au modélisateur des connaissances en physique du sol, en mécanique de fluides, en géomatique, en calcul numérique, en langage informatique, en logique, etc. Le problème est que la plupart du temps les résultats de la modélisation sont différents des valeurs observées dans la nature, particulièrement pour des événements extrêmes. Alors, il est naturel de se poser des questions comme: Pourquoi fait-on des modèles ? Ou encore, jusqu'où peut-on aller avec la modélisation ?

Dans la plupart des cas, le développement des modèles est fait à partir d'un objectif précis comme cela a été le cas dans cette thèse. Cela peut être la compréhension d'un processus spécifique, l'aide à la décision pour des aménagements ou la prévision des processus d'érosion. L'étape de définition de l'objectif est particulièrement importante dans le développement d'une modélisation car c'est dans cette étape que nous définissons ce que nous espérons de la modélisation, le domaine d'application, les processus à prendre en compte, la précision des résultats, etc. Ainsi l'objectif spécifique recherché peut être atteint même si les performances globales du modèle ne sont pas encore totalement satisfaisantes. Dans notre cas, ce travail de réflexion, de recherche et de développement d'un modèle nous aura permis d'aborder à la fois les aspects conceptuels et pratiques de la modélisation de l'érosion.

Il est clair que notre approche de modélisation, a comme bien d'autres des limites fondamentales en ce qui concerne la capacité de prédiction de l'érosion. Ces limites peuvent venir des différentes étapes de la modélisation : développement du code informatique, paramétrisation, application, etc.

Dans l'étape de développement du modèle, la phase d'exploration nous a amené à nous poser des questions concernant les procédures d'analyse de sensibilité des modèles d'érosion. Dans la plupart des cas, les variables hydrologiques, comme la conductivité hydraulique à saturation du sol, ont été considérées comme les plus sensibles. Ce résultat semble logique car s'il n'y a pas de ruissellement, l'érosion hydrique ne peut pas exister. Nous pensons cependant que les procédures d'analyse de sensibilité qui ont été pratiquées au cours des années pour les modèles d'érosion hydrique, ont sous-évalué la sensibilité des modèles aux paramètres d'érosion. Ceci en particulier du fait que les tests de sensibilité ont le plus souvent été effectués pour des conditions de pluies et de ruissellement fortes, qui favorisent certains processus érosifs.

L'étape de calage et de paramétrisation des modèles distribués nous a également conduit à certaines réflexions. Il est clair que, en se basant seulement sur les mesures

de MES à l'exutoire d'un bassin versant, un modèle distribué quelconque peut donner une infinité de solution pour la même mesure. Cela s'appelle l'équifinalité. En fait tout les types de modèles qui ont plus de un paramètre peuvent souffrir d'équifinalité. Imaginons un modèle très simple, par exemple $x+y = 10$. Il existe une infinité de valeurs des couple (x, y) permettant d'arriver au résultat espéré (10). La procédure classique de calage de modèle consiste à générer des valeurs de couples (x, y) et à garder celles qui donnent les plus petites différences entre résultat espéré et simulé. Le problème est que les valeurs produites de (x, y) ne sont pas toutes physiquement possibles, certains couples (x, y) peuvent être hors réalité. C'est là que la connaissance des experts peut nous aider. Pas seulement en donnant des limites pour les couples (x, y), mais aussi en essayant de lier les valeurs des paramètres physiques à des conditions observés sur le terrain. Le couplage des procédures de calage automatique avec la connaissance des experts peut être un bon moyen de réduire le problème d'équifinalité des modèles existants.

Même si les performances globales des modèles ne sont pas encore totalement satisfaisantes, la modélisation de l'érosion reste une étape nécessaire pour faire un état de nos connaissances et identifier les points de blocage à lever. Par ailleurs, l'utilisation de modèles est l'unique manière d'évaluer le risque d'érosion dans des régions où nous n'avons pas de mesure. Les modèles sont également les seuls outils permettant de tester des scénarios d'aménagement et ainsi aider à une meilleure gestion des bassins versants agricoles.

9.5 Perspectives

L'expérience acquise dans ce travail de thèse ainsi que les limites de notre approche que nous venons de discuter nous conduisent à proposer les pistes de recherche suivantes :

- Le modèle développé dans cette thèse nécessite d'être testé et évalué sur d'autres contextes, sur le même site avec des conditions de pluie et d'occupation du sol différentes, mais également sur d'autres bassins versants;

- Il serait nécessaire de développer des fonctions de formation des croûtes superficielles, afin de prendre en compte le changement d'infiltrabilité du sol et de l'érodibilité au cours de l'événement;

- Le manque de connaissance pour définir de façon a priori le nombre et la forme des rigoles reste un point faible sur lequel on doit travailler;

- Les interactions existant parfois entre hydrologie et érosion nécessiteraient que l'on arrive à coupler ces deux phénomènes. Cela concerne par exemple le choix des lois d'écoulement lorsque l'eau est très chargée en sédiments
- La fonction de connectivité, limitée au transfert de sédiments, nécessiterait d'être étendue au transfert d'eau, en recalculant les variables hydrologiques au même temps que les variables d'érosion, afin de pouvoir mieux représenter les processus de "filtrage" de sédiments;
- Il serait nécessaire d'introduire d'autres fonctions de connectivité, pour représenter d'autres types d'aménagements;
- On pourrait envisager de passer à une modélisation comprenant plusieurs classes de taille de particules, afin d'être plus réaliste sur la nature des sédiments érodés sur les sols cultivés;
- Il faudrait aussi envisager de prendre en compte d'autres types de transport de sédiments, comme le transport d'éléments grossiers par charriage, en plus du transport de sédiments en suspension;

Touts ces propositions sont nécessaires pour tenter d'améliorer la performance de modèle d'érosion du type de celui développé dans le cadre de cette thèse. Cependant ces implémentation ne sont pas une garantie absolue d'amélioration des performances. Le grand défi sera alors de faire évoluer la modélisation de l'érosion en évitant de multiplier les paramètres implémentés, et ainsi conserver un modèle suffisamment simple pour être utilisable à l'échelle du bassin versant.

References

Abu-Zreig, M., Rudra, R. P., Whiteley, H. R., Lalonde, M. N., Kaushik, N. K., 2003. Phosphorus removal in vegetated filter strips. J Environ Qual 32 (2), 613–619. 45

Abujamin, S., Abdurachman, A., Suwardjo, M., 1984. Contour grass strips as low cost conservation practice. In: Soil Erosion and Its Countermeasures, Chiang Mai, Thailand. 48

Ambroise, B., 1999. Genèse des débits dans les petits bassins versants ruraux en milieu tempéré: 2-modélisation systémique et dynamique. Revue des Sciences de l'Eau 12, 123–153. 76

Amezketa, E., 1999. Soil aggregate stability: a review. J. Sus. Agri. 14, 83–151. 25, 28

Amezketa, E., Singer, M., Le Bissonnais, Y., 1996. Testing a new procedure for measuring wet aggregate stability. Soil Science Society of America Journal 60, 888–894. 25

Appelboom, T. W., Chescheir, G. M., Skaggs, R. W., Hesterberg, D. L., 2002. Management practices for sediment reduction from forest roads in the coastal plains. Transactions Of The Asae 45 (2), 337–344. 45

Arnold, J. G., Williams, J. R., 1995. SWAT - Soil and Water Assessment Tool. Draft Users Manual, l. Temple, TX. 17, 93

Arnold, J. G., Williams, J. R., Srinivasan, R., King, K. W., 1996. The soil and water assessment tool (SWAT) user's manual. Tech. rep., Temple, TX. 57, 60

Arora, K., Mickelson, S. K., Baker, J. L., Tierney, D. P., Peters, C. J., 1996. Herbicide retention by vegetative buffer strips from runoff under natural rainfall. Transactions Of The Asae 39 (6), 2155–2162. 44

Ascough, J. C., Baffaut, C., Nearing, M. A., Liu, B. Y., 1997. The wepp watershed model: I. hydrology and erosion. Transactions of the ASAE 40, 921–933. 17, 60, 92

Babalola, O., Oshunsanya, S. O., Are, K., 2007. Effects of vetiver grass (vetiveria nigritana) strips, vetiver grass mulch and an organomineral fertilizer on soil, water and nutrient losses and maize (zea mays, l) yields. Soil & Tillage Research 96, 6–18. 45

Band, L. E., 1986. Topographic partition of watersheds with digital elevation models. Water Resour. Res. 22, 15–24. 42

Baptist, M. J., Babovic, V., Uthurburu, J. R., Keijzer, M., Uittenbogaard, R. E., Mynett, A., Verwey, A., 2007. On inducing equations for vegetation resistance. Journal of Hydraulic Research 45, 435–450. 48, 50

Barfield, B. J., Blevins, R. L., Fogle, A. W., Madison, C. E., Inamdar, S., Carey, D. I., Evangelou, V. P., 1998. Water quality impacts of natural filter strips in karst areas. Transactions Of The Asae 41 (2), 371–381. 44

Barfield, B. J., Tollner, E. W., Hayes, J. C., 1979. Filtration of sediment by simulated vegetation i. steady-state flow with homogenous sediment. Trans. ASAE 22 (3), 540–548. 53, 55

Barthés, B., Azontonde, A., Boli, B. Z., Prat, C., Roose, E., 2000. Field-scale run-off and erosion in relation to topsoil aggregate stability in three tropical regions (benin, cameroon, mexico). European Journal of Soil Science 51, 485–495. 25

Beasley, D. B., Huggins, L. F., Monke, E. J., 1980. Answers: a model for watershed planning. Trans Am Soc Agric Eng 23, 938–944. 2, 57

Behmardi, D., Nayeri, E. D., 2008. Introduction of Fréchet and Gâteaux derivative. App. Math. Sci. 2, 975–980. 134

Bennett, J. P., 1974. Concepts of mathematical modeling of sediment yield. Water Resources Research 10, 485–492. 99, 105, 222

Bennett, S. J., Pirim, T., Barkdoll, B. D., Apr. 2002. Using simulated emergent vegetation to alter stream flow direction within a straight experimental channel. Geomorphology 44 (1-2), 115–126. 52

Beuselinck, L., Govers, G., Hairsine, P. B., Sander, G. C., Breynaert, M., Feb. 2002. The influence of rainfall on sediment transport by overland flow over areas of net deposition. Journal of Hydrology 257 (1-4), 145–163. 60

Beven, K., Binley, A., 1992a. The future of distributed models: Model calibration and uncertainty prediction. Hydrological Processes 6, 279–289. 77

Beven, K., Kirkby, M., 1979. sa physically based, variable contributing area model of basin hydrology. Hydrological Science Bulletin 24(1), 196–201. 80

Beven, K. J., 1989. Changing ideas in hydrology – the case of physically based models. Journal of Hydrology 105, 157–172. 124, 196

Beven, K. J., 1993. Prophecy, reality and uncertainty in distributed hydrological modelling. Adv. Water Resour. 16, 41–51. 124

Beven, K. J., 2000. On the future of distributed modelling in hydrology. Hydrol. Process. 14, 3183–3184. 73

Beven, K. J., Binley, A. M., 1992b. The future of distributed models: model calibration and uncertainty prediction. Hydrol. Process. 6, 279–298. 126

Beven, K. J., Musy, A., Higy, C., 2001. L'unicité de lieu, d'action et de temps [Tribune libre]. Rev. Sci. Eau 14 (4), 525–533. 124

Blanco-Canqui, H., Gantzer, C. J., Anderson, S. H., Alberts, E. E., Thompson, A. L., 2004. Grass barrier and vegetative filter strip effectiveness in reducing runoff, sediment, nitrogen, and phosphorus loss. Soil Science Society Of America Journal 68 (5), 1670–1678. 45

Blöschl, G., 2001. Scaling in hydrology. Hydrol. Process. 15, 709–711. 124, 153

Blöschl, G., Sivapalan, M., 1995. Scale issues in hydrological modelling - a review. Hydrol. Process. 9, 251–290. 124, 153

Boardman, J., 1998. Modelling Soil Erosion by Water. Global Environmental Change. Springer-Verlag, Berlin Heidelberg„ Ch. Modelling soil erosion in real landscapes: a Western European perspective, pp. 17–29. 2

Boardman, J., 2006. Soil erosion science: Reflections on the limitations of current approaches. CATENA 68 (2-3), 73–86. 2, 3, 9, 113, 124, 178, 196

Boardman, J., Favis-Mortlock, D., 1998. Modelling Soil Erosion by Water. Springer-Verlag, Berlin Heidelberg, Ch. Modelling Soil Erosion by Water, pp. 3–5. 2, 9, 217

Boardman, J., Ligneau, L., De Roo, A., Vandaele, K., 1994. Flooding of property by runoff from agricultural land in northwestern europe. Geomorphology 10, 183–196. 1

Boiffin, J., Monnier, G., 1986. Assessment of soil surface sealing and crusting. Flanders Research Center for Soil Erosion and Soil Conservation. Ghent, Ch. Infiltration rate as affected by soil surface crusting caused by rainfall., pp. 210–217. 9

Bollinne, A., 1975. La mesure de l'intensité du splash sur sol limoneux. mise au point d'une tecnique de terrain et premiers. Pedologie 25, 199–210. 22

Borin, M., Vianello, M., Morari, F., Zanin, G., 2005. Effectiveness of buffer strips in removing pollutants in runoff from a cultivated field in north-east italy. Agric. Ecosyst. Environ. 105, 101–114. 43, 45

Borselli, L., Cassi, P., Torri, D., Nov. 2008. Prolegomena to sediment and flow connectivity in the landscape: A gis and field numerical assessment. CATENA 75 (3), 268–277. 64

Bracken, L. J., Croke, J., 2007. The concept of hydrological connectivity and its contribution to understanding runoff-dominated geomorphic systems. Hydrol. Proc. 21, 1749–1763. 39, 40, 63, 93

Brazier, R. E., Beven, K. J., Freer, J., Rowan, J. S., 2000. Equifinality and uncertainty in physically based soil erosion models: application of the glue methodology to wepp-the water erosion prediction project-for sites in the uk and usa. Earth Surface Processes and Landforms 25 (8), 825–845. 196, 204, 214, 225

Brunsden, D., 1993. Barriers to geomorphological change. (in: Landscape Sensitivity). Wiley, Chichester. 42

Bryan, R. B., May 1976. Considerations on soil erodibility indices and sheetwash. Catena 3 (1), 99–111. 15, 125

Bryan, R. B., 2000. Soil erodibility and processes of water erosion on hillslope. Geomorphology 1, 385–415. 2, 15, 16, 25, 29, 125

Cacuci, D. G., 1981. Sensitivity theory for non-linear systems. I. Non-linear functional analysis approach. Journal of Mathematical Physics 22, 2794–2802. 127, 152

Cacuci, D. G., 2003. Sensitivity and uncertainty analysis, Volume 1: Theory. Chapman & Hall. 127, 134, 152

Cacuci, D. G., D'Auria, F., 2006. State-of-the-art report on sensitivity and uncertainty analysis (SP4). Tech. rep., NURESIM- Platform for Nuclear Reactor Simulation - European Commission Community Research. 126

Cammeraat, L. H., Imeson, A. C., Sep. 1999. The evolution and significance of soil-vegetation patterns following land abandonment and fire in spain. CATENA 37 (1-2), 107–127. 56, 178, 220

Campana, T. R., 1999. Hydraulic resistance of submerged floodplain vegetation. Ph.D. thesis, IHE-Delft. 50

Campolongo, F., Braddock, R., 1999. Sensitivity analysis of the IMAGE Greenhouse model. Environ. Model. Software 14, 275–282. 126

Campolongo, F., Cariboni, J., Saltelli, A., 2007. An effective screening design for sensitivity analysis of large models. Environ. Model. & Software 22 (10), 1509–1518. 125

Castaings, W., Dartus, D., Le Dimet, F.-X., Saulnier, G.-M., 2007. Sensitivity analysis and parameter estimation for the distributed modeling of infiltration excess overland flow. Hydrol. Earth Syst. Sci. Discuss. 4, 363–405. 126

Cerdan, O., Le Bissonnais, Y., Couturier, A., Saby, N., 2002. Modelling interrill erosion in small cultivated catchments. Hydrological Processes 16, 3215–3226. 57, 123, 151, 153

Chahinian, N., 2004. Paramétrisation multi-critère et multi-échelle d'un modèle hydrologique spatialisé de crue en milieu agricole. Ph.D. thesis, UNIVERSITE DE MONTPELLIER II. 210

Chahinian, N., Moussa, R., Andrieux, P., Voltz, M., 2006a. Accounting for temporal variation in soil hydrological properties when simulating surface runoff on tilled plots. Journal of Hydrology 326, 135–15. 207, 209

Chahinian, N., Voltz, M., Moussa, R., Trotoux, G., 2006b. Assessing the impact of the hydraulic conductivity of a crusted soil on overland flow modelling at the field scale. Hydrological Processes 20, 1701–172. 207

Chan, C.-C., 1981. Evaluation of soil loss factors on cultivated slopelands of taiwan. Tech. rep., Food and Fertilizer Technology Center (FFTC). Taipei City,. 58, 59

Chaubey, I., Edwards, D. R., Daniel, T. C., Nicols, D., 1993. Effectiveness of vegetative filter strips in controlling losses of surface-applied poultry litter constituents. American Society of Agricultural Engineers No. 93-2011, 17 pp. 44

Cheviron, B., Gumiere, S. J., Le Bissonnais, Y., Raclot, D., Moussa, R., 2009a. A framework for sensitivity analysis of distributed physics based erosion models i. Water Resources Research in revision. 150, 207

Cheviron, B., Le Bissonnais, Y., Gumiere, S. J., Desprats, J. F., Cerdan, O., Darboux, F., Couturier, A., Raclot, D., 2009b. A framework for sensitivity analysis of distributed physics based erosion models ii: Application to four distributed erosion models. Water Resources Research submitted. 108, 188, 204, 207

Chow, V. T., Maidment, D. R., Mays, L. W., 1988. Applied Hydrology. McGraw-Hill International Editors. 99

Chu, S. T., 1978. Infiltration during unsteady rain. Water Resour.Res. 14 (3), 461–466. 53

Citeau, L., Bispo, A., Bardy, M., King, D., 2008. Gestion durable des sols. Versailles, 320 p. 197

Cooper, J. R., Gilliam, J. W., Daniels, R. B., Robarge, W. P., 1987. Riparian areas as filters for agricultural sediment. Soil Science Society Of America Journal 51 (2), 416–420. 45

CORPEN, 1997. Produits phytosanitaires et dispositifs enherbés, ministère de l'agriculture et de la pêche. Tech. rep., Ministère de l'aménagement du territoire et de l'environnement. 55

Corradini, C., Melone, F., Smith, R., 1994. Modelling infiltration during complex rainfall sequences. Water Resources Research 30, 2777–2784. 84

Corradini, C., Melone, F., Smith, R., 1997. A unified model for infiltration and redistribution during complexe rainfall patterns. Journal of Hydrology 192, 104–124. 84

Courant, R., Friedrichs, K., Lewy, H., 1928. Uber die partiellen differenzengleichungen der mathematischen physik. Mathematische Annalen 100, 32–74. 94, 181, 203

Coyne, M. S., Gilfillen, R. A., Villalba, A., Zhang, Z., Rhodes, R., Dunn, L., Blevins, R. L., 1998. Fecal bacteria trapping by grass filter strips during simulated rain. Journal Of Soil And Water Conservation 53 (2), 140–145. 44

Coyne, M. S., Gilfllen, R. A., Rhodes, R. W., Blevins, R. L., 1995. Soil and fecal coliform trapping by grass filter strips during simulated rain. J. Soil Water Conserv. 50, 405–408. 44

Croke, J., Mockler, S., Fogarty, P., Takken, I., 2005. Sediment concentration changes in runoff pathways from a forest road network and the resultant spatial pattern of catchment connectivity. Geomorphology 68, 257–268. 39

Crosetto, M., Tarantola, S., 2001. Uncertainty and sensitivity analysis: Tools for gis-based model implantation. Intl. J. Geo. Info. Sci. 15 (5), 415–437. 126

Daniels, R. B., Gilliam, J. W., 1996. Sediment and chemical load reduction by grass and riparian filters. Soil Sci. Soc. Am. J. 60, 246–251. 44

Darboux, F., Le Bissonnais, Y., 2007. Changes in structural stability with soil surface crusting: consequences for erodibility estimation. Eur. J. Soil Sci. 58 (0), 1107–1114. 16

Darboux, F., Robin, J. G., Fox, D., 2008. Evaluation of two soil conditioners for limiting post-fire erosion as part of a soil conservation strategy. Soil Use and Manag. 24, 366–372. ix, xv, 26, 27

Darcy, H., 1856. Les fontaines de la ville de Dijon. Dalmont, Paris. 85

de Jong, S. M., Paracchini, M. L., Bertolo, F., Folving, S., Megier, J., de Roo, A. P. J., Oct. 1999. Regional assessment of soil erosion using the distributed model semmed and remotely sensed data. CATENA 37 (3-4), 291–308. 57

de Marsily, G., 1994. On the use of models in hydrology [Free opinion] - De l'usage des modèles en hydrologie [Tribune libre]. Rev. Sci. Eau 7 (3), 219–234. 124, 215

De Roo, A. P. J., Jetten, V. G., 1999. Calibrating and validating the LISEM model for two data sets from the netherlands and south africa. CATENA 37 (3-4), 477–493. 214

De Roo, A. P. J., Offermans, R. J. E., Cremers, N. H. D. T., 1996a. LISEM: A single-event physically based hydrological and soil erosion model for drainage basins. II:

Sensitivity analysis, validation and application. Hydrological Processes 10 (8), 1119–1126. 2, 118, 152

De Roo, A. P. J., Wesseling, C. G., Ritsema, C. J., 1996b. LISEM: A single-event physically based hydrological and soil erosion model for drainage basins. I: theory, input and output. Hydrological Processes 10 (8), 1107–1117. 1, 3, 15, 17, 24, 31, 57, 61, 93, 123

de Vente, J., Poesen, J., Jun. 2005. Predicting soil erosion and sediment yield at the basin scale: Scale issues and semi-quantitative models. Earth-Science Reviews 71 (1-2), 95–125. 40, 196

Deletic, A., 1999. Sediment behaviour in grass filter strips. Water Science and Technology 39, 129–136. 54

Deletic, A., Jul. 2001. Modelling of water and sediment transport over grassed areas. Journal of Hydrology 248 (1-4), 168–182. 50, 54, 103, 105, 183

Deletic, A., Jan. 2005. Sediment transport in urban runoff over grassed areas. Journal of Hydrology 301 (1-4), 108–122. x, 54, 55, 103, 104, 105, 183

Deletic, A., Fletcher, T. D., 2006. Performance of grass filters used for stormwater treatment - a field and modelling study. Journal Of Hydrology 317 (3-4), 261–275. 43, 45, 65, 103, 183

Desmet, P. J. J., Govers, G., 1996. A gis procedure for automatically calculating the usle ls factor on topographically complex landscape units. J. of Soil and Water Conser. 51, 427–433. 17

Dijk, P. M. v., Kwaad, F. J. P. M., Klapwijk, M., 1996. Retention of water and sediment by grass strips. Hydrological Processes 10 (8), 1069–1080. 24, 25, 44

Dillaha, T. A., Reneau, R. B., Mostaghimi, S., Lee, D., 1989. Vegetative filter strips for agricultural nonpoint source pollution-control. Trans of ASAE 32, 513–519. 42, 43, 44, 46

Dillaha, T. A., Sherrard, J. H., Lee, D., Mostaghimi, S., Shanholtz, V. O., 1988. Evaluation of vegetative filter strips as a best management practice for feedlots. J. Water Pollut. Control Fed. 60, 1231–1238. 45

Diskin, M., Nazimov, N., 1995. Linear reservoir with feedback regulated inlet as a model for the infiltration process. Journal of Hydrology 172, 313–330. 84

Doherty, J., 2004. PEST - Model-independent parameter estimation, User Manual. Watermark Numerical Computing. 133, 153, 197, 205

Duan, Q., Sorooshian, S., Gupta, V., 1992. Effective and efficient global optimization for conceptual rainfall-runoff models. Water Resources Research 28(4), 1015–1031. 77

Dunkerley, D., 2003. Determining friction coefficients for interrill flows: the significance of fow filaments and backwater effects. Earth Surf. Process. Landf. 28, 475–491. 50, 52

Elliott, W. J. A. M., Liebenow, J., Laflen, M., Kohl, K. D., 1989. A compendium of soil erodibility data from wepp cropland soil field erodibility experiments 1987 & 1988. USDA-ARS National Soil Erosion Research Lab., West Lafayette, IN. NSERL Report No. 3. ix, xv, 20, 21, 28

Ellison, W. D., 1947. Soil erosion studies - part i. Agric. Eng. 28, 145–146. 22

Evans, R., Brazier, R., 2005. Evaluation of modelled spatially distributed predictions of soil erosion by water versus field based assessments. Environmental Science and Policy 8, 493–501. 9

Ewen, J., Parkin, G., O'Connell, E., 2000. Shetran: Distributed basin flow and transport modelling system. Journal of Hydrologic Engineering 5(3), 250–258. 2, 3, 40, 57, 61

Fasching, R. A., Bauder, J. W., 2001. Evaluation of agricultural sediment load reductions using vegetative filter strips of cool season grasses. Water Environment Research 73 (5), 590–596. 45

Favis-Mortlock, D. T., 1998. Modelling Soil Erosion by Water. Global Environmental Change. Springer-Verlag, Berlin Heidelberg, Ch. Evaluation of field-scale erosion models on the UK South Downs, pp. 43–53. 2, 9, 217

Ferreira, V. A., Weesies, G. A., Yoder, D. C., Foster, G. R., Renard, K. G., 1995. The site and condition specific nature of sensitivity analysis. J. Soil Water Conserv 50, 493–497. 29

Finkner, S. C., Nearing, M. A., Foster, G. R., Gilley, J. E., 1989. A simplified equation for modelling sediment transport capacity. Trans. Am. Soc. Agric. Eng. 32, 1545–1550. 61

Fitzjohn, C., Ternan, J. L., Williams, A. G., Feb. 1998. Soil moisture variability in a semi-arid gully catchment: implications for runoff and erosion control. CATENA 32 (1), 55–70. 56, 178, 220

Folly, A., Quinton, J. N., Smith, R. E., 1999. Evaluation of the eurosem model using data from the catsop watershed, the netherlands. Catena 37, 507–519. 2, 9, 217

Foster, G. R., 1982. Modeling the erosion process. Hydrologic modeling of small watersheds, 295–380. 61, 101, 102

Foster, G. R., Flanagan, D. C., Nearing, M. A., Lane, L. J., Risse, L. M., Finkner, S. C., 1995. Water Erosion Prediction Project (WEPP):technical documentation. Tech. rep., National Soil Erosion Research Laboratory. USDA-ARS-MWA.1196 SOIL Building. West Lafayette, IN 47907-1196 NSERL Report No.10. 101, 102

Foster, G. R., Lane, L. J., Nowlin, J. D., Laflen, J. M., Young, R. A., 1980. Creams: A field scale model for chemicals, runoff, and erosion from agricultural. Management Systems 8, 1–10. 15, 17

Fox, G. A., Sabbagh, G. J., Jan. 2009. Comment on "major factors influencing the efficacy of vegetated buffers on sediment trapping: A review and analysis," by xingmei liu, xuyang zhang, and minghua zhang in the journal of environmental quality 2008 37:1667-1674. J Environ Qual 38 (1), 1–3. 46

Frey, H. C., Patil, S. R., 2002. Identification and review of sensitivity analysis methods. Risk Analysis 22 (3), 553–578. 125, 152, 178

Fryirs, K., Brierley, G. J., 1999. Slope-channel decoupling in wolumla catchment, new south wales, australia: the changing nature of sediment sources following european settlement. Catena 35, 41–63. 39

Fryirs, K. A., Brierley, G. J., Preston, N. J., Kasai, M., 2007. Buffers, barriers and blankets: The (dis)connectivity of catchment-scale sediment cascades. Catena 70, 49–67. 55, 103, 178

Gâteaux, R., 1913. Sur les fonctionnelles continues et les fonctionnelles analytiques. Comptes-Rendus de l'Académie des Sciences 157, 325–327. 127, 134, 152

Ghadiri, H., Rose, C. W., Hogarth, W. L., 2001. The influence of grass and porous barrier strips on runoff hydrology and sediment transport. Transactions Of The ASAE 44 (2), 259–268. 45, 46

Gharabaghi, B., Rudra, R. P., Goel, P. K., 2006. Effectiveness of vegetative filter strips in removal of sediments from overland flow. Water Quality Research Journal Of Canada 41 (3), 275–282. 45, 46

Ghate, S. R., Burtle, G. J., Vellidis, G., Newton, G. L., May 1997. Effectiveness of grass strips to filter catfish (ictalurus punctatus) pond effluent. Aquacultural Engineering 16 (3), 149–159. 44

Gobin, A., Jones, R. J. A., Kirkby, M., Campling, P., Kosmas, C., Govers, G., Gentile, A. R., 2004. Pan-european assessment and monitoring of soil erosion by water. Environmental Science and Policy 7, 25–38. 123, 151, 154

Graf, W., 1988. Fluvial Processes in Dryland Rivers. Springer-Verlag: Berlin. 63

Green, W., Ampt, G., 1911. Studies on soil physics part i: The flow of air and water through soils. Journal of Agricultural Science 4, 1–24. 84, 85, 98

Gumiere, S. J., Delattre, L., Cheviron, B., Le Bissonnais, Y., Ben Slimane, A., 2009a. Multi-scale calibration and validation of a distributed water erosion model: Application in a mediterranean vineyards catchment. Journal of Soils and Sediments submitted, xx. 109, 151, 153

Gumiere, S. J., Le Bissonnais, Y., Raclot, D., 2008. Mhydas - Erosion: A physically based erosion model for watershed application. In: EGU Viena, Austria. 100

Gumiere, S. J., Le Bissonnais, Y., Raclot, D., 2009b. Soil resistance to interrill erosion: Model parameterization and sensitivity. Catena 77, 274–284. 118

Gumiere, S. J., Le Bissonnais, Y., Raclot, D., Cheviron, B., 2009c. Interface effects on sedimentological connectivity of agricultural catchments in erosion modelling: A review. Earth Surf. Process. Landf. acepted with major revision, xx. 82, 93, 142, 151

Gumiere, S. J., Moraes, J. M., Victoria, R. L., 2007. Calibration and validations of a soil-plant-atmosphere model at the national forest of tapajos, Para. Brazilian Journal of Water Research 1, 1–11. 207

Gumiere, S. J., Raclot, D., Cheviron, B., Le Bissonnais, Y., 2009d. MHYDAS-Erosion: A physically based spatially-distributed erosion model for agricultural catchment application. J. Soils Sediments. *Submitted*. 123, 125, 153, 179, 181, 203

Hairsine, P. B., Rose, C. W., 1992. Modeling water erosion due to overland flow using physical principles. II: rill flow. Water Resources Research 28, 245–250. 102

Hall, J. K., Hartwing, N. L., Hoffman, L. D., 1983. Application mode and alternate cropping effects on atrazine losses from a hillside. J. Environ. Qual. 12 (3), 336–340. 44

Harvey, A. M., 2001. Coupling between hillslopes and channels in upland fluvial systems: implications for landscape sensitivity illustrated from the howgill fells, northwest england. Catena 42, 225–250. 39, 102, 103

Haskins, G., Davey, 1991. Integrated quantity-quality modelling: Stage 3. Tech. rep., Department of Water Resources, Sydney, pp. 102. 2, 57, 61

Hayami, S., 1951. On the propagation of flood waves. Bulletin of the Disaster Prevention Research Institute, Kyoto University 1, 1–16. 99, 105

Hayes, J. C., Barifield, B. J., Barnhisel, R. I., 1979. Filtration of sediment by simulated vegetation ii. unsteady flow with non-homogeneous sediment. Trans. ASAE 22 (5), 1063–1067. 53

Hayes, J. C., Barifield, B. J., Barnhisel, R. I., 1984. Performance of grass filters under laboratory and field conditions. Trans. ASAE 27 (5), 1321–1331. 53

Hayes, J. C., Hairston, J. E., 1983. Modeling the long-term effectiveness of vegetative filter strips on on-site sediment control. Am. Soc. Agric. Eng. ASAE Paper 83-2081 St. Joseph, MI. 44

Helmers, M. J., Eisenhauer, D. E., Dosskey, M. G., Franti, T. G., Brothers, J. M., McCullough, M. C., 2005. Flow pathways and sediment trapping in a field-scale vegetative filter. Trans. ASAE 48, 955–968. 45

Helton, J. C., 1993. Uncertainty and sensitivity analysis techniques for use in performance assessment for radioactive waste disposal. Reliability Engineering and System Safety 42, 327–367. 29, 126, 178

Hessel, R., van den Bosch, R., Vigiak, O., 2006. Evaluation of the lisem soil erosion model in two catchments in the east african highlands. Earth Surface Processes and Landforms 31, 469–486. 24, 93, 196

Hier-Majumder, C. A., Travis, B. J., Belanger, E., Richard, G., Vincent, A. P., Yuen, D. A., 2006. Efficient sensitivity analysis for flow and transport in the earth's crust and mantle. Geophysical Journal International 166 (2), 907–922. 126

Hong, H. T. M., 1995. Hydraulic resistance of flexible roughness. Ph.D. thesis, IHE Delft. 50

Horton, R., 1933. The role of infiltration in the hydrologic cycle. American Geophysical Union Transactions 14, 446–460. 84

Hussein, J., Ghadiri, H., Yu, B., Rose, C., 2007. Sediment retention by a stiff grass hedge under subcritical flow conditions. Soil Science Society Of America Journal 71 (5), 1516–1523. 45

Ionescu-Bujor, M., Cacuci, D. G., 2004. A comparative review of sensitivity and uncertainty analysis of large-scale systems. I. deterministic methods. Nucl. Sci. Eng. 147 (3), 189–203. 126

Janeau, J. L., Briquet, J. P., Planchon, O., Valentin, C., 2003. Soil crusting and infiltration on steep slopes in northern thailand. Eur. J. Soil Sci. 54, 543–553. 25

Jetten, V., Boiffin, J., de Roo, A., 2005. Defining monitoring strategies for runoff and erosion studies in agricultural catchments: a simulation approach. Europ. J. Soil Sci. 47 (4), 579–592. 124

Jetten, V., Govers, G., Hessel, R., 2003. Erosion models: quality of spatial predictions. Hydrological Processes 17 (5), 887–900. 2, 9, 10, 35, 93, 124, 217

Jetten, V. G., de Roo, A. P. J., Favis-Mortlock, D., 1999. Evaluation of field - scale and catchment - scale soil erosion models. Catena 3, 521–541. 2, 9, 35, 93, 124, 196, 217

Johanson, R. C., Imhoff, J. C., Davis, H. H., 1980. Users manual for the hydrologic simulation program-fortran (hspf) version no. 5.0, epa-600/9-80-105. Tech. rep., USEPA Environmental Research Laboratory, Athens, GA. 57

Julien, P.-Y., 1998. Erosion and sedimentation. 102

Kamboj, S., Cheng, J.-J., Yu, C., 2005. Deterministic vs. probabilistic analyses to identify sensitive parameters in dose assessment using RESRAD. Health Phys. 88 (5), 104–109. 126

Kemper, W. D., Rosenau, R. C., 1986. Aggregate stability and size distribution In: Methods of Soil Analysis, Part 1, Agronomy Monographs vol. 9. American Society of Agronomy, Madison, WI. 28

Kinnell, P. I. A., 1993. Interrill erodibilities based on the rainfall intensity flow discharge erosivity factor. Aust. J. Soil Res 31, 319–32. 15, 27

Kinnell, P. I. A., 2005. Raindrop-impact-induced erosion processes and prediction: a review. Hydrological Processes 19, 2815–2844. 15, 18, 28, 96, 100

Kinnell, P. I. A., Risse, L. M., 1998. Usle-m: empirical modeling rainfall erosion through runoff and sediment concentration. Soil Sci. Soc. Am. J 62, 1667–1672. 17

Kirkby, M. J., Irvine, B. J., Jones, R. J. A., Govers, G., the PESERA team, 2008. The PESERA coarse scale erosion model for Europe. I. - model rationale and implementation. European Journal of Soil Science 59, 1293–1306. 123, 151, 154

Kleijnen, J. P. C., Helton, J. C., 1999. Statistical analysis of scatterplots to identify important factors in large-scale simulations. 2: Robustness of techniques. Reliab. Eng. Syst. Safety 65 (2), 187–197. 125

Klemes, V., 1986. Operational testing of hydrological simulation models. Hydrological Sciences 31, 13–24. 77

Kliment, Z., Kadlec, J., Langhammer, J., May 2008. Evaluation of suspended load changes using annagnps and swat semi-empirical erosion models. CATENA 73 (3), 286–299. 93, 196

Knapen, A., Poesen, J., Govers, G., Gyssels, G., Nachtergaele, J., 2007. Resistance of soils to concentrated flow erosion: A review. Earth-Sci. Rev. 80, 75–109. 15, 29, 102, 125, 151, 219

Knight, D. W., Shiono, K., 1996. Channel and floodplain hydraulics. In: Floodplain processes. Anderson, M.G., D.E. Walling, P. D. Bates editors. New York: John Wiley and Sons. 126

Knisel, W. G., 1980a. Creams, a field scale model for chemicals, runoff and erosion from agricultural management systems. U. C. R. Report USDA 26. 15, 57, 92

Knisel, W. G., 1980b. Creams: A field-scale model for non-point source pollution evaluation. gettysburg. Proc. Non-point Pollution Control Tools and Techniques for the Future Symposium 1, 100–106. 2

Lacas, J. G., Voltz, M., Gouy, V., Carluer, N., Gril, J. J., 2005. Using grassed strips to limit pesticide transfer to surface water: a review. Agron. Sustain. Dev. 25, 253–266. 46

Laflen, J. M., Elliot, W. J., Flanagan, D. C., Meyer, C. R., Nearing, M. A., 1997. Wepp-predicting water erosion using a process-based model. Journal of Soil And Water Conservation 52 (2), 96–102. 1, 40, 57, 62

Laflen, J. M., Elliot, W. J., Simanton, R., Holzhey, S., Kohl, K. D., 1991. Wepp soil erodibility experiments for rangeland and cropland soils. Journal of Soil and Water Conservation 46, 39–44. xv, 15, 21

Lagacherie, P., Rabotin, M., Colin, F., Moussa, R., Voltz, M., 2009. GeoMHYDAS: A discretization procedure for cultivated landscapes in distributed hydrologic modeling. Computers and geosciences, submitted. ix, 41, 42, 82, 94, 95, 181

Lawrence, D. S. L., 1997. Macroscale surface roughness and frictional resistance in overland flow. Earth Surface Processes and Landforms 22, 365–382. 50

Lawrence, D. S. L., 2000. Hydraulic resistance in overland flow during partial and marginal surface inundation: Experimental observations and modeling. WATER RESOURCES RESEARCH 36, 2381–2393. 64

Le Bissonnais, Y., 1996. Aggregate stability and assessment of soil crustability and erodibility: I. theory and methodology. European Journal of Soil Science 47, 425–437. 25, 28, 100

Le Bissonnais, Y., Blavet, D., De Noni, G., Laurent, J. Y., Asseline, J., Chenu, C., 2007. Erodibility of mediterranean vineyard soils: relevant aggregate stability methods and significant soil variables. European Journal of Soil Science 58, 188–195. 25

Le Bissonnais, Y., Cerdan, O., Lecomte, V., Benkhadra, H., Souchere, V., Martin, P., 2005. Variability of soil surface characteristics influencing runoff and interrill erosion. Catena 62, 111–124. 16

Le Bissonnais, Y., Lecomte, V., Cerdan, O., 2004. Grass strip effects on runoff and soil loss. Agronomie 24 (3), 129–136. 43, 45, 48

Le Bissonnais, Y., Montier, C., Jamagne, J., Daroussin, J., King, D., 2002. Mapping erosion risk for cultivated soil in France. Catena 46, 207–220. 123, 151, 154, 197

Le Bissonnais, Y., Singer, M., 1992. Crusting, runoff and erosion response to soil water content and successive rainfall events. Soil Sci. Soc. Am. J. 56, 1898–1903. 26, 206

Lecomte, V., 1999. Transferts de produits phytosanitaires par le ruisellement et l'érosion de la parcelle au bassin versant. modélisation spatiale. Ph.D. thesis, ENGREF et INRA-Orléans. 55, 65, 68, 178

Lee, K. H., Isenhart, T. M., Schultz, R. C., Mickelson, S. K., 2000. Multispecies riparian buffers trap sediment and nutrients during rainfall simulations. Journal Of Environmental Quality 29 (4), 1200–1205. 45

Legout, C., Leguédois, S., Bissonnais, Y. L., Issa, O. M., Feb. 2005. Splash distance and size distributions for various soils. Geoderma 124, 279–292. 23, 29

Leguédois, S., Planchon, O., Legout, C., Le Bissonnais, Y., 2005. Splash projection distance for aggregated soils: Theory and experiment. Soil Science Society of America Journal 69, 30–37. 23, 101

Lehman, F., Ackerer, P., 1996. Wamos-1d: Simulation of water movement in soil, model description and user's guide. Tech. rep., Rapport N 96 IMF-HMP 0321, Strasbourg, France. 84

Licciardello, F., Govers, G., Cerdan, O., Kirkby, M., Vacca, A., Kwaad, F. J. P. M., 2009. Evaluation of the PESERA model in two contrasting environments. Earth Surf. Process. Landforms. 34 (5), 629–640. 154

Ligdi, E. E., Morgan, R. P. C., Nov. 1995. Contour grass strips: a laboratory simulation of their role in soil erosion control. Soil Technology 8 (2), 109–117. 44

Lilburne, L., Tarantola, S., 2009. Sensitivity analysis of spatial models. Intl. J. Geo. Info. Sci. 23 (2), 151–168. 127, 179

Lim, T. T., R, E. D., Workman, S. R., Larson, B., Dunn, L., 1998. Vegetated filter strip removal of cattle manure constituents in runoff. Trans. ASAE 41, 1375–1381. 46

Line, D. E., 1991. Sediment trapping effectiveness of grass strips. Proceedings of the Fijth Federal Interagency Sedimentation Conference March 18-21, pp 56–63, Las Vegas. 44

Lions, J. L., 1968. Contrôle optimal des systèmes gouvernés par des équations aux dérivées partielles. 126

Littleboy, M., Silburn, M. D., Freebairn, D. M., Woodruff, D. R., Hammer, G. L., Leslie, J., 1992. Impact of soil erosion on production in cropping systems. i. development and

validation of a simulation model. Australian Journal of Soil Research 30, 757–774. 2, 57

Liu, G., Xu, M., Ritsema, C., 2003. A study of soil surface characteristics in a small watershed in the hilly, gullied area on the chinese loess plateau. CATENA 54, 31–44. 24

Liu, X., Zhang, X., Zhang, M., 2008. Major Factors Influencing the Efficacy of Vegetated Buffers on Sediment Trapping: A Review and Analysis. J Environ Qual 37 (5), 1667–1674. 46

Low, A. J., 1954. The study of soil structure in field and the laboratory. Journal of Soil Science 5, 57–74. 28

Lu, H., Moran, C., Prosser, I. P., Sep. 2006. Modelling sediment delivery ratio over the murray darling basin. Environmental Modelling & Software 21 (9), 1297–1308. 59, 60

Ludwig, B., Boiffin, J., Chadoeuf, J., Auzet, A. V., 1995. Hydrological structure and erosion damage caused by concentrated flow in cultivated catchments. Catena 25, 227–252. 43, 64

Madsen, H., 2000. Automatic calibration of a conceptual rainfall-runoff model using multiple objectives. Journal of Hydrology 235, 276–288. 76

Magette, W. L., Brinsfeld, R. B., Palmer, R. E., Wood, J. D., 1989. Nutrient and sediment removal by vegetated fiter strips. Trans. of ASAE 32, 663–667. 42, 44

Marquardt, D. W., 1963. An algorithm for least-squares estimation of non-linear parameters. Journal of the Society of Industrial and Applied Mathematics 11, 431–441. 205

Marrel, A., Iooss, B., Van Dorpe, F., Volkova, E., 2008. An efficient methodology for modeling complex computer codes with gaussian processes. Computational Statistics and Data Analysis 52, 4731–4744. 179

Masterman, R., Thorne, C. R., 1992. Predicting influence of bank vegetation on channel capacity. J. Hydr. Engrg., ASCE 118(7), 1052–1058. 51

McKay, M. D., Beckman, R. J., Conover, W. J., 1979. A comparison of three methods for selecting values of input variables in the analysis of output from a computer code. Technometrics 21 (1), 239–245. 125

McKergow, L. A., Weaver, D. M., Prosser, I. P., Grayson, R. B., Reed, A. E. G., 2003. Before and after riparian management: sediment and nutrient exports from a small agricultural catchment, western australia. Journal Of Hydrology 270 (3-4), 253–272. 45, 51

Merritt, W. S., Letcher, R. A., Jakeman, A. J., 2003. A review of erosion and sediment transport models. Environm. Model. Software 18 (8-9), 761–799. 3, 40, 124, 151

Meyer, L. D., Dabney, S. M., Harmon, W. C., 1995. Sediment-trapping effectiveness of stiff-grass hedges. Trans. Am. Soc. Agric. Eng. 38, 809–815. 44

Michaelides, K., Wainwright, J., 2002. Modelling the effects of hillslope-channel coupling on catchment hydrological response. Earth Surf. Process. Landf. 27, 1441–1457. 39

Mitas, L., Mitasova, H., 1998. Distributed soil erosion simulation for effective erosion prevention. Water Resources Research 34 (3), 505–516. 17

Mitchell, M., Campbell, C., 2001. Probabilistic exposure assessment of operator and residential exposure; a Canadian regulatory perspective. Annals of the Occupational Hygiene Society. 45, 43–47. 126

Morel-Seytoux, H., Khanji, J., 1974. Derivation of an equation of infiltration. Water Resources Research 10(4), 795–800. 85, 98

Morel-Seytoux, H. J., 1978. Derivation of equations for variable rainfall infiltration. Water Resources Research 14 (4), 561–568. 84, 85, 86, 94, 98, 181, 202

Morel-Seytoux, H. J., 1984. From excess infiltration to aquifer recharge: A derivation based on the theory of flow of water in unsaturated soils. Water Resour. Res. 20, 1230–1240. 85, 105

Morgan, R., 1978. Field studies of rainsplash erosion. Earth Surface Processes 3, 295–299. 22

Morgan, R. P. C., 2001. A simple approach to soil loss prediction: a revised Morgan-Morgan-Finney model. Catena 44, 305–322. xv, 15, 23, 196

Morgan, R. P. C., 2005. Soil Erosion and Conservation, 3rd edn. Blackwell Publishing. 3, 64, 68, 73, 220

Morgan, R. P. C., Quinton, J. N., Smith, R. E., Govers, G., Poesen, J. W. A., Auerswald, K., Chisci, G., Torri, D., Styczen, M. E., 1998a. The european soil erosion model (EUROSEM): a dynamic approach for predicting sediment transport from fields and small catchments. Earth Surface Processes and Landforms 23 (6), 527–544. xv, 1, 15, 17, 23

Morgan, R. P. C., Quinton, J. N., Smith, R. E., Govers, G., Poesen, J. W. A., Auerswald, K., Chisci, G., Torri, D., Styczen, M. E., 1998b. The european soil erosion model (EUROSEM): a dynamic approach for predicting sediment transport from fields and small catchments. Earth Surface Processes and Landforms 23 (6), 527–544. 2, 40, 57, 61, 92

Morris, M. D., 1991. Factorial sampling plans for preliminary computational experiments. Technometrics 33 (2), 161–174. 125, 126

Moussa, R., 1996. Analytical Hayami solution for the diffusive wave flood routing problem with lateral inflow. Hydrological Processes 10 (9), 1209–1227. 86, 90, 94, 99, 105, 151, 153, 181, 202

Moussa, R., Bocquillon, C., 1996a. Algorithms for solving the diffusive wave flood routing equation. Hydrological Processes 10 (1), 105–124. 89, 181, 202

Moussa, R., Bocquillon, C., 1996b. Criteria for the choice of flood-routing methods in natural channels. Journal Of Hydrology 186 (1-4), 1–30. 89, 151, 153

Moussa, R., Voltz, M., Andrieux, P., 2002. Effects of the spatial organization of agricultural management on the hydrological behaviour of a farmed catchment during flood events. Hydrological Processes 16 (2), 393–412. 94, 95, 98, 107, 142, 151, 153, 181, 197, 198, 199, 202, 207, 222

Mulungu, D. M. M., Munishi, S. E., 2007. Simiyu river catchment parameterization using SWAT model. Phys. Chem. Earth, Parts A/B/C 32 (15-18), 1032–1039. 125

Munoz-Carpena, R., Parsons, J. E., Gilliam, J. W., 1999. Modeling hydrology and sediment transport in vegetative filter strips. Journal Of Hydrology 214 (1-4), 111–129. x, 45, 53, 54, 55

Nearing, M. A., 1998. Why soil erosion models over-predict small soil losses and underpredict large soil losses. Catena 32, 15–22. 10, 93

Nearing, M. A., 2000. Evaluating soil erosion models using measured plot data: accounting for variability in the data. Earth Surf. Process. Landforms. 25, 1035–1043. 10, 76, 111, 117, 124, 196

Nearing, M. A., Deer-Ascough, L., Laflen, J. M., 1990. Sensitivity analysis of the WEPP hillslope profile erosion model. TRANS ASAE 33, 839–849. 2, 30, 31, 118, 123, 152, 178

Nearing, M. A., Foster, G. R., Lane, L. J., Finkner, S. C., 1989. A process-based soil erosion model for udsa: water erosion prediction project technology. Trans. of the ASAE 32(5), 1587–1593. 2

Nearing, M. A., Govers, G., Norton, L., Nov. 1999. Variability in soil erosion data from replicated plots. Soil Sci Soc Am J 63 (6), 1829–1835. 10, 117, 124

Nearing, M. A., Nicks, A. D., 1998. Modelling Soil Erosion by Water. Global Environmental Change. Springer-Verlag, Berlin Heidelberg, Ch. Evaluation of the Water Erosion Prediction Project (WEPP) model for hillslopes, pp. 43–53. 2, 9, 217

Neibling, W. H., Alberts, E. E., 1979. Composition and yields of soil particles transported through sod strips. ASAE St. Joseph MI Paper No 79-2065. 44

Nepf, H. M., 1999. Drag, turbulence, and diffusion in flow through emergent vegetation. Water Resour. Res. 35, 479–489. 48, 50

Nord, G., 2005. Modélisation à base physique des processus de l'érosion hydrique a l'échelle de la parcelle. Ph.D. thesis, Université Joseph Fourier, Grenoble I. 17, 28, 31, 101, 102, 123, 152

Norris, V. O. L., 1993. The use of buffer zones to protect water quality: a review. Water Resources Management 7, 257–272. 46

OpenFluid, 2009. L.I.S.A.H. Laboratory, UMR INRA-IRD-SupAgro, Montpellier, France. http://www.umr-lisah.fr/openfluid. 127, 153

Pappenberger, F., Beven, K. J., Ratto, M., Matgen, P., 2008. Multi-method global sensitivity analysis of flood inundation models. Adv. Water Resour. 31, 1–14. 125, 126, 152

Papy, F., Douyer, C., 1991. Influence des états de surface du territoire agricole sur le déclenchement des innondations catastrophiques. Agronomie 11(3), 201–215. 1

Parlange, J. Y., Haverkamp, R., 1989. In Unsaturated Flow in Hydrologic Modeling, Theory and Practice. Kluwer, Boston, MA, Ch. Infiltration and ponding time, pp. 95–126. 84

Parsons, A. J., Abrahams, A. D., Luk, S. H., 1991. Size characteristics of sediment in interrill overland flow on a semiarid hillslope, southern arizona. Earth Surface Processes and Landforms 16, 143–152. 19

Parsons, A. J., Wainwright, J., Abrahams, A. D., Simaton, R. J., 1997. Distributed dynamic modelling of interrill overland flow. Hydrological Processes 11, 1833–1859. 2

Parsons, A. J., Wainwright, J., Brazier, R. E., Powell, D. M., 2006. Is sediment delivery a fallacy? Earth Surface Processes and Landforms 31 (10), 1325–1328. 63

Parsons, A. J., Wainwright, J., Powell, D. M., Kaduk, J., Brazier, R. E., 2004. A conceptual model for determining soil erosion by water. Earth Surface Processes and Landforms 29, 1293–1302. 63

Parsons, J. E., Gilliam, J. W., Munoz-Carpena, R., Daniels, R. B., Dillaha, T. A., 1994. Nutrient and sediment removal by grass and riparian bu?ers. In Proc. 2nd Conf.: Environmentally Sound Agriculture., pp 147?154, In K.L. Campbell et al. (ed.) ASAE, St. Joseph, MI. 44

Parsons, J. E., Thomas, D. L., Huffman, R. L., 2001. Non-point source water quality models: Their use and application.development and application of comprehensive agricultural ecosystems models. Tech. rep., Final Report of USDA-CSREES Southern Region Research Project S-273, 200 pp. 40

Patty, L., Real, B., Gril, J. J., 1997. The use of grassed buffer strips to remove pesticides, nitrate, and soluble phosphorous compounds from runoff water. Pestic. Sci. 49, 243–251. 44

Peterjohn, W. T., Correl, D. L., 1984. Nutrient dynamics in an agricultural watershed: observations on the role of a riparian forest. Ecology 65 5, 1466–1475. 45

Petryk, S., Bosmajian, G. B., 1975. Analysis of flow through vegetation. Journal of the Hydraulics Division, ASCE 101(7), 871–884. 52

Philip, J., 1957. The theory of infiltration: 1. the infiltration equation and its solution. Soil Science 83(5), 345–358. 84

Poesen, J., Torri, D., 1988. The effect of cup size on splash detachment and transport measurements. Part II: field measurements. Catena Suppl. 12, 113–126. 22, 23, 28

Rachman, A., Anderson, S. H., Gantzer, C. J., Thompson, A. L., 2003. Influence of long-term cropping systems on soil physical properties related to soil erodibility. Soil Sci. Soc. Am. J. 67, 637–644. 16, 35

Raclot, D., Le Bissonnais, Y., Louchart, X., Andrieux, P., Moussa, R., Voltz, M., 2009. Soil tillage and scale effects on erosion from fields to catchment in a mediterranean vineyard area. Agriculture, Ecosystems & Environment 134 (3-4), 201–210. 197

Ratto, M., Tarantola, S., Saltelli, A., 2001. Sensitivity analysis in model calibration: Gsa-glue approch. Comput. Phys. Commun 136, 212–224. 118

Refsgaard, J. C., 1997. Parameterisation, calibration and validation of distributed hydrological models. Journal of Hydrology 198 (1-4), 69–97. 70, 73, 74, 76

Renard, K. G., Foster, G. R., 1983. Soil Conservation Principles of erosion by water. Dryland Agriculture. American Society of Agronomy, Soil Science Society of America, Madison, WI, USA, pp. 155-176. 59

Renard, K. G., Foster, G. R., Weesies, G. A., Porter, J. P., 1991. Rusle. revised universal soil loss equation. Journal of Soil and Water Conservation 46, 30–33. 17

Richards, A., 1931. Capillary conduction of liquids through porous mediums. Physics 1, 318–333. 84, 85

Richards, K. S., 1993. Channel Network Hydrology. Wiley, Chichester, Ch. Sediment delivery and the drainage network., pp. 221–254. 60

Robinson, C. A., Ghaffarzadeh, M., Cruse, R. M., 1996. Vegetative filter strip effects on sediment concentration in cropland runoff. Journal Of Soil And Water Conservation 51 (3), 227–230. 44

Ronen, Y., 1988. Uncertainty analysis. CRC Press, Boca Raton, Florida, Ch. The role of uncertainties, pp. 1–40. 126

Roose, E., 1977. Erosion et ruissellement en afrique de l'ouest. Tech. rep., Travaux et documents de l'ORSTOM, 108 pp. 58

Roose, E., Bertrand, R., 1971. Contribution à l'étude des bandes d'arrêt pour lutter contre l'érosion hydrique en afrique occidentale. Agron.Trop. 26 (11), 1270–1283. 44

Rosewell, C. J., 1986. Rainfall kinetic energy in eastern australia. Journal of Climate and Applied Meteorology 25, 1695–1701. 15

Rustomji, P., Prosser, I., 2001. Spatial patterns of sediment delivery to valley floors: sensitivity to sediment transport capacity and hillslope hydrology relations. Hydrological Processes 15, 1003–1018. 40

Sabbagh, G. J., Fox, G. A., Kamanzi, A., Roepke, B., Tang, J.-Z., Feb. 2009. Effectiveness of vegetative filter strips in reducing pesticide loading: Quantifying pesticide trapping efficiency. J Environ Qual 38 (2), 762–771. 48, 65

Saint-Venant, B., 1871. Théorie du mouvement non permanent des eaux, avec application aux crues des rivières et à l'introduction des marées dans leurs lits. Comptes-Rendus de l'Académie des Sciences 73, 147–154. 98

Salles, C., Poesen, J., 2000. Rain properties controlling soil splash detachment. Hydrological Processes 14 (2), 271–282. 15

Saltelli, A., 2002. Making best use of model evaluations to compute sensitivity indices. Computer Physics Communication 145, 580–297. 179

Saltelli, A., Chan, K., Scott, E. M. E., 2000. Sensitivity analysis. John Wiley. 29, 125, 126, 152, 179, 188

Saltelli, A., Tarantola, S., Campolongo, F., Ratto, M., 2004. Sensitivity analysis in practice. A guide to assessing scientific models. Wiley. 126, 178

Saltelli, A., Tarantola, S., Chan, K. P. S., 1999. A quantitative model independent method for global sensitivity analysis of model output. Technometrics 41, 39–56. 117, 178

Sander, G. C., Parlange, J. Y., Barry, D. A., Parlange, M. B., Hogarth, W. L., 2007. Limitation of the transport capacity approach in sediment transport modeling. Water Resour. Res 43, W02403. 61

Savat, J., Poesen, J., 1981. Detachment and transportation of loose sediments by raindrop splash: Part ii detachability and transport ability measurements. Catena 8 (1), 19–41. 22, 29

Schauder, H., Auerswald, K., 1992. Long-term trapping efficiency of a vegetated filter strip under agricultural use. Zeitschrift Fur Pflanzenernahrung Und Bodenkunde 155 (5-6), 489–492. 44

Schmitt, T. J., Dosskey, M. G., Hoagland, K. D., 1999. Filter strip performance and processes for different vegetation, widths, and contaminants. J. Environ. Qual. 28, 1479–1489. 45, 46, 48

Sheridan, G. J., So, H. B., Loch, R. J., Walker, C. M., 2000. Estimation of erosion model erodibility parameters from media properties. Australian Journal of Soil Research 38, 256–284. 15, 125

Sheridan, J. M., Lowrance, R., Bosch, D. D., 1999. Management effects on runoff and sediment transport in riparian forest buffers. Trans. ASAE 42, 55–64. 45

Shields, F. D., Smith, R. H., 1992. Effects of large woody debris removal on physical characteristics of a sand-bed river. Aquatic Conservation 2, 145–163. 52

Shiono, T., Yamamoto, N., Haraguchi, N., Yoshinaga, A., 2007. Performance of grass strips for sediment control in okinawa. Jarq-Japan Agricultural Research Quarterly 41 (4), 291–297. 45

Shrestha, G., Stahl, P. D., Ingram, L., 2005. Influence of reclamation management practices on soil bulk density and infiltration rates on surface coal mine lands in wyoming. In: National Meeting of the American Society of Mining and Reclamation. 48

ShuHui, Z., QingSong, D., BoZhi, W., 2006. Effects of mixed grass strip on reducing water and soil losses in sloping fields. Transactions of the Chinese Society of Agricultural Engineering 22 (5), 61–65. 45

Sieber, A., Uhlenbrook, S., 2005. Sensitivity analyses of a distributed catchment model to verify the model structure. J. Hydrol. 310, 216–235. 125

Silverman, B. W., 1986. Density Estimation. London: Chapman and Hall. 186

Sivapalan, M., 2003. Process complexity at hillslope scale, process simplicity at the watershed scale: is there a connection? [Invited commentary]. Hydrol. Process. 17, 1037–1041. 124, 153

Smith, R. E., Goodrich, D. C., Quinton, J. N., 1995. Dynamic, distributed simulation of watershed erosion: the KINEROS2 and EUROSEM models. Journal of Soil and Water Conservation 50 (5), 517–520. 2

Sobol, I. M., 1993. Sensitivity estimates for nonlinear mathematical models. Math. Model. Comput. Exp. 1, 407–417. 126, 188

Souchère, V., King, D., Daroussin, J., Papy, F., Capillon, A., 1998. Effects of tillage on runoff directions: consequences on runoff contributing areas within agricultural catchments. J. Hydrol. 206, 256–267. 153

Soulsby, R. L., 1997. Dynamics of marine sands - a manual for practical applications. Tech. rep., Thomas Telford, 250pp. 102

Soutter, M., Musy, A., 1999. Global sensitivity analysis of three pesticide leaching models using a monte carlo approach. Trans. ASAE 43 (4), 883?895. 118

Spatz, R., Walker, F., Hurle, K., 1997. Effect of grass buffer strips on pesticide runoff under simulated rainfall. Med. Fac. Landbouww. Univ. Gent. 62, 799–806. 46

Spear, R., Grieb, T. M., Shang, N., 1994. Parameter uncertainty and interaction in complex environmental models. Water Resour. Res. 30, 3159–3169. 179

Sreenivas, L., Johnston, J. R., Hill, H. O., 1947. Some relationships of vegetation and soil detachment in the erosion process. Soil Science Soc. Proceed 12, 471–474. 22

Srivastava, P., Edwards, D. R., Daniel, P. A., Moore, P. A., Costello, T. A., 1996. Performance of vegetative filter strips with varying pollutant source and filter strip lengths. Trans. ASAE 39, 2231–2239. 46

Stewart, B. A., Wischmeier, W. H., Woolhiser, D. A., 1975. Control of water pollution from cropland : A manual for guideline development. U.S.D.A. ix, 18, 19

Syversen, N., Borch, H., 2005. Retention of soil particle fractions and phosphorus in cold-climate buffer zones. Ecological Engineering 25 (4), 382–394. 45

Takken, I., Beuselinck, L., Nachtergaele, J., Govers, G., Poesen, J., Degraer, G., 1999. Spatial evaluation of a physically-based distributed erosion model (LISEM). Catena 37, 431–447. 2, 9, 196, 197, 214, 217, 225

Tang, Y., Reed, P. M., Wagener, T., van Werkhoven, K., 2006. Advancing the identification and evaluation of of distributed rainfall-runoff models using sobol's global sensitivity analysis. Water Resour. Res. 43, W06415, doi: 10.1029/2006WR005813. 126

Tingle, C. H., Shaw, D. R., Boyette, M., Murphy, G. P., 1998. Metolachlor and metribuzin losses in runoff as affected by width of vegetative filter strips. Weed Sci 46, 475–479. 44, 46

Tollner, E. W., Barifield, B. J., Haan, C. T., Kao, T. Y., 1976. Suspended sediment filtration capacity of simulated vegetation. Trans. ASAE 19 (4), 678–682. 53

Tollner, E. W., Barifield, B. J., Vachirakornwatana, C., Haan, C. T., 1977. Sediment deposition in simulated grass filters. Trans. ASAE 20 (5), 940–944. 53

Torri, D., Sfalanga, M., Del Sette, M., 1987. Splash detachment : runoff depth and soil cohesion. Catena 14, 149–155. 10

Toy, T. J., Foster, G. R., Renard, K. G., 2002. Soil Erosion: Processes, Prediction, Measurement and Control. John Wiley and Sons, New York 338 pp. 19, 27, 36

Turanyi, T., Rabitz, H., 2000. Sensitivity analysis. New York: John Wiley, Ch. Local methods and their applications., pp. 367–383. 127

USDA, 1972. National Engineering Handbook Section 4: Hydrology, Soil Conservation Service. US Department of Agriculture, Washington, D.C. 60, 65, 84

USDA, 1997. Predicting soil erosion by water: a guide to conservation planning with the revised universal soil loss equation (rusle). Tech. rep., US Department of Agriculture, Washington, D.C. 63

USDA, 2000. Conservation buffers to reduce pesticide losses. Natural Resources Conservation Service, 1–21. 48

USEPA, 1994. Swrrbwq windows interface users guide. Tech. rep., US Environmental Protection Agency. 57

Van der Knijff, J. M., Jones, R. J. A., Montanarella, L., 2000. Estimation du rique d'érosion en Italie. Tech. rep., EUR 19022 FR, Office for Official Publications of the European Communities, Luxembourg. 47pp. 154

Van Dijk, A. I. J. M., Meesters, A. G. C. A., Bruijnzeel, L. A., 2002. Exponential distribution theory and the interpretation of splash detachment and transport experiments. Soil Science Society of America Journal 66, 1466–1474. 23

van Griensven, A., Meixner, T., Grunwald, S., Bishop, T., Diluzio, M., Srinivasan, R., 2006. A global sensitivity analysis tool for the parameters of multi-variable catchment models. Journal of Hydrology (Amsterdam) 324 (1/4), 10–23. 125

Van Griensven, A., Meixner, T., Grunwald, S., Bishop, T., Diluzio, M., Srinivasan, R., 2006. A global sensitivity analysis tool for the parameters of multi-variable catchment models. Journal of Hydrology (Amsterdam) 324 (1/4), 10–23. 152

Van Oost, K., Govers, G., Desmet, P. J. J., 2000. Evaluating the effects of changes in landscape structure on soil erosion by water and tillage. Landscape Ecology 15 (6), 579–591. 17

Van Rompaey, A., Verstraeten, G., Van Oost, K., Govers, G., Poesen, J., 2001. Modelling mean annual sediment yield using a distributed approach. Earth Surface Processes and Landforms 26 (11), 1221–1236. 57

Vaucluse, C. A., 2000. Efficacité des bandes enherbées sur la qualité des eaux de ruissellement. Tech. rep., Groupement de développement agricole-Viticulture de Vaucluse. 46

Veihe, A., Quinton, J., 2000. Sensitivity analysis of EUROSEM using Monte Carlo simulation: I. hydrological, soil and vegetation parameters. Hydrological Processes 14, 915–926. 2, 30, 31, 118, 123, 152

Verstraeten, G., Poesen, J., de Vente, J., Koninckx, X., Mar. 2003. Sediment yield variability in spain: a quantitative and semiqualitative analysis using reservoir sedimentation rates. Geomorphology 50 (4), 327–348. 40

Vertessey, R. A., Watson, F. G. R., Rahman, J. M., Cuddy, S. D., Seaton, S. P., Chiew, F. H., Scanlon, P. J., Marston, F. M., Lymbuner, L., Jeanelle, S., Verbunt, M., 2001. New software to aid water quality management in the catchments and waterways of the south-east queensland region. In: In: Proceedings of the Third Australian Stream Management Conference. 40

Viney, N. R., Sivapalan, M., Deeley, D., 2000. A conceptual model of nutrient mobilisation and transport applicable at large catchment scales. Journal of Hydrology 240, 23–44. 40, 57

Wainwright, J., Parsons, A. J., 1998. Modelling Soil Erosion by Water. Springer-Verlag, Berlin, Ch. Sensitivity of sediment-transport equations to errors in hydraulic models of overland flow, pp. 271–284. 204

Wainwright, J., Parsons, A. J., Powell, D. M., Brazier, R., 2001. Soil Erosion for the 21st Century. American Society of Agricultural Engineers: St. Joseph, Michigan;, Ch. A new conceptual framework for understanding and predicting erosion by water from hillslopes and catchments, pp. 607– 610. 63

Wallerstein, N., Thorne, C. R., Doyle, M. W., 1997. Spatial distribution and impact of large woody debris in northern Mississippi. In Management of Landscapes Disturbed by Channel Incision. University of Mississippi: Mississippi, USA, 145-150. 52

Walling, D. E., 1983. The sediment delivery problem. J. of Hydrol. 65, 209–237. 60, 63

Walling, D. E., He, Q., Blake, W., 1999. Use of be-7 and cs-137 measurements to document short- and medium-term rates of water-induced soil erosion on agricultural land. Water Resour. Res. 35, 3865–3874. 64, 68, 220

Walsh, S., Brown, J., Bian, D. G., Allen, T. R., 1994. Effects of spatial scale on data certainty: an assessment through data dependency and sensitivity analyses. In: Proceedings of 1st international symposium on the spatial accuracy of natural resource databases Williamsburg, Virgina. 29

Wang, X. H., Yin, C. Q., Shan, B. Q., 2005. The role of diversied landscape buffer structures for water quality improvement in an agricultural watershed, north china. Agriculture, Ecosystems and Environment 107, 381–396. 39

Ward, J. M., Jackson, C. R., 2004. Sediment trapping within forestry streamside management zones: Georgia piedmont, usa. Journal Of The American Water Resources Association 40 (6), 1421–1431. 45

Warner, R. F., 2006. Natural and artificial linkages and discontinuities in a mediterranean landscape: Some case studies from the durance valley, france. Catena 66, 236–250. 41

Watson, D. A., Laflen, J. M., 1986. Soil strength, slope, and rainfall intensity effects on interrill erosion. Transactions of ASAE St Joseph 29, 98–102. 15

Wheater, H. S., Jakeman, A. J., Beven, K. J., 1993. Progress and directions in rainfall-runoff modelling in: Modelling Change in Environmental Systems. John Wiley and Sons, Chichester. 40

Williams, J. R., Berndt, H. D., 1977. Sediment yield prediction based on watershed hydrology. Trans. Of the ASAE, 1100–1104. 60

Wilson, C. A. M. E., Stoesser, T., Bates, P. D., 2005. Modelling of open channel flow throgh vegetation (in: Computational Fluid Dynamics: Applications in Environmental Hydraulics). John Wiley and Sons. ix, 48, 49, 50, 64

Wischmeier, W. H., 1976. Use and misuse of the universal soil loss equation. Journal Soil and Water Conservation 31, 5–9. 18

Wischmeier, W. H., Johnson, C. B., Cross, B. V., 1971. A soil erodibility nomograph for farmland and construction sites. Journal of Soil and Water Conservation 26, 189–193. 18

Wischmeier, W. H., Smith, D. D., 1978. Predicting rainfall erosion losses. Agricultural Handbook Washington U. S. D. A. 14, 15, 16, 17, 58, 59, 125

Woolhiser, D. A., Smith, R. E., Goodrich, D. C., 1990. Kineros, a kinematic runoff and erosion model: documentation and user manual. ars-77. Tech. rep., USDA-Agricultural Research Service. 2, 15, 17, 57, 61, 92

Wu, F. C., Shen, H. W., Chou, Y. J., 1999. Variation of roughness coefficients for unsubmerged and submerged vegetation. Journal of Hydraulic Engineering 9, 934–942. 48, 50

Yan, F.-L., Shi, Z.-H., Li, Z.-X., Cai, C.-F., 2008. Estimating interrill soil erosion from aggregate stability of ultisols in subtropical china. Soil and Tillage Research 100, 34–41. 25, 100, 221

Young, P. C., 1978. Modeling, Identification and Control in Environmental Systems. North Holland, Amsterdam, Ch. A general theory of modelling for badly defined dynamic systems, pp. 103–135. 179

Young, R. A., 1974. A method of measuring aggregate stability under waterdrop impact. Trans. Am. Soc. Agric. Eng 31, 1351–1354. 25

Young, R. A., Huntrods, T., Anderson, W., 1980. Effectiveness of vegetated buffer strips in controlling pollution from feedlot runoff. J Environ Qual 9, 483–487. 42, 45

Young, R. A., Onstad, C. A., Bosch, D. D., Anderson, W. P., 1987. Agnps: Agricultural non-point source pollution model: awatershed analysis tool. Tech. rep., U.S. Department of Agriculture, Washington, D.C. 17, 40, 57

Yu, B., Rose, C. W., Cielsiolka, C. A. A., Coughlan, K. J., Fentie, B., 1997. Towards a framework for runoff and soil loss prediction using guest technology. Australian Journal of Soil Research 35, 1191–1212. 2, 57

Zhang, B., Horn, R., Jan. 2001. Mechanisms of aggregate stabilization in ultisols from subtropical china. Geoderma 99 (1-2), 123–145. 100

Zhang, J.-t., Su, X.-h., Apr. 2008. Numerical model for flow motion with vegetation. Journal of Hydrodynamics, Ser. B 20 (2), 172–178. 52

Zhu, J. C., Gantzer, C. J., Anderson, S. H., Peyton, R. L., Alberts, E. E., 1995. Simulated small-channel bed scour and head cut erosion rates compared. Soil Science Society of America Journal 59, 211–218. 15

List of symbols, acronyms and abbreviations

List of Symbols, Acronyms and Abbreviations

A	is the total momentum-absorbing area of the stems
A_i	is the cross-sectional area of the i^{th} debris in the plane normal to the flow
A_s	is the index of stability calculated from MWD measurements
B	is the mean flow depth
b	is the width of the grass strip
B_0	is the open flow width (spacing between two nearby stems)
c	is sediment concentration
C_D	is the drag coefficient of vegetation
$clay$	is the fraction of clay in surface soil
D_A	is the roughness concentration due to LWD
d_s	is diameter of the particles
D_d	is the sediment deposition rate
d_{grass}	is the width of stems seen as cylinders
D_i	is the sediment inflow rate due to interrill erosion
d_i	is the detachment rate
D_r	is the sediment inflow rate due to rill erosion
d_{s*}	is adimensional sedimentological diameter
E_{NS}	the Nash-Sutcliffe efficiency
$F(t)$	is the cumulative infiltration
F_p	is the cumulative infiltration when ponding occurs
H	is the flow depth
h	is the depth of flow over vegetation
H_c	is the capillary height
h_{grass}	is the grass height
I	is the effective rainfall intensity
K	is the soil erodibility factor

k	is the detachability index
K_r	is rill erodibility
K_s	is the hydraulic conductivity at natural saturation
KE	is the total rainfall kinetic energy
Ki	is interrill erodibility
ko	is the organic matter sub factor
kp	is the soil profile permeability sub factor
ks	is the soil structure sub factor
kt	is the rill transport efficacy
l	its width of the vegetated filter
m_r	is the mass of soil particles detached
q	is unit flow discharge per meter width of the flow
q_s	is unit solid discharge by meter width of the flow
R	is the runoff amount
R_H	is the mean hydraulic radius
S	is local bedslope in rills or reach segments of the channel network
S_{factor}	is the slope factor
S_f	is local energy slope related to friction on the bed
$T_{r,s}$	is the sediment removal efficiency of the vegetated filter
TC	is the flow transport capacity
U	is double-averaged flow velocity
V	is the velocity between the vegetation blades
v_s	is the settling velocity
vfs	is the very fine sand in the surface soil
Vs	is the sedimentation velocity calculated by Stokes equation (laminar flow and sufficiently small sediment load)
x	is the distance in the streamwise direction
Y_i	is a generic observed value

α is an empirical exponent depending on roughness

η is the transport efficiency of sediment in the rill

μ is dynamic viscosity of water

ν is kinematic viscosity of water

ρ is the water density

ρ_s is density of the particles

τ is shear stress exerted on the bed by the flow

τ_c is critical shear stress over which detachment is initiated

θ is the slope angle

θ_i the water content at $t = 0$

θ_r is the residual water content

θ_s is the water content at natural saturation

$AGNPS$ Agricultural Non-Point Source pollution model

$ANSWERS$ Areal Nonpoint Source Watershed Environment Response Simulation

$CETI$ transport coefficient of interrill to rill

$CREAMS$ Chemicals Runoff and Erosion from Agricultural Management Systems

$EUROSEM$ European Soil Erosion Model

$GUEST$ Griffith University Erosion System Template

$HSPF$ Model Hydrologic Simulation Program Fortran

$KINEROS$ kinematic runoff and erosion model

$LASCAM$ Large Scale Catchment Model

$LISEM$ Limburg Soil Erosion Model

LMP Land management practices

MWD_{FW} is the mean weight diameter obtained by the fast-wetting treatment

MWD_{SW} is the mean weight diameter obtained by the slow-wetting treatment

MWD_{WS} is the mean weight diameter obtained by the stirring treatment

$RMSE$ Root Mean Square Error

$SEMMED$ Soil Erosion Model for Mediterranean Regions

$STREAM$ Sealing Transfer Runoff Erosion Agricultural Modification

$SWAT$ Soil and Water Assessment Tool

$SWIM$ Soil Water Models

$SWRRB - WQ$ Simulator for Water Resources in Rural Basins-Water Quality

$USLE$ Universal Soil Loss Equation

$WEPP$ Water Erosion Prediction Project